DEVELOPMENT OF CORE-SHELL STRUCTURE POLYMER COATED NANO-PARTICLES FOR TRIBOLOGICAL APPLICATIONS

by

KIMAYA VYAVHARE

DISSERTATION

Submitted in partial fulfillment of the requirements
for the degree of Doctor of Philosophy at
The University of Texas at Arlington
December, 2020
Arlington, Texas

Supervising Committee:

Dr. Pranesh B. Aswath, Supervising Professor

Dr. Richard B. Timmons

Dr. Efstathios "Stathis" I. Meletis,

Dr. Yaowu Hao

Dr. Daejong Kim

ACKNOWLEDGEMENTS

I wish to leave my gratitude to my supervisor, Dr. Pranesh Aswath for his never ending support and help through each step of the research process. He has been constant source of inspiration throughout my graduate program. He inspired me to continue doing research and encouraged me to pursue Ph.D. after my Masters, which has been the best decision of my life. He not only taught me scientific reasoning and problem solving skills but has also helped me to develop good presentation and communication skills. He always motivated me to work on my weaknesses and because of him I have transformed from a student to a professional.

I would like to say a big thanks to my great co-advisor, Dr. Richard B. Timmons for his great support on my project. It was very inspiring and exciting to work under his guidance and get so much useful experience and advice to bolster my technical knowledge.

I am extremely thankful to all of those with whom I have had the pleasure to work during my five years of graduate study. I appreciate the opportunity to do an internship at Argonne National Laboratory under the guidance of Dr. Ali Erdemir. I am grateful to all his scientific inputs and recommendations for this research work. In addition, I would like to thank renowned scientists at Argonne, Dr. Eryilmaz Levent, Dr. Delferro Massimiliano, Dr. Gokhan Chelik, and Dr. Ryan Hackler to introduce me to new material characterization technique and help me strengthen my research aptitude.

Beside these, I would like to acknowledge the time and efforts of my dissertation committee members, Dr. Efstathios Meletis, Dr. Yaowu Hao, and Dr. Daejong Kim. Your suggestions during my Ph.D. comprehensive exam provided me with more focused outlook and contributed towards completion of my research work. I would also like to acknowledge support and time of Dr. Brian Edwards, Dr. Jiechao C. Jiang and David Yan who trained me on different

analytical instruments and helped me trouble shoot technical problems related to my experimental work. Additionally, I would like to thank all the faculty and staff members of Material Science and Engineering department for their indispensable support throughout my graduate study. My sincere acknowledgment to Dr. Lucia Zuin, Dr. Tom Regier and Dr. Yongfeng Hu for their help with the XANES work and all the training at the Canadian Light Source. I would like to thank all the members of my research group and friends at UTA, Dr. Vinay Sharma, Sedhuraman Mathiravedu, Ami Shah, Aseem Athavale, and Kamal Awad who always kept me motivated and helped me to stay focused on my work.

Nothing has helped me more in the pursuit of this dissertation work than the support of my loving family. I would like to appreciate love and guidance of my mother, brother, and in-laws. Importantly, I wish to thank my supportive and loving husband, Dhruvang Patel who motivated me at my lowest points and provided me with the strength to see through the whole graduation.

LIST OF FIGURES

Chapter 1

Chapter 2

LIST OF TABLES

Chapter 2

Chapter 3

Chapter 4

ABSTRACT

DEVELOPMENT OF CORE-SHELL STRUCTURE POLYMER COATED NANO-ADDITIVES FOR TRIBOLOGICAL APPLICATIONS

Kimaya Vyavhare, PhD

University of Texas at Arlington, 2020

Supervising Professor: Pranesh B. Aswath

Lubricating oils are of paramount importance for controlling frictional energy losses in automotive engines and maintaining the overall performance of the vehicle components. These oils contain various P and S based chemical species to help reduce friction and wear of metallic parts, and thus, enhance durability and energy efficiency of engines. Unfortunately, the beneficiary performance of the current engine oil additive technology i.e. zinc dialkyl dithiophosphate (ZDDP) comes with a major drawback of reducing the lifespan and efficiency of an automobile's pollutant-reducing catalytic converter, thus increasing harmful emissions in the surrounding. This research work is a step towards making engines more efficient and sustainable through the development of functionalized nanoparticles as environment-friendly lubricant anti-wear additives. For this purpose, surface tailored nanoparticles were employed to deliver chemical species at tribological contacts for improving anti-friction and anti-wear characteristics. Plasma polymerization technology was used to coat or encapsulate nanoparticles with chemistries known to provide good tribological outcomes. In this study, different nanoparticles (ZnO, $CaCO_3$) were plasma treated with different chemistries (fluorine, boron) and tribologically tested along with other anti-wear additives including ashless thiophosphates additives to overcome the current challenges of lowering phosphorus content in engine oil and improving the fuel efficiency. The objective of this

thesis work is to study the tribological performance of plasma functionalized core-shell structure nanoparticles under boundary lubrication regime and develop a comprehensive understanding of their tribofilm properties and its implications on friction and wear outcomes. As the first approach, an experimental methodology was developed to synthesize core-shell structure ZnO nanoparticles coated with fluorocarbon polymer films and prepare oil formulations with a low concentration of ZDDP. These nano-lubricants were tribologically tested and properties of in-situ formed anti-wear tribofilms were studied using advanced surface characterization techniques like X-ray absorption near-edge spectroscopy (XANES), X-ray photoelectron spectroscopy (XPS), Scanning probe microscopy (SPM), and Scanning electron microscopy (SEM). Results indicate that core-shell structure ZnO nanoparticle can effectively deliver coated fluorine chemistry at a tribological interface to form advance tribofilms and significantly improve friction and wear properties. Additionally, the plasma polymerization approach was extended and applied to different coating chemistry like boron and nanoparticles like $CaCO_3$. Overall results indicate that the developed polymer-coated ZnO and $CaCO_3$ nanoparticles are very effective in reducing harmful levels of phosphorus in oils without compromising tribological properties. Additionally, they exhibit synergistic interactions with conventional additives to form robust tribofilms leading to enhanced friction and wear protection at sliding contacts. The surface tailored nanoparticles-based additives (ZnO, $CaCO_3$) developed in this study can contribute to research advancement in lubrication technology and, as such, lead to the development of more energy-efficient and environmentally friendly outcomes when used in automotive engines.

TABLE OF CONTENTS

Chapter 1. Introduction

1.1 Motivation

Transportation activities are a vital aspect of our day-to-day life and contribute gravely to global energy consumptions and environmental pollution. The major environmental impact of the automotive sector is due to fuel consumption and emissions of greenhouse gases that are driving global warming. [1] As a result, government agencies around the world have imposed rigorous standards for fuel efficiency, emissions, safety, and durability, for example: In the US, the Environment Protection Agency has set standards for new cars to reach 36 miles per gallon by 2025. [2] To improve fuel efficiency and decrease the amount of fuel required for vehicle operation, it is important to minimize energy losses from the vehicle engine.

More than half of the fuel energy use in an internal combustion engine goes to exhaust and cooling, while the rest is transferred to mechanical power out of which 33 % is used to overcome frictional losses in major mechanical parts. [3] As friction is a major consumer of engine energy (almost 25 – 30% of total energy), maintaining effective tribology of engine components seems to be a promising solution to curb fuel usage and hence reduce greenhouse gas emissions. [3] Improved tribological performance can be achieved in three ways: enhancing the tribological properties of the materials used for the mechanical parts; coating surfaces to improve tribological behavior; or developing lubricants that improve tribological behavior. [1] Of all the approaches used lubricant development offers the potential to provide low-friction at engine sliding contacts at a low cost. Most recently, in May 2020, OEMs launched new low viscosity oils for passenger cars following ILSAC GF-6 standards to meet the demands of better fuel economy, tailpipe emissions, and engine wear protection. Low-viscosity oils can effectively reduce viscous energy losses in-vehicle, however, their application requires engine components to operate in boundary

to mixed lubrication regimes for a prolonged time, thus causing increased friction and wear of engine components. This necessitates the formulation of low viscosity engine oils with high-performance anti-wear additives capable of forming solid tribofilms to enhance the durability of moving mechanical interfaces experiencing direct metal-metal contact in boundary lubrication regime.

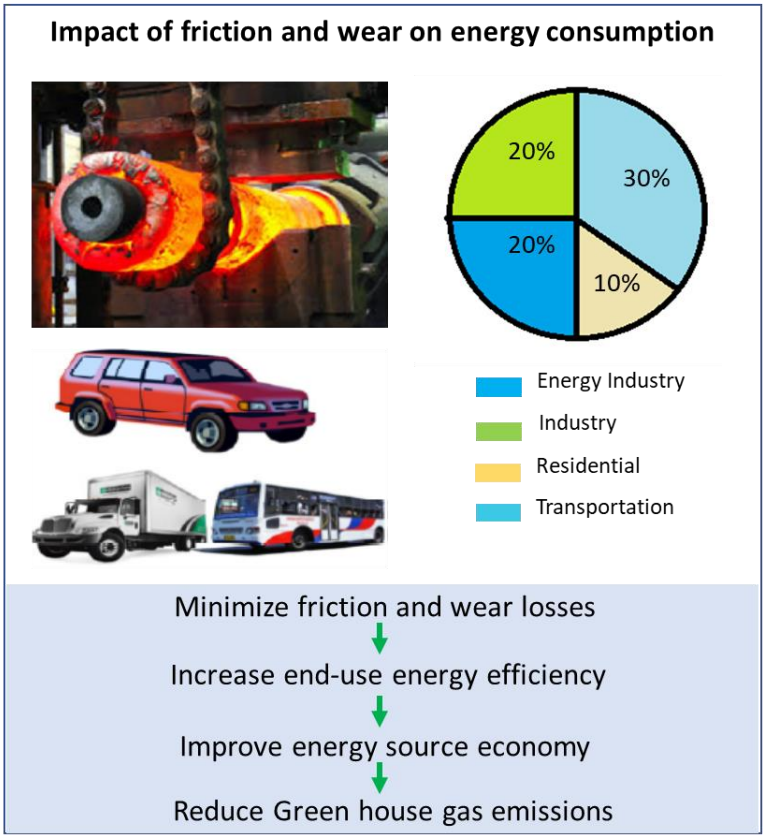

Figure 1. Contribution of the transportation sector to overall global energy consumption. [1]

The current additive technology uses zinc dialkyl dithiophosphate (ZDDP) class of anti-wear additives due to their ability to form effective tribofilms at sliding interfaces, which act as protective layers for the underlying metal. [4] This is in addition to ZDDP's low cost and good solubility in oil. However, despite being an effective anti-wear additive, thiophosphate byproducts of ZDDP contribute to the poisoning of catalytic converters, which increases automotive tailpipe emissions. [5–7] Because of this side-effect the amount of ZDDP in current GF6 engine oils is

restricted to 0.08 wt.% of phosphorus. With the continued growing concerns of global warming, coupled with the need for improved emission control technologies to meet stringent environmental regulations, automotive lubricant formulators will likely have to further reduce SAPS (sulfated ash, phosphorus, and sulfur) amounts, especially phosphorus to below 0.05 wt.% and eventually eliminate phosphorus and sulfur compounds in engine oils. [8–10] Moreover, the current ZDDP additive technology is inadequate to provide wear protection in low viscosity oils (GF-6, PAO6, Group V oils), and increasing their concentration is not an option considering stringent government regulations. Therefore, it is important to identify new anti-wear additive technology capable of either replacing or reducing the phosphorus concentration in engine oils and providing required tribological protection in the novel low-viscosity base stock blends.

With the advent of nanotechnology, nanomaterials/nanoparticles have emerged as high performance environmentally friendly additives for the next generation of lubricants. Nanosized additives provide better lubricating performance over their micron-sized counterparts due to their ability to compensate for the material loss by easily entraining within micro-sized surface asperities and depositing on the worn surface. However, the practical application of nano-additives faces several challenges such as poor solubility in nonpolar lubricants, agglomeration, and precipitation. This research work focuses on the development of functionalized metal oxide nanoparticles (ZnO and $CaCO_3$) as the lubricant additive to improve friction and wear of mineral base oil. In this study, a simple and effective plasma polymerization technique was employed to molecularly surface tailored nanoparticles and improve their dispersibility in base oils. Herein, nanoparticles are encapsulated with polymer coatings through a process of plasma-enhanced chemical vapor deposition (PECVD), hence forming a core-shell like structure.

The primary objective of this study is to develop nano-additive formulation with low phosphorus concentration and therefore, ZnO and $CaCO_3$ core-shell nano-additives were mixed with a significantly low concentration of ZDDP at 350 ppm of P in a mineral base oil. Specifically, ZnO and $CaCO_3$ nanoparticle chemistries were selected for this study to enhance formation of highly cross-linked metal phosphate based tribofilms which helps to improve anti-wear properties. A detailed systematic evaluation of the tribological behavior of unfunctionalized and plasma functionalized nanoparticles with and/ without ZDDP was performed through reciprocating tribological tester in the boundary lubrication regime. Advance surface sensitive techniques like high-resolution scanning electron microscopy (SEM), surface probe microscopy (SPM), X-ray photoelectron spectroscopy (XPS), and X-ray near-edge absorption spectroscopy (XANES) were employed to elucidate the chemical and physical properties of the tribofilms formed on the worn surfaces. Through these different techniques, the study aims to develop a phenomenological model of the structure of tribofilms and relate it to the tribological properties of nano-additives. Combined analysis of tribological test and tribo-surface characterization results is crucial in understanding the lubrication mechanism of these novel core-shell nano-additives. The outcomes of this research work reveal that core-shell nanoparticles can indeed reduce the amount of ZDDP in the engine oil, thus reducing the catalytic poisoning, while simultaneously improving the anti-wear performance and durability of engine components.

1.2 General Background

1.2.1 Tribology and Lubrication

Tribology is the science and engineering field dealing with the study and application of friction, lubrication, adhesion, and wear at the interacting surfaces in relative motion. The word tribology is derived from the Greek term “tribos” meaning rubbing so that the literal term would

be “science of rubbing.” Tribology is particularly important in today's world because a significant amount of energy is wasted due to friction in mechanical components or surfaces relative to motion. For example, in an internal combustion engine, more than half of the fuel energy generated goes to exhaust and cooling, while the rest is transferred to mechanical power out of which 33 % is used to overcome frictional losses in major mechanical parts. [3] As friction is a major consumer of engine energy (almost 25 – 30% of total energy), maintaining effective tribology of engine components seems to be a promising solution to curb fossil fuel usage and hence reduce greenhouse gas emissions. [3] Improved tribological performance can be achieved in three ways: enhancing the tribological properties of the materials used for the mechanical parts; coating surfaces to improve tribological behavior or developing advance lubrication that improves tribological behavior. [1]

Lubrication involves the introduction of a layer of material (liquid, solid, or both) between sliding surfaces to minimize shear strength and prevent friction and wear at the tribological contact. The material used to perform this task is called as a lubricant. The components in internal combustion engines are commonly lubricated with a liquid type of lubricant. For example, crank train, valve train, piston, connecting rod, and bearing assembly make up the most critical lubrication systems in engines and are continuously lubricated with lubricants primarily made of mineral or synthetic base carrier oil together with the additive package (detailed in section 1.2.2). The lubrication system where liquid lubricants are used experiences three different types of lubrication regimes depending on different variables like load, surface roughness, amount of lubricant, the velocity of sliding surfaces, fluid layer thickness, etc. These lubrication regimes are categorized as follows:

Fluid film lubrication – In fluid film lubrication type, the sliding surfaces are separated by a fluid film pressurized by an external supply. The thickness of the fluid film is great enough for the asperities on the sliding surfaces not to make contact, and therefore, the load is supported by the fluid film. In fluid film lubrication, the physical properties of the lubricant (e.g. viscosity, traction, load-bearing capability, etc.) determine the performance capability. Fluid film lubrication is divided into (i) hydrodynamic lubrication and (ii) elastohydrodynamic lubrication. In hydrodynamic lubrication fluid film separating the sliding surfaces is pressurized by viscous dragging of the lubricant into a narrowing gap. Again, the fluid film thickness is great enough for the surface asperities to come in contact. Journal bearings and thrust bearings are examples of hydrodynamic lubrication systems. On the contrary, under high loads, highly localized pressures within squeezed thin lubricant film lead to enhanced lubricant viscosity and to an elastic distortion of the surfaces which help to keep surface asperities apart. This form of fluid film lubrication is known as elastohydrodynamic lubrication. [11,12]

Boundary Lubrication – In boundary lubrication, direct asperity-asperity contact occurs between the sliding surfaces. This regime is observed at very high contact loads and low sliding speed. Even when liquid lubricants are used boundary lubrication occurs at the start-up and stopping of the instrument. Here, metal to metal contact results in shearing the surface asperities coming into contact, thus resulting in severe wear. Under boundary lubrication condition, lubricant additives primarily anti-wear additives (e.g. ZDDP, etc.) play a significant role in protecting sliding surfaces by either getting physically or chemically absorbed to the surfaces of moving parts or decomposing to form new ions to activate the substrate surfaces and subsequently reacting to form chemically active species which adhere onto the wear prone surfaces to enhance protection. The antiwear chemistries present in the lubricant aided by frictional heating, react with the freshly exposed

active surfaces and form protective surface thin films also known as tribofilms. Thus, in boundary lubrication, both the chemistry of the lubricant and the material properties of the interacting surfaces, dictate the performance of the lubricant.

Mixed Lubrication – Under more severe lubrication conditions, e.g. under extreme contact loads, the fluid film is no longer able to fully support the load and the surface asperities come into contact. Under these conditions, the lubrication regime becomes a mixed regime of boundary and EHD fluid film lubrication regimes. In real-life applications, tribological systems are comprised of different sizes of asperities, which when came in contact produces a wide range of stresses at the contact zone. Such systems do experience a mixed regime of boundary and elastohydrodynamic lubrication.

Mathematically lubrication regimes present at any tribological contact are identified by estimating fluid film thickness using the four most common elastohydrodynamic lubrication theories. [13] Fluid film thickness defines friction and wear outcomes of any tribological system lubricated with liquid lubricants. Besides, the ratio of fluid film thickness and surface roughness commonly referred to as lambda (λ) helps to determine the type of lubrication regime as follows:

$$\lambda = \frac{h_{min}}{\sigma^*} \qquad (1)$$

h_{min} = minimum thickness of the lubricant film.

σ^* = root mean square roughness of the two surfaces.

Based on the λ value, lubrication regimes can be divided into 3 types. Hydrodynamic lubrication ($\lambda > \sim 5$), elastohydrodynamic lubrication, or mixed lubrication ($1 < \lambda < 5$), and boundary lubrication ($\lambda < 1$). Within the same fluid lubrication system, the mechanism of lubrication can change as sliding condition changes, and this was first illustrated by Richard Stribeck in 1902 in the form of a graph known as the Stribeck curve. [14] Stribeck curve defines a relation between the coefficient

of friction and lubrication parameters (absolute viscosity of the oil, relative speed, component geometry, and load) and plays an important role in identifying the boundary, mixed and hydrodynamic lubrication regimes as shown in figure 2. [15]

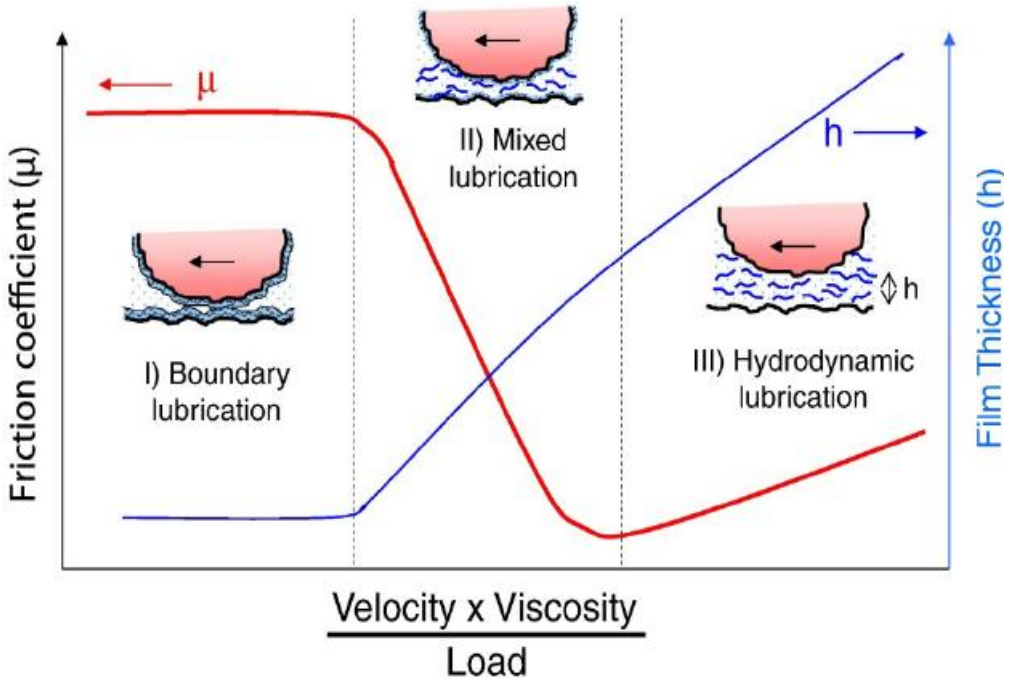

Figure 2. Friction coefficient plotted as a function of fluid viscosity and shear velocity divided by the load (Stribeck curve) with corresponding lubrication film thickness. The plot displays three lubrication regimes: Boundary lubrication, mixed lubrication, and hydrodynamic lubrication. [16]

In the Stribeck plot, as one moves from the left, the effect of very high loads, low sliding speed, and thin fluid film thickness results in direct contact between surface asperities of two bodies in relative motion. This condition is known as the boundary lubrication regime. In this case, direct contact between asperities leads to an extremely high coefficient of friction. With the further increase in speed and decrease in load, the surfaces begin to separate, and the fluid film starts to form. This gradual film formation leads to a reduction in surface contact and a corresponding drop

in the coefficient of friction. This regime is known as mixed lubrication. With the continued increase in viscosity and a decrease in load, fluid film thickness increases, and a condition is reached where surface asperities are completely separated. This regime is known as hydrodynamic lubrication. Because of the high fluid film thickness in this regime, fluid friction comes into play and results in a gradual increase in the coefficient of friction as shown at the farthest right side of the plot. Most of the tribological systems try to have combined mixed to hydrodynamic lubrication to maintain friction as less as possible. However, complex tribological systems like internal combustion engine experience operation at extremely high contact load and slow speed. In such scenarios, the boundary lubrication regime does exist and the performance, in this case, is controlled by the high-performance additive package in engine oil primarily anti-wear additives like ZDDP.

1.2.2 Lubricant Additives

Lubricants play a major role in providing good fuel economy and it also protects the engine parts from wear, thus directly relating to engine durability. Their performance and effectiveness mainly depend on their chemistry and composition. Generally, lubricant consists of 90 % base oil and 10 % additives. Additives serve many roles like anti-wear and anti-corrosive agents, antioxidants, extreme pressure (EP) additives, dispersants and detergents, rust and corrosion inhibitors, friction modifiers, foam depressants, viscosity index improvers, etc.

1.2.2.1 Zinc dialkyl dithiophosphate (ZDDP)

The lubricant additive ZDDP was introduced in engine oil in the 1940s and to date remains the additive of choice for almost all modern engine lubricants. [17] ZDDP plays different functions of wear prevention, antioxidant, and corrosion inhibition to ensure the reliable operation of sliding interfaces in the internal combustion engine. It is well known that ZDDPs dissociate in the

unforgiving conditions in a combustion engine to generate reaction products that, under high temperature and pressure, create sacrificial films, which protect the contacting surfaces from subsequent damage. [18] These films are commonly referred to as tribofilms and so far a considerable volume of research has been carried out to explore the properties and mechanism of formation of the ZDDP tribofilms. [19–24]

Academic research activity on ZDDPs in 1950 – 1960 showed that ZDDPs form phosphorus, zinc, and sulfur-rich chemical films only on the rubbing surfaces where actual sliding contact occurs and not on the rolling contacts or at the contacts where the hydrodynamic film thickness is significantly greater than the surface roughness. [17,25–27] In 1980 – 2000 combination of various surface analytical techniques like Auger electron spectroscopy, X-ray absorption near-edge spectroscopy, X-ray photoelectron spectroscopy, secondary ion mass spectrometry, etc. were used by researchers to elucidate the chemistry of ZDDP tribofilms and it was showed that the ZDDP tribofilms consists of a relatively thin sulfur-rich region close to the steel substrate and thicker layers of zinc and iron polyphosphates and/or phosphates as shown in figure 3. [28–41] Though the main cation present in the upper levels of the tribofilms pads is zinc, the proportion of iron to zinc increases progressively towards the metal surface.

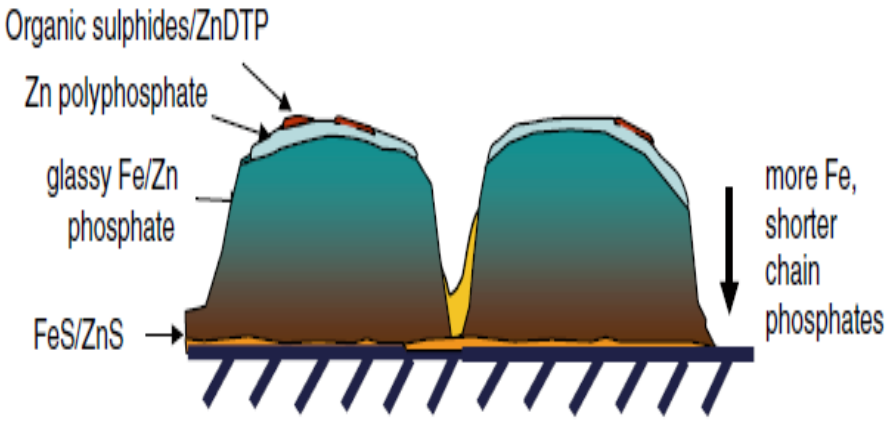

Figure 3. Schematic of ZDDP tribofilms pad structure and composition. [17]

Furthermore, in the late 1990s application of atomic force microscopy and in-situ spacer layer interferometric method resolved several contradictions on the thickness of ZDDP tribofilms and it was proved that the ZDDP tribofilms rapidly grow on rubbing surfaces in a pad-like structure consisting of flat-topped thick film regions about 3-5 μm in diameter separated by narrow regions where little or no film is present. [42–46] ZDDP tribofilms are typically 80-150 nm thick depending on the type of oil and rubbing conditions, for example, thicker films are observed in nonpolar base oil containing only ZDDP [47] and relatively thinner films are formed with fully formulated engine lubricants. [48] Research efforts have also been extended in determining precise molecular reaction pathways or steps leading to ZDDP tribofilm formation, and now it is believed that ZDDP tribofilms are formed due to stress-assisted, thermally activated chemical reactions at sheared contacts. [8,21] Gosvami et al. in 2015 used a single-asperity contact of an AFM tip sliding on an iron oxide substrate in ZDDP solution to study tribofilm formation and found out that the formation rate is exponentially dependent on both temperature and pressure i.e. ZDDP tribofilm formation is a mechanochemical process. [49] Most recently in 2020, Zhang and Spikes et al. used an alternative approach to prove the ZDDP tribofilm formation process is mechanochemical in origin by using a tribological test rig capable of testing ZDDP oil under full elastohydrodynamic conditions with negligible asperity contacts. [50] Results revealed that the initial decomposition of ZDDP to form thiophosphate byproducts is the rate-determining step for tribofilm formation and this decomposition reaction is driven by macroscopic shear stresses as well as temperature. They proposed that under full-film EHL conditions, ZDDP tribofilm formation is promoted by shear stress applied through the base oil molecules rather than hydrostatic pressure, which induces asymmetric stress on adsorbed ZDDP molecules to promote their decomposition and initiate rapid

phosphate polymerization. [50] However, despite the importance of ZDDP thiophosphate byproducts to form tribofilms, they can lead to poisoning of after-exhaust treatment systems which increases automotive tailpipe emissions. Importantly, existing ZDDP additive technology provides inadequate wear protection in ultralow viscosity lubricants, which are promoted to meet aggressive fuel efficiency and emission standards. Increasing the ZDDP concentration for low-viscosity lubricants is prohibited by already stringent emission regulations that ultimately aim to eliminate sulfur and phosphorus-containing additives in engine oil. Due to these restrictions and short-comings, the need for research is fueled to replace and/or reduce the amount of ZDDP in engine oil through development of new lubricant anti-wear additives such as boron based additives, ionic liquids, nanomaterials, etc.

1.2.2.2 Nanomaterials/Nanoparticles as lubricant additives

The advent of nanotechnology has expanded the realms of research towards the use of nanoparticles or nanomaterials as additives in lubricating oil. Nano lubricant approach is of considerable interest for overcoming the drawbacks of conventional lubricant additives and improving the performance of low-viscosity lubricants. Nanoparticles have unique physical and chemical characteristics which makes them promising candidates for lubricant additive applications including anti-wear and extreme pressure additives, as well as friction modifiers. The main advantages of nanoparticles are their small size in the nanometer range and high chemical reactivity which allows them to easily enter the microscale surface asperities of the friction interface or deposit in micro defects of friction surfaces to play the role of “self-repairing”. Additionally, most nanoparticles are environmentally friendly and therefore, their application can aid to minimize the use of hazardous additives and meet the requirements of green tribology.

To date, various nanomaterials such as carbon-based, inorganic fullerenes, metal, metal oxides, metal sulfides, nano-composites, and polymeric nanoparticles have been used in lubricating oil with potentially interesting friction and wear properties. Among the diverse class of nanomaterials, metal and metal oxide nanoparticles have received particular attention owing to their excellent friction-reducing, anti-wear, and self-repairing ability. Padgurskas et al. investigated the tribological properties of different mineral oils containing Fe, Cu, and Co nanoparticles and their combinations. Test results suggested that Cu-containing nano lubricants significantly reduced friction and wear compared to other NPs when added individually. In particular, the presence of Cu, Fe, and Co NPs reduced friction by 49%, 39%, and 20%, respectively, compared to lubricants without additives. [51] Ag and Au metal nanoparticles have also exhibited promising anti-wear and anti-friction properties. [52,53] Kumara et al. synthesized organic-modified Ag nanoparticles as an additive for PAO base oil and reported remarkable improvement in friction by 35% and wear by 85%. [54] Studies have been done with TiO_2 nanoparticles where they are found to stabilize the friction and form TiO_2 films on the contacting surfaces. [55–57] Metal oxide composite nanoparticles have also exhibited promising tribological properties. Wei et al. reported that a composite mixture of $Al2O_3/TiO_2$ nanoparticles provided superior anti-wear and anti-friction properties than the individual nanoparticles. [58,59] ZnO nanoparticles are also one of the promising green lubricant nano additives with stable structure, good thermal stability, and high surface area and energy. Considering these favorable properties, it is understandable that many studies have been conducted using ZnO nanoparticles as oil additives. [60–66] Alves et al. observed that ZnO nanoparticles exhibit good friction-reducing and antiwear abilities. [67] Battez et al. studied the tribological properties of ZnO nanoparticles as an additive in PAO base oil and found that ZnO nanoparticles can form tribofilms thereby showing

excellent tribological properties [61,68]. Nanoparticles of polytetrafluoroethylene (PTFE) [69], MoS_2 [70,71], TiO_2 [55], $La(OH)_3$ [72], PbS [73], LaF_3 [74], titanium borate [75], zinc borate [76], ferric oxide [77], calcium borate [78], Ni [79] and $CaCO_3$ [80,81] have also been explored for their use in lubricant oil. Some of the suggested mechanisms behind the excellent tribological performance of these nanoparticles are rolling effect [82], a protective film by tribochemical reactions [83], ball-bearing effect [84], adsorption on the surface to compensate for material loss, mending effect [85] and third body material transfer [86,87], which are summarized in figure 4.

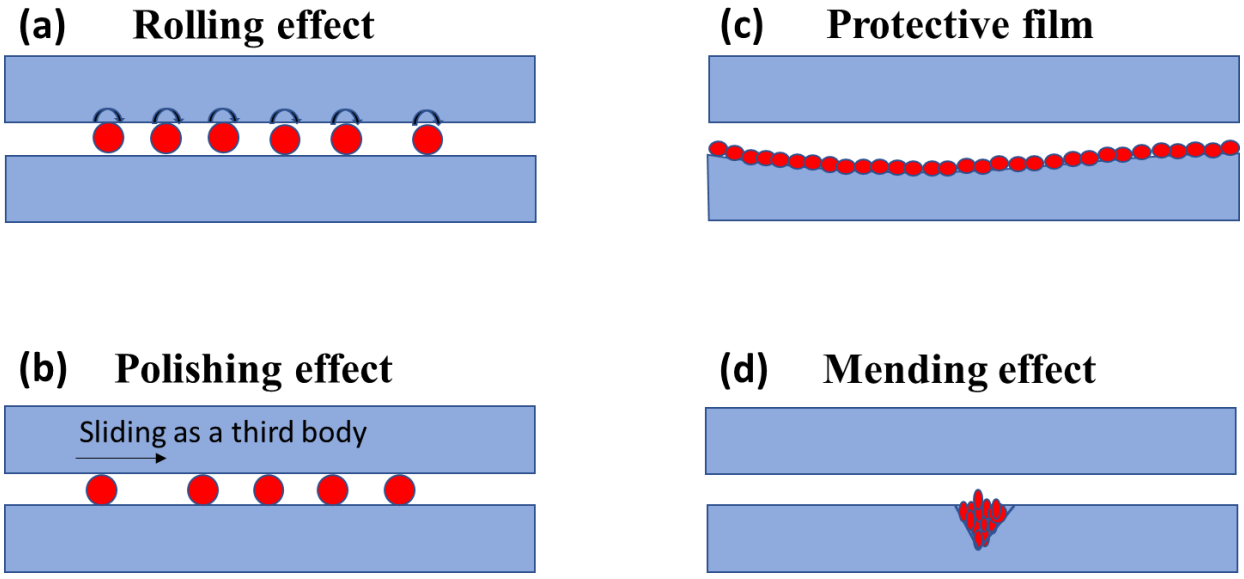

Figure 4. Schematic of possible lubrication mechanisms of nanoparticles.

To date, metal-containing nanoparticles have emerged as a new class of environmentally friendly lubricant additives capable of replacing hazardous sulfur and phosphorus-containing additives like ZDDP. However, several challenges remain for their practical tribological application. Metal and metal oxide nanoparticles exhibit poor solubility in nonpolar base oils, which causes problems of unstable suspension and sedimentation. Additionally, the high specific surface energy of nanoscale particles makes them prone to agglomeration and precipitation in the

base oil. The aggregation of nanoparticles limits their ability to protect tribological interfaces. Adequately dispersed nanoparticles can improve wear and friction resistance by forming tribofilms consisting of nanoparticle agglomerates, discrete nanoparticles, or nanoparticle-reinforced tribopolymer networks. There are two approaches to achieve adequate dispersion or suspension of nanoparticles in lubricant oil. The first is to incorporate dispersant along with nanoparticles in a base oil. The other is to synthesis surface tailored nanoparticles through physical or chemical methods like sol-gel, use of amphiphilic chemicals or alkoxysilanes, etc. Both strategies modify the surface of nanoparticles by absorption or chemical reaction to form an organic layer. Till 2005, various dispersants like Aliquat 336 [68], Estisol 242 [12], oleic acid [12], and sorbitol monostearate [47,105] were mixed with nanoparticles and studied to achieve stable dispersion of nanoparticles in the lubricant oil. However, these studies reported a very short stability time of nano-lubricants, in some cases dispersion was lost in less than two weeks. Furthermore, the amount of dispersant required was more than the amount of the nanoparticles in this method, and the properties of nano-lubricant were changed. Also, the dispersant can absorb the contacting surfaces and hindered the tribochemistry and tribofilm forming capability of nanoparticles. For example, Rabaso et al. reported loss of tribological benefits of inorganic fullerene-like MoS_2 nanoparticles when used in the mineral oil with succinimide-based dispersants. They observed that the succinimide-based dispersant can improve the dispersion of the nanoparticles in the oil by reducing agglomeration, however, affects the tribochemistry of the contact, by excessive adsorption on the steel surfaces preventing adhesion of a low friction MoS_2 on the interacting surfaces, ultimately leading to poor friction and wear properties. Due to several shortcomings of the dispersant method, various surface modification techniques were used to prepare well-dispersed nano-lubricants like chemically reacting surfactants with nanoparticles before addition in lubricant oil, using a

surfactant to modify the precursor and synthesizing nanoparticles with a pre-attached surfactant, surface silanization with alkoxysilanes, surface-induced-atom-transfer-radical polymerization, water bath or probe ultrasonication, etc. Some of the most recent research has focused on the interaction of ionic liquid and nanoparticles. These studies reported improvement in the dispersion stability of nano-lubricants due to the synergistic interaction of ionic liquids with nanoparticles. In this thesis, an interesting approach of plasma-assisted chemical vapor deposition is used to molecularly surface tailored metal oxide nanoparticles to achieve a uniform and stable dispersion in a mineral base oil.

1.2.3 Plasma enhanced chemical vapor deposition (PECVD)

Plasma enhanced chemical vapor deposition (PECVD) or plasma-assisted chemical vapor deposition (PACVD) is a thin film fabrication technique of polymeric materials, which has successfully overcome the disadvantages of wet chemical fabrication and other deposition methods. [88] Plasma polymerization is a complex process and takes place through initiation, propagation, and termination stages. In the PECVD process, a high energy plasma discharge is used to dissociate a gaseous or liquid precursor into sub-monomers or free-radical fragments and ions. A free radical in the plasma stream initiates the process of polymerization of the precursor resulting in the formation of the polymer, which gets deposited on the substrate. And due to the presence of the radicals in each chain of the produced polymer, cross-linking of the polymer also occurs; therefore, the final resulting plasma polymer coating has a cross-linked structure. [89,90] The structure of the plasma polymeric thin films is not similar to the conventional polymers because of the higher density of cross-linked and branched structures. [90,91] Films synthesized through plasma polymerization have good adhesion to the substrate materials and usually exhibit good stability in air and various chemical solvents. Usage of inert gas plasma in PECVD extends

its applicability to a wide range of precursors, reactive organic, inorganic, and inert materials. [92,93] Composition of these polymerized films can be controlled through optimization of internal plasma parameters like homogeneity of discharge, distribution of various species in the plasma, and energy of the species, and the external parameters such as reactor geometry, applied voltage, frequency, total pressure, flow rate, temperature, and length of the deposition. [89,94]

PECVD is a versatile deposition technique that is used in a variety of applications like developing electrical insulation and conductive films, fabrication of integrated circuits, transistors, photovoltaic, photonic, and dielectric devices, surface treatment of biological implants, synthesizing biomaterials for applications in biosensors, etc. PECVD is also well recognized for the functionalization of nanoparticles/nanomaterials through the addition of functional groups such as amine, carboxylic, and silane groups. Timmons and co-workers have successfully demonstrated the significance of RF plasma polymerization technique for functionalization and surface modification of nanoparticles using a 360º rotating plasma reactor. For example, they employed a pulsed plasma polymerization process to introduce amine ($-NH_2$) groups to surfaces of superparamagnetic iron nanoparticles (γ-Fe_2O_3) for biomedical applications. In this study, the pulsed plasma PECVD technique is used to molecularly surface tailor metal oxide nanoparticles to enhance their tribological properties and develop core-shell structure nano-additives for automotive lubricants. These plasma functionalized nano-additives show a promising way to reduce the amount of ZDDP in the engine oil, while simultaneously improving the anti-wear and anti-friction benefits. Application of plasma polymerization to synthesize lubricant additives is not limited to a specific nanoparticle-polymer film system and thus it can be utilized for different mechanical systems other than an internal combustion engine.

1.3 Research Objectives

The primary objective of the proposed research project is to develop low phosphorus-containing environment-friendly engine oil lubrication through the use of surface-modified nanoparticles based additives. In pursuit of this goal, the research work concentrates on the use of plasma polymerization techniques to functionalize nanoparticles with chemistries known to be favorable for tribological application. This approach is applied to different nanoparticles to make core-shell nanostructures, wherein nanoparticles are functionalized with multilayered coatings. These functionalized nanoparticles are then mixed with oils and their performance is evaluated under tribological conditions similar to actual operating conditions in the internal combustion engine. Detailed mechanistic aspects will be explored through different advanced characterization tools to understand the lubrication mechanism of these functionalized nanoparticles. It is hoped that the findings from this work will contribute to the development of a promising alternative for harmful existing lubricant additives like ZDDP and hence, will be extremely valuable to the field of lubrication science.

Hypothesis…..

It has been widely accepted by the researchers in this field of science that the antiwear and/antifriction performance of the well-known additives (like ZDDP, MoDTC, PTFE) depends upon their capability to form protective films called as tribofilms at contact surfaces under high temperature and shear forces. For example, the antiwear mechanism of industrially dominant additive, ZDDP involves its thermal and tribological degradation leading to the formation of an amorphous glassy antiwear film comprised of metal polyphosphates and/ metal sulfides/sulfates. Chemical processes involved in this mechanism are known to be influenced by the availability of active elements like P or S provided due to the degradation of ZDDP. Also, in recent years, nanoparticles have emerged as potential friction modifiers and antiwear additives. Various

mechanisms for their behavior have been proposed, such as nanoparticles can disintegrate and form layered structure tribofilm, they can act as a third body and prevent the material loss, etc.

Based on this fundamental understanding of the additive lubrication mechanism, the author postulate that the plasma functionalized nanoparticles would act as a carrier and deliver coated chemistries at the tribological interfaces to form protective glassy antiwear films. Additionally, nanoparticles can itself contribute to additional antifriction and antiwear protection of the rubbing surfaces. This bifold mechanism would be expected to provide improved tribological performance than existing lubricant additives. Preliminary, this approach involves coating nanoparticles in the form of polymeric thin-film through plasma surface treatment. Functionalization chemistries will be similar to those that have been shown to form antiwear films and benefit in tribological applications. Later, these nanoparticles will be subjected to tribological testing and various analytical tools will be used to study tribofilms formed under the lubricated mechanical rubbing action. The knowledge of the chemical nature and composition of formed tribofilms will then complement the proposed hypothesis.

1.3.1 Developing Core-shell Structure Nanoparticles

The most important aspect of this research work is the careful selection of the nanoparticles considering particle size, shape, oxidative, chemical, and thermal stability, and cost factor. Nanoparticles like ZnO, and $CaCO_3$ which have been proven to exhibit good antiwear and antifriction capabilities were selected for the study. The main rationale behind using ZnO and $CaCO_3$ is to exploit the benefit of extra Zn and Ca chemistries to promote formation of cross-linked polyphosphate-based tribofilms leading to improved friction and wear properties. Secondly, perfluorohexane, trimethyl boroxine, and glycidyl methacrylate monomers were selected for plasma polymerization considering their properties like vapor pressure, toxicity, and handling

stability. Plasma polymerization process optimization was carried out by finding perfect experimental parameters such as RF power input, the duty cycle for pulsing signal, monomer pressure, coating time, and monomer flow rate to get the best possible coating stability and thickness. For this purpose, initial studies were performed using Si wafers and KBr discs to examine film deposition and stability in the air. Later, FTIR characterization was used to identify the presence of the desired chemical functional group. Additionally, chemical composition data on developed functionalized nanoparticles were obtained using XANES surface-sensitive technique.

1.3.2 Evaluating Tribological Performance of Functionalized Nanoparticles with and Against ZDDP

Environmental regulations and human health concerns drive the research in the development of low phosphorus-containing engine oil additives. Zinc dialkyl dithiophosphate (ZDDP) is one of the most prominent additives to dominate the lubrication landscape despite being the main source of phosphorus in conventional engine oil and thus, a contributor to automotive catalytic deactivation and environmental emissions. This proposed research work aims on evaluating the potential of functionalized nanoparticles to either replace or reduce the amount of ZDDP currently used in engine oils. Hence, as the first approach to developing low phosphorus oils, formulations were prepared with an additive mixture of functionalized nanoparticles and very less concentration of ZDDP. Antiwear behavior of these novel nano-additives was scrutinized under mixed to boundary lubrication condition under pure sliding contact and wear results were compared with ZDDP antiwear additive at identical test conditions.

1.3.3 Multiscale Tribofilm Characterization and Understanding Lubricating Mechanism

The second objective of this study is to understand the chemical properties of the tribofilms formed under the lubrication of functionalized nano-additives. An in-depth characterization of the worn surface morphology was performed using advance characterization techniques like XPS, XANES, AFM, and HR-SEM. Knowledge gained on the physiochemical properties of in-situ formed tribofilms shed insight into the mechanism of wear and tribofilm formation using nanoparticles by themselves and in synergistic mixtures with ZDDP. In the final approach, phenomenological models of tribofilms formed under nano-additives lubrication were suggested by combining the knowledge gained from the overall surface characterization results.

1.3.4 Extending Approach to Different Nanoparticles and Chemistries

The plasma polymerization process developed by the tribological research group of material science and engineering at UTA is very versatile and can be extended to different nanoparticles and monomers to prepare high-performance nano-additives. Herein, the plasma functionalized approach was extended to deliver chemistries at tribological surfaces to provide better anti-wear and anti-friction properties by using ZnO and $CaCO_3$ nanoparticles and fluorine and boron coating chemistries. Additionally, the anti-wear and anti-friction behavior of functionalized nanoparticles was investigated with new generation additives like ashless dithiophosphates.

1.4 Dissertation Structure

This dissertation consists of six chapters. An outline and summary of each chapter are presented below.

Chapter 1. Introduction: This chapter gives the reader a broad overview of the research work carried out and forms the basis for the following chapters of this dissertation. A brief background

on the fundamentals of tribology and lubricant additives is provided in this chapter. Literature review and details on anti-wear lubricant additive ZDDP, nanoparticles application in lubrication, in-situ tribofilm formation, and plasma-enhanced chemical vapor deposition are also mentioned. It highlights the fundamental drive for this research work and outlines general objectives followed by a detailed hypothesis and specific aims.

Chapter 2. Tribochemistry of fluorinated ZnO nanoparticles and ZDDP lubricated interface and implications for enhanced anti-wear performance at boundary lubricated contacts: This chapter highlights the initial practical application of the proposed hypothesis of using plasma polymerization technique to synthesize lubricant nano-additives. Details on experimental methods used to develop core-shell structure ZnO nanoparticles and tribological testing under boundary lubrication conditions are provided in this chapter. Here, perfluorohexane and glycidyl methacrylate monomer were used to coat ZnO nanoparticles initially with fluorocarbon coating followed with methacrylate-based coatings. Tribofilms formed by fluorinated core-shell ZnO nano-additives based lubrication were characterized using AFM, SEM, XANES, and XPS. The results of this study suggest that the plasma polymerization technique can be effectively applied to develop nano-additives capable of forming tribofilms and improving tribological properties like that of conventional additives like ZDDP, ionic liquids, borate esters, etc.

Chapter 3. Polymer coated ZnO nanoparticles driven robust interfacial tribofilms leading to improved wear protection under boundary lubrication regime: In this chapter, plasma polymerization experimental approach was extended to different coating chemistry and boron coated core-shell ZnO nanoparticles were synthesized by using trimethyl boroxine monomer. The synergistic interaction and enhanced tribological performance of fluorinated ZnO nanoparticles observed from research work discussed in chapter 3 formed basis for this chapter and sparked the

idea of coating ZnO nanoparticles with other tribologically beneficial chemistries like boron. Wear and friction results and tribofilm characterization results discussed in this chapter also suggests that boron coated ZnO nanoparticles interact synergistically with ZDDP.

Chapter 4. Tribofilm formation, friction and wear properties of a plasma functionalized $CaCO_3$ nanoparticles in the presence of ashless dithiophosphate and ZDDP anti-wear additives: In this chapter, an experimental methodology for developing polymer-coated core-shell structure nano-additives was applied to different nanoparticles, $CaCO_3$. Boron-coated $CaCO_3$ was tribologically evaluated with ashless dithiophosphate (DDP) and ZDDP anti-wear additives. Once again, core-shell structure $CaCO_3$ nano-additives interacted synergistically with both DDP and ZDDP. XANES and SPM techniques gave critical insights into the differences in the chemistry of tribofilms formed due to the interaction of boron-coated ZnO with DDP and ZDDP.

Chapter 5. General Conclusions: This chapter summarizes the major findings of this dissertation and interconnects the results of each chapter to support the central idea of this research work. It also provides insight into the future work and how the developed plasma polymerization technique of functionalizing nanoparticles could be extended to other tribological and lubrication applications.

References

[1] K. Holmberg, A. Erdemir, Influence of tribology on global energy consumption, costs and emissions, Friction. 5 (2017) 263–284. doi:10.1007/s40544-017-0183-5.

[2] Bruker Nano Surfaces, The Benefits of Engine Tribology Within the Automotive Industry, AZo Mater. (2017) 1–10. https://www.azom.com/article.aspx?ArticleID=13763.

[3] K. Holmberg, A. Erdemir, Global impact of friction on energy consumption, economy and environment, FME Trans. 43 (2015) 181–185. doi:10.5937/fmet1503181H.

[4] H. Spikes, The history and mechanisms of ZDDP, Tribol. Lett. 17 (2004) 469–489. doi:10.1023/B:TRIL.0000044495.26882.b5.

[5] B.G. Bunting, K. More, S. Lewis, T. Toops, Phosphorous Poisoning and Phosphorous Exhaust Chemistry with Diesel Oxidation Catalysts, in: SAE Tech. Pap., SAE International, 2005. doi:10.4271/2005-01-1758.

[6] M. Desanker, X. He, J. Lu, P. Liu, D.B. Pickens, M. Delferro, T.J. Marks, Y.-W. Chung, Q.J. Wang, Alkyl-Cyclens as Effective Sulfur- and Phosphorus-Free Friction Modifiers for Boundary Lubrication, ACS Appl. Mater. Interfaces. 9 (2017) 9118–9125. doi:10.1021/acsami.6b15608.

[7] A. Erdemir, Review of engineered tribological interfaces for improved boundary lubrication, Tribol. Int. 38 (2005) 249–256. doi:https://doi.org/10.1016/j.triboint.2004.08.008.

[8] H.S. Khare, I. Lahouij, A. Jackson, G. Feng, Z. Chen, G.D. Cooper, R.W. Carpick, Nanoscale Generation of Robust Solid Films from Liquid-Dispersed Nanoparticles via in Situ Atomic Force Microscopy: Growth Kinetics and Nanomechanical Properties, ACS Appl. Mater. Interfaces. 10 (2018) 40335–40347. doi:10.1021/acsami.8b16680.

[9] V. Wong, S. Tung, Overview of automotive engine friction and reduction trends–Effects of surface, material, and lubricant-additive technologies, Friction. 4 (2016) 1–28. doi:10.1007/s40544-016-0107-9.

[10] H. Spikes, Low- and zero-sulphated ash, phosphorus and sulphur anti-wear additives for engine oils, Lubr. Sci. 20 (2008) 103–136. doi:10.1002/ls.57.

[11] D. Dowson, Developments in lubrication - the thinning film, J. Phys. D. Appl. Phys. 25 (1992) A334--A339. doi:10.1088/0022-3727/25/1a/050.

[12] B.J. Hamrock, D. Dowson, Isothermal Elastohydrodynamic Lubrication of Point Contacts: Part III—Fully Flooded Results, J. Lubr. Technol. 99 (1977) 264–275. doi:10.1115/1.3453074.

[13] R. Mourhatch, Tribological and antiwear mechanisms of fluorinated zinc dialkyl dithiophosphate in comparison to zinc dialkyl dithiophosphate in engine oils, (2008).

[14] M. Woydt, R. Wäsche, The history of the Stribeck curve and ball bearing steels: The role of Adolf Martens, Wear. 268 (2010) 1542–1546. doi:https://doi.org/10.1016/j.wear.2010.02.015.

[15] X. Lu, M. Khonsari, E. Gelinck, The Stribeck Curve: Experimental Results and Theoretical Prediction, J. Tribol. Asme - J TRIBOL-TRANS ASME. 128 (2006). doi:10.1115/1.2345406.

[16] J.M. Coles, D.P. Chang, S. Zauscher, Molecular mechanisms of aqueous boundary lubrication by mucinous glycoproteins, Curr. Opin. Colloid Interface Sci. 15 (2010) 406–416. doi:https://doi.org/10.1016/j.cocis.2010.07.002.

[17] H.A. Spikes, The History and Mechanisms of ZDDP, Tribol. Lett. 17 (2004) 469–489. doi:10.1023/B:TRIL.0000044495.26882.b5.

[18] M.A. Nicholls, T. Do, P.R. Norton, M. Kasrai, G.M. Bancroft, Review of the lubrication of metallic surfaces by zinc dialkyl-dithiophosphates, Tribol. Int. 38 (2005) 15–39. doi:https://doi.org/10.1016/j.triboint.2004.05.009.

[19] H. Spedding, R.C. Watkins, The antiwear mechanism of zddp's. Part I, Tribol. Int. 15 (1982) 9–12. doi:https://doi.org/10.1016/0301-679X(82)90101-3.

[20] W.A. Glaeser, D. Baer, M. Engelhardt, In situ wear experiments in the scanning Auger spectrometer, Wear. 162–164 (1993) 132–138. doi:https://doi.org/10.1016/0043-1648(93)90494-7.

[21] J. Zhang, H. Spikes, On the Mechanism of ZDDP Antiwear Film Formation, Tribol. Lett.

63 (2016) 24. doi:10.1007/s11249-016-0706-7.

[22] V. Sharma, A. Erdemir, P.B. Aswath, An analytical study of tribofilms generated by the interaction of ashless antiwear additives with ZDDP using XANES and nano-indentation, Tribol. Int. 82 (2015) 43–57. doi:10.1016/j.triboint.2014.09.019.

[23] R. Mourhatch, P.B. Aswath, Tribological behavior and nature of tribofilms generated from fluorinated ZDDP in comparison to ZDDP under extreme pressure conditions—Part 1: Structure and chemistry of tribofilms, Tribol. Int. 44 (2011) 187–200. doi:10.1016/j.triboint.2010.10.018.

[24] H. Fujita, H.A. Spikes, The formation of zinc dithiophosphate antiwear films, Proc. Inst. Mech. Eng. Part J J. Eng. Tribol. 218 (2004) 265–278. doi:10.1243/1350650041762677.

[25] M.J. Furey, Film Formation by an Antiwear Additive in an Automotive Engine, A S L E Trans. 2 (1959) 91–100. doi:10.1080/05698195908972361.

[26] E.H. Loeser, R.C. Wiquist, S.B. Twiss, Cam and Tappet Lubrication. IV–Radioactive Study of Sulfur in the EP Film, A S L E Trans. 2 (1959) 199–207. doi:10.1080/05698195908972371.

[27] E.H. Loeser, R.C. Wiquist, S.B. Twiss, Cam and Tappet Lubrication III — Radioactive Study of Phosphorus in the EP Film, A S L E Trans. 1 (1958) 329–335. doi:10.1080/05698195808972348.

[28] H. Spedding, R.C. Watkins, The antiwear mechanism of zddp ’ s Part I, (1982) 9–12.

[29] I. Sieber, K. Meyer, H. Kloss, A. Schöpke, Characterization of boundary layers formed by different metal dithiophosphates in a four-ball machine, Wear. 85 (1983) 43–56. doi:https://doi.org/10.1016/0043-1648(83)90334-4.

[30] M.L.S. Fuller, M. Kasrai, G.M. Bancroft, K. Fyfe, K.H. Tan, Solution decomposition of zinc dialkyl dithiophosphate and its effect on antiwear and thermal film formation studied by X-ray absorption spectroscopy, Tribol. Int. 31 (1998) 627–644. doi:https://doi.org/10.1016/S0301-679X(98)00084-X.

[31] E.S. Ferrari, K.J. Roberts, M. Sansone, D. Adams, A Multi-Edge X-ray Absorption

Spectroscopy Study of the Reactivity of Zinc Di-alkyl-di-thiophosphates Anti-Wear Additives 2. In Situ Studies of Steel/Oil Interfaces, 1999. doi:10.1016/S0043-1648(99)00286-0.

[32] K. Varlot, M. Kasrai, J.M. Martin, B. Vacher, G.M. Bancroft, E.S. Yamaguchi, P.R. Ryason, Antiwear film formation of neutral and basic ZDDP: influence of the reaction temperature and of the concentration, Tribol. Lett. 8 (2000) 9–16. doi:10.1023/A:1019162529554.

[33] M.L.S.F.R.F.R.M.N.L.K.M. Bancroft, The use of X-ray absorption spectroscopy for monitoring the thickness of antiwear films from ZDDP, Tribol. Lett. 8 (2000) 187. doi:10.1023/A:1019195404055.

[34] J.M. Palacios, Films formed by antiwear additives and their incidence in wear and scuffing, Wear. 114 (1987) 41–49. doi:https://doi.org/10.1016/0043-1648(87)90014-7.

[35] H.J. Mathieu, R. Schumacher, D. Landolt, Detection of tribofragments of phosphorus compounds by AES and SIMS, Wear. 132 (1989) 99–110. doi:https://doi.org/10.1016/0043-1648(89)90205-6.

[36] J.M. Martin, J.L. Mansot, I. Berbezier, H. Dexpert, The nature and origin of wear particles from boundary lubrication with a zinc dialkyl dithiophosphate, Wear. 93 (1984) 117–126. doi:10.1016/0043-1648(84)90064-4.

[37] J.M. Martin, J.L. Mansot, I. Berbezier, M. Belin, G. Balossier, Microstructural aspects of lubricated mild wear with zinc dialkyldithiophosphate, Wear. 107 (1986) 355–366. doi:https://doi.org/10.1016/0043-1648(86)90165-1.

[38] M. Belin, J.M. Martin, J.L. Mansot, Role of Iron in the Amorphization Process in Friction-Induced Phosphate Glasses, Tribol. Trans. 32 (1989) 410–413. doi:10.1080/10402008908981907.

[39] J.M. Martin, M. Belin, J.L. Mansot, H. Dexpert, P. Lagarde, Friction-Induced Amorphization with ZDDP—An EXAFS Study, A S L E Trans. 29 (1986) 523–531. doi:10.1080/05698198608981716.

[40] Z. Yin, M. Kasrai, G.M. Bancroft, K.F. Laycock, K.H. Tan, Chemical characterization of

antiwear films generated on steel by zinc dialkyl dithiophosphate using X-ray absorption spectroscopy, Tribol. Int. 26 (1993) 383–388. doi:https://doi.org/10.1016/0301-679X(93)90076-D.

[41] Z. Yin, M. Kasrai, M. Fuller, G.M. Bancroft, K. Fyfe, K.H. Tan, Application of soft X-ray absorption spectroscopy in chemical characterization of antiwear films generated by ZDDP Part I: the effects of physical parameters, Wear. 202 (1997) 172–191. doi:https://doi.org/10.1016/S0043-1648(96)07272-9.

[42] A.J. Pidduck, G.C. Smith, Scanning probe microscopy of automotive anti-wear films, Wear. 212 (1997) 254–264. doi:https://doi.org/10.1016/S0043-1648(97)00081-1.

[43] O.L. Warren, J.F. Graham, P.R. Norton, J.E. Houston, T.A. Michalske, Nanomechanical properties of films derived from zinc dialkyldithiophosphate, Tribol. Lett. 4 (1998) 189–198. doi:10.1023/A:1019194903262.

[44] J.F. Graham, C. McCague, P.R. Norton, Topography and nanomechanical properties of tribochemical films derived from zinc dialkyl and diaryl dithiophosphates, Tribol. Lett. 6 (1999) 149–157. doi:10.1023/A:1019124026402.

[45] M. Aktary, M.T. McDermott, G.A. McAlpine, Morphology and Nanomechanical Properties of ZDDP Antiwear Films as a Function of Tribological Contact Time, Tribol. Lett. 12 (2002) 155–162. doi:10.1023/A:1014755123184.

[46] K. Topolovec-Miklozic, T.R. Forbus, H.A. Spikes, Film thickness and roughness of ZDDP antiwear films, Tribol. Lett. 26 (2007) 161–171. doi:10.1007/s11249-006-9189-2.

[47] H. FUJITA, R.P. GLOVNEA, H.A. SPIKES, Study of Zinc Dialkydithiophosphate Antiwear Film Formation and Removal Processes, Part I: Experimental, Tribol. Trans. 48 (2005) 558–566. doi:10.1080/05698190500385211.

[48] M. Ratoi, V.B. Niste, H. Alghawel, Y.F. Suen, K. Nelson, The impact of organic friction modifiers on engine oil tribofilms, RSC Adv. 4 (2014) 4278–4285. doi:10.1039/C3RA46403B.

[49] N.N. Gosvami, J.A. Bares, F. Mangolini, A.R. Konicek, D.G. Yablon, R.W. Carpick, Mechanisms of antiwear tribofilm growth revealed in situ by single-asperity sliding

contacts, Science (80-.). 348 (2015) 102–106. doi:10.1126/science.1258788.

[50] J. Zhang, J.P. Ewen, M. Ueda, J.S.S. Wong, H.A. Spikes, Mechanochemistry of Zinc Dialkyldithiophosphate on Steel Surfaces under Elastohydrodynamic Lubrication Conditions, ACS Appl. Mater. Interfaces. 12 (2020) 6662–6676. doi:10.1021/acsami.9b20059.

[51] J. Padgurskas, R. Rukuiza, I. Prosyčevas, R. Kreivaitis, Tribological properties of lubricant additives of Fe, Cu and Co nanoparticles, Tribol. Int. 60 (2013) 224–232. doi:https://doi.org/10.1016/j.triboint.2012.10.024.

[52] H. Song, J. Huang, X. Jia, W. Sheng, Facile synthesis of core–shell Ag@C nanospheres with improved tribological properties for water-based additives, New J. Chem. 42 (2018) 8773–8782. doi:10.1039/C8NJ01382A.

[53] S. Beckford, J. Cai, J. Chen, M. Zou, Use of Au Nanoparticle-Filled PTFE Films to Produce Low-Friction and Low-Wear Surface Coatings, Tribol. Lett. 56 (2014) 223–230. doi:10.1007/s11249-014-0402-4.

[54] C. Kumara, H. Luo, D.N. Leonard, H.M. Meyer, J. Qu, Organic-Modified Silver Nanoparticles as Lubricant Additives, ACS Appl. Mater. Interfaces. 9 (2017) 37227–37237. doi:10.1021/acsami.7b13683.

[55] F. Ilie, C. Covaliu, Tribological Properties of the Lubricant Containing Titanium Dioxide Nanoparticles as an Additive, Lubricants. 4 (2016) 12. doi:10.3390/lubricants4020012.

[56] M. Laad, V.K.S. Jatti, Titanium oxide nanoparticles as additives in engine oil, J. King Saud Univ. - Eng. Sci. 30 (2018) 116–122. doi:10.1016/j.jksues.2016.01.008.

[57] A. Charanpahari, S. Ingole, D.V. Bhatt, A. Kakade, J. Menghani, S.S. Umare, Tribological behavior of nano TiO2 as an additive in base oil, Wear. 301 (2013) 776–785. doi:10.1016/j.wear.2013.01.037.

[58] T. Luo, X. Wei, H. Zhao, G. Cai, X. Zheng, Tribology properties of Al2O3/TiO2 nanocomposites as lubricant additives, Ceram. Int. 40 (2014) 10103–10109. doi:10.1016/j.ceramint.2014.03.181.

[59] D. Jiao, S. Zheng, Y. Wang, R. Guan, B. Cao, The tribology properties of alumina/silica composite nanoparticles as lubricant additives, Appl. Surf. Sci. 257 (2011) 5720–5725. doi:10.1016/j.apsusc.2011.01.084.

[60] N.G. Demas, R.A. Erck, C. Lorenzo-martin, O.O. Ajayi, G.R. Fenske, Experimental Evaluation of Oxide Nanoparticles as Friction and Wear Improvement Additives in Motor Oil, 2017 (2017).

[61] A. Hern, R. Gonz, J.L. Viesca, J.E. Fern, A. Machado, R. Chou, J. Riba, CuO , ZrO 2 and ZnO nanoparticles as antiwear additive in oil lubricants, 265 (2008) 422–428. doi:10.1016/j.wear.2007.11.013.

[62] R.B. Rastogi, D. Kumar, Synthesis, Characterization, and Tribological Evaluation of SDS-Stabilized Magnesium-Doped Zinc Oxide (Zn 0.88 Mg 0.12 O) Nanoparticles as E ffi cient Antiwear Lubricant Additives, (2016). doi:10.1021/acssuschemeng.6b00472.

[63] L. Wu, Y. Zhang, G. Yang, S. Zhang, L. Yu, P. Zhang, RSC Advances oxide nanoparticles as the lubricant additive in poly-alpha ole fi n and diisooctyl sebacate base oils †, (2016) 69836–69844. doi:10.1039/c6ra10042b.

[64] F.J. Carrión, J. Sanes, M.D. Bermúdez, Effect of ionic liquid on the structure and tribological properties of polycarbonate – zinc oxide nanodispersion, 61 (2007) 4531–4535. doi:10.1016/j.matlet.2007.02.044.

[65] X.X. XUE Weiguo , ZHAO Zhenghua , WANG Peng , JIN Zhiliang, Performance Study of Zinc Oxide Nanoparticles for Lubricant Oil, 1118 (2015) 195–204. doi:10.4028/www.scientific.net/AMR.1118.195.

[66] A. Hernández, J.E. Fernández, R. Tucho, J.M. Cuetos, R. Chou, SOME ASPECTS OF OIL LUBRICANT ADDITIVATION WITH ZnO NANOPARTICLES, (2006) 24–26.

[67] S.M. Alves, B.S. Barros, M.F. Trajano, K.S.B. Ribeiro, E. Moura, Tribology International Tribological behavior of vegetable oil-based lubricants with nanoparticles of oxides in boundary lubrication conditions, Tribiology Int. 65 (2013) 28–36. doi:10.1016/j.triboint.2013.03.027.

[68] A.H. Battez, J.E.F. Rico, A.N. Arias, J.L.V. Rodriguez, R.C. Rodriguez, J.M.D.

Fernandez, The tribological behaviour of ZnO nanoparticles as an additive to PAO6, 261 (2006) 256–263. doi:10.1016/j.wear.2005.10.001.

[69] V. Sharma, R. Timmons, A. Erdemir, P.B. Aswath, Plasma-Functionalized Polytetrafluoroethylene Nanoparticles for Improved Wear in Lubricated Contact, ACS Appl. Mater. Interfaces. 9 (2017) 25631–25641. doi:10.1021/acsami.7b06453.

[70] S.D. Bagi, P.B. Aswath, Role of MoS2 morphology on wear and friction under spectrum loading conditions, Lubr. Sci. 27 (2015) 429–449. doi:10.1002/ls.1296.

[71] V. An, Y. Irtegov, C. de Izarra, Study of Tribological Properties of Nanolamellar WS 2 and MoS 2 as Additives to Lubricants, J. Nanomater. 2014 (2014) 1–8. doi:10.1155/2014/865839.

[72] L. Hao, J. Li, X. Xu, T. Ren, Preparation, Characterization, and Tribological Evaluation of Triethanolamine Monooleate-Modified Lanthanum Borate Nanoparticles, Proc. Inst. Mech. Eng. Part J J. Eng. Tribol. 224 (2010) 1163–1171. doi:10.1243/13506501JET817.

[73] S. Chen, W. Liu, Oleic acid capped PbS nanoparticles: Synthesis, characterization and tribological properties, Mater. Chem. Phys. 98 (2006) 183–189. doi:https://doi.org/10.1016/j.matchemphys.2005.09.043.

[74] J. Zhou, Z. Wu, Z. Zhang, W. Liu, H. Dang, Study on an antiwear and extreme pressure additive of surface coated LaF3 nanoparticles in liquid paraffin, Wear. 249 (2001) 333–337. doi:10.1016/S0043-1648(00)00547-0.

[75] Z.S. Hu, J.X. Dong, Study on antiwear and reducing friction additive of nanometer titanium borate, Wear. 216 (1998) 87–91. doi:https://doi.org/10.1016/S0043-1648(97)00249-4.

[76] J.. Dong, Z.. Hu, A study of the anti-wear and friction-reducing properties of the lubricant additive, nanometer zinc borate, Tribol. Int. 31 (1998) 219–223. doi:10.1016/S0301-679X(98)00017-6.

[77] Z.. Hu, J.. Dong, G.. Chen, Study on antiwear and reducing friction additive of nanometer ferric oxide, Tribol. Int. 31 (1998) 355–360. doi:10.1016/S0301-679X(98)00042-5.

[78] G. Zhao, Q. Zhao, W. Li, X. Wang, W. Liu, Tribological properties of nano-calcium borate as lithium grease additive, Lubr. Sci. 26 (2014) 43–53. doi:10.1002/ls.1227.

[79] S. Qiu, Z. Zhou, J. Dong, G. Chen, Preparation of Ni Nanoparticles and Evaluation of Their Tribological Performance as Potential Additives in Oils, J. Tribol. 123 (2001) 441. doi:10.1115/1.1286152.

[80] Q. Sunqing, D. Junxiu, C. Guoxu, Wear and friction behaviour of $CaCO_3$ nanoparticles used as additives in lubricating oils, Lubr. Sci. 12 (2000) 205–212. doi:10.1002/ls.3010120207.

[81] X. Ji, Y. Chen, G. Zhao, X. Wang, W. Liu, Tribological properties of CaCO 3 nanoparticles as an additive in lithium grease, Tribol. Lett. 41 (2011) 113–119. doi:10.1007/s11249-010-9688-z.

[82] Y.Y. Wu, W.C. Tsui, T.C. Liu, Experimental analysis of tribological properties of lubricating oils with nanoparticle additives, Wear. 262 (2007) 819–825. doi:10.1016/j.wear.2006.08.021.

[83] W. Liu, S. Chen, An investigation of the tribological behaviour of surface-modified ZnS nanoparticles in liquid paraffin, Wear. 238 (2000) 120–124. doi:https://doi.org/10.1016/S0043-1648(99)00344-0.

[84] S. Tarasov, A. Kolubaev, S. Belyaev, M. Lerner, F. Tepper, Study of friction reduction by nanocopper additives to motor oil, Wear. 252 (2002) 63–69. doi:10.1016/S0043-1648(01)00860-2.

[85] G. Liu, X. Li, B. Qin, D. Xing, Y. Guo, R. Fan, Investigation of the mending effect and mechanism of copper nano-particles on a tribologically stressed surface, Tribol. Lett. 17 (2004) 961–966. doi:10.1007/s11249-004-8109-6.

[86] Y.-B. Guo, S.-W. Zhang, The Tribological Properties of Multi-Layered Graphene as Additives of PAO2 Oil in Steel–Steel Contacts, Lubricants. 4 (2016) 30. doi:10.3390/lubricants4030030.

[87] H.D. Huang, J.P. Tu, L.P. Gan, C.Z. Li, An investigation on tribological properties of graphite nanosheets as oil additive, Wear. 261 (2006) 140–144.

doi:10.1016/j.wear.2005.09.010.

[88] Y. Hamedani, P. Macha, T.J. Bunning, R.R. Naik, M.C. Vasudev, Plasma-Enhanced Chemical Vapor Deposition: Where we are and the Outlook for the Future, in: S. Neralla (Ed.), Chem. Vap. Depos., IntechOpen, Rijeka, 2016. doi:10.5772/64654.

[89] S.R. Peri, B. Habersberger, B. Akgun, H. Jiang, J. Enlow, T.J. Bunning, C.F. Majkrzak, M.D. Foster, Variations in cross-link density with deposition pressure in ultrathin plasma polymerized benzene and octafluorocyclobutane films, Polymer (Guildf). 51 (2010) 4390–4397. doi:https://doi.org/10.1016/j.polymer.2010.07.026.

[90] B. Nisol, F. Reniers, Challenges in the characterization of plasma polymers using XPS, J. Electron Spectros. Relat. Phenomena. 200 (2015) 311–331. doi:https://doi.org/10.1016/j.elspec.2015.05.002.

[91] P.W. Kramer, Y.S. Yeh, H. Yasuda, Low temperature plasma for the preparation of separation membranes, J. Memb. Sci. 46 (1989) 1–28. doi:https://doi.org/10.1016/S0376-7388(00)81167-9.

[92] K.D. Anderson, J.M. Slocik, M.E. McConney, J.O. Enlow, R. Jakubiak, T.J. Bunning, R.R. Naik, V. V Tsukruk, Facile plasma-enhanced deposition of ultrathin crosslinked amino acid films for conformal biometallization., Small. 5 (2009) 741–749. doi:10.1002/smll.200801843.

[93] M.C. Vasudev, H. Koerner, K.M. Singh, B.P. Partlow, D.L. Kaplan, E. Gazit, T.J. Bunning, R.R. Naik, Vertically Aligned Peptide Nanostructures Using Plasma-Enhanced Chemical Vapor Deposition, Biomacromolecules. 15 (2014) 533–540. doi:10.1021/bm401491k.

[94] B. PERI, B. BORAH, R.A.J.K. DASH, Effect of RF power and gas flow ratio on the growth and morphology of the PECVD SiC thin film s for MEMS applications, Bull. Mater. Sci. 38 (2015) 1105–1112. doi:10.1007/s12034-015-0881-4.

CHAPTER 2

TRIBOCHEMISTRY OF FLUORINATED ZnO NANOPARTICLES AND ZDDP LUBRICATED INTERFACE AND IMPLICATIONS FOR ENHANCED ANTI-WEAR PERFORMANCE AT BOUNDARY LUBRICATED CONTACTS

Kimaya Vyavhare, Richard B. Timmons, Ali Erdemir, Brian Edwards, and Pranesh B. Aswath

Submitted to: Wear (October 2020)

ABSTRACT

Surface-capped zinc oxide (ZnO) nanoparticles were engineered to deliver beneficial anti-wear and anti-friction chemistries at sliding interfaces with a focus on potentially reducing environmentally hazardous zinc dialkyl dithiophosphate (ZDDP) additive in automotive lubricants, without compromising tribological performance. A plasma polymerization technique was employed to coat ZnO nanoparticles, initially with fluorine rich polymer films to enhance the formation of surface protective tribofilms, followed by methacrylate-based coatings to reduce agglomeration and, simultaneously, induce stable dispersion of nanoparticles in the base oils. Formulation with an additive mixture of fluorinated ZnO and ZDDP (350 ppm phosphorus level) exhibited a reduction in the coefficient of friction and significantly improved wear performance. The improved tribological performance is attributed to the synergistic interaction between fluorinated ZnO and ZDDP and to the physical and chemical properties of the formed tribofilms. In-situ electrical contact resistance data highlighted the role of fluorinated ZnO nano-additives in reducing the incubation time for stable tribofilm formation. AFM, SEM, XANES, and XPS results revealed that oils with fluorinated ZnO form relatively thick, patchy tribofilms with hierarchical chemical structure enriched with zinc polyphosphates, coupled with minor amounts of metal fluorides, zinc and iron sulfates and sulfides, further improving wear resistance under low concentration of ZDDP.

KEYWORDS

Anti-wear additives, ZDDP tribofilms, ZnO nanoparticles, plasma functionalization, XANES, nano-additives.

1. INTRODUCTION

The current trends toward improved fuel economy and tighter emission controls have pushed the automobile industry toward low viscosity engine oils formulated with increasingly efficient additives [1–3]. Thinner engine oils reduce hydrodynamic friction and increase engine efficiency. However, in contrast, their usage can require engine components to operate in boundary to mixed lubrication regimes, thus causing increased friction and wear of rubbing surfaces. This necessitates the formulation of engine oils with high-performance anti-wear additives capable of forming solid tribofilms to enhance durability of moving mechanical interfaces experiencing direct contact in the internal combustion engine.

Tied in with the demands of fuel economy and efficiency is a concern of the effect of phosphorus and sulfur-containing anti-wear additives on the efficiency of exhaust after-treatment devices [4,5]. One such example is of zinc dialkyldithiophosphate (ZDDP) additive which is universally used in automotive lubricants due to its multifaceted functions and relatively inexpensive cost. The ZDDP undergoes thermo-mechanical decomposition to form surface-bound phosphate tribofilms capable of effectively preventing wear and failure of tribological contacts [6–9]. However, despite being an effective anti-wear additive, the amount of ZDDP utilized in current GF6 engine oils is restricted to 800 ppm of phosphorus, because formation of thiophosphate byproducts contribute to poisoning of catalytic converters thus increasing automotive tailpipe emissions [10–12]. With the continued growing concerns of global warming, coupled with the need for improved emission control technologies to meet stringent environmental regulations, lubrication formulators will likely have to further reduce SAPS (sulfated ash, phosphorus, and sulfur) amounts, especially phosphorus to below 500 ppm [2,4]. Clearly, it is important to develop

novel high-performance additive technologies capable of either reducing or replacing ZDDP thus providing better wear protection of engine components operating with low-viscosity lubrication.

In recent years, inorganic metal oxide nanoparticles like TiO_2 [13–15], SiO_2 [16–20], CuO [21,22], ZnO [23–26], and Fe_3O_4 [27] have been suggested as promising environment-friendly lubricant additives to reduce friction and wear between the sliding surfaces. Nanosized additives provide better lubricating performance over their micron-sized counterparts due to their ability to compensate for the material loss by easily entraining within micro-sized surface asperities and depositing on the worn surface. However, the practical application of nano-additives faces several challenges such as poor solubility in nonpolar lubricants, agglomeration, and precipitation [28]. To date, three major methods have been employed to improve the dispersibility of nanomaterials in lubricant base stocks: addition of dispersants, ultrasonic dispersion, and chemical surface modification [29]. Uniform dispersion of nano-additives in the lubricating oils is very crucial to protect and minimize wear losses of sliding contacts. Several experimental studies have reported the efficacy of dispersed nanoparticles to generate protective interfacial tribofilms composed of nanoparticle agglomerates, sintered nanoparticles, or nanoparticle reinforced tribopolymer networks [23,30–40]. For example, Battez et al. used organic dispersants to achieve uniform suspension of ZnO nanoparticles in polyalphaolefin (PAO6) oil. They showed improvement in the extreme pressure behavior of PAO6 and ZnO mixtures with the increase in ZnO concentration and correlated it to the ability of dispersed ZnO nanoparticles to deposit tribofilms on the wear track [34]. Sui et al. used an extensive chemical method to synthesize hairy silica nanoparticles, grafted with alkyl and amino organic ligands, for use as high-performance SiO_2 nano-additive for PAO lubricants. The presence of bifunctional ligands was shown to enhance the adsorption of nanoparticles on the metal surfaces to form protective tribofilms, rather than just filling the grooves

on the wear tracks [20]. Khare et al. investigated the mechanism of anti-wear tribofilms formed with a dispersion of ZrO_2 nanoparticles capped with organic ligands in a PAO4 synthetic oil. Using in-situ atomic force microscopy, they proposed that the dispersed ZrO_2 nanoparticles interact with the sliding nanoscale interfaces to form tribofilms, through a process of stress-activated tribosintering [41].

In the present study, core-shell structure polymer-coated ZnO nanoparticles are developed and are used in combination with extremely low amount of ZDDP (350 ppm of P) to improve anti-wear and anti-friction properties of very low phosphorus containing oils. Considering good thermal and chemical stability, non-toxicity, commercial feasibility, it is understandable that few studies have been conducted using ZnO nanoparticles as lubricant additive [23,24,26,34,42,43]. Alves et al. observed that ZnO nanoparticles exhibit good friction-reducing and antiwear abilities when used as an additive in the vegetable based oil lubricant [44]. Battez et al. showed improvement in the extreme pressure properties of ZnO nanoparticles dispersed in a polyalphaolefin oil and attributed the performance to their ability to deposit tribofilms on the contact. Through SEM-EDS results it was hypothesized that tribofilms were developed via a process of tribosintering [23], however, neither the tribofilm forming mechanism nor the properties of tribofilms were verified experimentally or through reliable characterization technique. A distinguishing feature of this research work is that the plasma enhanced chemical vapor deposition (PECVD) technique was employed to molecularly surface tailor ZnO nanoparticles with multilayered polymer coatings. Initially, ZnO nanoparticles were encapsulated with fluorocarbon-based polymer films, followed with subsequent deposition of methacrylate-based coatings. Such bi-layered shell coatings not only help to induce adequate dispersion of nanoparticles in the oil but, importantly, also delivers tribologically beneficial anti-wear chemistries (like fluorine) at the sliding interface. We aim to

use fluorine coated ZnO nanoparticles in the oil containing reduced amount of ZDDP and explore the nature of the interaction of ZnO nanoparticles with ZDDP to develop an understanding of how nano-additives will behave in a commercial fully formulated oil. Additionally, as the tribochemical reactions occurring at sliding interfaces control the friction and wear outcomes, this study concentrates on determining the physiochemical properties of the interfacial tribofilms and understanding tribofilm forming mechanism of novel core-shell structure fluorinated ZnO nanoparticles.

Herein, a detailed systematic evaluation of the tribological behavior of non-functionalized and functionalized ZnO nanoparticles, with or without ZDDP, was performed through tribological testing in the boundary lubrication regime. In addition to measurements of friction values and wear volume loss, electrical contact resistance data was measured, *in-situ*, during tribological tests to help elucidate the dynamics of tribofilm formation. Topography and morphology of tribofilms generated from nanoparticle lubricant additives were studied through high resolution scanning electron microscopy (SEM) and surface probe microscopy (SPM). To identify the compounds formed due to tribochemical reactions and their distribution across the interface, X-ray photoelectron spectroscopy (XPS) and X-ray near-edge absorption spectroscopy (XANES) were applied. In particular, a thorough analysis of tribo-surface characterization was carried out to propose a phenomenological model of tribofilms and anti-wear mechanism. The outcomes of this study reveal that fluorinated ZnO core-shell nanoparticles can indeed reduce the amount of ZDDP in the engine oil, thus reducing the aforementioned catalytic poisoning, while simultaneously improving the anti-wear performance and durability of engine components.

2. EXPERIMENTAL DETAILS

2.1. Materials

ZnO nanoparticles, having a manufacturer measured size of 10-30 nm, were purchased from Sky Spring Nanomaterials. Perfluorohexane (C_6F_{14}) and glycidyl methacrylate ($C_7H_{10}O_3$) were procured from Sigma Aldrich. Group III mineral base stock (GS Caltex Kixx Lubo 4 cSt) was used for preparing test oils. The ZDDP used in this study, derived from secondary alcohol, the details of which can be found elsewhere [45,46].

2.2. Synthesis of ZnO Core-Shell Structure Nano-additives

ZnO core-shell structure nano-additives were prepared by encapsulating ZnO nanoparticles with fluorine rich coatings through a plasma-enhanced chemical vapor deposition process. A homebuilt 360º rotating plasma reactor was selected in this research work to achieve uniform deposition of plasma films and minimize nanoparticles aggregation during the coating process. ZnO nanoparticles were coated with fluorocarbon plasma-induced films, using perfluorohexane as monomer. The deposition process was carried out using a continuous wave (CW) plasma for initial 10 mins, followed with sequential reduced to lower duty cycle pulsed plasmas from 20:20 (plasma on time:plasma off times in seconds) to 20:60, for 10 minute periods at each ratio. Applying CW plasma first ensures good adhesive strength between the coating and the substrate, and the lower duty cycle pulsating plasma provides a gradient layer structure with each layer tightly bound to another. The monomer pressure was maintained at 300 mT and RF power was kept at 60 W throughout the process. X-ray photoelectron spectroscopy (XPS) was employed to characterize and ensure fluorine rich plasma coatings on the ZnO nanoparticles exposed to perfluorohexane plasma. Figure 1 shows the fluorine 1s XPS spectra for plasma functionalized ZnO nanoparticles. The peaks around 689-690 eV binding energy represent the presence of organic films containing carbon-bonded fluorine on the surface of ZnO nanoparticles. Additionally,

developed plasma fluoropolymer coatings were characterized using FTIR and results are added in Supporting Information section (refer figure S1).

Subsequently, another plasma coating was deposited on top of these particles using glycidyl methacrylate as the precursor monomer. The purpose of this secondary methacrylate coating is to protect initially deposited fluorocarbon films and, simultaneously, assist in the subsequent dispersion of nanoparticles in the non-polar oil. The plasma process for methacrylate coatings was run at 100 W power and 70 mT pressure. Coatings were deposited using CW plasma for 20 mins followed with a 20:50 (in secs) pulsating signal for 40 min.

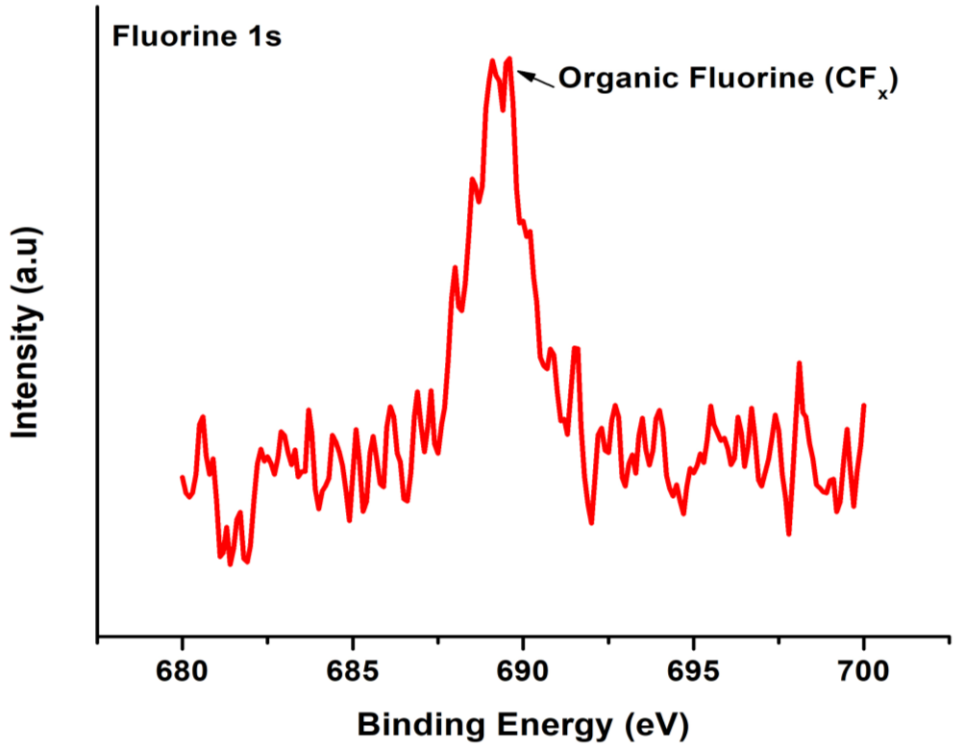

Figure 1. Fluorine 1s XPS spectrum for fluorinated ZnO nanoparticles.

2.3. Preparation of Nano-lubricant

Plasma functionalized ZnO nanoparticles were added to the base oil at 0.33 wt.% and formulations were prepared with or without ZDDP. 0.33 wt.% concentration for nanoparticles was selected as it is close to the percolation threshold of non-functionalized ZnO nanoparticles providing better tribological benefits. Results of tribological test carried out to determine percolation threshold of non-functionalized ZnO are provided in Supporting Information (refer to figure S2). Additionally, it should be noted, we have observed that plasma functionalized PTFE nanoparticles at a similar concentration of 0.33 wt.% resulted in improved tribological performance [47]. Table 1 provides details of the oil formulations used in this study. Since the current level of phosphorus used by the lubricant industry is between 600-800 ppm, oil blends were prepared with ZDDP at two different phosphorus levels: i) 700 ppm and ii) 350 ppm to evaluate and compare the tribological performance of the low phosphorus nano-lubricants with that of conventional lubricant. To achieve homogenous mixtures, functionalized nanoparticles were mixed in the base oil using probe sonication for about 30 mins. After sonication, the dispersion of ZnO nanoparticles was observed to be retained in the base oil over the two weeks observation time (refer to figure S3).

Table 1. Overview of Test Oil Formulations and Additives

Coded Name	**Details of Formulations**
BO	Group III base oil (without any additives)
ZnO	Base oil + ZnO (added at 0.33 wt.%)
ZDDP_350	Base oil + ZDDP (added at 350 ppm of P)
ZDDP_350 + ZnO	Base oil + ZDDP (350 ppm of P) + ZnO (0.33 wt.%)
ZnOFM	Base oil + ZnOFM (fluorinated ZnO nanoparticles added at 0.33 wt.%)

ZDDP_350 + ZnOFM	Base oil + ZDDP (350 ppm of P) + ZnOFM (fluorinated ZnO nanoparticles added at 0.33 wt.%)
ZDDP_700	Base oil + ZDDP (added at 700 ppm of P)

2.4. Tribological Evaluation of ZnO Nano-additives

The tribological performance of nano-lubricants was evaluated by high-frequency reciprocating rig friction and wear tester with a cylinder-on-flat configuration. Schematic of the test configuration and detail of test parameters for cylinder on reciprocating flat contact under pure sliding are shown in Table 2.

Table 2. Schematic of Tribological Test Configuration and Details of Test Parameters

Tribological Test	Cylinder-on-flat line contact test configuration
	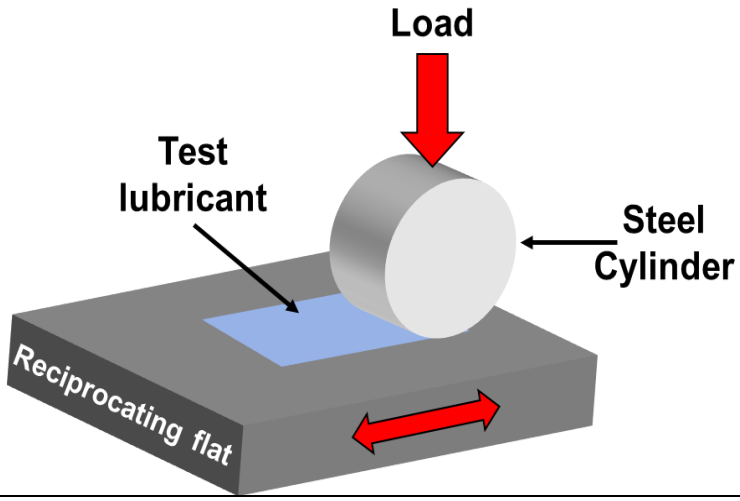
Cylinder	52100 Steel (58-60 HRc); 4 mm × 6 mm; Sa: 8-9 nm.
Flat	52100 Steel (58-60 HRc); 12 mm × 12 mm; Sa: 8-9 nm.
Applied Load	82 N
Initial Hertzian Contact Pressure	500 MPa

Maximum Hertzian Contact Pressure	530 MPa
Temperature	100 ºC
Speed	300 rpm
Stroke length	6 mm
Duration	60 min; 240 min

The tribometer with reciprocating movement was selected based on the standards for evaluating lubricants, but test parameters like contact pressure and sliding velocity and line sliding contact were adapted to simulate tribological conditions experienced at the piston ring and cylinder liner contact in an automobile engine. In the internal combustion engine, the highest wear at the piston ring-cylinder liner contact occurs for the top dead center (TDC) during the power stroke, where the conditions like high contact pressure, slow sliding velocity, and boundary lubrication condition prevail leading to maximum wear losses. The focus of this study is to evaluate the anti-wear capability of developed nano-additive for automobile applications. Therefore, a high frequency reciprocating cylinder-on-flat configuration operating at high load and low-speed testing condition was selected to mimic line contact in the automobile engine's piston ring on cylinder interaction. Similar test conditions were used by previous researchers for tribological automotive applications [48–53]. Wear at piston-cylinder contact also occurs during the bottom dead center or mid-stroke region under mixed-hydrodynamic lubrication regime, however, the wear behavior of these zones is not the focus of this study.

As the highest wear of the piston ring-cylinder liner occurs under boundary lubrication conditions, mathematical calculations were carried out to ensure the boundary lubrication regime does exist under selected testing parameters. The lubrication regime was confirmed by calculating fluid film thickness (using the Dowson-Higginson equation [54,55]) and lambda value (using the

ratio of fluid film thickness and surface roughness). Lambda value was less than unity and thus, suggested operation of tribological tests under boundary lubrication. All test specimens were thoroughly cleaned with Stoddard solution, isopropanol, and acetone before the start of the test. 10 µl of test oil was introduced between the cylinder and flat contact. Two tests were performed for base oil formulation (BO), while three tests were carried out for all other test formulations like ZnO, ZnOFM, ZDDP_350, ZDDP_350 + ZnO, ZPP_350 + ZnOFM, and ZDDP_700 for 60 min duration. These repeats for 60 min tests were carried out with especially oils containing nano-additives to ensure variation in the wear outcomes and their overall performance (including tribofilm properties). Additionally, tribological tests were performed for 240 min duration for all test oils under similar load and speed to evaluate tribological performance and durability of functionalized ZnO additives over prolonged rubbing conditions. After completion of the test, samples were cleaned with heptane and were preserved for characterization by submerging in the additive-free PAO (poly-α-olefin) oil.

The tribological test setup used in this study was built in-house at Argonne National Laboratory and was equipped to record the coefficient of friction (COF) and electrical contact resistance (ECR) data in-situ during the test. To collect ECR data, the electric circuit was set-up by applying a potential between the conducting steel cylinder and flat. During the test, the electric potential builds up across two counter steel surfaces and is recorded, along with the COF values, as functions of rubbing time. ECR data helps to track the formation of non-conductive tribofilms at the cylinder and flat interface.

Counter-bodies (i.e. both cylinder and flat test specimen) after tribological tests were employed to assess wear rate and wear performance using optical microscopy and white light interferometry. The material loss or wear volume of the flat was very difficult to calculate, as it

was manifested as scratches and material deposition. Wear analysis of flat test specimen was confirmed through optical images and surface profiling, and results are added in the Supporting Information section (refer to figure S4). As the material loss of flat specimen was negligible, wear scars developed on the cylinder test specimen was used to evaluate the wear performance of formulated nano-lubricants. Initially, wear scar width was measured at nine locations by imaging the wear scar on the optical microscope and then an average of the wear scar width was used to calculate wear volume loss. Additionally, the Bruker Contour GT interferometer was employed to examine the 3D surface profile of the worn-off surface of the cylinder. Wear surface developed on the flat was later subjected to the previously described surface characterization and analysis of the physical and chemical properties of tribofilms.

2.5. Characterization of Tribofilms

The topography and morphology of tribofilms formed with lubrication of nano-additives and ZDDP were investigated by microscopic examination of the worn surfaces generated on the flat test specimens. SEM (model type: Hitachi S-3000N) was used, in secondary electron mode at an accelerating voltage of 10-20 kV, to image worn surfaces at a magnification of 2000X. Additionally, high-resolution surface probe microscopy (SPM) 3D images of the rubbed surfaces were acquired using atomic force microscopy in contact mode to study surface characteristics and elucidate wear mechanisms in play at tribological contacts.

The chemical nature of the tribofilms formed in-situ during tribological tests were characterized using X-ray photoelectron spectroscopy (XPS) and X-ray absorption near-edge spectroscopy (XANES). The XPS surface analysis was conducted with a Kratos Axis Ultra using a monochromatic Al Kα X-ray source. The beam spot was an elliptical with dimensions 300 µm × 700 µm. XPS spectra were obtained by sputtering the samples using an ion gun (beam energy

4.20 keV) for about 4 min and then irradiating center/edge regions of the worn surfaces with a beam of X-ray at power of 150 W. A survey scan was conducted to identify the major elements present, while high-resolution scans were obtained for elements of interest (Zn, Fe, P, F, O). XPS data were processed using the Casa XPS Software. The spectra calibration was carried out by setting the binding energy of the C1s peak to 284.8 eV.

XANES experiments were performed at the Canadian Light Source synchrotron facility. The phosphorus L (P-L) edge spectra were collected at the variable line spacing plane grating monochromator (VLS-PGM) beam station that operated at the energy range of 5.5-250 eV with a photon resolution of more than 10000 E/ Δ E. The zinc L (Zn-L), iron L (Fe-L), and oxygen K (O-K) edge spectra were acquired using a spherical grating monochromator (SGM) beamline operating at the energy range of 250-2000 eV, with a photon resolution of more than 5000 E/ Δ E. Spectra at both VLS-PGM and SGM beam stations were collected using 100 μm × 100 μm beam spot size. XANES spectra were acquired in total electron yield (TEY) and fluorescence yield (FY) mode for all samples. TEY spectra are more surface sensitive, whereas FY spectra give information from the bulk of the samples.

3. RESULTS AND DISCUSSION

3.1. Coefficient of Friction and Wear Volume

The coefficient of friction (COF) data collected in-situ during tribological tests is summarized in figure 2. These friction profiles roughly represent the presence or exclusion of the tribofilms formed by the additives in the oil at the tribological contacts. Friction profiles for BO and ZnO appear to be very unstable with high friction values indicating that no tribofilms were formed on the counter surface during these tests. The friction response for ZDDP_350 is relatively

stable with some variance in the friction values at the end of the test. Interestingly, formulation with ZDDP and non-fluorinated ZnO additive mixture exhibits low COF values for the first 25 minutes of the test, but as the test continues rapid increase and drops are observed, indicating that smooth surface providing low shear strength was gradually formed and removed during this test. The friction response of fluorinated ZnO-based lubrication appears to be comparatively stable than ZDDP_350 and ZnO. COF data for lubrication with an additive mixture of ZDDP and fluorinated ZnO nanoparticles exhibits the most stable frictional response, with the least COF values. The friction profile for ZDDP_700 is unstable at the beginning of the test, however, near the end it appears to be similar to that of ZDDP_350 + ZnOFM based lubrication.

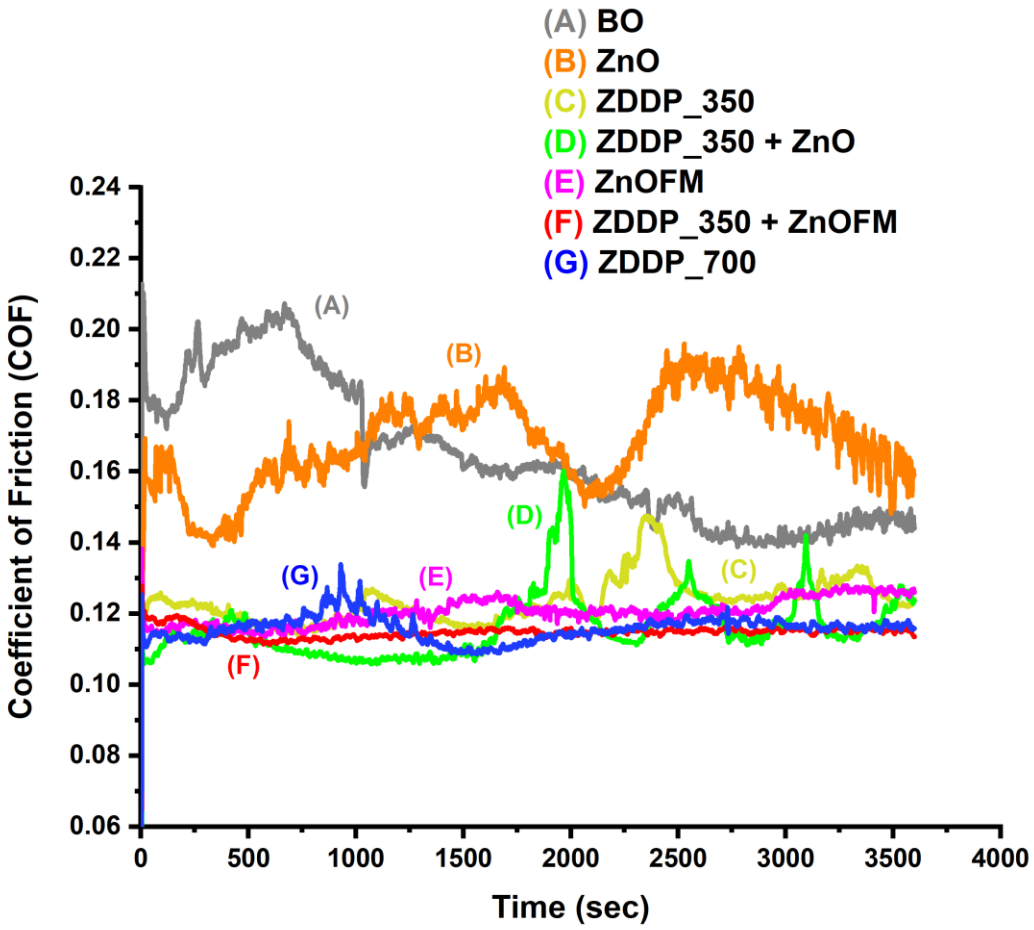

Figure 2. Coefficient of friction as a function of HFRR test time for all seven oil formulations.

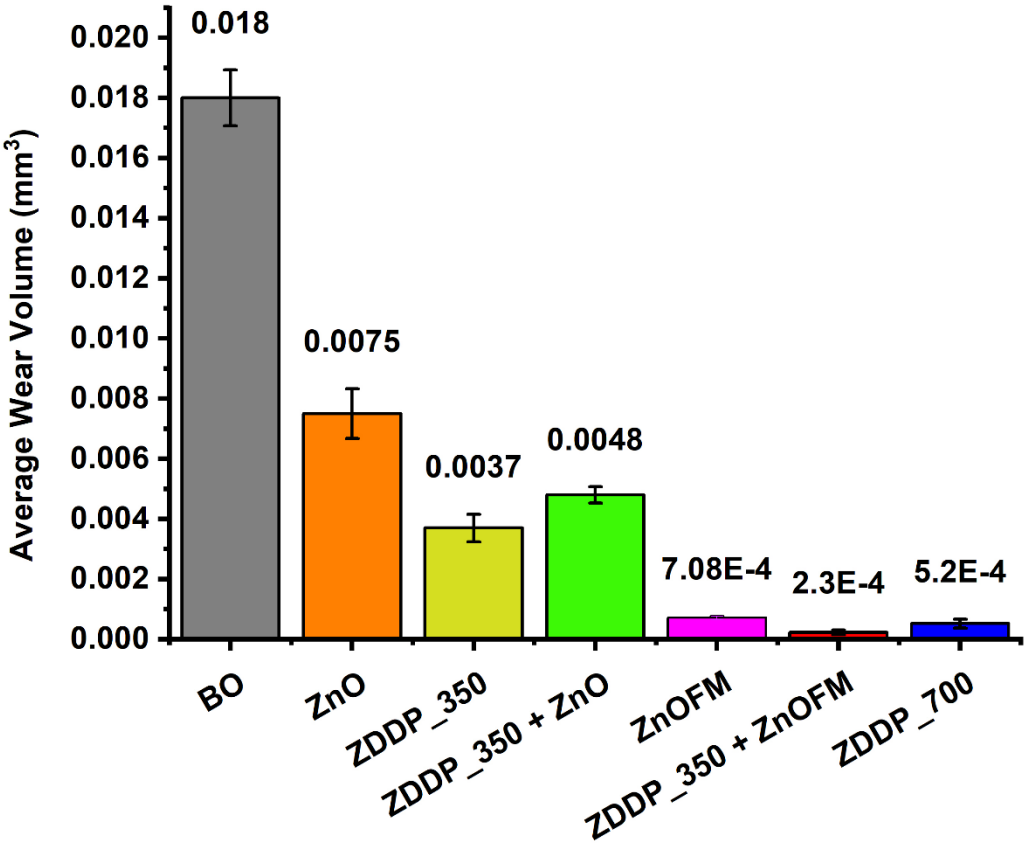

Figure 3. Wear volume losses of cylindrical steel pins for all seven oil formulations.

Wear volume losses were calculated by measuring average wear scar width on the cylindrical pins after each test using optical microscopy and are summarized in figure 3. Black error bars shown in figure 3 represent the standard deviation between the wear volume values calculated for two repeat tribological tests. As anticipated base oil without any additives exhibits the worst wear outcomes. The addition of non-fluorinated ZnO and ZDDP at 350 ppm of P by themselves in the oil has improved the wear performance. However, surprisingly, a mixture of these additives in the base oil resulted in an increase in the wear volume. This suggests that ZDDP exhibits antagonistic behavior when used with non-fluorinated ZnO nanoparticles. When fluorinated ZnO nanoparticles were employed with ZDDP 350, best wear outcomes are observed.

In fact, wear results are better than that of a formulation containing ZDDP at 700 ppm. Similar inferences can be deduced from the optical profilometry results shown in supporting section (figure S5), wherein cylinder lubricated with ZDDP_350 + ZnOFM lubrication is also showing minimal volume loss and surface damage of all. Thus, the friction and wear results reflect synergism between fluorinated ZnO and ZDDP. Additionally, results indicate the benefit of ZnO nanoparticles coated with extra fluorine chemistry in enhancing the anti-wear properties of ZDDP even at a reduced amount of phosphorus of 350 ppm.

To ensure the ability of the developed fluorinated ZnO nano-additives to protect tribological interfaces overextended rubbing time, tribological tests were also conducted for the 4 hour testing duration. Friction and wear results of 4 hour tribological tests are added in the supporting section. Similar to a 1 hour tribological test, oil with fluorinated ZnO and ZDDP additive mixture for 4 hour test exhibits stable friction values and lower wear volume losses and thus, strongly confirming the effectiveness of fluorinated ZnO nano-additives to protect tribological contacts over long rubbing times.

3.2. Electrical Contact Resistance

Dynamics of tribofilms formed by lubricant additives at the rubbing surfaces can be successfully examined using ECR measurements. ZDDP forms amorphous glassy short or long-chain polyphosphates-based tribofilms, which are known to have very high electrical resistivity. At the initial stage of the tribological test when tribofilms are not formed, direct contact of surface asperities of two bodies in relative motion result in very low contact resistance. However, as the test progresses with the formation of protective tribofilms, the resistance between the contacting surfaces increases and can be used as a way of determining effectiveness of tribofilm formation. The voltage drop across the tribocontact of a steel cylinder and flat ranges from 0 to 100 mV. Plots

in figure 4 display potential drop measured in-situ during the tribological test as a function of rubbing time.

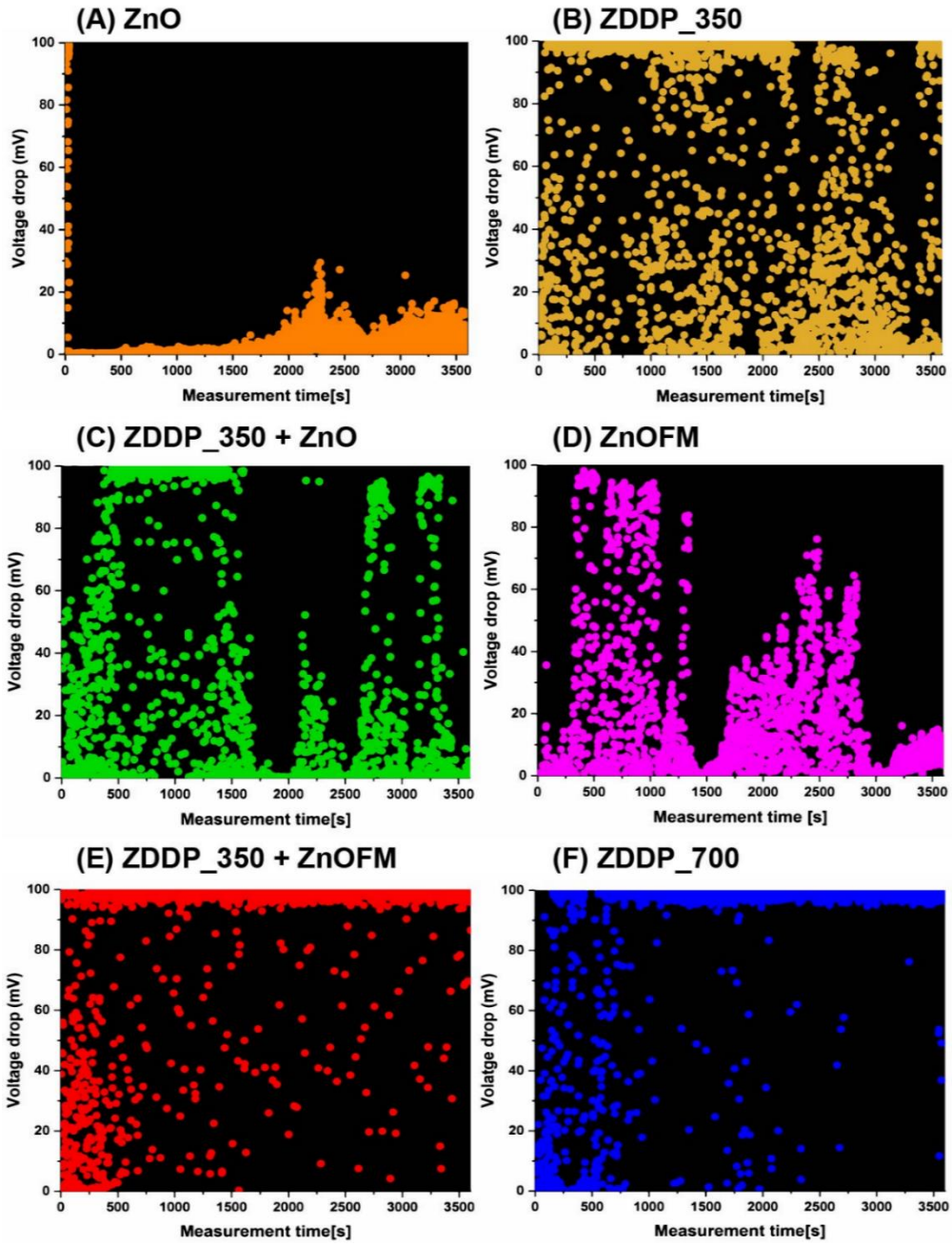

Figure 4. Electrical contact resistance data recorded during tribological test of formulations **(A)** ZnO; **(B)** ZDDP_350; **(C)** ZDDP_350 + ZnO; **(D)** ZnOFM; **(E)** ZDDP_350 + ZnOFM; **(F)** ZDDP_700.

The segregation of data points around 0 mV suggests the absence of non-conductive tribofilms at the contact while data points around 100 mV represent the formation of stable interfacial tribofilms by lubricant additives. ECR data for non-functionalized ZnO nano-additives clearly indicate that no tribofilms were formed during this test. For ZDDP_350, data points appear to be scattered and there was a clear breakdown of the films at the end of the test as evidenced from the drop in potential after ~2250 sec. This indicates that ZDDP, at the lesser concentration of 350 ppm of P, is not enough to form stable tribofilms and protect interacting surfaces against high shear stresses.

In the case of ZDDP_350+ZnO, potential drop at 100 mV at the beginning of the test followed by a sudden decrease to 0 mV indicates stable tribofilms were formed at the initial stages, however, were apparently gradually removed due to interactions between ZDDP and non-functionalized ZnO nanoparticles. This strongly suggests non-functionalized ZnO hinders stable tribofilm formation and their interaction with ZDDP is antagonistic in nature, as also supported by the friction and wear data. ECR data for a formulation containing fluorinated ZnO nanoparticles does hint formation of films at the lubricating interface as opposed to non-functionalized ZnO. Nanoparticles are known to form tribofilms through physical adsorption and/ deposition on the wear tracks, however, in this case as ZnO is semi-conductive, the ECR technique by itself cannot be used effectively to interpret the presence of these nanoparticle-based tribofilms. XPS surface characterization confirming the formation of ZnO rich tribofilms by the lubricant containing fluorinated ZnO nano-additives is available in the Supporting Information (refer figure S6).

Interestingly, the formulation containing fluorinated ZnO and ZDDP (ZDDP_350+ZnOFM) exhibits more stable tribofilm formation than ZDDP_350, with an incubation time of ~500 sec. It is important to note that providing extra zinc and fluorine

chemistries from ZnOFM additives in addition to ZDDP reduces the incubation time for tribofilm formation and leads to form stable film till the end of the test, as contrasted to the tribofilm formation for the formulation ZDDP_350 that fails near the completion of the test. Additionally, in the case of ZDDP_700, tribofilms were initially breaking down and the stability was achieved around 800 sec. These differences in the incubation time and stability clearly demonstrate the additional benefit from plasma coatings in effectively promoting the formation of protective tribofilms which cannot be achieved by the ZDDP alone, certainly not at the lesser concentration of 350 ppm of P.

3.3. Topography of the Interfacial Tribofilms using SEM and AFM

The secondary electron SEM images of the worn surfaces derived after the tribological test are shown in figure 5. A typical SEM image of the wear scar formed with lubrication containing anti-wear additives exhibits bright and dark regions. The bright region represents the surface features derived from conductive metal surfaces (Fe substrate), while the dark region indicates the presence of non-conductive tribofilms. SEM image of ZDDP_350 lubricated wear surface exhibits regions of mild scratches that are covered with small patches of tribofilms (evidenced from dark patches in the SEM image). Wear surface lubricated under the formulation of non-fluorinated ZnO with ZDDP_350 appears to have rougher regions with deep scratches along with some micro pitting, indicating abrasive wear mechanism was in play during this test. On the other hand, surface lubricated with an additive mixture of fluorinated ZnO with ZDDP_350 exhibits better coverage of tribofilms with the patch sizes larger than what is seen in ZDDP_350. Similarly, in comparison with ZDDP_350, ZDDP_700 shows relatively darker spots and mild scratches suggesting the presence of large patches of non-conductive tribofilms over the wear surface.

To further compliment the findings of SEM results, SPM images were obtained using AFM in the direct contact mode. SPM images shown in figure 6 are procured by probing 45 µm × 45 µm area of the wear surface while keeping the Z-axis (± 400 nm) constant.

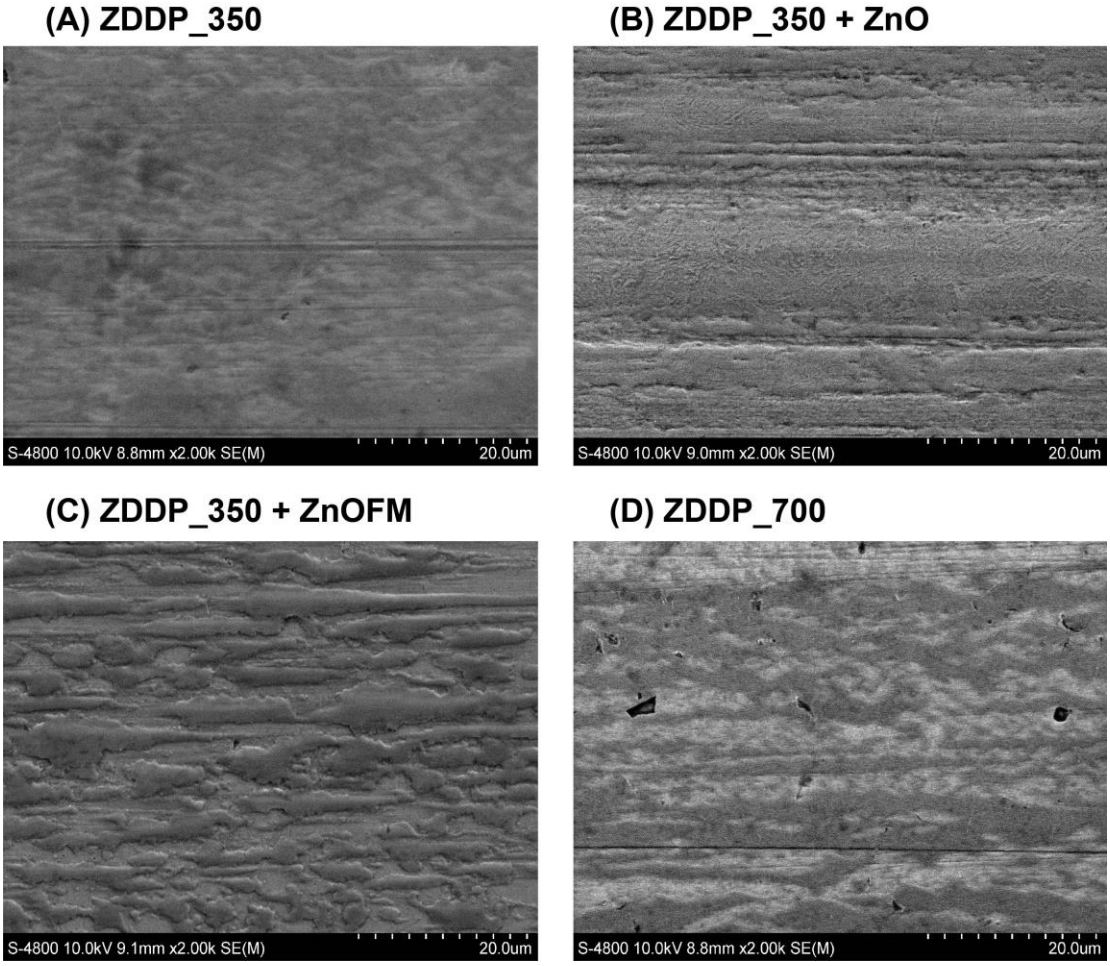

Figure 5. SEM images illustrating morphology of wear surfaces derived from **(A)** ZDDP_350; **(B)** ZDDP_350 + ZnO; **(C)** ZDDP_350 + ZnOFM; **(D)** ZDDP_700.

The topography of wear surface lubricated with ZDDP_350 clearly shows the formation of patchy and porous tribofilms with small pad/island-like features which are typical of ZDDP tribofilms [48,49,56]. SPM image of ZDDP_350 + ZnO lubricated surface exhibits deep scratches with high peak to valley heights supporting results of severe wear losses and inadequate tribofilm

formation with the additive interaction of ZDDP and non-fluorinated ZnO nanoparticles. SPM images of both ZDDP_700 and ZDDP_350 + ZnOFM reveal the presence of thick, smooth and continuous patches of tribofilms covering rough surface asperities.

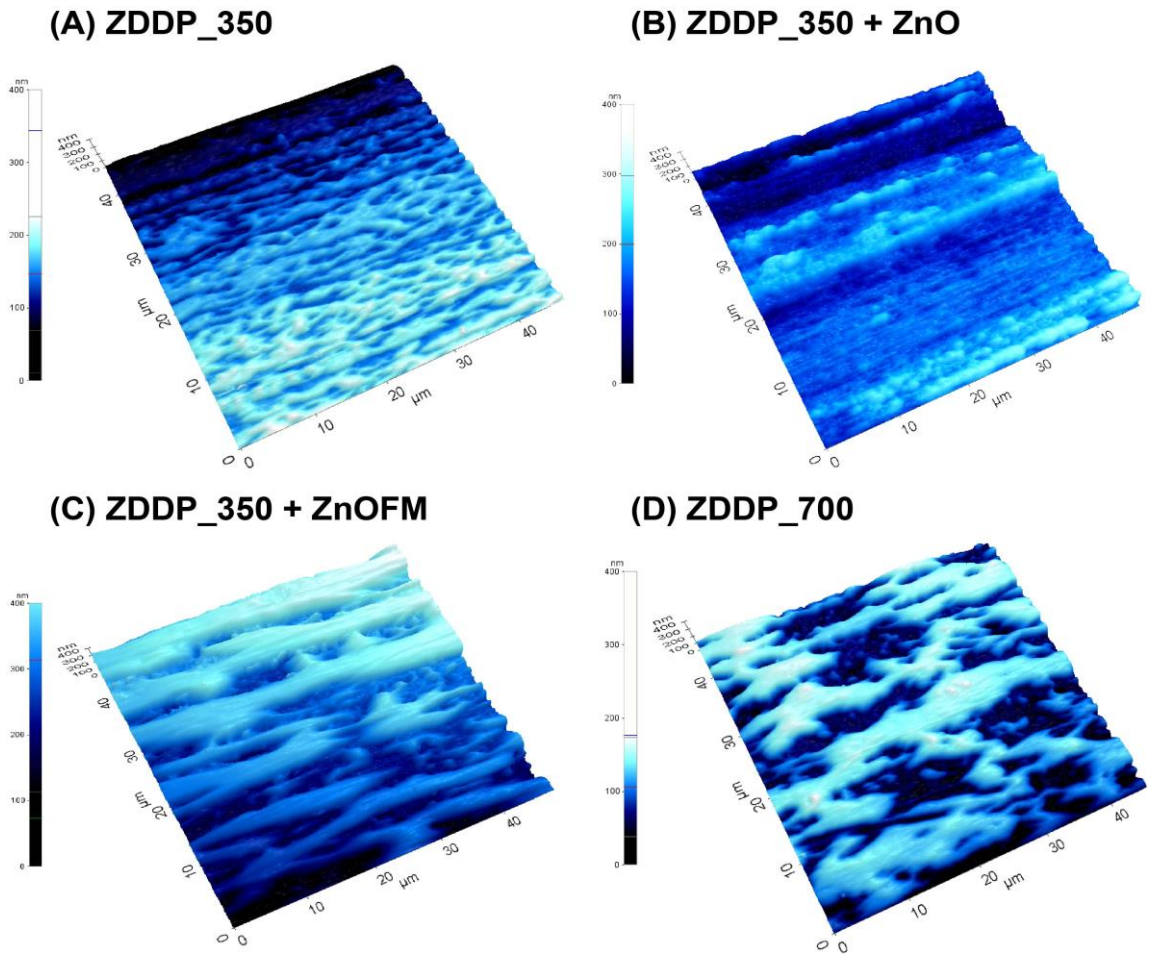

Figure 6. SPM images detailing 3D wear profile and topography of the wear scars derived from formulations **(A)** ZDDP_350; **(B)** ZDDP_350 + ZnO; **(C)** ZDDP_350 + ZnOFM; **(D)** ZDDP_700.

Differences in the surface profiles for ZDDP_350 and ZDDP_350 + ZnOFM indicates that the friction and wear benefits due to fluorinated ZnO nanoparticles, with lower concentration of ZDDP, could be the reflection of differences in physical/chemical properties of the formed tribofilms.

3.4. Chemical Characterization of Tribofilms

3.4.1. XANES

3.4.1.1. Phosphorus Characterization (P $L_{2,3}$-edge)

Phosphorus L-edge XANES spectra for various oil formulations subjected to a 1 hour tribological test along with the relevant model compounds are presented in figure 7. The P L-edge spectra were recorded in both TEY (left side) and FY (right side) modes, wherein the TEY technique probes ~ 5 nm of the surface and FY method probes ~ 60 nm [57]. Thus, the information identified through P L-edge provides better detail of the chemistry (at the uppermost surface and in the bulk of tribofilms) as the sampling depth is close to the average thickness of the tribofilms (~ 50-100 nm in most cases) [58–60]. TEY spectra as shown in figure 8(a) are characteristic of polyphosphates glasses, as observed in our previous studies of ZDDP tribofilms [14,47–49,51,53,61,62]. P L-edge spectra of model compounds show distinguished peaks (marked as **a**, **a'**, **b**, **c**, **c'** and **d**) corresponding to specific electronic transitions of phosphorus 2p electrons. Details on each peak and their significance can be found elsewhere [49,59,63,64]. Peak positions in the spectra of ZDDP_350 tribofilms are highly similar to the positions of iron phosphate ($FePO_4$), in particular, the position of pre-edge **a** in the tribofilm aligns closely with peak **a'** of iron phosphate. The broad main absorption peak of ZDDP_350 tribofilms covers both **c** and **c'** peak positions of zinc and iron phosphates respectively. This indicates that the mixture of zinc and iron phosphates exists, with the Fe^{2+} or Fe^{3+} as the major cation on the surface of these tribofilms rather than Zn^{2+}. TEY spectra for ZDDP_350 + ZnO exhibits extremely low-intensity main absorption peaks and it is difficult to determine whether it is from zinc or iron phosphates. This observation hints the absence or very low concentration of glassy phosphate films in the near-surface region of the tribofilms.

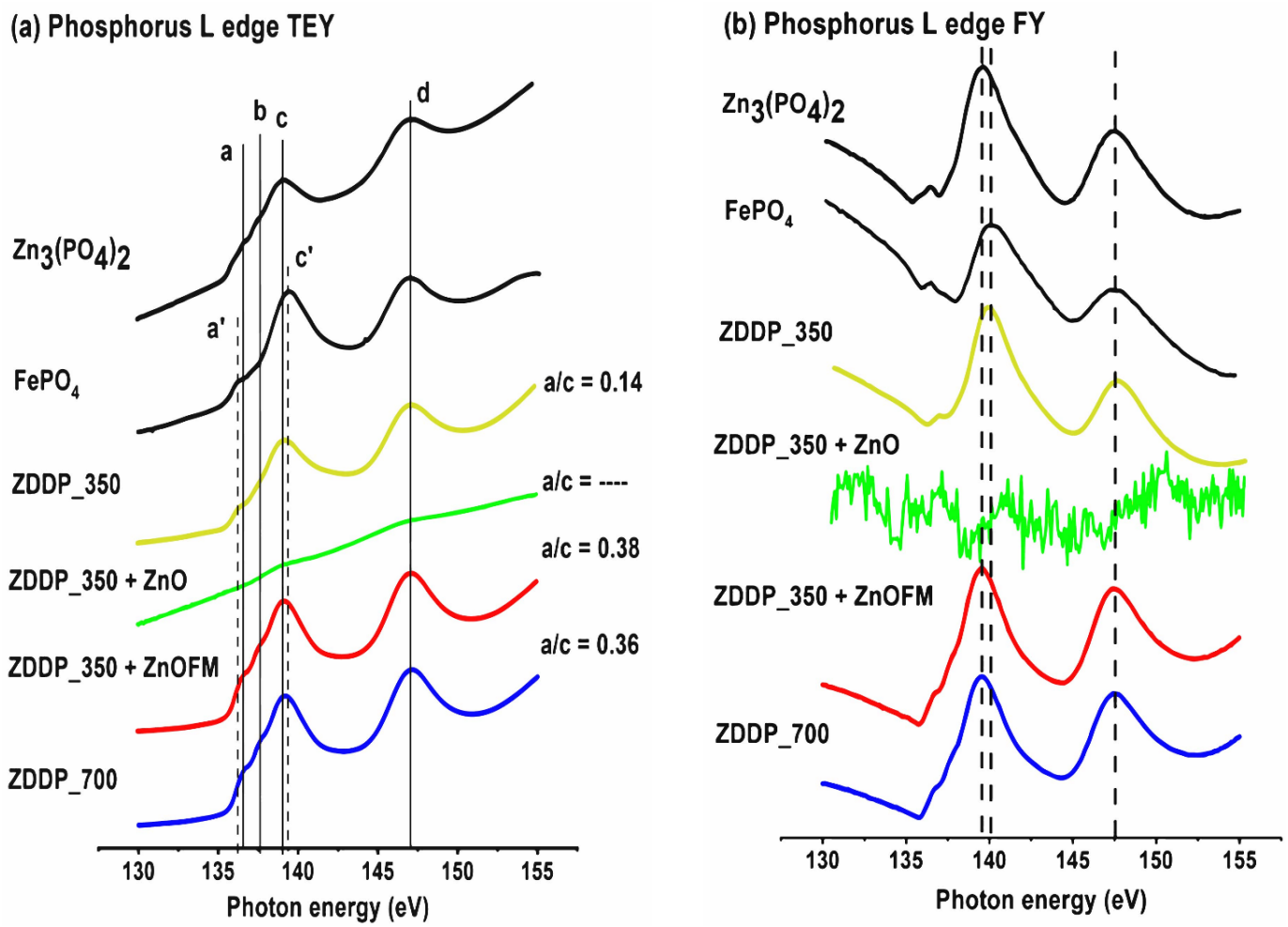

Figure 7. Phosphorus L edge XANES (a) TEY spectra (b) FY spectra of model compounds and tribofilms generated with ZDDP_350, ZDDP_350 + ZnO, ZDDP_350 + ZnOFM, and ZDDP_700.

TEY spectra for ZDDP_350 + ZnO exhibits extremely low-intensity main absorption peaks and it is difficult to determine whether it is from zinc or iron phosphates. This observation hints the absence or very low concentration of glassy phosphate films in the near-surface region of the tribofilms. On the contrary, samples ZDDP_350 + ZnOFM and ZDDP_700 exhibit the very strong intensity of characteristic peaks and reveals the presence of phosphates in the tribofilms. Comparison of peak position with model compounds strongly indicates zinc phosphates as the dominant species at the surface whereas the contribution from iron phosphates to the chemical

makeup of these films is limited. The difference in the intensity of peak **a** relative to peak **c** shown in P L edge TEY XANES spectra has been previously used to determine the chain length of polyphosphates [57]. Kim et al. [65,66] and Yin et al. [63] have proposed that the ratio of peak intensities **a**/**c** increases with the increase in polyphosphate chain length, wherein the **a**/**c** ratio below 0.2 is attributed to orthophosphate or pyrophosphate; the value between 0.2 to 0.3 represents short-chain polyphosphate; the value between 0.3 to 0.6 indicates medium-chain polyphosphate and the ratio greater than 0.6 indicates long-chain polyphosphates. Figure 7(a) clearly indicates that the near-surface regions of tribofilms formed under this study are comprised of short/medium chain polyphosphates. It is important to note that the lubrication with fluorinated ZnO nanoparticles and ZDDP_350 has resulted in the formation of longer chain polyphosphates compared to the oil containing only ZDDP_350.

Phosphorus based bulk chemistry of tribofilms can be elucidated from the FY XANES spectra shown in figure 7(b). The main absorption peak for ZDDP_350 appears to be in between peak position **c** and **c'** suggesting the presence of a mixture of zinc and iron phosphates in the bulk of these tribofilms. FY spectra for ZDDP_350 + ZnO clearly indicates the absence of phosphorus-based compounds in the chemical make-up of tribofilms formed with this lubrication. FY spectra of samples ZDDP_350 + ZnOFM and ZDDP_700 are almost similar and, upon comparing with model compounds, strongly indicate that the majority core of tribofilms are comprised primarily of zinc polyphosphates.

3.4.1.2. Zinc Characterization (Zn $L_{3,2}$-edge)

Figure 8 shows the Zn L-edge spectra of the model compounds ZnO, $ZnSO_4$, $Zn_3(PO_4)_2$, and ZnF_2, together with spectra of the tribofilms, as recorded in TEY and FY modes. Peaks **a** and

b in the Zn L-edge spectra of all samples (except ZDDP_350 + ZnO) matches very well with the characteristic peaks of zinc phosphate.

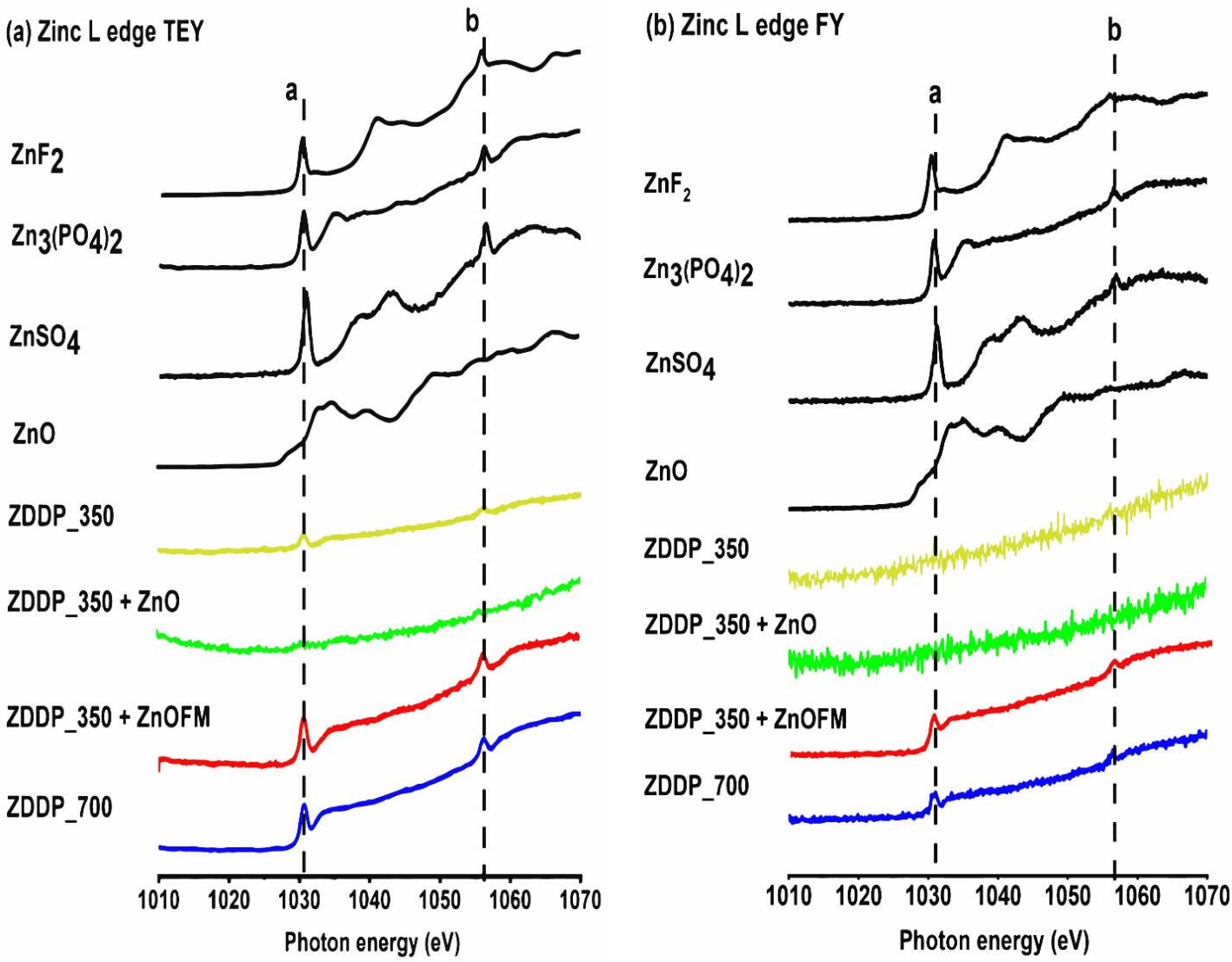

Figure 8. Zinc L edge XANES (a) TEY spectra (b) FY spectra of model compounds and tribofilms generated with ZDDP_350, ZDDP_350 + ZnO, ZDDP_350 + ZnOFM, and ZDDP_700.

The sample with ZDDP_350 exhibits the presence of zinc phosphate in the near-surface region (TEY), while interestingly no signal for Zn is observed in the bulk (FY) of the tribofilms. The tribosurfaces generated from the mixture of ZDDP_350 and non-functionalized ZnO

nanoparticles appear to have no signal for zinc in both TEY and FY mode. The sample with the binary additive mixture of ZDDP_350 and fluorinated ZnO nanoparticles exhibits a strong presence of zinc phosphates in the surface and bulk of the tribofilm. It appears there is higher concentration of zinc phosphate (higher intensity of peak **a**) in the film generated from ZDDP_350 + ZnOFM than the film from ZDDP_350 suggesting the contribution of ZnOFM nanoparticles in promoting the formation of stable phosphate-rich tribofilm. The TEY and FY spectra for ZDDP_700 resemble ZDDP_350 + ZnOFM with only a difference in the intensity of peaks **a** and **b**, thus indicating slightly less concentration (low intensity of peak **a**) of zinc phosphates in these films. Additionally, a close comparison of tribofilm spectra with the spectra of $ZnSO_4$ hints of a small contribution from zinc sulfate in the tribofilm while the majority proportion of zinc is associated with phosphorus.

3.4.1.3. Oxygen Characterization (O K-edge)

O K-edge spectra of tribofilm samples and model compounds are displayed in figure 9. Pre-edge and main absorption peak positions in ZDDP_350 spectra appear to be very similar to $FePO_4$ spectra, however, the main absorption peak (around 542 eV) is very broad and suggests the presence of zinc bound sulfur/phosphorus species in addition to iron phosphate. Spectra of ZDDP_350 + ZnO sample exhibits similar characteristic features of Fe_2O_3 spectra and thus, further confirms antagonistic interaction between ZDDP and non-functionalized ZnO nanoparticles resulting in severe wear and oxidation of exposed steel substrate. On the contrary, the O K-edge spectra of the ZDDP_350 + ZnOFM sample reveals a strong presence of zinc phosphates (aligned peak **a**, **b**, and **c**) in the tribofilms. The main absorption peak is broad and overlaps with peak **c** and **d** indicating less concentration of iron-bound phosphorus and sulfur species in these tribofilms. O K-edge spectra of ZDDP_700 is quite similar to ZDDP_350 + ZnOFM spectra and thus,

indicates tribofilms are primarily composed of zinc phosphate with a minor concentration of iron phosphate and zinc sulfate.

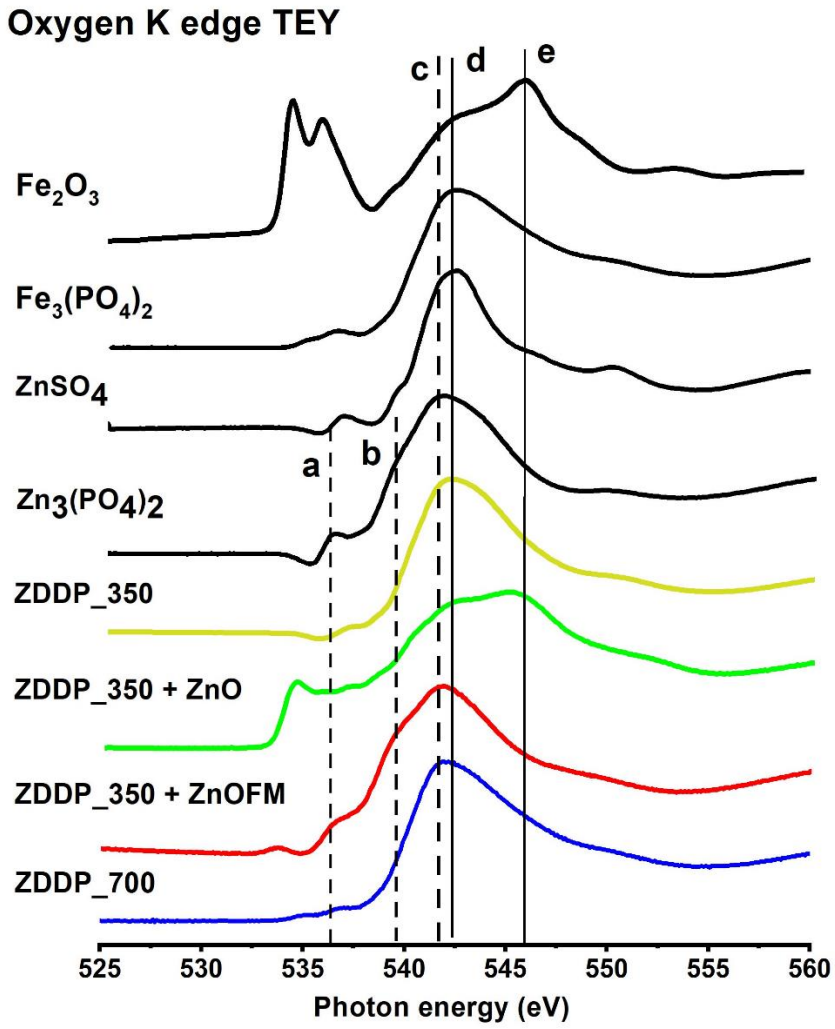

Figure 9. Oxygen K edge XANES TEY spectra of model compounds and tribofilms generated with ZDDP_350, ZDDP_350 + ZnO, ZDDP_350 + ZnOFM, and ZDDP_700.

3.4.1.4. Iron Characterization (Fe $L_{3,2}$-edge)

The TEY Fe-L edge spectra of the iron-containing model compounds $Fe_3(PO_4)_2$, Fe_2O_3, $FePO_4$, FeF_3, and FeS are compared with Fe-L edge spectra of tribofilm samples in figure 10. Fe-

L edge spectra display two main peaks (marked as **a** and **b**/**c**) for both Fe $^{2+}$ and Fe $^{3+}$ model compounds with the only difference being the relative intensities of these peaks. When the oxidation state of iron is increased from Fe $^{2+}$ ($Fe_3(PO_4)_2$) to Fe $^{3+}$ (Fe_2O_3/$FePO_4$), the intensity of second peak (**b**/**c**) is increased [67]. Thus, in this study, the most intense peak is used for fingerprint analysis.

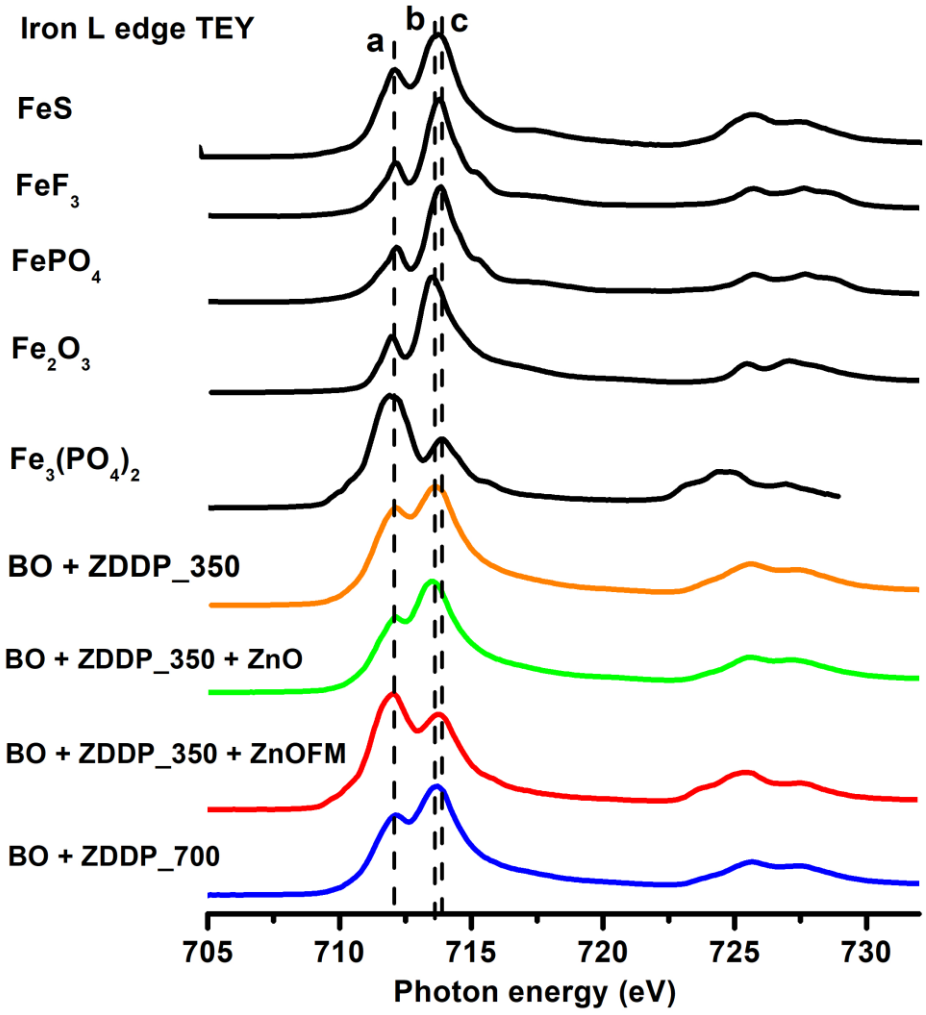

Figure 10. Iron L edge XANES TEY spectra of model compounds and tribofilms generated with ZDDP_350, ZDDP_350 + ZnO, ZDDP_350 + ZnOFM, and ZDDP_700.

The spectra from ZDDP_350 exhibits high intensity broad second peak suggesting the presence of Fe^{3+} associated with the mixture Fe_2O_3 and $FePO_4$ in the near-surface region of

tribofilms. The sample with ZDDP_350 + ZnO has the main peaks (**a** and **b)** exactly aligned with the characteristic peaks of the Fe_2O_3 model compound. The ZDDP_350 + ZnOFM sample has high-intensity peak **a** in exact alignment with $Fe_3(PO_4)_2$ model compound indicating that the near-surface region of these tribofilms is less oxidized, with the significant amount of iron present in the form of iron phosphates. Additionally, the intensity of peak **c** in the tribofilm sample is slightly greater than the $Fe_3(PO_4)_2$ suggesting that tribofilm may have a minor concentration of Fe^{3+} compounds (FeS/ Fe_2O_3/$FePO_4$). On the contrary, spectra of ZDDP_700 clearly show the dominance of Fe^{3+} and indicates the presence of different iron species or mixtures of Fe_2O_3, $FePO_4$, and FeS. These observations further support the formation of protective iron phosphate-rich tribofilms due to synergistic interactions of fluorinated ZnO nanoparticles with ZDDP at the tribological interface.

3.4.2 XPS

XPS can contribute in elucidating the tribofilm chemistry through its ability to record elemental composition and to identify the chemical state of elements through binding energies of atoms. As discussed in wear measurement and XANES results, a very interesting difference is observed for formulations containing only ZDDP and an additive mixture of ZDDP with fluorinated ZnO nanoparticles, and therefore samples lubricated under these two formulations were selected for detailed chemical analysis using XPS. Figure 11 depicts high-resolution XPS spectra obtained for P, Zn, F, O, and Fe elements. XPS spectra reveal information from the 5-8 nm of the tribofilm surfaces. XPS Zn 2p and P 2p core peaks for both samples A and B are almost identical with a distinctive difference in the peak intensity. Zn 2p peaks at the binding energies of ~ 1022.4 eV and ~ 1045.5 eV for sample B with fluorinated ZnO nanoparticles appears to be at relatively higher intensities than sample A.

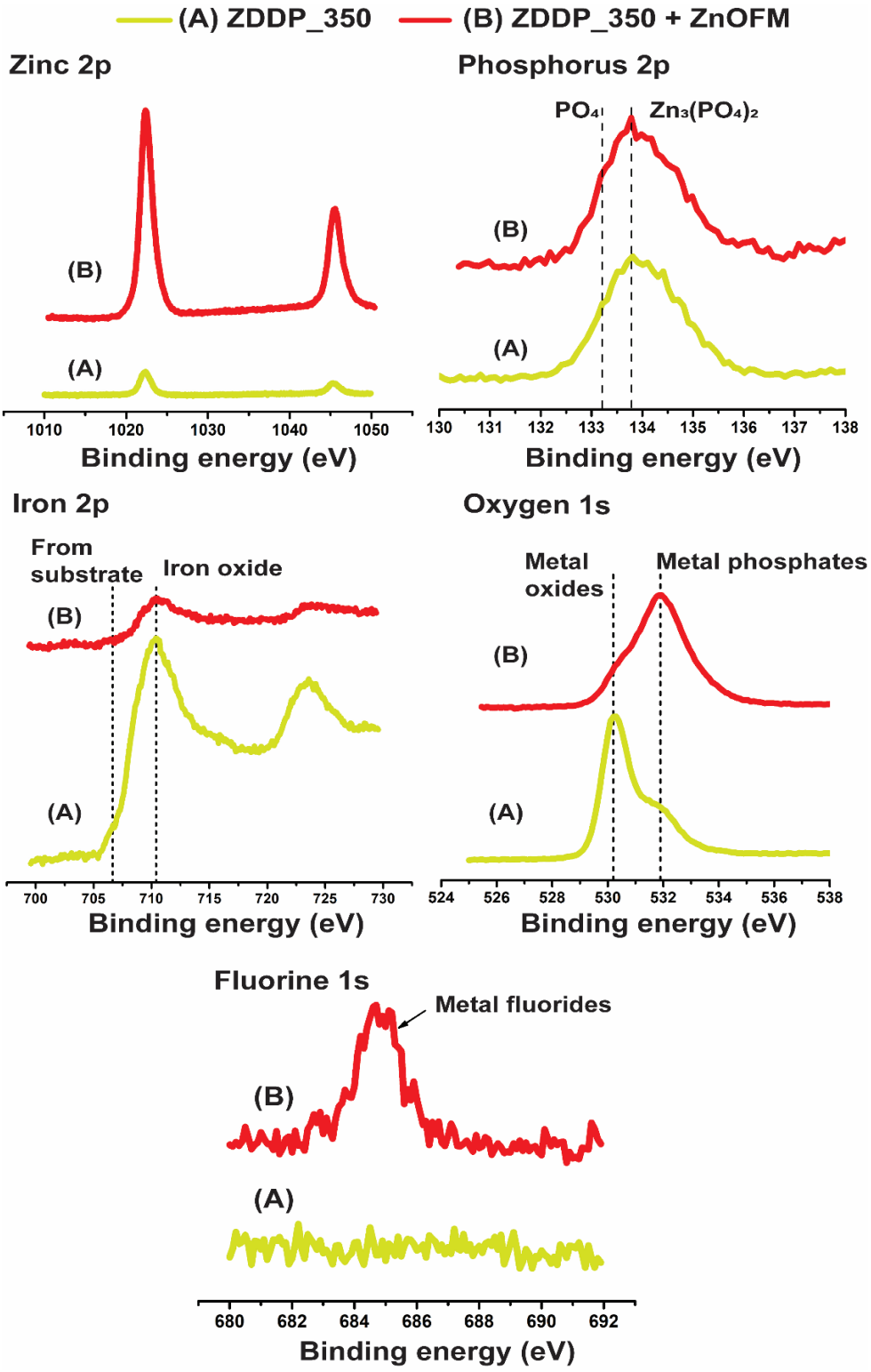

Figure 11. XPS spectra for flat test specimens derived from formulations (A) ZDDP_350; (B) ZDDP_350 + ZnOFM.

Additionally, the information from O 1s spectra reveals the rich chemistry with an interesting shift in the binding energies of a core level peak. The sample with only ZDDP exhibits strong signal for metal oxides (~ 530.2 eV) and weak signal for metal phosphates (~ 531.9 eV), while sample lubricated with fluorinated ZnO based oil shows a weak signal for metal oxides and a strong signal for metal phosphates. This strongly indicates the potential of the additive mixture of ZDDP and fluorinated ZnO nanoparticles to form stable metal phosphate tribofilms with Zn and P rich composition. The Fe 2p core-level spectrum exhibits two peaks at binding energies of ~ 710.4 eV and ~ 723.4 eV, corresponding to the $2p_{3/2}$ and $2p_{1/2}$ components of Fe^{2+}, respectively. Detection of these peaks with a noisy signal can be attributed to the presence of iron oxides on both samples, probably in the sub-surface regions of the tribofilms. Additionally, a high intensity of Fe 2p core peaks for the sample clearly suggests more exposure of nascent steel substrate to oxygen during sliding wear and formation of unstable protective phosphate-based tribofilms during the ZDDP_350 tribological test. XPS spectra for F 1s exhibit crucial information on the contribution of fluorine plasma films in providing improved friction and wear benefits during the tribological test. The F 1S spectra show a high-intensity peak for metal fluorides (~ 685 eV) for the sample with fluorinated ZnO nanoparticles, while the sample with only ZDDP detects no signal for fluorine, thereby suggesting plasma functionalized ZnO nanoparticles were successfully able to deliver fluorine chemistry at the tribological interface. Overall XPS results hint the incorporation of extra Zn and F atoms from core-shell ZnO nano-additives in the chemical structure of glassy phosphate tribofilms and their contribution in promoting stable tribofilm formation with the low concentration of ZDDP (350 ppm of P) in the oil.

3.5. Anti-wear Mechanism and Phenomenological Make-up of Tribofilms

The addition of fluorinated ZnO nanoparticles to ZDDP_350 lowered and stabilized friction values and remarkably improved wear performance as compared to base oil containing no additives. Interestingly, ZDDP_350+ZnOFM also exhibited superior tribological performance than ZDDP_350. Elucidating the differences in the properties of tribofilms formed with formulation (A) ZDDP_350+ZnOFM and (B) ZDDP_350 can provide critical insights into the role of plasma functionalized ZnO in enhancing the anti-wear performance of ZDDP.

Combined SPM, XANES and XPS results were used to create feasible layered models of tribofilms for these samples as shown in figure 12. The in-operando stress-induced tribofilms formed with formulation (A) has a layered pad-like structure. The bottom layer close to a steel substrate is comprised of iron oxides, while the center region has the presence of zinc and/ iron sulfates and/sulfides. The upper region 5-60 nm of tribofilms is dominated with the formation of glassy zinc phosphates with a trace amount of iron phosphates formed near the bulk region of tribofilm. The topmost layer up to 5-8 nm exhibits the presence of metal fluorides presumably formed due to the contribution of fluorine atoms from the plasma coated ZnO nanoparticles. The schematic of the layered tribofilm formed with ZDDP_350 formulation is shown in figure 12(B). Interestingly, top layers in ZDDP_350 tribofilms are dominated with iron-bound phosphorus in contrast to ZDDP_350+ZnOFM wherein zinc phosphate was present in the near-surface region of tribofilms. Beneath these top layers of short-chain iron phosphates are iron and/ zinc sulfates/sulfides. The bulk of ZDDP_350 tribofilms contains the majority of iron oxides, while the contribution from phosphorus and sulfur chemistries is not significant.

We hypothesize that the improved stability of ZnO nanoparticles in the base oil-induced due to methacrylate polymeric coatings facilitate adsorption and entrainment of core-shell nanoparticles between surface asperities in contact at the tribological interface. The high

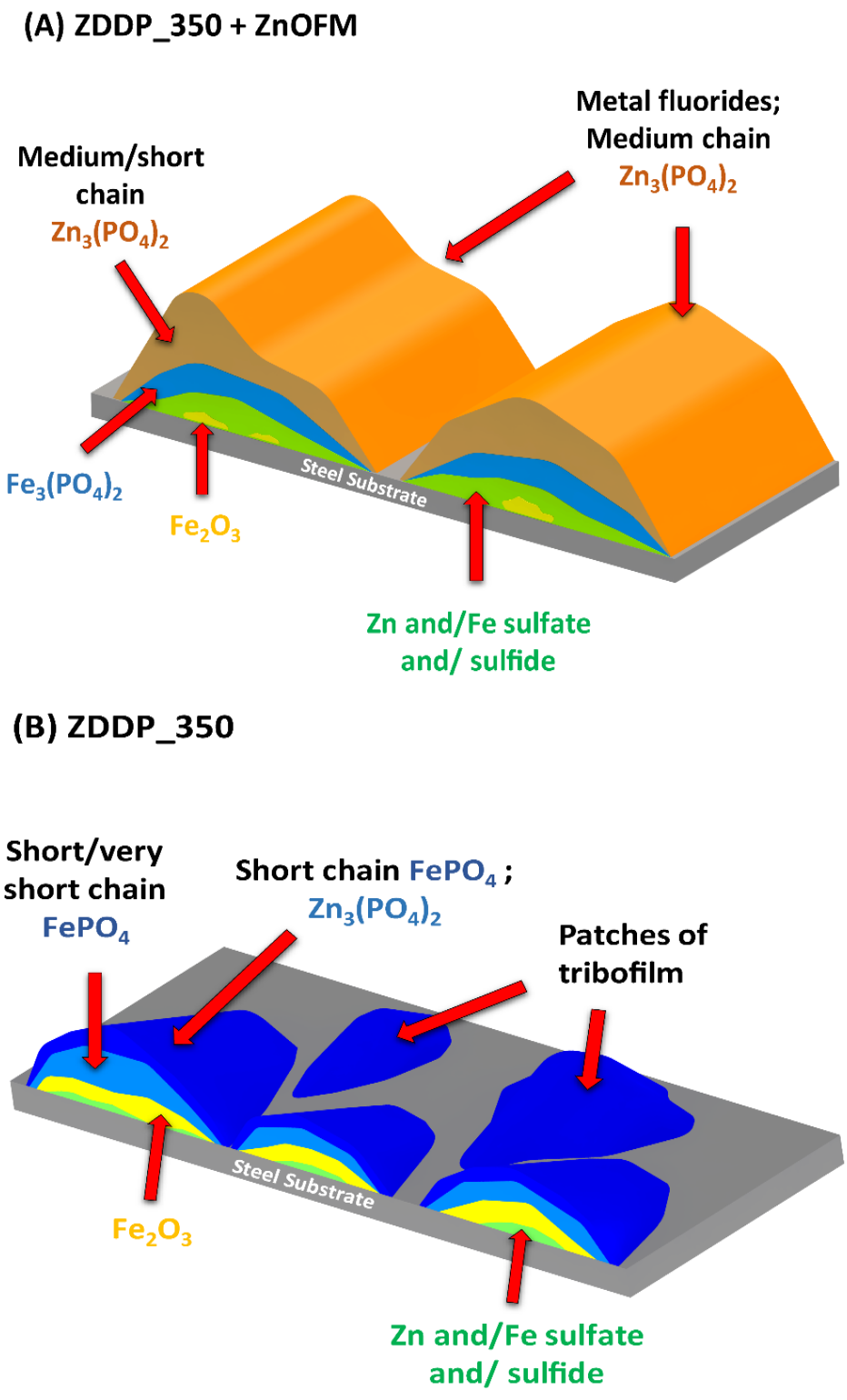

Figure 12. Schematics of tribofilms generated from samples (A) ZDDP_350 + ZnOFM (B) ZDDP_350.

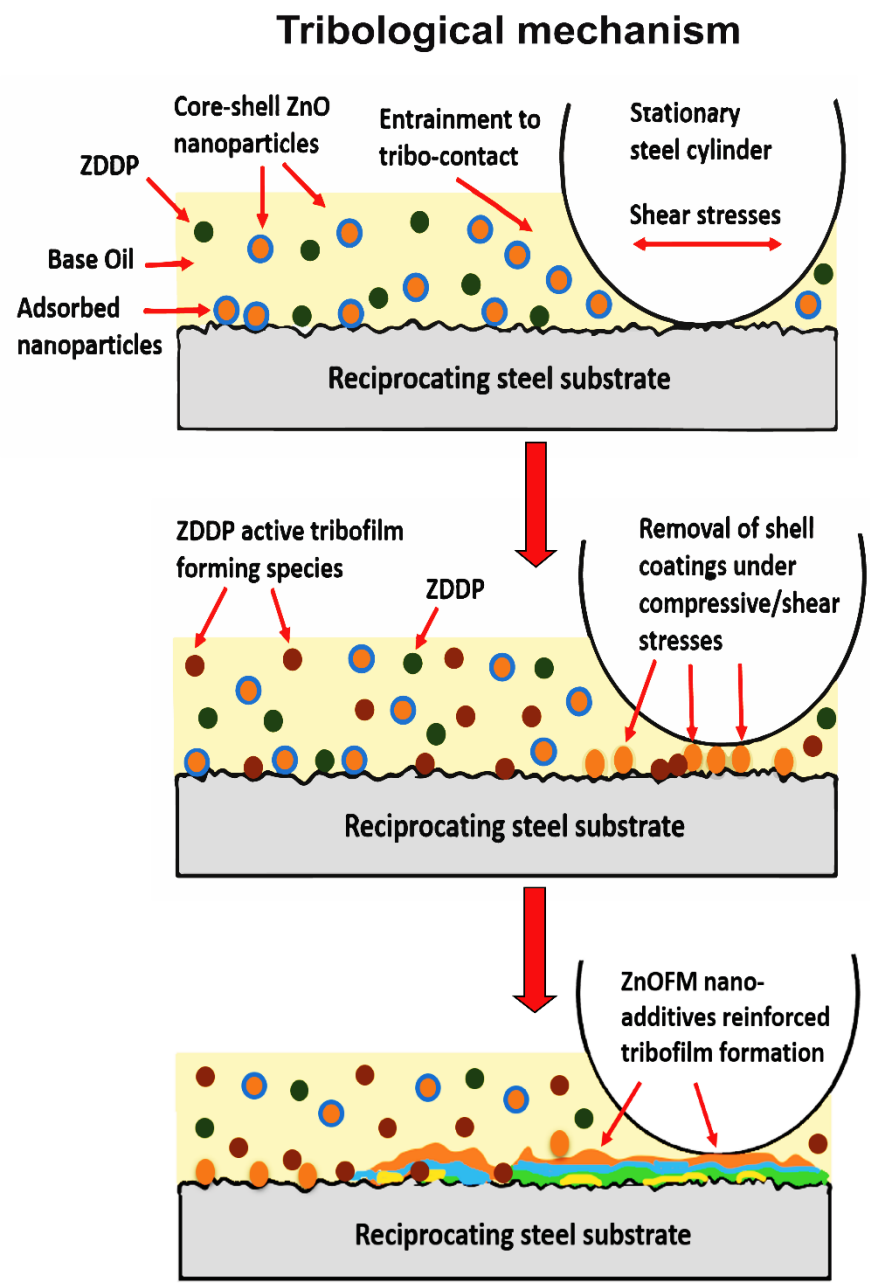

Figure 13. Schematic diagram explaining anti-wear mechanism and tribofilm formation in the presence of lubrication containing fluorinated ZnO nanoparticles.

temperature and shear/compressive stresses experienced at the asperity contacts can remove shells of encapsulated nano-additives and induce interactions between chemical species of ZnOFM and ZDDP.

Phenomenological model of fluorinated ZnO nanoparticles tribological mechanism is shown in figure 13. The determination of the exact steps involved in this synergistic interaction is beyond the scope of this research work. It is also interesting to note that the chain length and concentration of zinc phosphates present in the tribofilms generated by ZnOFM+ZDDP_350 are greater than that of ZDDP_350. It can be postulated that the extra Zn atoms provided from ZnOFM are enhancing cross-linking of phosphate films and promoting the increased formation of zinc polyphosphates which were initially formed by ZDDP at the interface.

4. CONCLUSIONS

This study demonstrates the efficacy of surface capped ZnO nano-additives to deliver tribologically beneficial chemistry at the interface and their contribution in the operando formation of surface protective tribochemical films. Core-shell ZnO nanoparticles coated with fluorocarbon polymeric films were synthesized by pulsed plasma polymerization and were used as additives to formulate nano-lubricants with a reduced amount of ZDDP. Fluorinated ZnO nano-additives exhibited remarkably significant improvement in lubricating performance, especially in terms of wear protection in comparison to ZDDP. In fact, the oil blend formulated with fluorinated ZnO nanoparticles and reduced amount of ZDDP (350 ppm of P) outperformed the formulation with the industrially used amount of ZDDP (700 ppm of P). However, when non-functionalized ZnO nanoparticles were used in lubricating oil by themselves, or in combination with ZDDP, worst friction and wear outcomes were observed. This deterioration in tribological properties was attributed to the antagonistic interaction of non-functionalized ZnO nanoparticles and ZDDP and their failure to promote stable tribofilm formation at the interface.

In the testing conditions employed in this study, synergistic interactions between fluorinated ZnO and ZDDP generated patchy chemical tribofilms with relatively higher thickness

than that of the only ZDDP derived tribofilms. Compared to only ZDDP (350 ppm of P) containing lubrication, a mixture of fluorinated ZnO and ZDDP (350 ppm of P) formed tribofilms much faster and this highlighted the prominent role of extra F and Zn atoms in promoting the generation of stable interfacial tribofilms.

XANES and XPS analysis revealed that tribofilms derived from the mixture of fluorinated ZnO and ZDDP has the surface and bulk chemistry dominated with zinc polyphosphates with small, but certainly beneficiary, presence of metal fluorides in the near-surface region. In contrast, lubrication with only ZDDP (350 ppm of P) resulted in the formation of thin surface layers of zinc and/ iron polyphosphates covering bulk (the majority of layers) with iron oxide films. The advanced tribological performance of nano-additives is attributed to these differences in the physical and chemical properties of tribofilms. The key steps involved in the anti-wear performance of additive mixture of capped ZnO nanoparticles and ZDDP are the entrainment of nano-additives at the tribological interface, removal of shell coatings under shear/compressive stresses, and subsequent contribution of extra Zn and F atoms from nano-additives in enhancing cross-linking and concentration of zinc phosphates films generated by ZDDP.

In summation, this work clearly indicates that the encapsulated ZnO nano-additives notably protect wear of sliding surfaces and thus, show great potential for replacement, and/or reduction, of the advantageous, but problematic, phosphorus-containing additives used in conventional lubricants.

ACKNOWLEDGMENTS

Tribological tests were conducted at Argonne National Laboratory. The support provided by Dr. Ali Erdemir is gratefully acknowledged. XANES experiments were conducted at the

Canadian Light Source, Saskatoon, Saskatchewan, Canada that is supported by NSERC, NRC, CIHR and the University of Saskatchewan.

SUPPORTING INFORMATION

Friction and wear tribological test results for optimum concentration ZnO and 4 hour duration tests are supplied as the supporting information. FTIR characterization results of plasma polymer coatings and digital image of formulated nano-lubricant is also provided. Optical profilometry characterization results of wear scar developed on cylinder test specimen are included with 2D and 3D images. Additionally, XPS Fluorine 1s spectra for ZnOFM test specimen exhibiting presence of fluorinated ZnO nanoparticle rich tribofilm is added for the reference.

REFERENCES

[1] W.B. Anderson, G.H. Guinther, Engine Oil Fuel Economy: Benefits and Potential Debits of Low Viscosity Engine Oil, in: SAE Tech. Pap., SAE International, 2019.

[2] V. Wong, S. Tung, Overview of automotive engine friction and reduction trends–Effects of surface, material, and lubricant-additive technologies, Friction. 4 (2016) 1–28. doi:10.1007/s40544-016-0107-9.

[3] V. Macián, B. Tormos, S. Ruiz, G. Miró, Low viscosity engine oils: Study of wear effects and oil key parameters in a heavy duty engine fleet test, Tribol. Int. 94 (2016) 240–248. doi:https://doi.org/10.1016/j.triboint.2015.08.028.

[4] H. Spikes, Low- and zero-sulphated ash, phosphorus and sulphur anti-wear additives for engine oils, Lubr. Sci. 20 (2008) 103–136. doi:10.1002/ls.57.

[5] R.B. Rastogi, J.L. Maurya, V. Jaiswal, Low sulfur, phosphorus and metal free antiwear additives: Synergistic action of salicylaldehyde N(4)-phenylthiosemicarbazones and its different derivatives with Vanlube 289 additive, Wear. 297 (2013) 849–859. doi:https://doi.org/10.1016/j.wear.2012.10.003.

[6] S. HA, The history and mechanism of ZDDP, Tribol. Lett. - TRIBOL LETT. 17 (2004) 469–489. doi:10.1023/B:TRIL.0000044495.26882.b5.

[7] J. Zhang, H. Spikes, On the Mechanism of ZDDP Antiwear Film Formation, Tribol. Lett. 63 (2016) 24. doi:10.1007/s11249-016-0706-7.

[8] H. Fujita, H.A. Spikes, The formation of zinc dithiophosphate antiwear films, Proc. Inst. Mech. Eng. Part J J. Eng. Tribol. 218 (2004) 265–278. doi:10.1243/1350650041762677.

[9] N.N. Gosvami, J.A. Bares, F. Mangolini, A.R. Konicek, D.G. Yablon, R.W. Carpick, Mechanisms of antiwear tribofilm growth revealed in situ by single-asperity sliding contacts, Science (80-.). 348 (2015) 102–106. doi:10.1126/science.1258788.

[10] B.G. Bunting, K. More, S. Lewis, T. Toops, Phosphorous Poisoning and Phosphorous Exhaust Chemistry with Diesel Oxidation Catalysts, in: SAE Tech. Pap., SAE International, 2005. doi:10.4271/2005-01-1758.

[11] M. Desanker, X. He, J. Lu, P. Liu, D.B. Pickens, M. Delferro, T.J. Marks, Y.-W. Chung, Q.J. Wang, Alkyl-Cyclens as Effective Sulfur- and Phosphorus-Free Friction Modifiers for Boundary Lubrication, ACS Appl. Mater. Interfaces. 9 (2017) 9118–9125. doi:10.1021/acsami.6b15608.

[12] A. Erdemir, Review of engineered tribological interfaces for improved boundary lubrication, Tribol. Int. 38 (2005) 249–256. doi:https://doi.org/10.1016/j.triboint.2004.08.008.

[13] R. Zhang, D. Qiao, X. Liu, Z. Guo, L. Hu, L. Shi, Well Dispersive TiO2 Nanoparticles as Additives for Improving the Tribological Performance of Polyalphaolefin Gel Lubricant, Ind. Eng. Chem. Res. 57 (2018) 10379–10390. doi:10.1021/acs.iecr.8b01694.

[14] V. Sharma, R.B. Timmons, A. Erdemir, P.B. Aswath, Interaction of plasma functionalized TiO2 nanoparticles and ZDDP on friction and wear under boundary lubrication, Appl. Surf. Sci. 489 (2019) 372–383. doi:https://doi.org/10.1016/j.apsusc.2019.05.359.

[15] L. Zhang, L. Chen, H. Wan, J. Chen, H. Zhou, Synthesis and Tribological Properties of Stearic Acid-Modified Anatase (TiO2) Nanoparticles, Tribol. Lett. 41 (2011) 409–416. doi:10.1007/s11249-010-9724-z.

[16] H. Xie, B. Jiang, J. He, X. Xia, F. Pan, Lubrication performance of MoS2 and SiO2 nanoparticles as lubricant additives in magnesium alloy-steel contacts, Tribol. Int. 93 (2016) 63–70. doi:https://doi.org/10.1016/j.triboint.2015.08.009.

[17] D.X. Peng, Y. Kang, R.M. Hwang, S.S. Shyr, Y.P. Chang, Tribological properties of diamond and SiO2 nanoparticles added in paraffin, Tribol. Int. 42 (2009) 911–917. doi:https://doi.org/10.1016/j.triboint.2008.12.015.

[18] B.T. Seymour, W. Fu, R.A.E. Wright, H. Luo, J. Qu, S. Dai, B. Zhao, Improved Lubricating Performance by Combining Oil-Soluble Hairy Silica Nanoparticles and an Ionic Liquid as an Additive for a Synthetic Base Oil, ACS Appl. Mater. Interfaces. 10 (2018) 15129–15139. doi:10.1021/acsami.8b01579.

[19] B.T. Seymour, R.A.E. Wright, A.C. Parrott, H. Gao, A. Martini, J. Qu, S. Dai, B. Zhao, Poly(alkyl methacrylate) Brush-Grafted Silica Nanoparticles as Oil Lubricant Additives: Effects of Alkyl Pendant Groups on Oil Dispersibility, Stability, and Lubrication Property,

ACS Appl. Mater. Interfaces. 9 (2017) 25038–25048. doi:10.1021/acsami.7b06714.

[20] T. Sui, B. Song, Y. Wen, F. Zhang, Bifunctional hairy silica nanoparticles as high-performance additives for lubricant, Sci. Rep. 6 (2016) 22696. doi:10.1038/srep22696.

[21] V. Cortes, J.A. Ortega, Evaluating the Rheological and Tribological Behaviors of Coconut Oil Modified with Nanoparticles as Lubricant Additives, Lubricants. 7 (2019). doi:10.3390/lubricants7090076.

[22] V.S. Jatti, T.P. Singh, Copper oxide nano-particles as friction-reduction and anti-wear additives in lubricating oil, J. Mech. Sci. Technol. 29 (2015) 793–798. doi:10.1007/s12206-015-0141-y.

[23] A.H. Battez, R. González, J.L. Viesca, J.E. Fernández, J.M.D. Fernández, A. Machado, R. Chou, J. Riba, CuO, ZrO2 and ZnO nanoparticles as antiwear additive in oil lubricants, Wear. 265 (2008) 422–428. doi:https://doi.org/10.1016/j.wear.2007.11.013.

[24] and G.R.F. Nicholaos G. Demas, Robert A. Erck, Cinta Lorenzo-Martin, Oyelayo O. Ajayi, Experimental Evaluation of Oxide Nanoparticles as Friction and Wear Improvement Additives in Motor Oil, J. Nanomater. (2017). doi:https://doi.org/10.1155/2017/8425782.

[25] W.G. Xue, Z.H. Zhao, P. Wang, Z.L. Jin, X.H. Xu, X.G. Zhou, Performance Study of Zinc Oxide Nanoparticles for Lubricant Oil, in: Curr. Micro-Nano Sci. Technol., Trans Tech Publications Ltd, 2015: pp. 195–204. doi:10.4028/www.scientific.net/AMR.1118.195.

[26] M. Ferreira Trajano, E. Moura, K. Ribeiro, S. Alves, Study of Oxide Nanoparticles as Additives for Vegetable Lubricants, Mater. Res. 17 (2014) 1124–1128. doi:10.1590/1516-1439.228213.

[27] G. Zhou, Y. Zhu, X. Wang, M. Xia, Y. Zhang, H. Ding, Sliding tribological properties of 0.45% carbon steel lubricated with Fe3O4 magnetic nano-particle additives in baseoil, Wear. 301 (2013) 753–757. doi:https://doi.org/10.1016/j.wear.2013.01.027.

[28] K. Vyavhare, P.B. Aswath, Tribological Properties of Novel Multi-Walled Carbon Nanotubes and Phosphorus Containing Ionic Liquid Hybrids in Grease, Front. Mech. Eng. 5 (2019) 15. doi:10.3389/fmech.2019.00015.

[29] I.E. Uflyand, V.A. Zhinzhilo, V.E. Burlakova, Metal-containing nanomaterials as lubricant additives: State-of-the-art and future development, Friction. 7 (2019) 93–116. doi:10.1007/s40544-019-0261-y.

[30] Y.Y. Wu, W. Tsui, T. Liu, Experimental analysis of tribological properties of lubricating oils with nanoparticle additives, Wear. 262 (2007) 819–825. doi:10.1016/j.wear.2006.08.021.

[31] J. Zhou, Z. Wu, Z. Zhang, W. Liu, Q. Xue, Tribological behavior and lubricating

mechanism of Cu nanoparticles in oil, Tribol. Lett. 8 (2000) 213–218. doi:10.1023/A:1019151721801.

[32] J. Zhou, J. Yang, Z. Zhang, W. Liu, Q. Xue, Study on the structure and tribological properties of surface-modified Cu nanoparticles, Mater. Res. Bull. 34 (1999) 1361–1367. doi:https://doi.org/10.1016/S0025-5408(99)00150-6.

[33] A.H. Battez, R. González, D. Felgueroso, J.E. Fernández, M. del Rocío Fernández, M.A. García, I. Peñuelas, Wear prevention behaviour of nanoparticle suspension under extreme pressure conditions, Wear. 263 (2007) 1568–1574. doi:https://doi.org/10.1016/j.wear.2007.01.093.

[34] A.H. Battez, J.E.F. Rico, A.N. Arias, J.L.V. Rodriguez, R.C. Rodriguez, J.M.D. Fernandez, The tribological behaviour of ZnO nanoparticles as an additive to PAO6, Wear. 261 (2006) 256–263. doi:https://doi.org/10.1016/j.wear.2005.10.001.

[35] D. Kim, L.A. Archer, Nanoscale Organic−Inorganic Hybrid Lubricants, Langmuir. 27 (2011) 3083–3094. doi:10.1021/la104937t.

[36] Y. Gao, G. Chen, Y. Oli, Z. Zhang, Q. Xue, Study on tribological properties of oleic acid-modified TiO2 nanoparticle in water, Wear. 252 (2002) 454–458. doi:https://doi.org/10.1016/S0043-1648(01)00891-2.

[37] B. Li, X. Wang, W. Liu, Q. Xue, Tribochemistry and antiwear mechanism of organic--inorganic nanoparticles as lubricant additives, Tribol. Lett. 22 (2006) 79–84. doi:10.1007/s11249-005-9002-7.

[38] H. Kato, K. Komai, Tribofilm formation and mild wear by tribo-sintering of nanometer-sized oxide particles on rubbing steel surfaces, Wear. 262 (2007) 36–41. doi:https://doi.org/10.1016/j.wear.2006.03.046.

[39] B.M. Ginzburg, O.F. Kireenko, A.A. Shepelevskii, L.A. Shibaev, D.G. Tochilnikov, A.M. Leksovskii, Thermal and Tribological Properties of Fullerene-Containing Composite Systems. Part 2. Formation of Tribo-Polymer Films during Boundary Sliding Friction in the Presence of Fullerene C60, J. Macromol. Sci. Part B. 44 (2005) 93–115. doi:10.1081/MB-200044604.

[40] F. Svahn, S. Csillag, Formation of Low-Friction Particle/Polymer Composite Tribofilms by Tribopolymerization, Tribol. Lett. 41 (2011) 387–393. doi:10.1007/s11249-010-9721-2.

[41] H.S. Khare, I. Lahouij, A. Jackson, G. Feng, Z. Chen, G.D. Cooper, R.W. Carpick, Nanoscale Generation of Robust Solid Films from Liquid-Dispersed Nanoparticles via in Situ Atomic Force Microscopy: Growth Kinetics and Nanomechanical Properties, ACS Appl. Mater. Interfaces. 10 (2018) 40335–40347. doi:10.1021/acsami.8b16680.

[42] Kalyani, R.B. Rastogi, D. Kumar, Synthesis, Characterization, and Tribological Evaluation of SDS-Stabilized Magnesium-Doped Zinc Oxide (Zn0.88Mg0.12O)

Nanoparticles as Efficient Antiwear Lubricant Additives, ACS Sustain. Chem. Eng. 4 (2016) 3420–3428. doi:10.1021/acssuschemeng.6b00472.

[43] L. Wu, Y. Zhang, G. Yang, S. Zhang, L. Yu, P. Zhang, Tribological properties of oleic acid-modified zinc oxide nanoparticles as the lubricant additive in poly-alpha olefin and diisooctyl sebacate base oils, RSC Adv. 6 (2016) 69836–69844. doi:10.1039/C6RA10042B.

[44] S.M. Alves, B.S. Barros, M.F. Trajano, K.S.B. Ribeiro, E. Moura, Tribological behavior of vegetable oil-based lubricants with nanoparticles of oxides in boundary lubrication conditions, Tribol. Int. 65 (2013) 28–36. doi:https://doi.org/10.1016/j.triboint.2013.03.027.

[45] K. Parekh, X. Chen, P.B. Aswath, Synthesis of Fluorinated ZDDP Compounds, Tribol. Lett. 34 (2009) 141–153. doi:10.1007/s11249-008-9373-7.

[46] S. Bagi, K. Vyavhare, P.B. Aswath, Tribological characteristics of greases with and without metallo-organic friction-modifiers, Tribol. - Mater. Surfaces Interfaces. (2018) 1–14. doi:10.1080/17515831.2018.1542790.

[47] V. Sharma, R. Timmons, A. Erdemir, P.B. Aswath, Plasma-Functionalized Polytetrafluoroethylene Nanoparticles for Improved Wear in Lubricated Contact, ACS Appl. Mater. Interfaces. 9 (2017) 25631–25641. doi:10.1021/acsami.7b06453.

[48] V. Sharma, C. Gabler, N. Doerr, P.B. Aswath, Mechanism of tribofilm formation with P and S containing ionic liquids, Tribol. Int. 92 (2015) 353–364. doi:10.1016/j.triboint.2015.07.009.

[49] V. Sharma, A. Erdemir, P.B. Aswath, An analytical study of tribofilms generated by the interaction of ashless antiwear additives with ZDDP using XANES and nano-indentation, Tribol. Int. 82 (2015) 43–57. doi:10.1016/j.triboint.2014.09.019.

[50] W. Thomas, C.-B. Ulrike, L. Claudia, D. Ferenc, T. Sándor, S.-B. Johannes, J. Martin, Wear of different material pairings for the cylinder liner – piston ring contact, Ind. Lubr. Tribol. 70 (2018) 687–699. doi:10.1108/ILT-07-2017-0218.

[51] V. Sharma, N. Doerr, P.B. Aswath, Chemical–mechanical properties of tribofilms and their relationship to ionic liquid chemistry, RSC Adv. 6 (2016) 22341–22356. doi:10.1039/C6RA01915C.

[52] R. Mourhatch, P.B. Aswath, Tribological behavior and nature of tribofilms generated from fluorinated ZDDP in comparison to ZDDP under extreme pressure conditionsPart II: Morphology and nanoscale properties of tribofilms, Tribol. Int. 44 (2011) 201–210. doi:10.1016/j.triboint.2010.10.035.

[53] V.S.J.B.T.P.B. Aswath, Tribological Interaction of Plasma-Functionalized Polytetrafluoroethylene Nanoparticles with ZDDP and Ionic Liquids, Tribol. Lett. 66 (2018) 107. doi:10.1007/s11249-018-1060-8.

[54] D. Dowson, G.R. Higginson, Reflections on Early Studies of Elasto-Hydrodynamic Lubrication, in: R.W. Snidle, H.P. Evans (Eds.), IUTAM Symp. Elastohydrodyn. Micro-Elastohydrodynamics, Springer Netherlands, Dordrecht, 2006: pp. 3–21.

[55] A. Dyson, H. Naylor, A.R. Wilson, Paper 10: The Measurement of Oil-Film Thickness in Elastohydrodynamic Contacts, Proc. Inst. Mech. Eng. Conf. Proc. 180 (1965) 119–134. doi:10.1243/PIME_CONF_1965_180_072_02.

[56] R. Mourhatch, P.B. Aswath, Tribological behavior and nature of tribofilms generated from fluorinated ZDDP in comparison to ZDDP under extreme pressure conditions—Part II: Morphology and nanoscale properties of tribofilms, Tribol. Int. 44 (2011) 201–210. doi:10.1016/j.triboint.2010.10.035.

[57] M. Nicholls, M. Najman, Z. Zhang, M. Kasrai, P. Norton, P. Gilbert, The contribution of XANES spectroscopy to tribology, Can. J. Chem. 85 (2007) 816–830. doi:10.1139/V07-093.

[58] S. Wan, A.K. Tieu, Q. Zhu, H. Zhu, S. Cui, D.R.G. Mitchell, C. Kong, B. Cowie, J.A. Denman, R. Liu, Chemical nature of alkaline polyphosphate boundary film at heated rubbing surfaces, Sci. Rep. 6 (2016) 26008. doi:10.1038/srep26008.

[59] K. Vyavhare, S. Bagi, M. Patel, P.B. Aswath, Impact of Diesel Engine Oil Additives–Soot Interactions on Physiochemical, Oxidation, and Wear Characteristics of Soot, Energy & Fuels. 33 (2019) 4515–4530. doi:10.1021/acs.energyfuels.8b03841.

[60] T. Cebe, N. Ahuja, F. Monte, K. Awad, K. Vyavhare, P. Aswath, J. Huang, M. Brotto, V. Varanasi, Novel 3D-printed methacrylated chitosan-laponite nanosilicate composite scaffolds enhance cell growth and biomineral formation in MC3T3 pre-osteoblasts, J. Mater. Res. 35 (2020) 58–75. doi:DOI: 10.1557/jmr.2018.260.

[61] R. Mourhatch, P.B. Aswath, Tribological behavior and nature of tribofilms generated from fluorinated ZDDP in comparison to ZDDP under extreme pressure conditions—Part 1: Structure and chemistry of tribofilms, Tribol. Int. 44 (2011) 187–200. doi:10.1016/j.triboint.2010.10.018.

[62] A. Somayaji, P.B. Aswath, The Role of Antioxidants on the Oxidation Stability of Oils with F-ZDDP and ZDDP, and Chemical Structure of Tribofilms Using XANES, Tribol. Trans. 52 (2009) 511–525. doi:10.1080/10402000902745499.

[63] Z. Yin, M. Kasrai, M. Fuller, G.M. Bancroft, K. Fyfe, K.H. Tan, Application of soft X-ray absorption spectroscopy in chemical characterization of antiwear films generated by ZDDP Part I: the effects of physical parameters, Wear. 202 (1997) 172–191. doi:https://doi.org/10.1016/S0043-1648(96)07272-9.

[64] Z. Yin, M. Kasrai, G.M. Bancroft, K. Fyfe, M.L. Colaianni, K.H. Tan, Application of soft X-ray absorption spectroscopy in chemical characterization of antiwear films generated by ZDDP Part II: the effect of detergents and dispersants, Wear. 202 (1997) 192–201. doi:https://doi.org/10.1016/S0043-1648(96)07273-0.

[65] B. Kim, R. Mourhatch, P.B. Aswath, Properties of tribofilms formed with ashless dithiophosphate and zinc dialkyl dithiophosphate under extreme pressure conditions, Wear. 268 (2010) 579–591. doi:10.1016/j.wear.2009.10.004.

[66] B. Kim, Tribological performance of ashless antiwear additives under extreme pressure conditions, (2010).

[67] S. Yang, D. Wang, G. Liang, Y.M. Yiu, J. Wang, L. Liu, X. Sun, T.-K. Sham, Soft X-ray XANES studies of various phases related to LiFePO4 based cathode materials, Energy Environ. Sci. 5 (2012) 7007–7016. doi:10.1039/C2EE03445J.

Supporting Information

1) FTIR characterization of plasma fluoropolymer film deposited on ZnO nanoparticles.

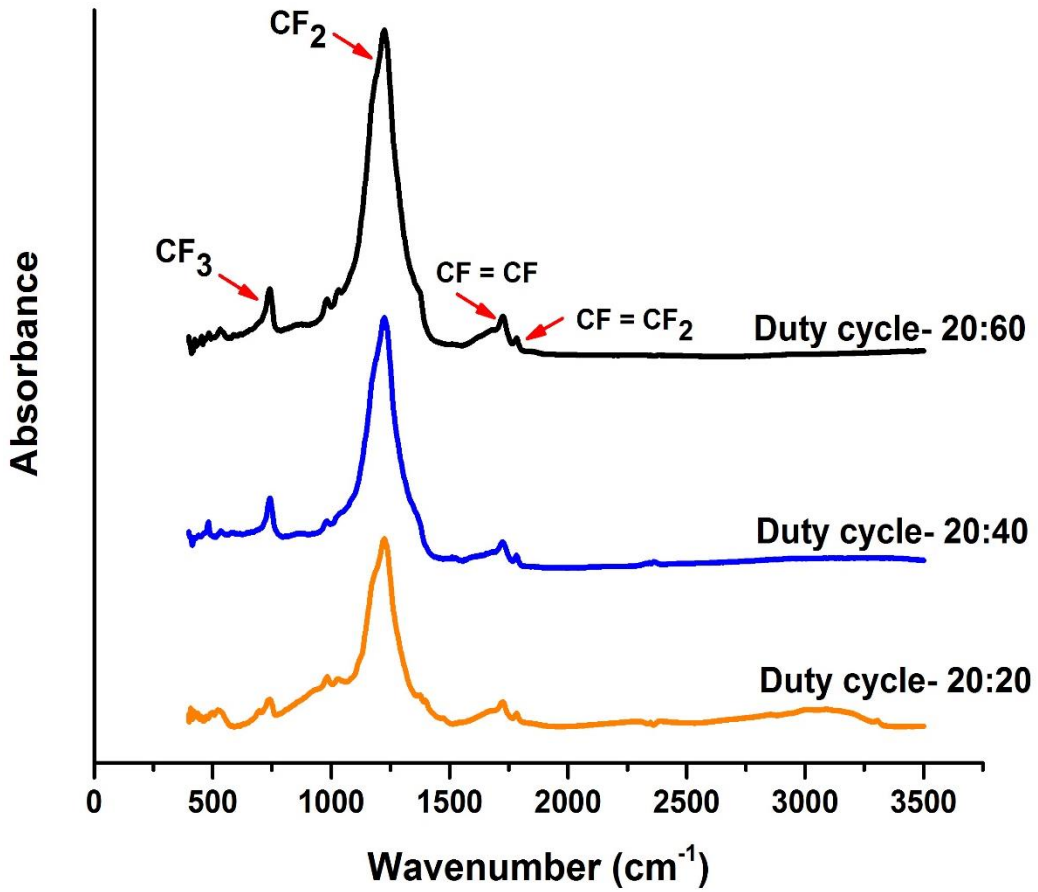

Figure S1. FTIR spectra of plasma films deposited from perfluorohexane monomer at different duty cycle.

2) Wear results obtained after tribological test conducted for determining optimum concentration of non-functionalized ZnO nanoparticles. Results clearly indicates improved anti-wear performance at 0.3 wt.% concentration of ZnO nanoparticles.

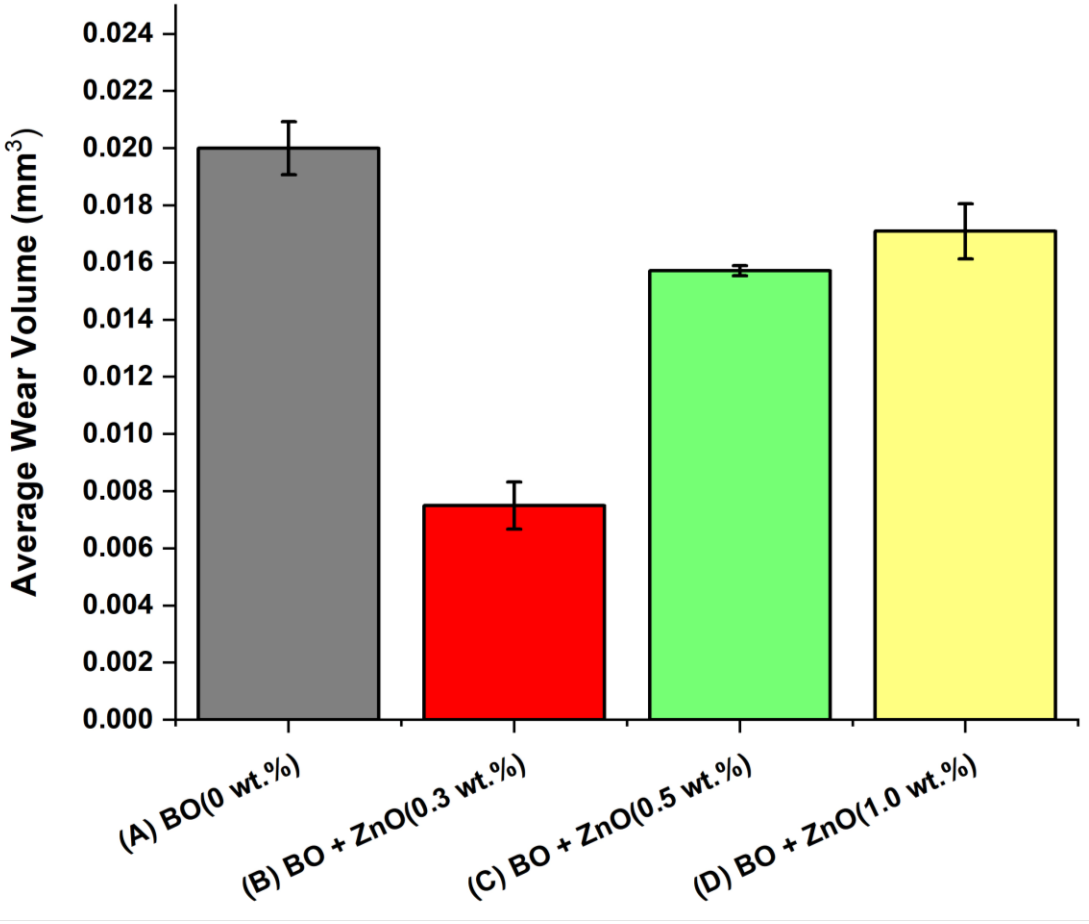

Figure S2. Average wear volume of results of oil formulations containing non-functionalized ZnO nanoparticles at 0, 0.3, 0.5, and 1.0 wt.% in Group III base oil.

3) Uniform dispersion of fluorinated ZnO nanoparticles in Group III base oil.

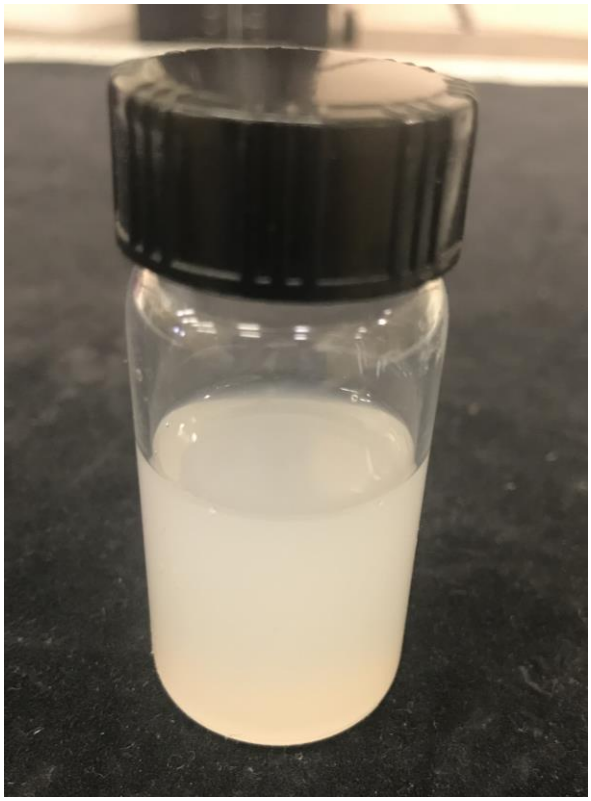

Figure S3. Image of oil formulation prepared with fluorinated ZnO and Group III base oil after sonication.

4) Optical images of the wear scar developed on flat steel test specimen.

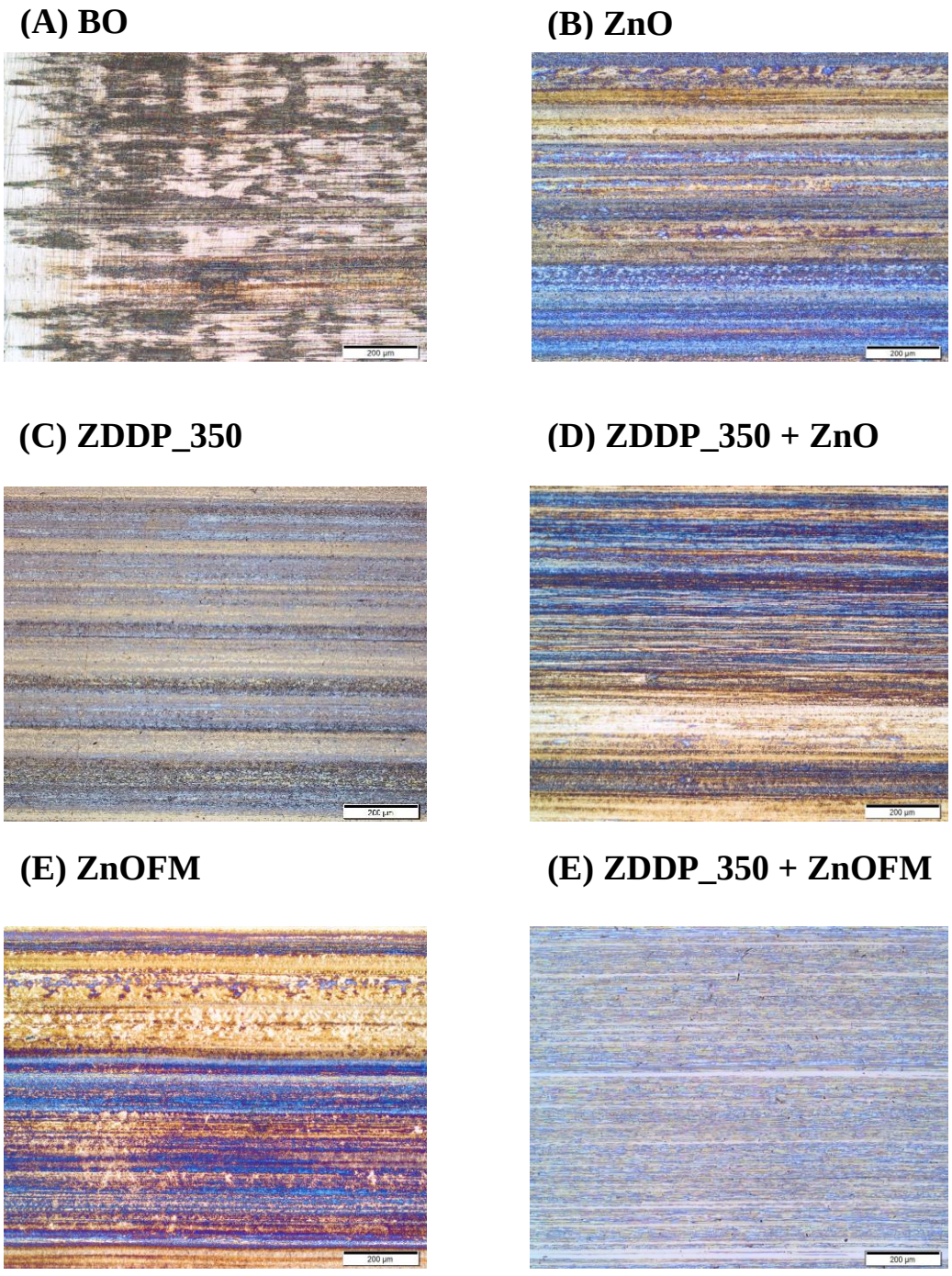

Figure S4. Optical images of the wear scar developed on flat steel specimen with test oils (A) BO; (B) ZnO; (C) ZDDP_350; (D) ZDDP_350 + ZnO; (E) ZnOFM; (F) ZDDP_350 + ZnOFM.

5) 4 Hour tribological tests to determine tribological performance of developed fluorinated ZnO nano-additives for extended rubbing time.

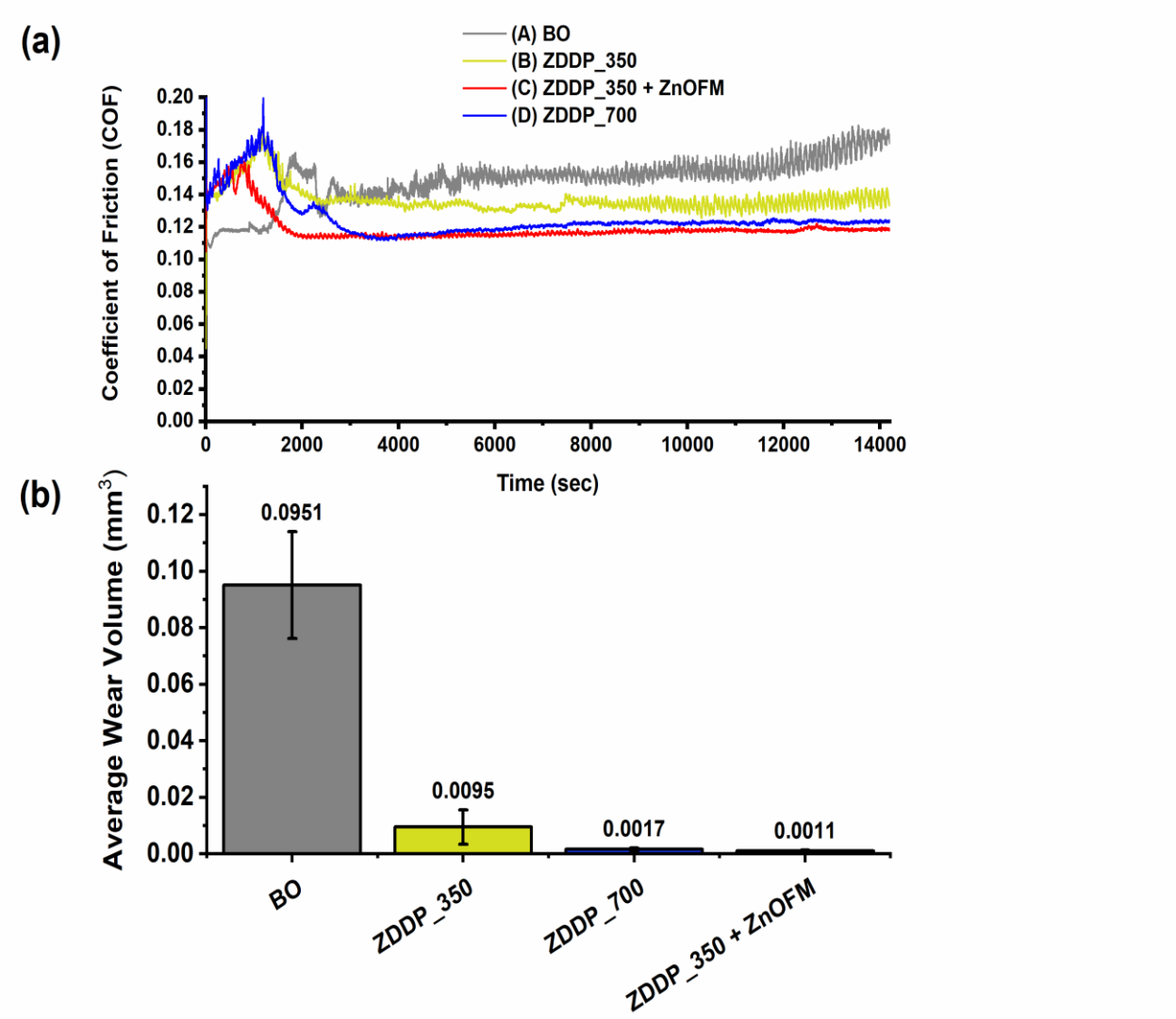

Figure S5. Tribological results of 4 hour duration test (a) Friction plots (b) Wear volume data.

6) Wear scar developed on steel cylinder specimen characterized using optical profilometry.

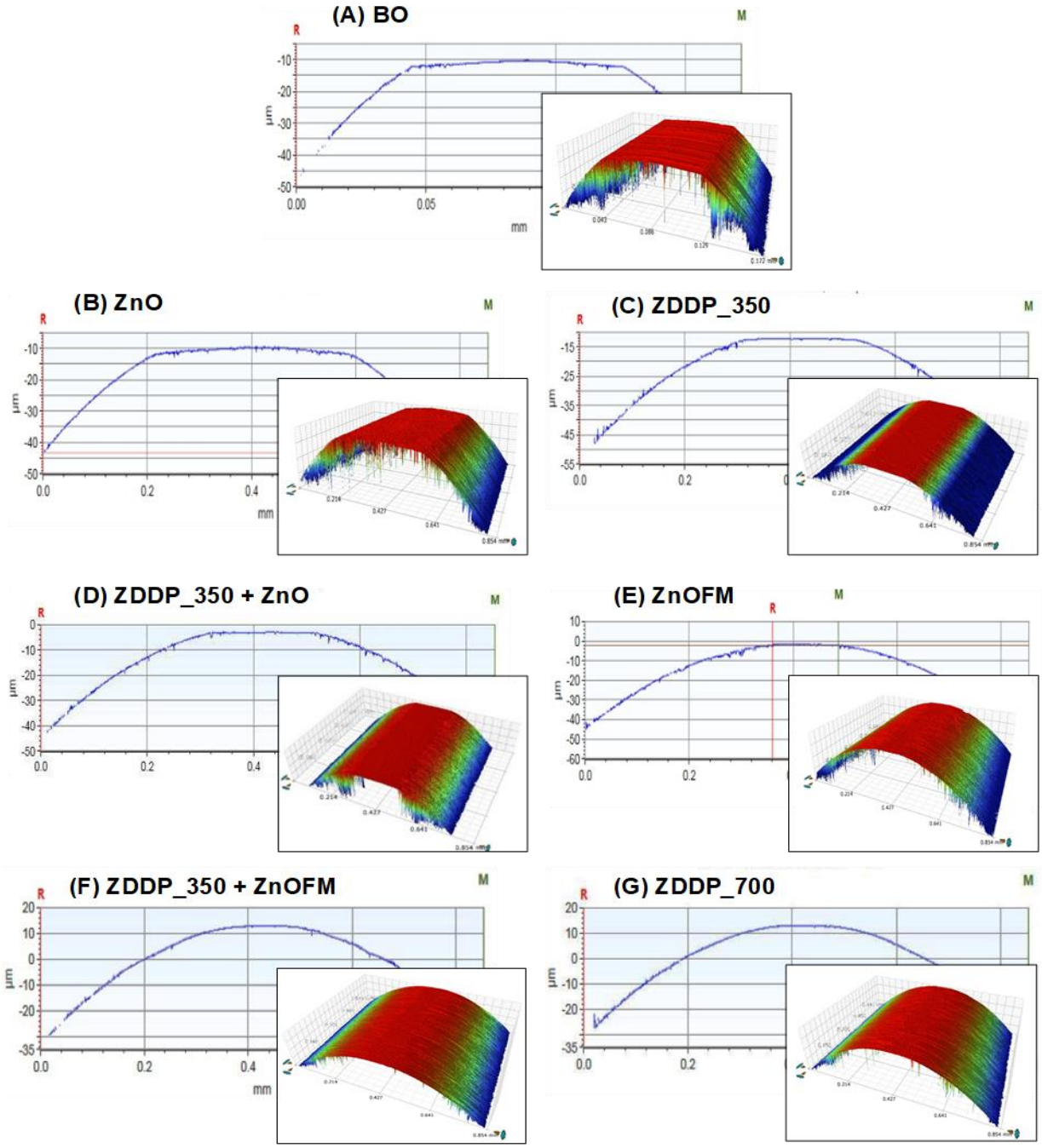

Figure S6. Two and three- dimensional representation of the volume loss of cylinder test specimens obtained using optical profilometry.

7) XPS characterization of tribofilms formed by fluorinated ZnO nanoparticles based lubrication for 1 Hour tribological test.

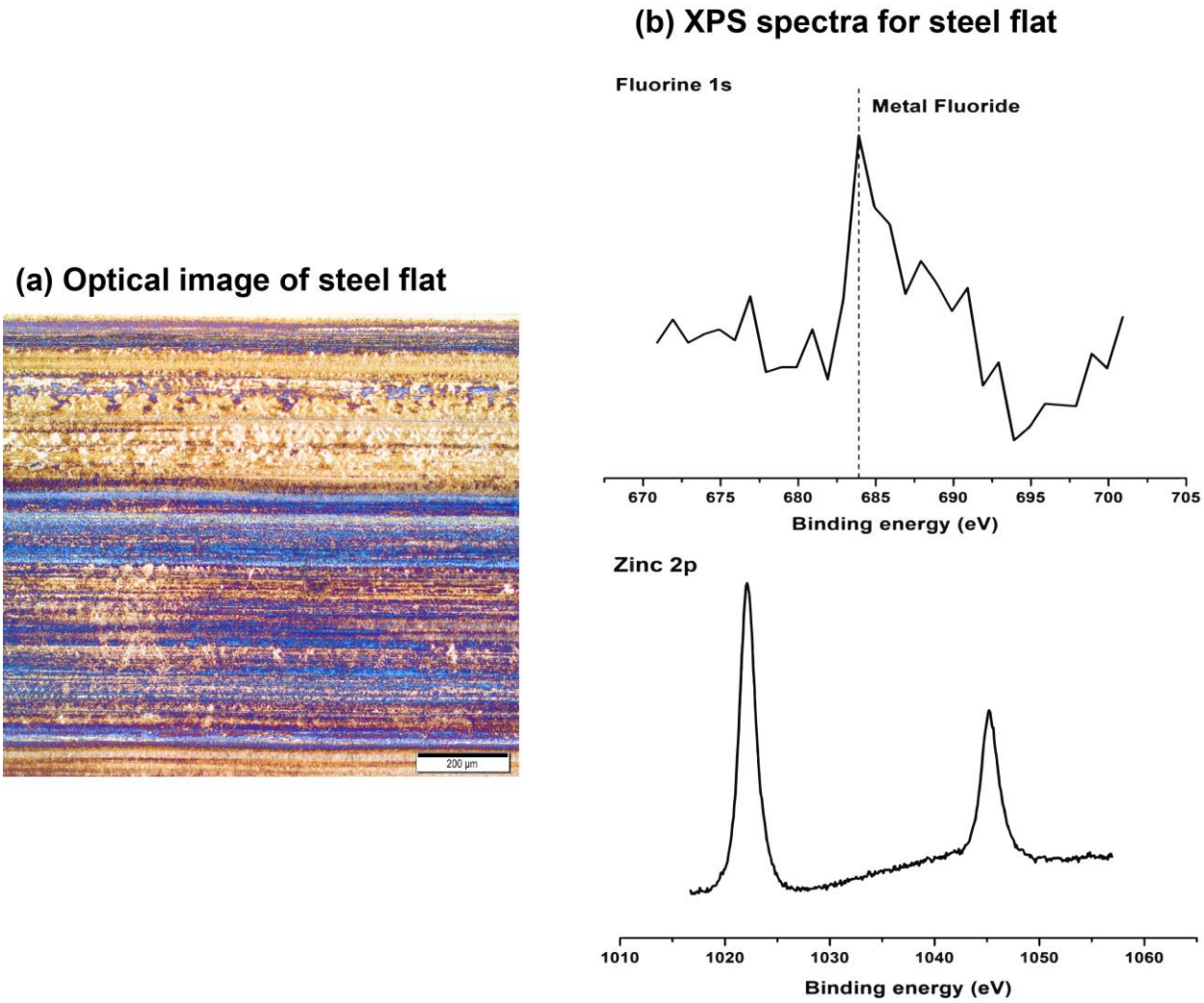

Figure S7. Characterization of wear scar developed during ZnOFM 1 hour tribological test (a) Optical image of wear surface of the steel flat (b) XPS fluorine 1s and zinc 2p spectra for flat steel specimen.

CHAPTER 3

POLYMER COATED ZnO NANOPARTICLES DRIVEN ROBUST INTERFACIAL TRIBOFILMS LEADING TO IMPROVED WEAR PROTECTION UNDER BOUNDARY LUBRICATION REGIME

Kimaya Vyavhare, Richard B. Timmons, Ali Erdemir, Brian Edwards, and Pranesh B. Aswath

Submitted to: Langmuir (September 2020)

ABSTRACT

This work provides a comprehensive characterization of the tribochemistry across the interfaces formed between sliding ferrous surfaces and polymer-coated and/ un-coated ZnO lubricant additives from the perspective of developing nano-lubricants to improve friction and wear of moving engine components. The functionalized nano-additives were synthesized by encapsulating ZnO nanoparticles with boron and acrylate-based polymer films as-deposited via plasma polymerization. Subsequently, various oil formulations were prepared with non-functionalized ZnO and boron coated ZnO nanoparticles (ZnOBM), including mixtures containing the conventional additive zinc dialkyl dithiophosphate (ZDDP). Tribological tests were carried out using reciprocating cylinder-on-flat tribometer operating under boundary lubrication regime. Extensive characterization techniques like atomic force microscopy, X-ray absorption near-edge spectroscopy and X-ray photoelectron spectroscopy were employed to elucidate morphology, topography, and chemical composition of interfacial tribofilms. Mechanical test results revealed that ZnOBM additives (by themselves) and in combination with ZDDP significantly improve wear performance (up to 95%) compared to the base oil. Electrical contact resistance results acquired in-situ during tribological tests demonstrated that lubricants containing ZnOBM nanoparticles at sliding interfaces undergo tribochemical reactions to form stable tribofilms that reduce friction and wear. Spectral analyses indicated that ZnOBM nanoparticles, by themselves, form iron borate and zinc oxide-based interfacial tribofilms and lead to superior tribological performance. Interestingly, ZnOBM nanoparticles interact synergistically with ZDDP to form a hierarchical interface of boron-doped tribofilms, with zinc-iron polyphosphates at the surface and iron oxide, zinc, and/ iron sulfides in the bulk. These encouraging results suggest the potential effective use of the developed ZnOBM nanoparticles as a high-performance automotive lubricant additive.

1. INTRODUCTION

Achieving the optimum lubrication of tribological interfaces in minimizing friction and wear in internal combustion engines remains an important goal in terms of achieving improved energy efficiency, minimized fuel consumption, and reduced automotive gas emissions.[1] The moving mechanical interfaces of engine components frequently operate under boundary lubrication and are protected against friction and wear by solid sacrificial films known as "tribofilms". The efficacy of tribofilms to ensure slippage and long wear life relies on the effective interaction of lubricant additives-solid contacts, film formation kinetics, mechanical, and chemical properties of the tribofilms. Clearly, the tribological performance of boundary lubricated sliding contacts are strongly dependent on the ability of lubricant additives to form effective tribofilms.

Lubricants, containing nanoscale material additives, have been investigated for over a decade in terms of tribological applications. Due to their small size and relatively large surface areas, nanomaterials can easily penetrate within microscale asperities of diverse geometrical contacts, fill the nano-grooves or serve as a roller on the interface, thus providing increased contact surfaces to distribute high shear stresses, and reduce friction and wear.[2] Additionally, the application of nanomaterials as an engine oil additive provides superior wear protection, with less adverse impact on the exhaust emission catalysts, compared with the conventional engine oil additives like ZDDP.[3–12] Extensive research efforts have been devoted to evaluating both the potential of metal[13–17] and metal oxide[18–24] nanoparticles to improve tribological protection of interfaces operating under mixed or boundary lubrication. Among these additives, zinc oxide (ZnO) nanoparticles have received considerable interest reflecting their non-toxicity, high surface energy, unique antioxidant, electrical, and thermal conductivity properties. Several researchers have attributed tribological properties of ZnO nanoparticles to their size and concentration in the

base oils.[25–30] ZnO nanoparticles can improve anti-wear performance by creating a lubricant film and reduce the friction of moving surfaces. Kalyani et al. examined the effect of the particle size of ZnO nanoparticles on the tribological behavior of paraffin oil and, using SEM-EDX elemental analysis of worn surfaces, confirmed the adsorption of ZnO nano-additives on the rubbing surfaces.[31] However, relatively high surface energy makes ZnO nanoparticles significantly susceptible to agglomeration and precipitation in the nonpolar lubricant base stock. These dispersibility problems negatively affect tribological performance and make nano-additives inactive at the high stress moving contacts.

In this paper, we report a significant advance in this line of research centered on the use of surface-modified ZnO nanoparticles additives to create stable protective tribofilms and improve tribological performance. In the present study, chemical surface tailoring of ZnO nanoparticles was achieved using plasma-enhanced chemical vapor deposition technique (PECVD) to deposit films of specific composition on these particles to not only provide adequate dispersions in the oil but to also evaluate the potential value of added chemical moieties (i.e boron-based films) in terms of improving overall tribofilm efficacy. In effect, the ZnO nanoparticles are used as active carriers to provide boron chemistry at the tribological contacts to assist in the formation of anti-wear films of oxide glasses, similar to that of glassy phosphate-based tribofilms formed by phosphorus in ZDDP. We postulated that boron coated ZnO nano-additives might form both chemically reacted tribofilms and tribo-stress compacted films to enhance significantly the wear protection of boundary lubricated moving interfaces.

It is well established that formation and removal kinetics of interfacial tribofilms, enriched with triboactive elements from lubricant additives, can favorably improve wear protection and friction reduction. Extensive surface and in-situ interfacial characterizations have been carried out

on tribofilms derived from phosphorus-containing lubricant additives, such as ZDDP and ionic liquids.[32–44] For example, Ramoun et al. used auger electron spectroscopy, X-ray absorption near-edge spectroscopy (XANES), and nano-indentation techniques to evaluate chemical and physical properties of ZDDP derived tribofilms and reported that films are grown from bottom to top in chemically varying layered structures, wherein the top layer is enriched with zinc and iron phosphates.[45,46] The driving force for the formation of such phosphate-based tribofilms was investigated by Gosvami et al.[47] and Zhang et al.[32] They proposed that ZDDP derived tribofilms formed as a result of stress-assisted, thermally activated chemical reactions at the sheared contacts and that the growth rate increases exponentially with both temperature and compressive stresses. In contrast, Mosey et al., using first-principles molecular dynamics simulation, suggested that the tribofilms are formed due to pressure-induced cross-linking of zinc phosphate molecules generated from thermal or catalytic decomposition of ZDDP at the tribological contact.[48] They proposed that zinc atoms act as a network forming agents to connect loosely interacting zinc phosphate molecules providing higher cross-linked, longer chain polyphosphates films.[49], Unlike ZDDP, metal-free additives, require a source of metal cations to form tribofilms. Most recently, Zhou et al. showed that ionic liquid tribofilms, enriched in iron phosphates and iron oxides, form through multi-step processes including direct interaction of nascent ferrous surface, IL decomposition products, and wear debris mixing via mechanical and chemical deposition.[50] The aforementioned tribofilm formation mechanism or growth models for phosphorus-containing additives are not applicable to nano-additives. Well dispersed nanoparticles in lubricating oils provide tribological benefits via any one or combination of the following lubricating mechanism: rolling effect, mending effect, polishing effect, tribofilm formation. Tribofilm formation is the most prevailing theory and most researchers have attributed better lubrication performance of nano-lubricants to

the adsorption and formation of protective layers of nanoparticles on the rubbing surfaces.[2] Tribofilms formed by nano-additives are reported to be composed of nano-particles agglomerates, discrete nanoparticles, or nano-particle reinforced tribopolymer networks.[51] For example, Sui et al. proposed that bifunctionalized hairy silica nanoparticles when used as lubricant additive fill the nanogrooves and form protective films on the wear surface, which continuously delaminate and regenerate during the rubbing process. The tribofilm forming mechanism was attributed to the functionalization of silica nanoparticles with amino and alkyl ligands.[52] Recently, Khare et al. used colloidal probe atomic force microscopy to study in-situ kinetics of nanoparticle tribofilm growth at nanoscale resolution. They proposed that tribofilms from nanoparticle anti-wear additive nucleate due to entrapment of nanoparticles at surface irregularities and grow via a process of stress-induced tribosintering.[51]

Based on the tribofilm lubricating mechanism of both phosphorus-based anti-wear additives and nano-materials, we hypothesized that the combination of boron-coated ZnO nanoparticles, with a significantly lower amount of ZDDP (350 ppm of phosphorus) as a lubricant additive, could lead to a further improvement in tribological performance. The complex stress-assisted thermochemical reactions between ZDDP decomposed products, boron, zinc oxide, and nascent metal surface during the rubbing process would hopefully enhance tribofilm formation, strengthen the protective tribofilms through cross-linking, and improve the binding of the tribofilm to the metallic substrate, ultimately leading to enhanced anti-wear and anti-friction protection. Additionally, as noted earlier, ZDDP poisons catalytic exhaust treatment systems and thus increase automotive tailpipe emissions. As such, a reduction of ZDDP concentrations is of significant interest with respect to developing improved environmentally friendly lubricants. Currently, additive technology contains ZDDP at 700-800 ppm of phosphorus and any further reduction in

phosphorus concentration will significantly decrease wear protection in low viscosity oils. We postulated that the additional chemistries provided by coated ZnO nanoparticles might permit reduction of ZDDP, without compromising tribological properties. For that reason, a concentration of ZDDP of only 350 ppm was tested in these experiments. To explore this hypothesis, ZnO nanoparticles (20-30 nm size) were surface modified by PECVD and were initially encapsulated with boron based polymer films followed with acrylate based coatings to promote dispersion of ZnO nanoparticles in the base oil. Test oil formulations were prepared with both functionalized and non-functionalized ZnO nanoparticles, in combination with and without ZDDP, to draw comparative conclusions. In this study, the tribological experiments were conducted on a ferrous interface, under boundary lubrication condition. Electrical contact resistance (ECR) measurements were collected *in-situ* during the rubbing test to correlate the presence or absence of tribofilm formation with frictional behavior and to assess the time required to form stable tribofilms. Advanced surface characterization techniques, i.e. AFM, XANES, and XPS, were employed to elucidate the fundamental tribochemistry at the interface between the boundary layer nano-lubricant and ferrous rubbing surfaces. The spectroscopic results obtained permit identification of the chemical composition of the layered tribofilms formed due to interaction of coated ZnO and ZDDP additives. From these data, a lubricating mechanism of boron coated ZnO nano-additives is proposed. Understanding how the interface between novel ZnO nanoparticle lubricant additives and sliding surfaces works through tribochemical characterization will enable development of nano-lubricants for automotive applications with a potential of reducing energy consumption and harmful emissions.

2. EXPERIMENTAL METHODOLOGY

2.1 Materials

ZnO nanoparticles, 10-30 nm in size, were obtained from a commercial source (Sky Spring Nanomaterials). Trimethylboroxine and glycidyl methacrylate were purchased from Sigma Aldrich. The anti-wear additive ZDDP was procured from Oronite. It was derived from secondary alcohol, the details of which can be found elsewhere.[53] Group III mineral base stock (GS Caltex Kixx Lubo 4 cSt) was used for preparing test oil formulations.

2.2 Preparation of Boron-coated ZnO Nano-additives

A plasma enhanced chemical vapor deposition (PECVD) technique was employed to encapsulate ZnO nanoparticles with boron rich polymer films. This technique allows precise control over the chemistry and thickness of the films. In this study, a home built 360 º rotating reactor was used as shown in figure 1(a) to minimize nanoparticle aggregation to help achieve more uniform deposition of plasma polymer films on the ZnO nanoparticles. Initially, ZnO nanopartciles were subjected to a boron rich plasma created using trimethylboroxine organic monomer. The process parameters for plasma deposition were as follows: power – 60 W; monomer pressure – 120 mT; monomer flow rate – 2 sccm; RF frequency – 13.56 MHz. Herein, a continuous wave signal was applied first at 60 W power for 20 mins and later, pulsating plasma signal was used with sequentially reducing duty cycle from 20:30 to 20:60 (plasma on : plasma off times in ms) for 10 min each. Total deposition time was 60 min. Fourier transform infrared spectroscopy (FTIR) and XANES was conducted to examine chemical composition of plasma films deposited from trimethyl boroxine monomer. FTIR and XANES spectra of these films shown in Supporting Information section (Figure S1) confirms presence of borate-based polymer films on the surface of ZnO nanoparticles. To increase the subsequent dispersibility of nano-additives in the mineral oil, the boron-coated ZnO nanoparticles were then encapsulated with methacrylate based polymer films using glycidyl methacrylate as a precursor monomer. Coatings containing methacrylate

ligands were deposited at power – 100 W, monomer pressure – 70 mT, continuous wave plasma – 20 min, pulsating plasma with duty cycle (20:50) – 40 min. Details on plasma reactor and pulsating plasma polymer coatings can be found in our previous research work. [54,55]

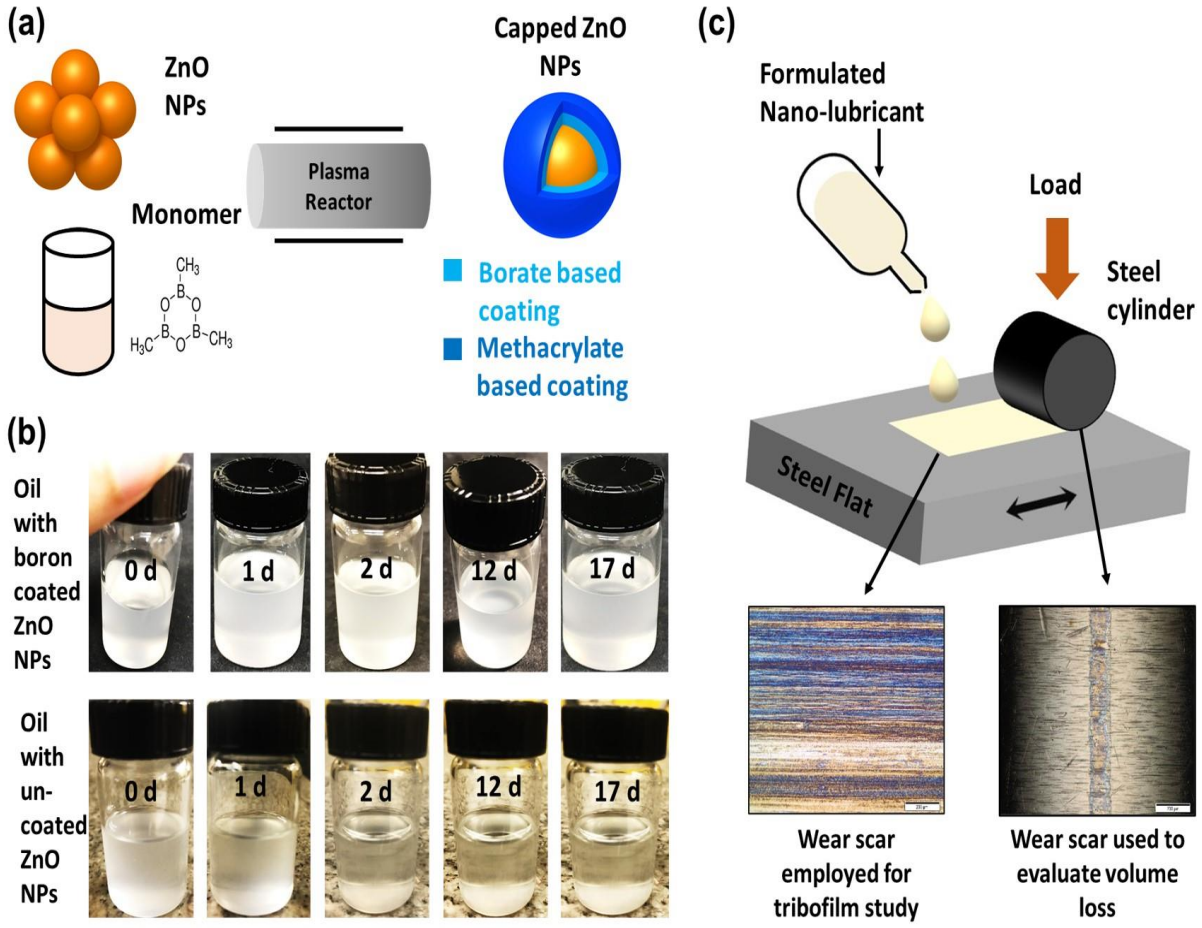

Figure 1. Schematic of (a) Synthesis of core-shell structure boron coated ZnO nanoparticles; (b) Digital pictures of test oils formulated with boron coated ZnO nanoparticles and uncoated ZnO nanoparticles depicting dispersibility of nanoparticles for 17 days; (c) Tribological tests conducted in the cylinder-on-flat configuration.

Developed plasma functionalized core-shell structure ZnO nanoparticles were later mixed into Group III mineral base oil at 0.3 wt.% , with or without ZDDP additive. Initially, tribological tests were conducted with oils containing non-functionalized ZnO nanoparticles to determine

optimum concentration of 0.3 wt.% at which improvement in both wear and friction was achieved. Results of concentration tribological tests are provided in Figure S2, Supporting Information. Therefore, in this study all nano-lubricants were prepared by mixing nanoparticles at 0.3 wt.%. The composition of the various test oil formulations utilized are provided in Table 1. Since one of the aims of this research work is to reduce phosphorus concentration in the lubricants, oil blends were formulated by adding ZDDP at only 350 ppm of phosphorus. In contrast, conventional engine lubricants contain ZDDP at 600 – 800 ppm of phosphorus.

Table 1. Details of Oil Formulations Used for Tribological Tests

Coded name	**Formulation details**
BO	Group III mineral base oil without any additives
BO + ZnO	Non-functionalized ZnO nanoparticles added at 0.3 wt.% in base oil
BO + ZnOBM	Boron coated ZnO nanoparticles added at 0.3 wt.% in base oil
BO + ZDDP	ZDDP mixed at 350 ppm of phosphorus in base oil
BO + ZDDP + ZnO	ZDDP at 350 ppm of phosphorus and non-functionalized ZnO nanoparticles at 0.3 wt.% mixed in base oil
BO + ZDDP + ZnOBM	ZDDP at 350 ppm of phosphorus and boron coated ZnO nanoparticles at 0.3 wt.% mixed in base oil

Homogenous mixing of boron-coated ZnO nanoparticles was achieved through probe sonication for 20 min. Figure 1(b) illustrates the dramatic differences in the dispersibility of coated and uncoated ZnO nanoparticles in the base oil observed over span of two weeks. For a formulation containing uncoated ZnO nanoparticles, an upper layer appears to be clearing out merely after 1 day, indicating instability and sedimentation of non-functionalized ZnO in the mineral base oil. However, a stable and homogenous system was observed with the plasma coated ZnO nanoparticles- based formulation during the entire test period of 20 days, highlighting the ability

of deposited methacrylate plasma coatings to prevent agglomeration or sedimentation of nanomaterials in the polar base oil.

2.3 Tribological Tests

A high-frequency reciprocating rig tribometer, in cylinder-on-flat test configuration, was employed to assess the anti-friction and anti-wear performance of formulated nano-lubricants as shown in figure 1(c). For this purpose, AISI 52100 steel cylinder of 4 mm × 6 mm dimension (Surface roughness (Sa): 8-9 nm; Hardness: 60-62 HRc) and steel flat of 12 mm × 12 mm dimension (Surface roughness (Sa): 10 nm; Hardness: 59-60 HRc) was utilized. Tribological tests were conducted at 100 ºC under an 82 N load for 60 min duration. A flat steel substrate was set in reciprocating motion at a stroke length of 6 mm and with a speed of 300 rpm. The rationale behind selecting line contact test configuration and above mentioned test parameters is to closely simulate the operating contact pressure and temperature experienced during piston and cylinder liner interaction in an internal combustion engine. After completion of tribological tests, the wear scars developed on both cylinder and flat were subjected for tribological performance evaluation and tribofilm analysis, respectively as depicted in figure 1(c). Before the start of the test, all steel samples were cleaned with Stoddard solution, isopropanol, and acetone. 10 µl of oil formulation was introduced at the sliding interface and boundary lubrication condition was maintained throughout the completion of the test. All tests were repeated twice to examine variations in friction and wear results for each formulation. After the completion of tribological tests, flat and cylinder specimens were stored in additive-free PAO (poly-α-olefin) oil for tribo-surface characterization.

2.4 Tribofilm Characterization Techniques

Wear scars generated on the flat steel test specimens after completion of the tribotests were employed to elucidate chemical and physical properties of tribofilms. The topography and

morphology of tribological surfaces were studied using AFM in direct contact mode. A sharp conductive AFM tip was used to raster scan the sample and acquire high resolution 3D images of wear scars detailing surface characteristics.

XANES was employed to evaluate the chemistry and geometric makeup of the chemical compounds in the tribofilms. XANES experiments were conducted at the Canadian Light Source synchrotron facility. Phosphorus and Sulfur K-edge spectra were obtained at a soft X-ray microcharacterization beamline (SXRMB), operating at the energy range from 1.7 keV to 10 keV with a photon resolution more than 3.3 x 10-4 InSb (111). The photon beam spot size was kept at 1 mm × 2 mm. The phosphorus L-edge and boron K-edge spectra were collected at a variable line spacing plane grating monochromator (VLSPGM) beamline, which provides an energy range from 5.5 eV to 250 eV, a photon resolution of more than 10000 E/ΔE, and was operated using 100 µm × 100 µm beam spot size. The zinc and iron L-edge and oxygen K-edge spectra were acquired at a spherical grating monochromator (SGM) beamstation using 100 µm × 100 µm beam spot size at the energy range of 250-2000 eV and a photon resolution of more than 5000 E/ΔE. Spectra at the SGM beamline were collected using 100 µm × 100 µm beam spot size. XANES spectra were acquired in total electron yield (TEY) by probing the near-surface region of the sample and in fluorescence yield (FY) mode by measuring photon-absorption from the bulk of the sample. For XANES analysis, flat steel samples were cleaned thoroughly using hexane to remove oil residue and then loaded inside the vacuum chamber. Each sample was scanned at two different spots (center, left edge, or right edge of the wear scar) to confirm uniformity of the results.

A Kratos Axis Ultra system, equipped with a monochromatic Al Kα X-ray source, was used for XPS analyses. XPS spectra were collected by sputtering the samples using an ion gun (beam energy 4.20 keV) for about 4 min. Center/edge regions of the worn surfaces were irradiated

with a X-ray beam of 300 µm × 700 µm spot size and power of 150 W. A survey scan was conducted to identify the major elements present, while high-resolution scans were obtained for elements of interest (Zn, Fe, P, F, O).

3. RESULTS AND DISCUSSION

3.1 Friction and wear behavior

The coefficient of friction (COF) data recorded in-situ during tribological test as a function of time is presented in figure 2(a). Friction profiles for two repeat tribological tests were essentially similar and, for that reason, instantaneous COF results from only one test is shown in detail for each of the six different formulations in figure 2(a). An average COF was calculated for the last 10 min of both tests and is represented, for all formulations, in figure 2(b). Average COFs for the last 10 minutes were used to eliminate initial variability and, at the same time, to more effectively compare friction behavior, or improvement in steady state friction, for the various additives after extended sliding duration.

Friction profile for the BO sample shown in figure 2(a) exhibits varying and unstable friction response with the highest COF values compared to other formulations. Similarly, COF graph for BO + ZnO sample appears to have severe variance and high friction values throughout the test. However, in sharp contrast with these two samples, the friction coefficient obtained for oil containing only coated ZnO nanoparticles exhibits impressively lower and stable friction values. The friction response for sample (D) with only ZDDP is relatively stable for the first 35 min of the test but then exhibits higher COF values compared to oils containing coated ZnO nanoparticles (sample (C) and (F)) at longer test times. The most dramatic variation in friction behavior is observed for sample (D), containing a mixture of non-functionalized ZnO and ZDDP,

wherein for the initial 20 min the friction coefficient remained low, in fact lowest of all but then started to increase with great variance and instability.

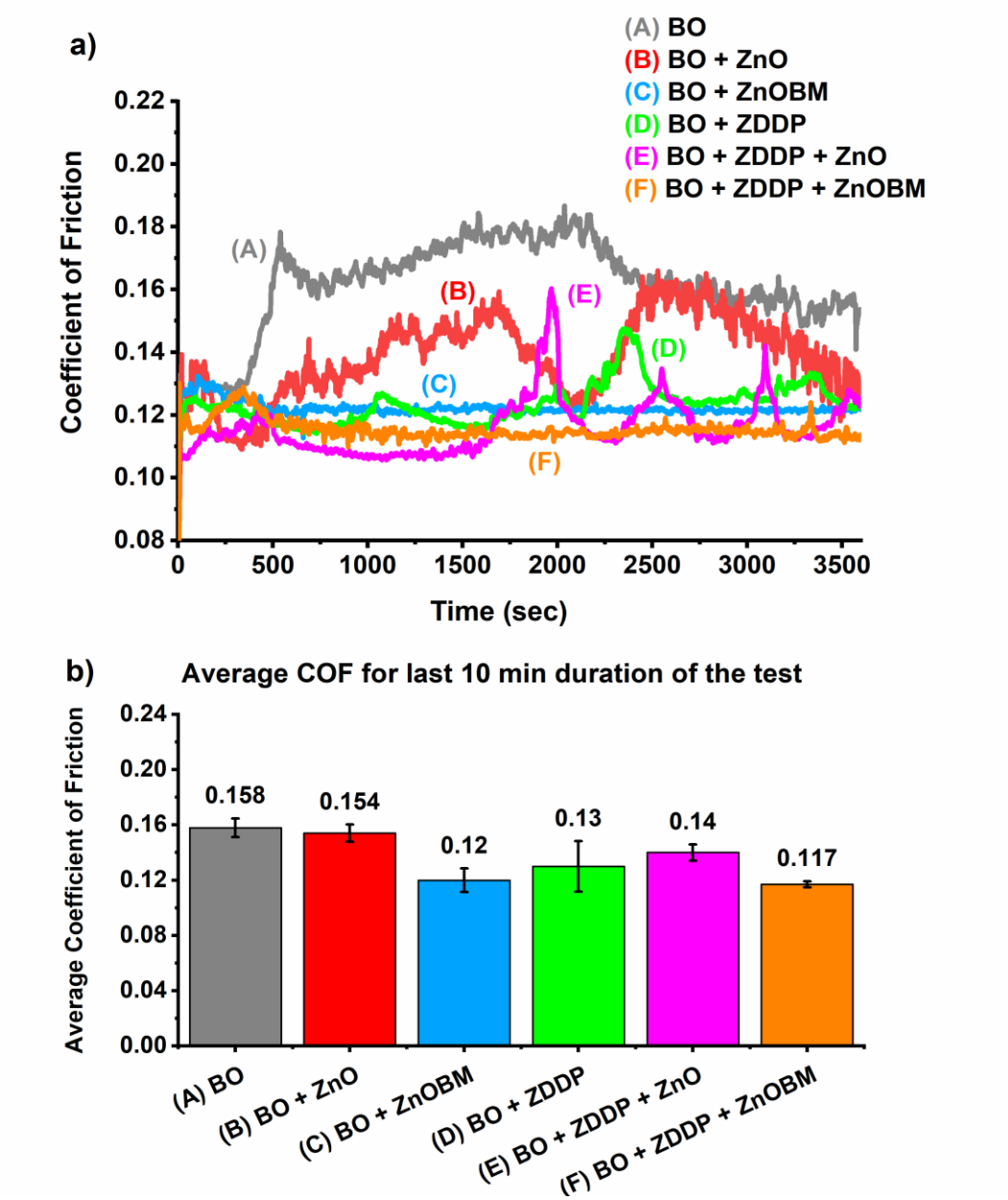

Figure 2. (a) Coefficient of friction measured as a function of time (b) average coefficient of friction for last 10 min duration of the test for formulations (A) BO; (B) BO + ZnO; (C) BO + ZnOBM; (D) BO + ZDDP; (E) BO + ZDDP + ZnO; (F) BO + ZDDP + ZnOBM.

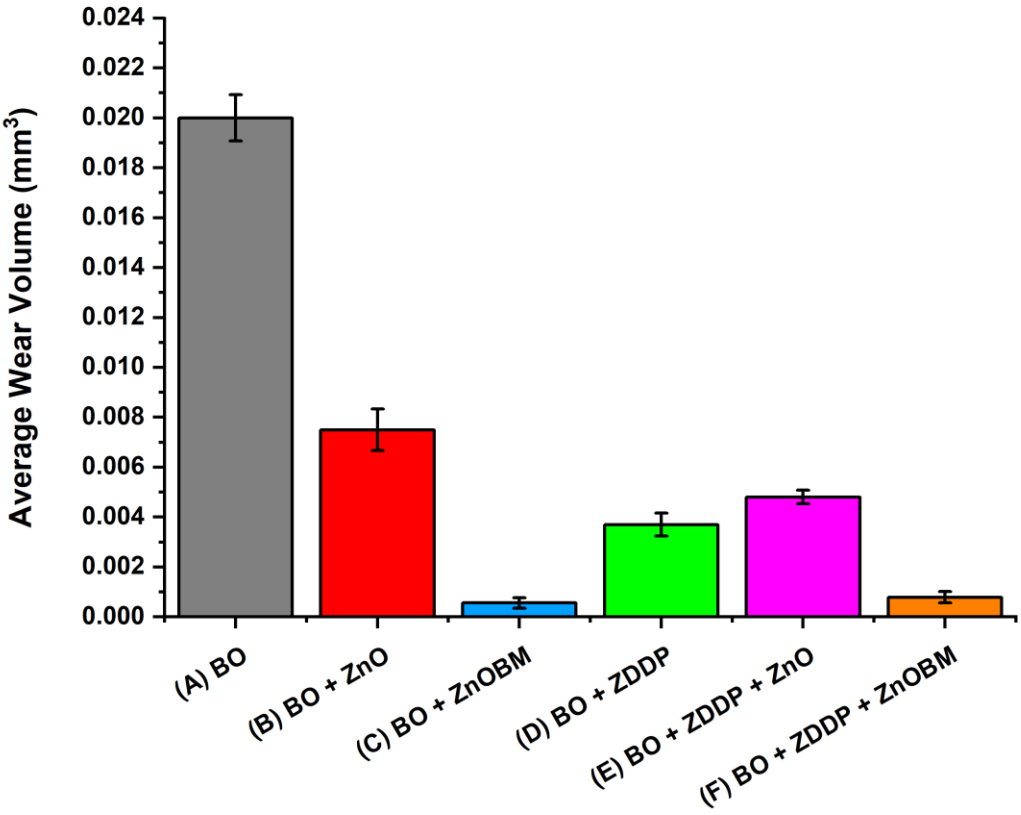

Figure 3. Wear performance of the lubricants assessed through volume loss of the cylindrical test specimens for formulations (A) BO; (B) BO + ZnO; (C) BO + ZnOBM; (D) BO + ZDDP; (E) BO + ZDDP + ZnO; (F) BO + ZDDP + ZnOBM.

The friction response of sample (D) is comparatively poorer than sample (C) with only ZDDP, which indicates that the presence of non-functionalized ZnO hindered the performance of ZDDP and instead of lowering friction fails to protect counter surfaces against high shear stresses. Sample (F) with the mixture of ZDDP and encapsulated ZnO nanoparticles exhibits the steadiest friction response of all with lower COF values especially after 20 min of the test. Additionally, analysis of the data shown in figure 2(b) indicate that the samples (B) and (D) showed 2% and 18% reduction

respectively, and samples (C) and (F) resulted in 24% and 26% reduction respectively compared to the BO sample (A).

Wear performance of nano-additives was assessed through analysis of wear scar developed on the cylinder test specimen using optical profilometer and microscope. Figure 3 displays volume loss measured after tribological tests of all formulations. To measure wear volume, average wear scar width value was obtained using optical microscopic images of the wear scars developed on the cylinder test specimens. It was very difficult to calculate the wear volume or material loss on flat test specimen as wear was exhibited through material redeposition and surface scratches (see Figure S3, Supporting Information). Therefore, to assess wear performance, wear scars developed on cylinder test specimens were used. Black error bars shown in Figure 3 represent the standard deviation between the wear volume values calculated for two repeat tribological tests. The BO sample exhibited the worst wear outcomes of all as no performance enhancing additives were added in this test oil. Sample (B) has high volume loss compared to the rest of the nano-lubricants, which also correlates with the coefficient of friction and wear profile analysis discussed earlier. On the other hand, boron coated ZnO nano-additive sample (C) exhibits better anti-wear performance (i.e. lower wear volume) in comparison with only non-functionalized ZnO (B) and only ZDDP (D). Surprisingly, wear volume for sample (E), containing a mixture of ZDDP with non-functionalized ZnO nanoparticles, is higher than the sample (D) with only ZDDP. Several studies have reported synergistic interaction of nanoparticles like WS_2, PTFE, MoS_3 with ZDDP anti-wear additives.[54,56–58] However, in this present study antagonistic interaction can be identified between non-functionalized ZnO nanoparticles and ZDDP, which resulted in high wear losses and high coefficients of friction. Notably, addition of encapsulated ZnO nanoparticles with ZDDP improved the wear performance, especially in comparison to wear data of sample (D) with only

ZDDP and sample (B) with only non-functionalized ZnO nanoparticles based lubrication. Similar, wear performance analysis can be made from the optical micrographs and 2D and 3D surface profilometry results shown in figure S4 in the supporting information section. The wear profile and pin surface of samples (C) and (F) in figure S4 appear to be quite similar and exhibit improved surface protection against high shear stresses achieved through boron coated ZnO nano-additives based lubrication.

Tribological test results reveal the advantage of functionalization of nanoparticles and extra anti-wear chemistries provided via boron coated ZnO nanoparticles in enhancing anti-friction and anti-wear protection under boundary lubrication regime. The effect of synergistic interaction between coated ZnO and ZDDP on tribofilm formation and properties of tribofilms is further evaluated and discussed in the follow sections.

3.2 Incubation time for the tribofilm formation

The tribometer used in this study was equipped with an electric setup wherein 100 mV potential was applied between countersurfaces of steel cylinder and flat to record electrical contact resistance (ECR). The ECR measurements monitor the *in-situ* formation of the protective tribofilms at the sliding interface during the test.[59] When the conductive steel cylinder and flat move against each other, the additives added in the oil form non-conductive glassy tribofilms at the interface which ultimately increases the resistance and voltage drop across the two counter surfaces. When no tribofilms are formed, direct contact between steel surface asperities results into very low resistance and voltage drops to 0 mV. It is well known that ZDDP forms glassy polyphosphate tribofilms. Thus, the ECR data in this study can be used to effectively determine the incubation times and overall dynamics of the tribofilms formations.

Figure 4 displays the voltage drop values recorded in-situ as a function of the test time.

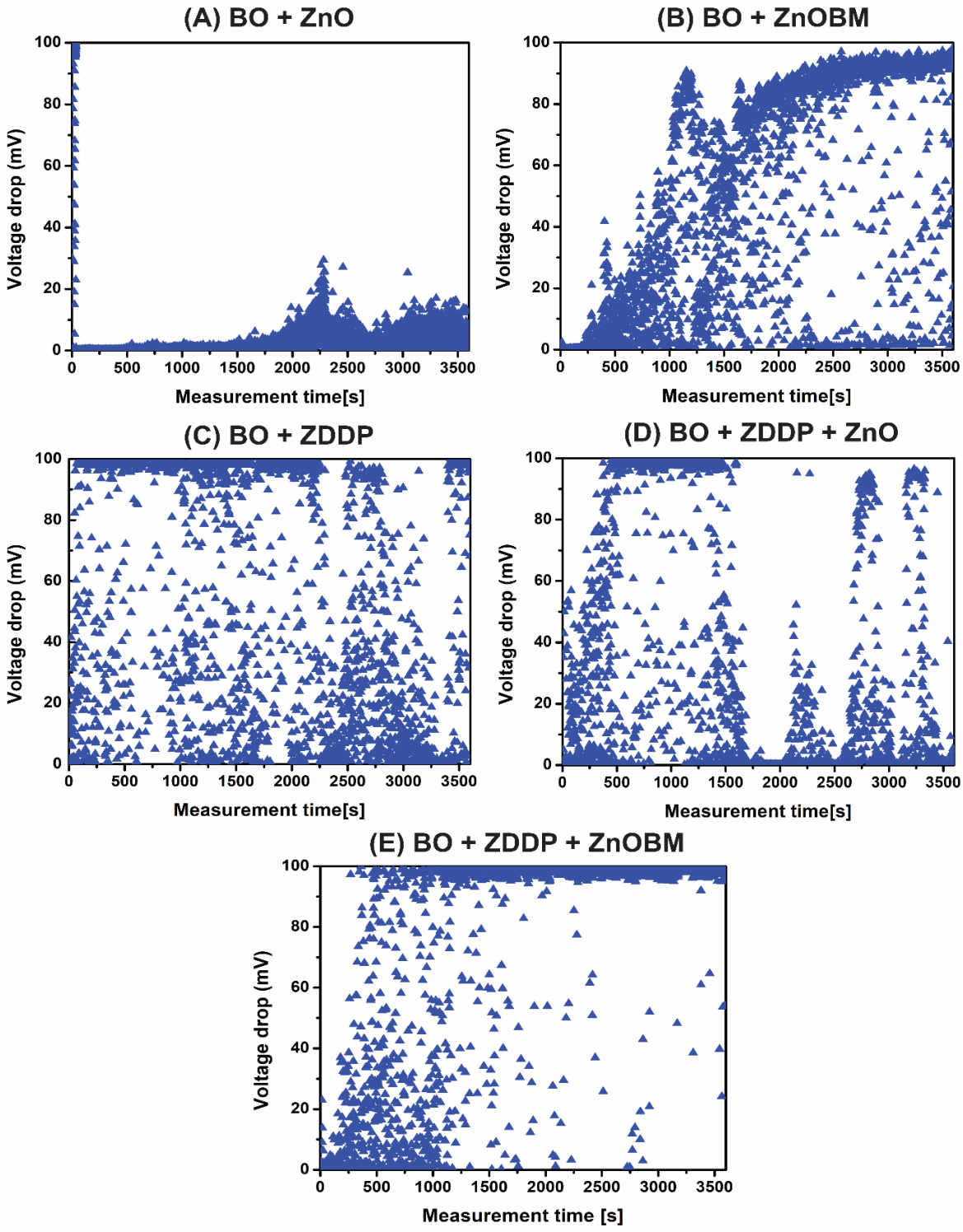

Figure 4. Electrical contact resistance data plotted as the function of test time for formulations (A) BO + ZnO; (B) BO + ZnOBM; (C) BO + ZDDP; (D) BO + ZDDP + ZnO; (E) BO + ZDDP + ZnOBM.

Voltage drop readings represented as red dots, segregated or close to 100 mV, correspond to more net coverage of tribofilms at the surface while the values close to 0 mV indicate that no stable interfacial tribofilms were formed by lubricant additives. ECR data for non-functionalized ZnO nano-additives clearly indicates that no tribofilms were formed during this test as the majority of data points are close to 0 mV. In contrast, the voltage data points for the sample with functionalized nanoparticles (ZnOBM) appear to be dispersed initially but after the first 25 min numerous data points are in the high region of the plot (75-98 mV) compared to sample (A), thus suggesting that functionalization of the ZnO nanoparticles with additional boron species available at the interface promotes tribofilm formation. The ECR plot for ZDDP sample (C) shows that the voltage drop reaches a maximum value in a very early stage of the test, thus suggesting a very short incubation time for the tribofilm formation in this case. It is important to note here that the data points are scattered and there is a clear breakdown of tribofilms near the end of the test. These observations indicate that the ZDDP added at 350 ppm of phosphorus was probably not enough to form stable tribofilms throughout the completion of the test. The ECR graph for BO + ZDDP + ZnO sample clearly shows removal of initially formed tribofilms further confirmation of the antagonistic interaction of non-functionalized ZnO nanoparticles and ZDDP. Interestingly, the ECR plot for the sample with the mixture of functionalized ZnO and ZDDP demonstrated stable tribofilm formation after merely only 10 min of testing. Additionally, the voltage drop data points are segregated, and not so dispersed as those of sample (C), highlighting the benefit of boron coated ZnO nanoparticles in promoting stable tribofilm formation, even in the presence of the low concentration of phosphorus (350 ppm).

3.3 Tribological Surface Characterization

3.3.1 Atomic Force Microscopy (AFM) Analysis

AFM was employed, in direct contact mode, to elucidate the general morphology of the worn surfaces generated with the six different test samples. Surface areas of 45 × 45 μm area were probed for each sample, keeping the z-axis (± 400 nm) constant. The topographical images obtained are shown in figure 5. Each sample was scanned at four different spots. The BO + ZnO sample exhibits regions of high surface roughness and deep scratches, and thus correlates to the higher material loss discussed earlier. The 3D wear profile of the ZDDP lubricated surface exhibits pad like morphology identifying the presence of patchy and porous tribofilms in the direction of sliding . ZDDP is well-known to form tribofilms on the sliding surfaces with island like features separated by valleys that prevent wear at the tribological interface.[61] Interestingly, topography of the surface generated with the additive mixture of non-functionalized ZnO nanoparticles and ZDDP shows the absence of anti-wear pads and the presence of regions of deep scratches with high peak to valley ratios. These observations further support removal of protective tribofilms due to antagonistic interaction between ZDDP and non-functionalized ZnO nanoparticles. On the contrary, SPM images of worn surfaces lubricated with only functionalized ZnO nanoparticles (BO + ZnOBM) and with the additive mixture of functionalized ZnO and ZDDP (BO + ZDDP + ZnOBM) reveal the presence of smooth continuous long patches of tribofilms, elongated in the direction of sliding. The binary additive system of ZnOBM and ZDDP appears to have formed comparatively thicker anti-wear pads than only ZDDP based lubrication and thus demonstrates the additional benefit of boron chemistry to form protective tribofilms at the sliding surface.

3.3.2 XANES Analysis of Interfacial Tribofilms

Results discussed in the earlier sections of ECR and surface analysis by AFM indicate that the improved tribological performance of functionalized ZnO nanoparticles might be due to the differences in the properties and formation mechanisms of the interfacial tribofilms.

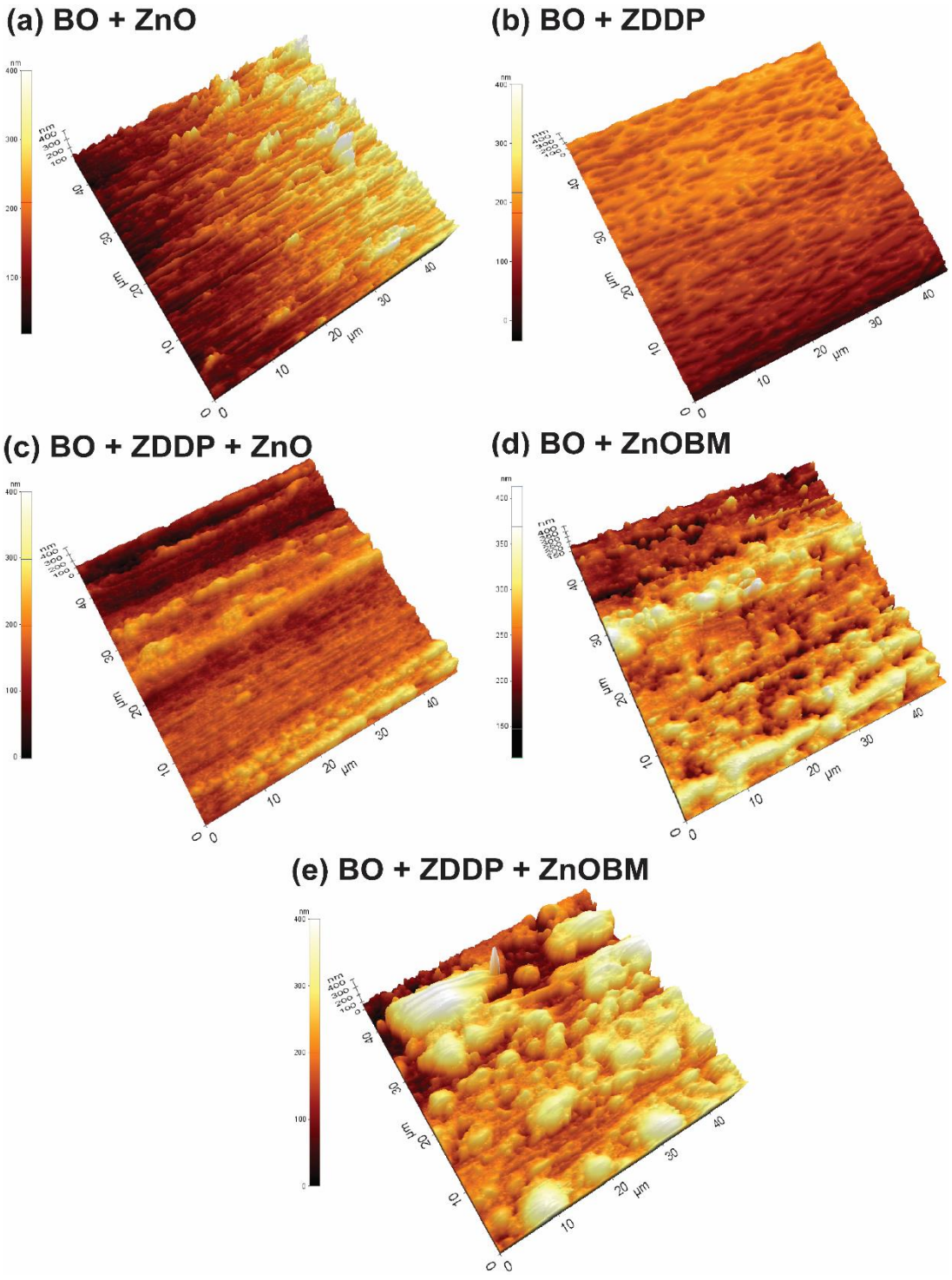

Figure 5. AFM topographical images of the wear scar generated on the flat steel specimen for formulations (a) BO; (b) BO + ZnO; (c) BO + ZnOBM; (d) BO + ZDDP; (e) BO + ZDDP + ZnO; (f) BO + ZDDP + ZnOBM.

To elucidate differences in the chemical composition of the tribofilms generated by different additive combinations, XANES analysis was used to investigate local coordination chemistry of critical elements in these tribofilms, namely zinc (Zn L-edge), sulfur (S K-edge), phosphorus (P L-edge and P K-edge), boron (B K-edge), and iron (Fe L-edge). XANES was operated in total electron yield (TEY) and fluorescence yield (FY) modes and results from both modes are coupled to determine qualitative distribution of compounds at different sampling depth. In TEY mode, the near-surface region (5-60 nm) of the sample is probed, while the information from the bulk (> 800nm) is obtained using FY mode.

Phosphorus Characterization (P $L_{2,3}$-edge and K-edge)

The local geometry and chemical information of the P containing species in the tribofilms is evaluated through P L-edge and P K-edge XANES. Since the L-edge has better photon resolution and narrower linewidth, the P L-edge is more sensitive to determine the structural and chemical characteristics than that of the P K-edge. It is reported that the sampling depth is ~ 5 nm for P L-edge TEY mode, ~ 60 nm for P L-edge FY, and ~ 50 nm for P K-edge TEY.[62,63] Therefore, the simultaneous P L-edge TEY and P L-edge FY and P K-edge FY analysis can provide complementary information about the phosphorus based chemistry at the uppermost surface and in the bulk of the tribofilm.

Figure 6(a) and 6(b) illustrates P L-edge TEY and FY spectra of tribofilms generated from different anti-wear additive chemistries along with that from model compounds. P L-edge TEY spectra exhibit three characteristic peaks, identified as peaks **(i)** or **(i')**, **(ii)** or **(ii')**, and **(iii)**. The transition of P 2p electrons to the 3p-like antibonding states results in the main absorption edge peak **(ii)** or **(ii').**[64] The pre-edge shoulder in P L-edge spectra, i.e. peak **(i)** and **(i')** originates from the transition of the spin-orbit split of P 2p electrons into the first unoccupied 3s antibonding

state.[64,65] Peak **(iii)** is a characteristic peak of phosphate coordination irrespective of the cation which arises due to P 2p to 3d electron transition.[66] TEY spectra for tribofilms generated with only ZDDP based lubrication exhibits strong main absorption peak aligned to that of the $FePO_4$ model compound. However, its corresponding FY spectra displays very noisy signal and low intensity characteristic peak superimposing with $FePO_4$ model compound. These results suggest that the phosphorus is primarily present as iron phosphates in the tribofilm and the concentration of phosphorus bonded species decreases from the surface to bulk of the tribofilm. The tribosurface generated from the additive mixture of non-functionalized ZnO and ZDDP has very weak signals for phosphorus in both TEY and FY mode, which make it difficult to determine whether the signal is from zinc or iron phosphates in the films. These observations confirm that the interaction of non-functionalized ZnO and ZDDP is detrimental and did not promote stable formation of tribofilms at the sliding surfaces, and as a result, poor wear performance was observed as noted earlier. The main absorption edge of the TEY spectra from the BO + ZDDP + ZnOBM sample aligns well with the iron phosphate model compound.

However, it is important to note that the full width half maxima of the characteristic peak is greater than the width of the peak **(ii')** of $FePO_4$ and the broader characteristic peak of the sample also overlaps with the peak **(ii)** of $Zn_3(PO_4)_2$. This hints a small contribution from zinc phosphate in the chemical makeup of the tribofilms, while the majority proportion of the phosphorus is associated with iron in the near-surface region of these films. Furthermore, upon comparing the main absorption edge of FY spectra with the model compounds using a drop line, the energy of the main peak was found to be in between the main absorption edge of $Zn_3(PO_4)_2$ and $FePO_4$ suggesting the presence of a mixture of zinc phosphate and iron phosphate in the bulk of the tribofilms formed with boron coated ZnO and ZDDP additive mixture.

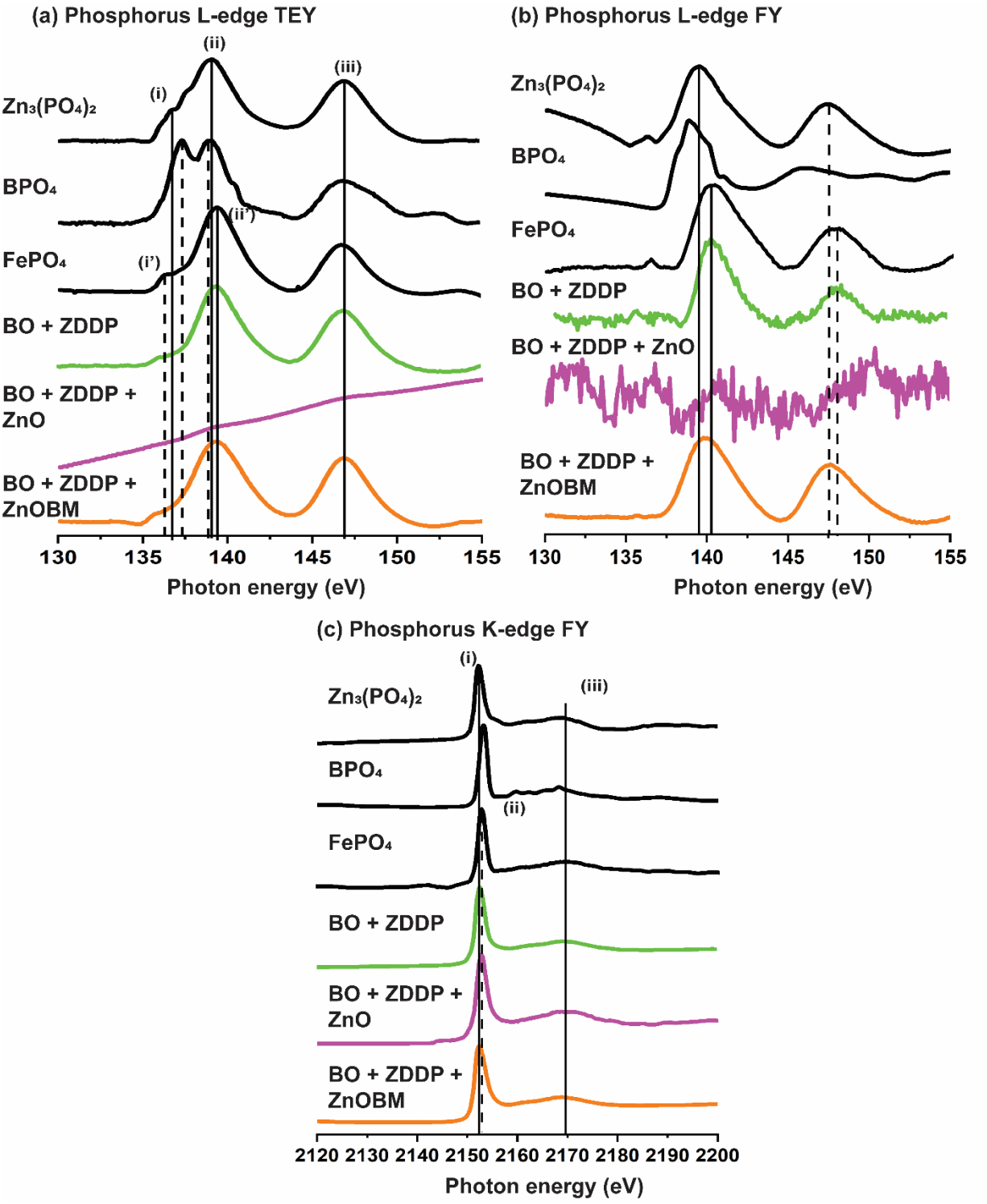

Figure 6. XANES phosphorus L-edge recorded in (a) TEY mode and (b) FY mode, and (c) phosphorus K-edge in TEY mode of model compounds and samples: BO + ZDDP, BO + ZDDP + ZnO, and BO + ZDDP + ZnOBM.

The P K-edge spectra of tribofilm samples collected in TEY mode is presented and compared with reference compounds $Zn_3(PO_4)_2$, BPO_4, and $FePO_4$ in figure 6(c). The main absorption edge in P K-edge TEY spectra is attributed to the transition of a P 1s electron into an unoccupied valence electronic state formed by the overlap of P sp^3 hybrid and O 2p orbitals. The characteristic peak for zinc phosphate **(i)** is at slightly lower photon energy than peak **(ii)** for iron phosphate. Additionally, the iron phosphate spectrum has a distinctive pre-edge peak which helps to differentiate it from zinc phosphate. BPO_4 has an absorption peak at 2153.3 eV higher than that of $Zn_3(PO_4)_2$ and $FePO_4$. P K-edge TEY spectra of tribofilm sample formed with the mixture of non-functionalized ZnO nanoparticles and ZDDP exhibits peak **(ii)** which is associated with iron phosphate. A slight pre-edge is also evident in the P K-edge TEY spectra which further confirms presence of iron phosphate based tribofilms on the worn surface. The main absorption peak for BO + ZDDP and BO + ZDDP + ZnOBM samples appears to be aligned with the peak **(i)** of zinc phosphate. However, the presence of $FePO_4$ cannot be eliminated completely as the absorption peak **(ii)** of $FePO_4$ slightly overlaps with the characteristic peak of the samples. These results indicate that the bulk chemistry of these tribofilm samples is comprised of the mixture of zinc and iron phosphates with the dominance of zinc phosphates.

Zinc Characterization (Zn L-edge)

Figure 7(a) presents the Zn L-edge XANES spectra for tribofilms and some relevant model compounds, recorded in the TEY mode. Zn L-edge features (1030 – 1045 eV) are associated with the transition of Zn 2p electron to the Zn 4s and antibonding Zn 3d states. Additional details on the characteristics can be found elsewhere.[63] Zn L-edge spectra of the sample generated with only ZDDP based lubrication strongly indicates that the environment around zinc ions is associated more with phosphates than sulfates or sulfides.

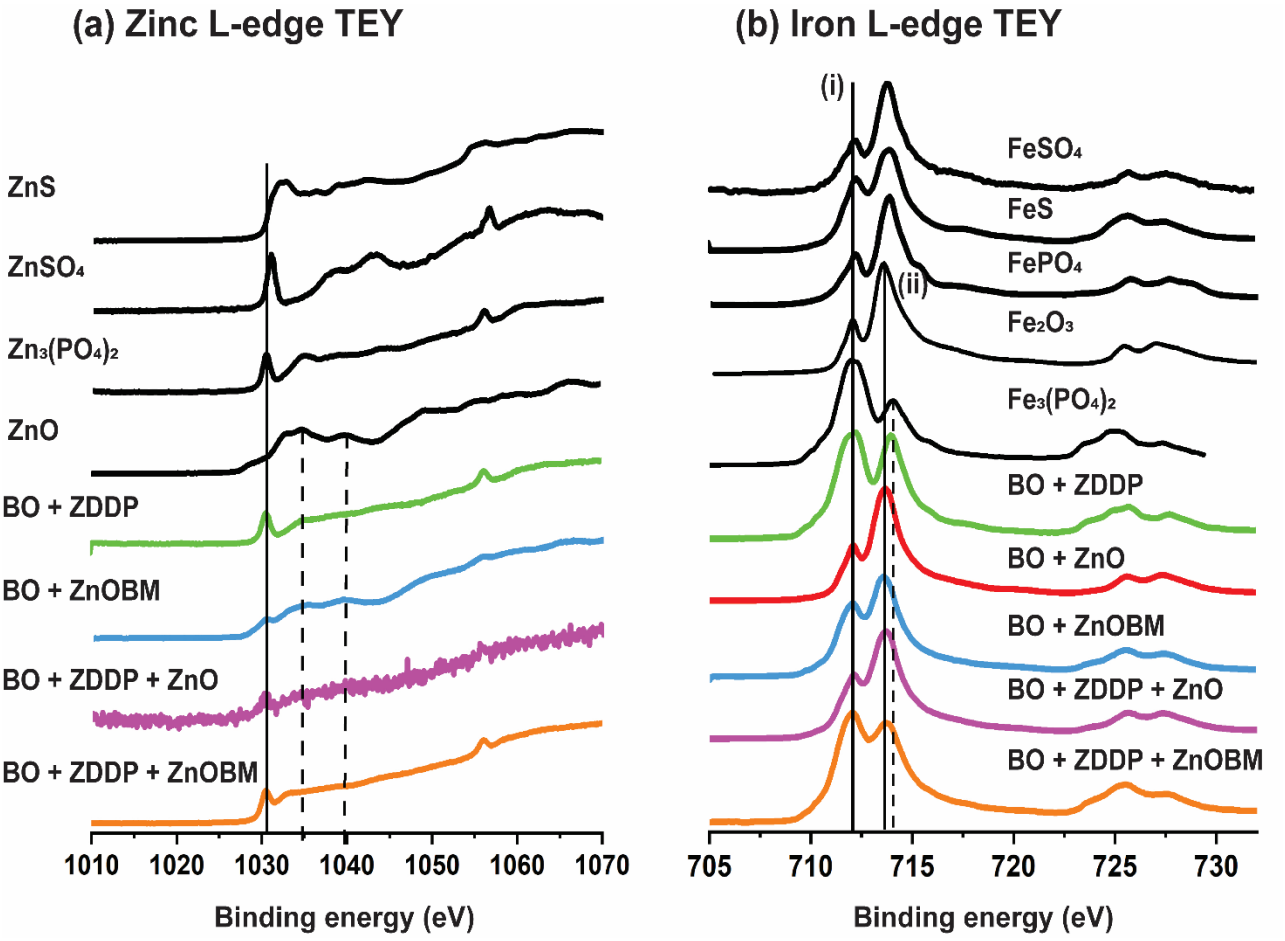

Figure 7. (a) XANES zinc L-edge recorded in TEY mode and (b) XANES iron L-edge recorded in FY mode of model compounds and samples: BO + ZDDP, BO + ZnO, BO + ZnOBM, BO + ZDDP + ZnO, and BO + ZDDP + ZnOBM.

On the contrary, Zn L-edge spectra from only functionalized ZnO sample appears to be different than the spectra of BO + ZDDP and $Zn_3(PO_4)_2$ model compound. The shape, peak position and intensity closely resembles with ZnO model compound and thus, indicates presence of protective anti-wear ZnO based tribofilms at the sliding surface lubricated with encapsulated ZnO nano-additives. The tribosurfaces generated with the mixture of ZDDP and ZnO (non-functionalized) have a very weak signal for zinc and indicates absence of Zn based phosphates, sulfates, and sulfides. Interestingly, the features of the spectra for the BO + ZDDP + ZnOBM

sample closely aligns with that of zinc phosphate model compounds. This information further substantiates the inferences derived from the phosphorus L-edge results and establishes that the tribofilms generated by mixture of ZDDP and functionalized ZnO contains both zinc and iron phosphates at the near surface region (~ 50 – 60 nm).

Iron Characterization (Fe $L_{2,3}$-edge)

Figure 7(b) shows the stacked TEY of Fe L-edge spectra of various iron containing reference compounds and tribological samples. The Fe L-edge of reference compounds exhibit main absorption edge peaks **(i)** and **(ii)**. Analyzing splitting and intensity of these peaks is very beneficial in tracking different oxidation states of iron. For example, spectra of model compounds, $Fe_3(PO_4)_2$ and $FePO_4$ reveal that the intensity ratio between main absorption peaks **(i)** and **(ii)** changes with the change in oxidation state of iron. When Fe^{2+} changes to Fe^{3+}, the second peak becomes the prominent one. Spectra of the BO + ZDDP sample exhibit characteristic splitting and main peaks **(i)** and **(ii)** with almost the same intensity, indicating that the tribofilms are comprised of mixture of different iron phosphates with a slightly major concentration of $Fe_3(PO_4)_2$. Additionally, samples with only ZnO nanoparticles, only ZnOBM nanoparticles, and mixture of ZDDP with ZnO nanoparticles have their main peak position aligned with the Fe_2O_3 model compound. However, the features in the TEY spectra of sample BO + ZDDP + ZnOBM are superimposing with the spectra of $FePO_4$ model compound and thus, indicate that iron is primarily associated with phosphates and not with sulfates or sulfides.

Boron Characterization (B K-edge)

The boron chemistry in the tribofilms was also investigated to elucidate the role of surface modified ZnO nanoparticles in providing better anti-wear and anti-friction properties. The B K-edge TEY XANES spectra, shown in figure 8(a), exhibit three characteristic features; a peak at

~194 eV (associated with trigonal B), a broader peak at 197-199 eV (the edge feature of tetrahedral B), and a broad peak at 200-201 eV for tetrahedral B and 203-204 eV for trigonal B.[67] Tribofilms formed with boron-coated ZnO nanoparticles-based lubrication reveal the presence of boron in trigonal co-ordination as the sharp peak at ~194 eV can be identified in its B K-edge spectra aligned with B_2O_3 and H_3BO_3 model compounds. The spectra for sample BO + ZDDP + ZnOBM exhibit a very distinctive broad peak at 197 eV with a shoulder at 194.7 eV which matches with the iron borates (Fe_3BO_6, $FeBO_3$) in the literature.[68] Since the results of Fe L-edge spectra (figure7(b)) revealed the presence of Fe^{3+}, the combined analysis of Fe L-edge and B K-edge further confirms that these tribofilms are comprised of iron borates, in addition to iron phosphates, wherein iron is present as Fe_3BO_6 or $FeBO_3$ or $FePO_4$ in an Fe^{3+} oxidation state. Additionally, in figure 7(b) peak **(i)** appears to be shifted by 0.7 eV, in comparison to reference compounds, which also suggest the formation of borate complex.[67,69] Based on these results, it can be concluded that encapsulated ZnO nanoparticles were able to deliver beneficial boron chemistry at the sliding interface and contribute to tribofilm formation.

Sulfur Characterization (S K-edge)

Sulfur K-edge TEY spectra for tribofilms are shown in figure 8(b) and are compared with model reference compounds. Acquisition depth of the collected emission electrons is about 50 nm at the S K-edge and, accordingly, the information acquired from TEY mode do not refer to the surface but to the bulk of tribofilms.[70] Sulfur can exist in different oxidation states (-2 to +6) and the information derived from S K-edge is extremely useful in differentiating among the chemical species of sulfur through characteristic peaks **(i)**, **(ii)** and **(iii)**. As shown in figure 8(b), the energy at the main absorption edge for different model compounds shifts toward lower energy as the oxidation states are reduced.

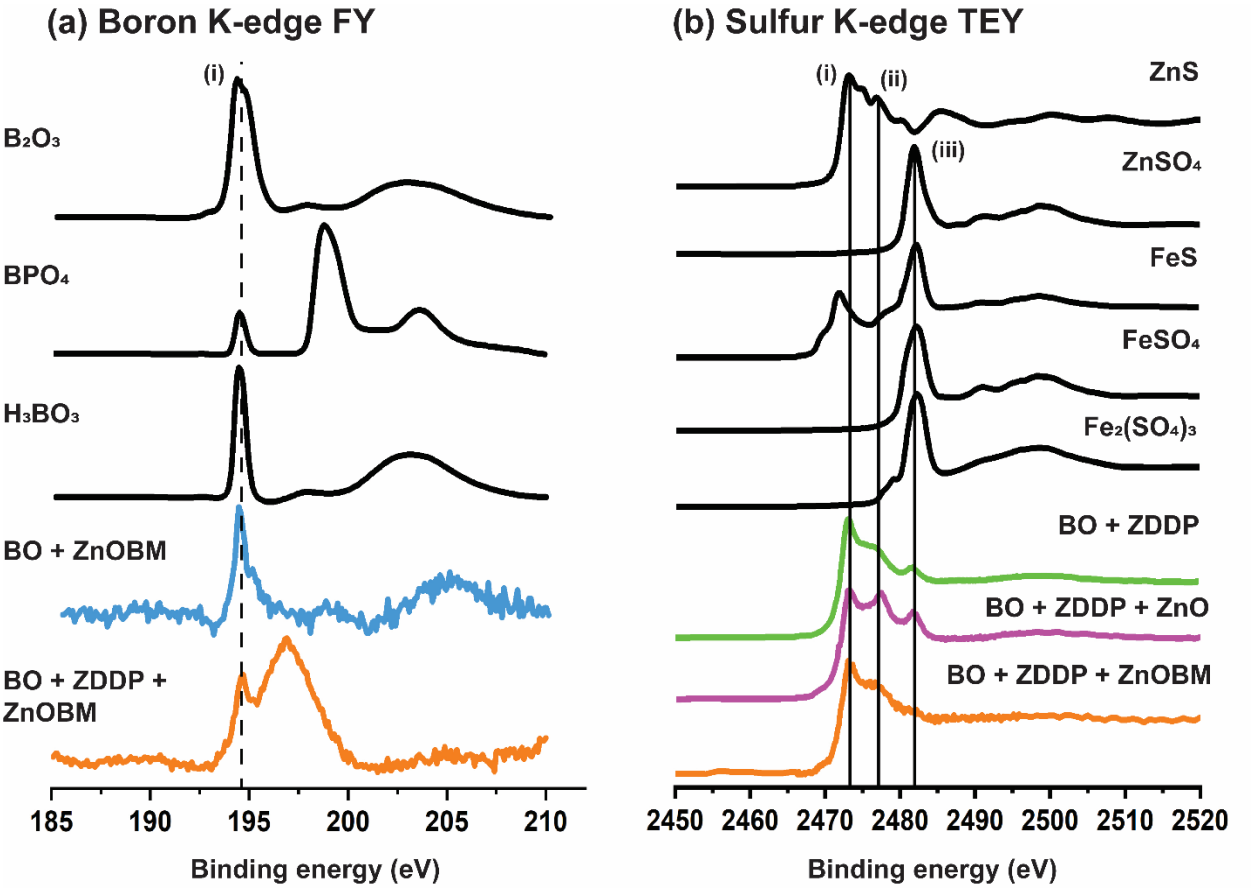

Figure 8. (a) XANES boron K-edge recorded in FY mode and (b) XANES sulfur K-edge recorded in TEY mode of model compounds and samples: BO + ZDDP, BO + ZnOBM, BO + ZDDP + ZnO, and BO + ZDDP + ZnOBM.

Peak **(iii),** around ~2482 eV, corresponds to sulfate species (S^{+6}) (i.e. $ZnSO_4$, $FeSO_4$, $Fe_2(SO_4)_3$), while peaks **(i)** and **(ii)** represent the main absorption edge for sulfides (S^{-2}) such as ZnS at ~2473 eV and FeS at ~2471 eV. Spectra for samples BO + ZDDP and BO + ZDDP + ZnO are very similar to that of ZnS spectra with the presence of additional peak **(iii)** corresponding to zinc sulfate. This indicates that zinc sulfide is the main chemical state of sulfur, but there is also some smaller presence of zinc sulfate in these tribofilms. Interestingly, S K-edge spectra for the BO + ZDDP + ZnOBM sample exhibited a very weak signal, but a peak **(ii)** aligning with ZnS compound can be identified. This indicate that the tribofilms formed due to interaction of ZDDP

and functionalized ZnO nano-additives contains sulfur in very minute concentration in the form of zinc sulfide 50 nm beneath the surface.

3.3.3 XPS analysis of the interfacial tribofilms

The elemental composition of the tribofilms generated with the lubricant containing only ZDDP, only functionalized ZnO nanoparticles and the mixture of ZDDP with functionalized ZnO nanoparticles were examined using high resolution XPS spectroscopy. XPS provides valuable compositional information of the top 0 to 5-8 nm of the surface and, as such, compliments findings of the XANES studies to help understand the lubricating mechanism of nano-additives. Figure 9 displays zinc, phosphorus, boron, oxygen XPS spectra acquired from the aforementioned tribosurfaces.

Zinc (Zn) 2p

The Zn 2p spectra, as shown in figure 9(a), are identical for all three samples, exhibiting two peaks at ~1022.2 eV ($2p_{3/2}$) and ~1045.4 eV ($2p_{1/2}$) due to spin-orbit splitting.[71] However, there is a clear difference in the intensity of characteristic peaks within these samples indicative of the differences in the relative amount of zinc bounded species in the tribofilms. For the BO + ZDDP sample, the signal for zinc is relatively weak and is attributed to the presence of zinc phosphate on the surface. On the contrary, sample BO + ZDDP + ZnOBM exhibits sharp and strong intensity peaks for Zn 2p highlighting additional contribution from ZnO nanoparticles to the phosphorus based tribofilms. Spectra from BO + ZnOBM further compliments the finding from the XANES study, thus confirming the formation of zinc based tribofilms on the sliding surface lubricated with functionalized ZnO nanoparticles.

Phosphorus (P) 2p

The plot shown in figure 9(b) reveals the strong presence of phosphorus in the tribofilms formed by ZDDP alone and, as well, in the additive mixture of ZDDP with ZnOBM. The peak

position at ~133.7 eV is attributed to iron phosphates while the peak position at ~133.3 eV to zinc phosphates. For the BO + ZDDP sample, it appears that both zinc phosphates and iron phosphates contribute to the overall phosphorus signal. The spectra of BO + ZDDP + ZnOBM sample suggest that the dominant phosphorus based chemical species in the tribofilms are zinc phosphates with relatively low amounts of iron phosphates.

Iron (Fe) 2p

Figure 9(c) is useful in determining the chemical state of iron atoms present in the tribofilms. The observed Fe 2p XPS spectra exhibit characteristic peak shape and positioning at the binding energy of ~ 712 eV, which is consistent with the XPS spectra of Fe_2O_3 model compound.[72] Additionally, there is no strong signal at 707 eV corresponding to metallic iron in steel substrate.[73,74] These observations imply that the Fe atoms are in the highest oxidation state Fe^{3+} and confirm the presence of iron oxides (Fe_2O_3) in the tribofilms. Interestingly, comparison of the intensity of the Fe $2p_{3/2}$ peak in figure 9(c) provides some explicit information on the concentration of iron oxides in the tribofilms. The plot for the BO + ZDDP sample shows stronger signal for iron and thus suggest that tribofilms formed in this case are mainly rich in iron oxide. Weak signal for iron in the BO + ZDDP + ZnOBM tribofilm sample indicates that the major contributions to the chemical make-up of the films are from zinc and iron phosphates, which are protecting the sliding surface from wear.

Oxygen (O) 1s

Oxygen 1s spectra, as shown in figure 9(d), gives an insight into the different oxygen bonded atoms and their contribution to the overall chemical nature of the tribofilms formed with the different additive chemistries. The oxygen signal consists of three peaks, wherein the low binding energy peak **(i)** at 530.1 ±0.1 eV is attributed to iron oxide,[75,76] while the main peak **(iii)** at ~ 531.8 ±0.1 eV originates from non-bridging oxygen in poly-phosphate chains and from other

oxygen containing groups such as carbonates, hydroxides or sulphates.[71,77,78] In some cases, an additional signal (peak **(ii)**) at 530.5 ±0.1 eV is detected and is attributed to the presence of zinc oxide.[78] The peak at 533.4 eV is assigned to B-O, which links phosphate groups to form phosphate chains.[71] The oxygen spectra for only ZDDP tribofilm sample shows intense peak for metal oxide primarily from iron oxide (Fe_2O_3), which is consistent with the information from the iron 2p spectra. The O 1s spectra for tribofilm sample BO + ZnOBM has a low intensity peak **(ii)** at 530.35 eV primarily from zinc oxide (not from iron oxide), and a broad peak between 531 and 532 eV energy range probably due to presence of carbonate species, as there is no phosphorus available in this lubrication. The tribofilm sample generated with ZDDP and boron coated ZnO nanoparticles shows a strong signal for metal phosphates, in comparison to metal oxides, again corroborating the formation of zinc and iron phosphate based beneficiary tribofilms at the tribological contacts.

Boron (B) 1s

To understand the role of boron coated ZnO nano-additives in promoting stable tribofilm formation in providing enhanced anti-wear and anti-friction protection, B 1s XPS spectra was recorded. Figure 9(e) exhibits a B 1s plot for tribofilm samples generated with only functionalized ZnOBM nanoparticles and with the mixture of ZDDP and ZnOBM. For the BO + ZnOBM sample, B 1s spectra has a peak at binding energy 191.7 (± 0.1 eV) which corresponds to the binding energy of B_2O_3 model compound[79], thus suggesting the presence of borates in this tribofilm. It is important to note that sample BO + ZDDP + ZnOBM exhibits XPS peaks with much broader full width half maxima than the BO + ZnOBM. Zhang et. al. has reported that P 2s XPS cross section coincides with B 1s cross section [79] and, as a result, if phosphorus is present in the sample it interferes significantly with boron characterization and B 1s spectra. This is especially true if the phosphorus concentration is high in the sample. Therefore, in this case, it is reasonable to assume that the strong signal at 191.3 eV is due to the presence of the mixture of zinc and iron phosphates (as

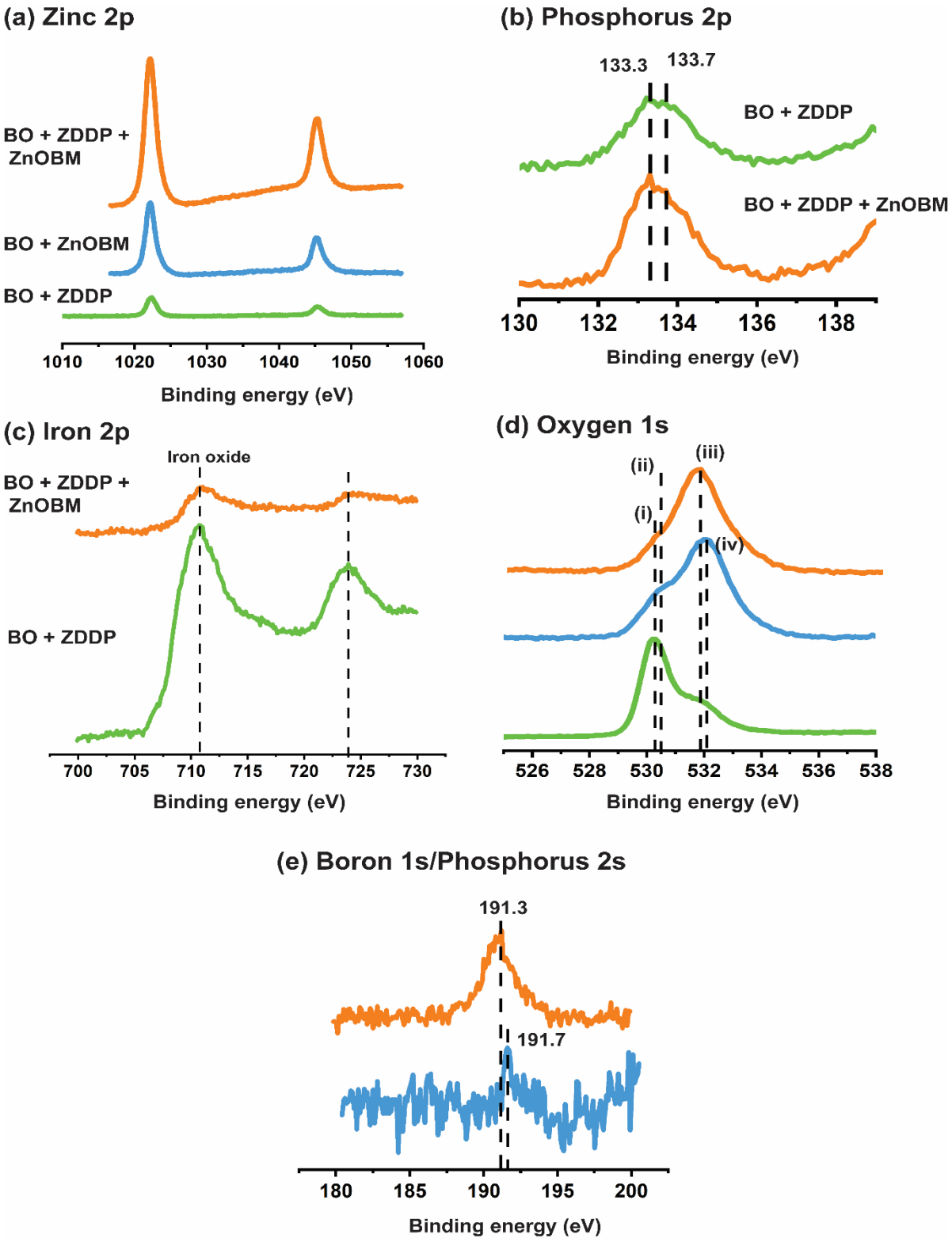

Figure 9. XPS spectra for (a) Zinc 2p, (b) Phosphorus 2p. (c) Iron 2p, (d) Oxygen 1s, and (e) Boron 1s for tribological samples.

detected through XANES P L-edge TEY spectra) at the surface of the tribofilms, while the low intensity peak at 191.7 eV is from the borates. Overall, these results indicate that boron species provided through plasma functionalized ZnO nanoparticles are aiding in protective tribofilm formation, thus helping to improve anti-wear performance even at the low concentration of ZDDP.

3.4 Chemical make-up of the tribofilms and lubricating mechanism

The friction and wear characteristics of the sliding contacts under mixed and boundary lubrication are primarily governed by the interfacial tribofilms. The tribofilms formed due to complex thermo-mechanical interaction of lubricant and sliding surfaces exhibit lower hardness and elastic moduli than the underlying substrate, which allows them to distribute applied contact pressure thus sacrificially cushion shearing stresses at the interface to effectively prevent wear. In this study, ~ 100 nm heterogenous patchy tribofilms are formed over the ferrous contacts, wherein the thickness and composition of these films appear to be varying with the lubricant additive chemistry. Information from AFM, XANES, and XPS are correlated in this section to create schematics of layered films, representing the hierarchical composition developed across the tribofilm thickness, to elucidate wear mechanism of nano-additives, as shown in figure 10. AFM results clearly demonstrated non-continuous pad like structure of tribofilms separated by valleys, however, for the simplicity of understanding a pictorial view of a continuous long tribofilm patch, with vertically varying chemical composition, is shown in figure 10(a). The schematic of tribofilm sample BO + ZDDP exhibits a layered structure dominant with iron phosphates in the near-surface region of the film and iron oxides in the near-metal interface. XANES P L, P K, and Fe L-edge spectra and XPS elemental results on P, Fe, and O provided the information for this schematic. As evident from P L and Zn L-edge TEY spectra, zinc phosphates are also present in lesser amount in the topmost region of this tribofilm. Sulfides are located between phosphates and iron oxides.

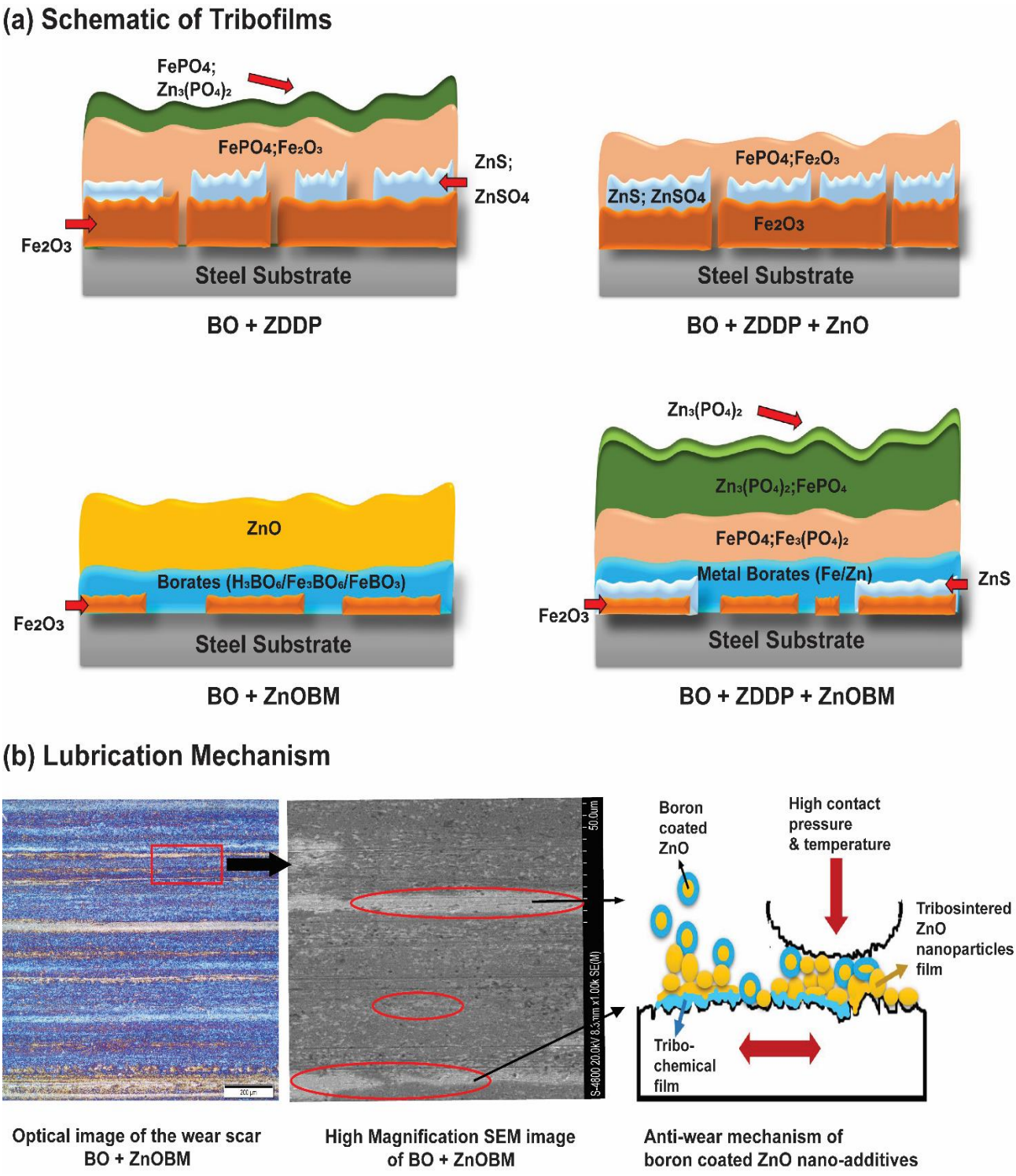

Figure 10. (a) Phenomenological models of tribofilms generated from lubricants BO + ZDDP, BO + ZDDP + ZnO, BO + ZnOBM, and BO + ZDDP + ZnOBM. (b) Schematic of lubricating anti-wear mechanism of ZnOBM nano-additives.

Additionally, zinc, phosphorus, iron, oxygen, and sulfur data, from both XANES and XPS, provide insights in the chemical architecture of tribofilms formed from the additive mixture of non-functionalized ZnO and ZDDP (BO + ZDDP + ZnO). These tribofilms are enriched in iron oxides with minor concentration of iron phosphates. It is postulated that the incompatibility of ZDDP and non-functionalized ZnO nanoparticles to form stable phosphate films resulted in severe material loss of the iron substrate and exposed nascent iron surface to react with oxygen, ultimately leading to such tribofilm structure. Chemical composition of these tribofilms further corroborates findings of ECR and high wear losses in this case. Chemistry of tribofilms derived from boron coated ZnO nanoparticles based lubrication is distinctly different from the tribofilms formed by ZDDP as shown in figure 10(a). XANES Zn L-edge TEY spectra and XPS O 1s spectra for BO + ZnOBM sample support the presence of zinc throughout the thickness of the tribofilm, primarily in the form of zinc oxides. Additionally, boron XANES and XPS spectra suggest the formation of a complex glassy structure near the metal interface region, consisting of boron oxide, hydrogen borates, and iron borates. The tribofilm model for BO + ZDDP + ZnO represents arrangement of different chemical species wherein it has trace amounts of iron oxide and zinc sulfide in the bottom layers but above it, near the surface, it contains high concentrations of iron and zinc phosphates. As evident from B K and Fe L-edge XANES and B 1s XPS spectra, this tribofilm also contains a mixture of different metal borates, including the strong presence of iron borates.

Based on the chemical properties of tribofilms, ECR results and tribological test results, an anti-wear mechanism is proposed for plasma functionalized ZnOBM nano-additives and is schematically displayed in figure 10(b). The detection of boron based compounds in the bulk of the tribofilm indicates that the ZnOBM nano-additives were able to deliver boron chemistry at the tribological interface via compressive stress induced removal of polymer shells, which were

initially encapsulating ZnO nanoparticles. Presence of iron borates in the case of both BO + ZnO and BO + ZDDP + ZnO tribofilm samples further indicate that the surface protective anti-wear films were partly formed due to stress induced tribochemical reaction between boron and nascent iron substrate. Additionally, formation of strong Zn-based tribofilms, on the worn surfaces lubricated with ZnOBM nano-additives, could be attributed to the stress-induced tribosintering anti-wear mechanism of nanoparticles. In this anti-wear mechanism, metallic nanoparticles are welded without melting at sliding surfaces forming a compact surface protective tribofilm, capable of providing load-bearing effect and limiting direct metal-metal contact.[80–84] As reported by Viesca et al. carbon coated Cu nanoparticles as additives in PAO6 lubricant reduces friction and wear by the tribosinterization of nanoparticles due to being compacted on the contact surfaces at high temperatures and pressure generated by friction.[85] To further investigate the wear mechanism of the ZnOBM nano-additives and substantiate findings of XANES, AFM, and XPS on nanoparticles induced tribofilm, the wear scar developed on the flat specimen was examined using SEM. As shown in figure 10(b), the optical image displays a wear surface covered with a large and thick protective film and a high-magnification micrograph of the marked region exhibits groves and scratches covered with protective film. In comparison to the metal surface, protective film formed by nanoparticles appears to be flat and smooth, which can effectively reduce friction and wear. Thus, based on surface characterization results, it is reasonable to propose that ZnOBM lubricating mechanism include formation of interfacial anti-wear tribofilms through combination of tribochemical reaction and tribosintering of nanoparticles to significantly improve anti-wear and anti-friction characteristics.

Finally, it is important to note the differences in the vertically heterogenous structure of tribofilm formed by BO + ZDDP and BO + ZDDP + ZnOBM oils. Tribofilm model for the mixture

of ZDDP and ZnOBM exhibits the dominance of zinc phosphates in comparison to that of tribofilms formed by only ZDDP containing oil, where surface of tribofilms is enriched in iron phosphates. Earlier studies have shown that the presence of the long chain zinc phosphates yield better tribological properties and are generally considered to be more beneficial than iron phosphates.[49] Thus, the chemistry of tribofilms formed by synergistic interaction of ZDDP and ZnOBM highlights the participation of tribosintered ZnOBM nanoparticles in promoting stable formation of advantageous zinc phosphate films and strengthening the protective layer to improve the overall lubrication performance of mineral base oil containing merely 350 ppm of phosphorus.

4. CONCLUSION

This research work illustrates that boron coated ZnO nanoparticles when used by themselves and in combination with 350 ppm of ZDDP in the base oil can effectively improve anti-wear performance and provide lower friction coefficients compared to oils containing only ZDDP, or ZDDP with non-functionalized ZnO nanoparticles. Notably, this study reports reduction in the amount of ZDDP or phosphorus concentration to 350 ppm using surface capped ZnO nanoparticles without compromising tribological protection of the sliding contacts.

Using high contact stress, cylinder on flat reciprocating tribometer with ECR test setup, the effect of functionalized and non-functionalized nano-additives on the overall dynamics of tribofilm formation was studied. It was observed that non-functionalized ZnO nanoparticles by themselves were not able to form tribofilms at the sliding surfaces and when used with ZDDP, they removed preformed tribofilms and hindered stable tribofilm formation. However, in sharp contrast, it was discovered that surface molecularly tailored and adequately dispersed ZnO nanoparticles are extremely effective in providing anti-wear film formation at the tribological interface.

Results derived from AFM, XPS, and XANES surface characterization techniques were correlated to understand the physical and chemical nature of tribofilms formed with nano-additives. Thin patchy tribofilms are formed when surfaces in contact are lubricated with formulation containing only ZDDP whereas in the case of additive mixture of ZDDP and coated ZnO nanoparticles tribofilms are comprised of thicker pads and are continuous in nature. Tribofilms formed with oil containing only ZDDP dominantly contains iron phosphates and iron oxides with minor concentration of zinc phosphate/sulfate/sulfide. In contrast, lubrication containing both ZDDP and boron coated ZnO nanoparticles resulted in the formation of majority layers of zinc and/iron phosphates and iron borates covering bulk layers of iron oxides, and iron and zinc sulfates and/sulfides. The improved tribological performance of this additive combination is attributed to the stable tribofilm formation with crosslinked zinc and iron polyphosphates network and iron borates due to extra Zn and B atoms introduced at the tribological interface by surface capped nanoparticles.

The enhanced anti-wear protection, coupled with reduction of ZDDP concentration, reported here will help automotive engine oil formulators to resolve concerns of catalytic converter poisoning and greenhouse gas emissions. Additionally, the knowledge gained here on tribological performance of ZnO plasma functionalized nanoparticles and their tribofilm properties will help promote further development of nano-lubricants for tribological applications that will extend the durability and energy efficiency of a multitude of other mechanical systems.

ACKNOWLEDGMENTS

This research work used tribological facilities at Applied Materials Division of Argonne National Laboratory with the support and guidance of Dr. Ali Erdemir. XANES experimental work was performed at Canadian Light Source, Saskatoon, Saskatchewan, Canada that is supported by NSERC, NRC, CIHR and the University of Saskatchewan. Support provided by Center of

Chemicals, Materials, and Biology (CCMB) at the University of Texas at Arlington is gratefully acknowledged.

SUPPORTING INFORMATION

FTIR and XANES characterization of plasma polymer films deposited on ZnO nanoparticles are provided as the supporting information. Optical microscopy results of wear scar developed on flat test specimen and profilometry 2D and 3D images of wear scar developed on cylinder test specimen for all test formulations are also provided. Friction and wear results of tribological tests carried out to determine optimum concentration of ZnO nanoparticles to be mixed in mineral base oil are also added for the reference.

REFERENCES

(1) Anderson, W. B.; Guinther, G. H. Engine Oil Fuel Economy: Benefits and Potential Debits of Low Viscosity Engine Oil. In *SAE Technical Paper*; SAE International, 2019.

(2) Kong, L.; Sun, J.; Bao, Y. Preparation, Characterization and Tribological Mechanism of Nanofluids. *RSC Adv.* **2017**, *7* (21), 12599–12609. https://doi.org/10.1039/C6RA28243A.

(3) Nicholaos G. Demas, Robert A. Erck, Cinta Lorenzo-Martin, Oyelayo O. Ajayi, and G. R. F. Experimental Evaluation of Oxide Nanoparticles as Friction and Wear Improvement Additives in Motor Oil. *J. Nanomater.* **2017**. https://doi.org/https://doi.org/10.1155/2017/8425782.

(4) Zhang, L.; Chen, L.; Wan, H.; Chen, J.; Zhou, H. Synthesis and Tribological Properties of Stearic Acid-Modified Anatase (TiO2) Nanoparticles. *Tribol. Lett.* **2011**, *41* (2), 409–416. https://doi.org/10.1007/s11249-010-9724-z.

(5) Peng, D. X.; Kang, Y.; Hwang, R. M.; Shyr, S. S.; Chang, Y. P. Tribological Properties of Diamond and SiO2 Nanoparticles Added in Paraffin. *Tribol. Int.* **2009**, *42* (6), 911–917. https://doi.org/https://doi.org/10.1016/j.triboint.2008.12.015.

(6) Alves, S. M.; Barros, B. S.; Trajano, M. F.; Ribeiro, K. S. B.; Moura, E. Tribological Behavior of Vegetable Oil-Based Lubricants with Nanoparticles of Oxides in Boundary Lubrication Conditions. *Tribol. Int.* **2013**, *65*, 28–36. https://doi.org/https://doi.org/10.1016/j.triboint.2013.03.027.

(7) Battez, A. H.; González, R.; Viesca, J. L.; Fernández, J. E.; Fernández, J. M. D.; Machado, A.; Chou, R.; Riba, J. CuO, ZrO2 and ZnO Nanoparticles as Antiwear Additive in Oil Lubricants. *Wear* **2008**, *265* (3), 422–428. https://doi.org/https://doi.org/10.1016/j.wear.2007.11.013.

(8) Zhou, G.; Zhu, Y.; Wang, X.; Xia, M.; Zhang, Y.; Ding, H. Sliding Tribological Properties of 0.45% Carbon Steel Lubricated with Fe3O4 Magnetic Nano-Particle Additives in Baseoil. *Wear* **2013**, *301* (1), 753–757. https://doi.org/https://doi.org/10.1016/j.wear.2013.01.027.

(9) Xie, H.; Jiang, B.; He, J.; Xia, X.; Pan, F. Lubrication Performance of MoS2 and SiO2 Nanoparticles as Lubricant Additives in Magnesium Alloy-Steel Contacts. *Tribol. Int.* **2016**, *93*, 63–70. https://doi.org/https://doi.org/10.1016/j.triboint.2015.08.009.

(10) Zhang, R.; Qiao, D.; Liu, X.; Guo, Z.; Hu, L.; Shi, L. Well Dispersive TiO2 Nanoparticles as Additives for Improving the Tribological Performance of Polyalphaolefin Gel Lubricant. *Ind. Eng. Chem. Res.* **2018**, *57* (31), 10379–10390. https://doi.org/10.1021/acs.iecr.8b01694.

(11) Gao, Y.; Chen, G.; Oli, Y.; Zhang, Z.; Xue, Q. Study on Tribological Properties of Oleic Acid-Modified TiO2 Nanoparticle in Water. *Wear* **2002**, *252* (5), 454–458. https://doi.org/https://doi.org/10.1016/S0043-1648(01)00891-2.

(12) Zhou, Y.; Leonard, D. N.; Meyer III, H. M.; Luo, H.; Qu, J. Does the Use of Diamond-Like Carbon Coating and Organophosphate Lubricant Additive Together Cause Excessive Tribochemical Material Removal? *Adv. Mater. Interfaces* **2015**, *2* (15), 1500213. https://doi.org/10.1002/admi.201500213.

(13) Sunqing, Q.; Zhou, Z.; Junxiu, D.; Chen, G. Preparation of Ni Nanoparticles and Evaluation of Their Tribological Performance as Potential Additives in Oils . *J. Tribol.* **1999**, *123* (3), 441–443. https://doi.org/10.1115/1.1286152.

(14) Zhou, J.; Wu, Z.; Zhang, Z.; Liu, W.; Xue, Q. Tribological Behavior and Lubricating Mechanism of Cu Nanoparticles in Oil. *Tribol. Lett.* **2000**, *8* (4), 213–218. https://doi.org/10.1023/A:1019151721801.

(15) Desanker, M.; Johnson, B.; Seyam, A. M.; Chung, Y.-W.; Bazzi, H. S.; Delferro, M.; Marks, T. J.; Wang, Q. J. Oil-Soluble Silver–Organic Molecule for in Situ Deposition of Lubricious Metallic Silver at High Temperatures. *ACS Appl. Mater. Interfaces* **2016**, *8* (21), 13637–13645. https://doi.org/10.1021/acsami.6b01597.

(16) Choi, Y.; Lee, C.; Hwang, Y.; Park, M.; Lee, J.; Choi, C.; Jung, M. Tribological Behavior of Copper Nanoparticles as Additives in Oil. *Curr. Appl. Phys.* **2009**, *9* (2, Supplement), e124–e127. https://doi.org/https://doi.org/10.1016/j.cap.2008.12.050.

(17) Chen, Y.; Zhang, Y.; Zhang, S.; Yu, L.; Zhang, P.; Zhang, Z. Preparation of Nickel-Based Nanolubricants via a Facile In Situ One-Step Route and Investigation of Their Tribological Properties. *Tribol. Lett.* **2013**, *51* (1), 73–83. https://doi.org/10.1007/s11249-013-0148-4.

(18) Li, B.; Wang, X.; Liu, W.; Xue, Q. Tribochemistry and Antiwear Mechanism of Organic--Inorganic Nanoparticles as Lubricant Additives. *Tribol. Lett.* **2006**, *22* (1), 79–84. https://doi.org/10.1007/s11249-005-9002-7.

(19) Xue, Q.; Liu, W.; Zhang, Z. Friction and Wear Properties of a Surface-Modified TiO2

Nanoparticle as an Additive in Liquid Paraffin. *Wear* **1997**, *213* (1), 29–32. https://doi.org/https://doi.org/10.1016/S0043-1648(97)00200-7.

(20) Li, X.; Cao, Z.; Zhang, Z.; Dang, H. Surface-Modification in Situ of Nano-SiO2 and Its Structure and Tribological Properties. *Appl. Surf. Sci.* **2006**, *252* (22), 7856–7861. https://doi.org/https://doi.org/10.1016/j.apsusc.2005.09.068.

(21) Kim, D.; Archer, L. A. Nanoscale Organic−Inorganic Hybrid Lubricants. *Langmuir* **2011**, *27* (6), 3083–3094. https://doi.org/10.1021/la104937t.

(22) Ali, M. K. A.; Xianjun, H.; Mai, L.; Qingping, C.; Turkson, R. F.; Bicheng, C. Improving the Tribological Characteristics of Piston Ring Assembly in Automotive Engines Using Al2O3 and TiO2 Nanomaterials as Nano-Lubricant Additives. *Tribol. Int.* **2016**, *103*, 540–554. https://doi.org/https://doi.org/10.1016/j.triboint.2016.08.011.

(23) Xue, W. G.; Zhao, Z. H.; Wang, P.; Jin, Z. L.; Xu, X. H.; Zhou, X. G. Performance Study of Zinc Oxide Nanoparticles for Lubricant Oil. In *Current Micro-Nano Science and Technology*; Advanced Materials Research; Trans Tech Publications Ltd, 2015; Vol. 1118, pp 195–204. https://doi.org/10.4028/www.scientific.net/AMR.1118.195.

(24) Berman, D.; Mutyala, K. C.; Srinivasan, S.; Sankaranarayanan, S. K. R. S.; Erdemir, A.; Shevchenko, E. V; Sumant, A. V. Iron-Nanoparticle Driven Tribochemistry Leading to Superlubric Sliding Interfaces. *Adv. Mater. Interfaces* **2019**, *6* (23), 1901416. https://doi.org/10.1002/admi.201901416.

(25) Uflyand, I. E.; Zhinzhilo, V. A.; Burlakova, V. E. Metal-Containing Nanomaterials as Lubricant Additives: State-of-the-Art and Future Development. *Friction* **2019**, *7* (2), 93–116. https://doi.org/10.1007/s40544-019-0261-y.

(26) Battez], A. [Hernández; González, R.; Viesca, J. L.; Fernández, J. E.; Fernández], J. M. [Díaz; Machado, A.; Chou, R.; Riba, J. CuO, ZrO2 and ZnO Nanoparticles as Antiwear Additive in Oil Lubricants. *Wear* **2008**, *265* (3), 422–428. https://doi.org/https://doi.org/10.1016/j.wear.2007.11.013.

(27) Demas, N. G.; Erck, R. A.; Lorenzo-Martin, C.; Ajayi, O. O.; Fenske, G. R. Experimental Evaluation of Oxide Nanoparticles as Friction and Wear Improvement Additives in Motor Oil. *J. Nanomater.* **2017**, *2017*, 8425782. https://doi.org/10.1155/2017/8425782.

(28) Chen, Y.; Renner, P.; Liang, H. Dispersion of Nanoparticles in Lubricating Oil: A Critical Review. *Lubricants* **2019**, *7* (1), 7. https://doi.org/10.3390/lubricants7010007.

(29) Huang, L.; Zhou, C.; Zhang, Y.; Zhang, S.; Zhang, P. DBHP-Functionalized ZnO Nanoparticles with Improved Antioxidant Properties as Lubricant Additives. *Langmuir* **2019**, *35* (12), 4342–4352. https://doi.org/10.1021/acs.langmuir.9b00093.

(30) Wu, L.; Zhang, Y.; Yang, G.; Zhang, S.; Yu, L.; Zhang, P. Tribological Properties of Oleic Acid-Modified Zinc Oxide Nanoparticles as the Lubricant Additive in Poly-Alpha Olefin and Diisooctyl Sebacate Base Oils. *RSC Adv.* **2016**, *6* (74), 69836–69844. https://doi.org/10.1039/C6RA10042B.

(31) Kalyani; Rastogi, R. B.; Kumar, D. Synthesis, Characterization, and Tribological Evaluation of SDS-Stabilized Magnesium-Doped Zinc Oxide (Zn0.88Mg0.12O) Nanoparticles as Efficient Antiwear Lubricant Additives. *ACS Sustain. Chem. Eng.* **2016**, *4* (6), 3420–3428. https://doi.org/10.1021/acssuschemeng.6b00472.

(32) Zhang, J.; Spikes, H. On the Mechanism of ZDDP Antiwear Film Formation. *Tribol. Lett.* **2016**, *63* (2), 24. https://doi.org/10.1007/s11249-016-0706-7.

(33) Spikes, H. Low- and Zero-Sulphated Ash, Phosphorus and Sulphur Anti-Wear Additives for Engine Oils. *Lubr. Sci.* **2008**, *20* (2), 103–136. https://doi.org/10.1002/ls.57.

(34) Li, Y.-R.; Pereira, G.; Lachenwitzer, A.; Kasrai, M.; Norton, P. R. X-Ray Absorption Spectroscopy and Morphology Study on Antiwear Films Derived from ZDDP Under Different Sliding Frequencies. *Tribol. Lett.* **2007**, *27* (3), 245–253. https://doi.org/10.1007/s11249-007-9213-1.

(35) Najman, M. N.; Kasrai, M.; Bancroft, G. M. Investigating Binary Oil Additive Systems Containing P and S Using X-Ray Absorption near-Edge Structure Spectroscopy. *Wear* **2004**, *257* (1–2), 32–40. https://doi.org/10.1016/S0043-1648(03)00537-4.

(36) Zhou, Y.; Qu, J. Ionic Liquids as Lubricant Additives: A Review. *ACS Appl. Mater. Interfaces* **2017**, *9* (4), 3209–3222. https://doi.org/10.1021/acsami.6b12489.

(37) Yin, Z.; Kasrai, M.; Bancroft, G. M.; Fyfe, K.; Colaianni, M. L.; Tan, K. H. Application of Soft X-Ray Absorption Spectroscopy in Chemical Characterization of Antiwear Films Generated by ZDDP Part II: The Effect of Detergents and Dispersants. *Wear* **1997**, *202* (2), 192–201. https://doi.org/https://doi.org/10.1016/S0043-1648(96)07273-0.

(38) Yin, Z.; Kasrai, M.; Fuller, M.; Bancroft, G. M.; Fyfe, K.; Tan, K. H. Application of Soft X-Ray Absorption Spectroscopy in Chemical Characterization of Antiwear Films Generated by ZDDP Part I: The Effects of Physical Parameters. *Wear* **1997**, *202* (2), 172–

191. https://doi.org/https://doi.org/10.1016/S0043-1648(96)07272-9.

(39) Sharma, V.; Gabler, C.; Doerr, N.; Aswath, P. B. Mechanism of Tribofilm Formation with P and S Containing Ionic Liquids. *Tribol. Int.* **2015**, *92*, 353–364. https://doi.org/10.1016/j.triboint.2015.07.009.

(40) Wan, S.; Tieu, A. K.; Zhu, Q.; Zhu, H.; Cui, S.; Mitchell, D. R. G.; Kong, C.; Cowie, B.; Denman, J. A.; Liu, R. Chemical Nature of Alkaline Polyphosphate Boundary Film at Heated Rubbing Surfaces. *Sci. Rep.* **2016**, *6* (1), 26008. https://doi.org/10.1038/srep26008.

(41) Sharma, V.; Doerr, N.; Aswath, P. B. Chemical–Mechanical Properties of Tribofilms and Their Relationship to Ionic Liquid Chemistry. *RSC Adv.* **2016**, *6* (27), 22341–22356. https://doi.org/10.1039/C6RA01915C.

(42) Sharma, V.; Erdemir, A.; Aswath, P. B. An Analytical Study of Tribofilms Generated by the Interaction of Ashless Antiwear Additives with ZDDP Using XANES and Nano-Indentation. *Tribol. Int.* **2015**, *82*, 43–57. https://doi.org/10.1016/j.triboint.2014.09.019.

(43) Qu, J.; Meyer, H. M.; Cai, Z.-B.; Ma, C.; Luo, H. Characterization of ZDDP and Ionic Liquid Tribofilms on Non-Metallic Coatings Providing Insights of Tribofilm Formation Mechanisms. *Wear* **2015**, *332–333*, 1273–1285. https://doi.org/10.1016/j.wear.2015.01.076.

(44) Kim, B.; Jiang, J. C.; Aswath, P. B. Mechanism of Wear at Extreme Load and Boundary Conditions with Ashless Anti-Wear Additives: Analysis of Wear Surfaces and Wear Debris. *Wear* **2011**, *270* (3–4), 181–194. https://doi.org/10.1016/j.wear.2010.10.058.

(45) Mourhatch, R.; Aswath, P. B. Tribological Behavior and Nature of Tribofilms Generated from Fluorinated ZDDP in Comparison to ZDDP under Extreme Pressure Conditions—Part 1: Structure and Chemistry of Tribofilms. *Tribol. Int.* **2011**, *44* (3), 187–200. https://doi.org/10.1016/j.triboint.2010.10.018.

(46) Kim, B.; Mourhatch, R.; Aswath, P. B. Properties of Tribofilms Formed with Ashless Dithiophosphate and Zinc Dialkyl Dithiophosphate under Extreme Pressure Conditions. *Wear* **2010**, *268* (3–4), 579–591. https://doi.org/10.1016/j.wear.2009.10.004.

(47) Gosvami, N. N.; Bares, J. A.; Mangolini, F.; Konicek, A. R.; Yablon, D. G.; Carpick, R. W. Mechanisms of Antiwear Tribofilm Growth Revealed in Situ by Single-Asperity Sliding Contacts. *Science.* **2015**, *348* (6230), 102–106. https://doi.org/10.1126/science.1258788.

(48) Mosey, N. J.; Müser, M. H.; Woo, T. K. Molecular Mechanisms for the Functionality of

Lubricant Additives. *Science.* **2005**, *307* (5715), 1612–1615. https://doi.org/10.1126/science.1107895.

(49) Mosey, N. J.; Woo, T. K.; Kasrai, M.; Norton, P. R.; Bancroft, G. M.; Müser, M. H. Interpretation of Experiments on ZDDP Anti-Wear Films through Pressure-Induced Cross-Linking. *Tribol. Lett.* **2006**, *24* (2), 105–114. https://doi.org/10.1007/s11249-006-9040-9.

(50) Zhou, Y.; Leonard, D. N.; Guo, W.; Qu, J. Understanding Tribofilm Formation Mechanisms in Ionic Liquid Lubrication. *Sci. Rep.* **2017**, *7* (1), 8426. https://doi.org/10.1038/s41598-017-09029-z.

(51) Khare, H. S.; Lahouij, I.; Jackson, A.; Feng, G.; Chen, Z.; Cooper, G. D.; Carpick, R. W. Nanoscale Generation of Robust Solid Films from Liquid-Dispersed Nanoparticles via in Situ Atomic Force Microscopy: Growth Kinetics and Nanomechanical Properties. *ACS Appl. Mater. Interfaces* **2018**, *10* (46), 40335–40347. https://doi.org/10.1021/acsami.8b16680.

(52) Sui, T.; Song, B.; Wen, Y.; Zhang, F. Bifunctional Hairy Silica Nanoparticles as High-Performance Additives for Lubricant. *Sci. Rep.* **2016**, *6* (1), 22696. https://doi.org/10.1038/srep22696.

(53) Parekh, K.; Chen, X.; Aswath, P. B. Synthesis of Fluorinated ZDDP Compounds. *Tribol. Lett.* **2009**, *34* (2), 141–153. https://doi.org/10.1007/s11249-008-9373-7.

(54) Sharma, V.; Timmons, R.; Erdemir, A.; Aswath, P. B. Plasma-Functionalized Polytetrafluoroethylene Nanoparticles for Improved Wear in Lubricated Contact. *ACS Appl. Mater. Interfaces* **2017**, *9* (30), 25631–25641. https://doi.org/10.1021/acsami.7b06453.

(55) Sumitsawan, S.; Cho, J.; Sattler, M. L.; Timmons, R. B. Plasma Surface Modified TiO2 Nanoparticles: Improved Photocatalytic Oxidation of Gaseous m-Xylene. *Environ. Sci. Technol.* **2011**, *45* (16), 6970–6977. https://doi.org/10.1021/es2012963.

(56) Ratoi, M.; Niste, V. B.; Walker, J.; Zekonyte, J. Mechanism of Action of WS2 Lubricant Nanoadditives in High-Pressure Contacts. *Tribol. Lett.* **2013**, *52* (1), 81–91. https://doi.org/10.1007/s11249-013-0195-x.

(57) Tomala, A.; Vengudusamy, B.; Rodríguez Ripoll, M.; Naveira Suarez, A.; Remškar, M.; Rosentsveig, R. Interaction Between Selected MoS2 Nanoparticles and ZDDP Tribofilms. *Tribol. Lett.* **2015**, *59* (1), 26. https://doi.org/10.1007/s11249-015-0552-z.

(58) Aswath, V. S. J. B. T. P. B. Tribological Interaction of Plasma-Functionalized

Polytetrafluoroethylene Nanoparticles with ZDDP and Ionic Liquids. *Tribol. Lett.* **2018**, *66*, 107. https://doi.org/10.1007/s11249-018-1060-8.

(59) Yamaguchi, E. S.; Ryason, P. R.; Hansen, T. P. Electrical Contact Resistance Studies on Zinc Dithiophosphates. *Tribol. Lett.* **1997**, *3* (1), 27–33. https://doi.org/10.1023/A:1019175509680.

(60) Sharma, V.; Doerr, N.; Erdemir, A.; Aswath, P. B. Interaction of Phosphonium Ionic Liquids with Borate Esters at Tribological Interfaces. *RSC Adv.* **2016**, 53148–53161. https://doi.org/10.1039/c6ra11822d.

(61) Spikes, H. A. The History and Mechanisms of ZDDP. *Tribol. Lett.* **2004**, *17* (3), 469–489. https://doi.org/10.1023/B:TRIL.0000044495.26882.b5.

(62) Kasrai, M.; Lennard, W. N.; Brunner, R. W.; Bancroft, G. M.; Bardwell, J. A.; Tan, K. H. Sampling Depth of Total Electron and Fluorescence Measurements in Si L- and K-Edge Absorption Spectroscopy. *Appl. Surf. Sci.* **1996**, *99* (4), 303–312. https://doi.org/https://doi.org/10.1016/0169-4332(96)00454-0.

(63) Nicholls, M.; Najman, M. N.; Zhang, Z.; Kasrai, M.; Norton, P. R.; Gilbert, P. U. P. A. The Contribution of XANES Spectroscopy to Tribology. *Can. J. Chem.* **2007**, *85* (10), 816–830. https://doi.org/10.1139/v07-093.

(64) Tan, D. L. ; G. M. B. ; M. K. ; M. E. F. ; X. H. F. ; K. H. High-Resolution Si and P K- and L-Edge XANES Spectra of Crystalline SiP2O7 and Amorphous SiO2-P2O5. *Am. Mineral.* **1994**, *79* (7–8), 785–788.

(65) Kruse, J.; Leinweber, P.; Eckhardt, K.-U.; Godlinski, F.; Hu, Y.; Zuin, L. Phosphorus {\it L}${\sb 2,3}$-Edge XANES: Overview of Reference Compounds. *J. Synchrotron Radiat.* **2009**, *16* (2), 247–259. https://doi.org/10.1107/S0909049509000211.

(66) Vyavhare, K.; Bagi, S.; Patel, M.; Aswath, P. B. Impact of Diesel Engine Oil Additives–Soot Interactions on Physiochemical, Oxidation, and Wear Characteristics of Soot. *Energy & Fuels* **2019**, *33* (5), 4515–4530. https://doi.org/10.1021/acs.energyfuels.8b03841.

(67) Fleet, M. E.; Muthupari, S. Boron K-Edge XANES of Borate and Borosilicate Minerals. *Am. Mineral.* **2000**, *85* (7–8), 1009–1021. https://doi.org/10.2138/am-2000-0716.

(68) Fofanov, D. Synthesis, Characterization and Physical Properties of Metal Borides, Universität Hamburg, Von-Melle-Park 3, 20146 Hamburg, 2006.

(69) Fleet, M. E.; Muthupari, S. Coordination of Boron in Alkali Borosilicate Glasses Using

XANES. *J. Non. Cryst. Solids* **1999**, *255* (2), 233–241. https://doi.org/10.1016/S0022-3093(99)00386-5.

(70) Varlot, K.; Kasrai, M.; Bancroft, G. M.; Yamaguchi, E. S.; Ryason, P. R.; Igarashi, J. X-Ray Absorption Study of Antiwear Films Generated from ZDDP and Borate Micelles. *Wear* **2001**, *249* (12), 1029–1035. https://doi.org/10.1016/S0043-1648(01)00586-5.

(71) Heuberger, R.; Rossi, A.; Spencer, N. D. XPS Study of the Influence of Temperature on ZnDTP Tribofilm Composition. *Tribol. Lett.* **2007**, *25* (3), 185–196. https://doi.org/10.1007/s11249-006-9166-9.

(72) Preisinger, M.; Krispin, M.; Rudolf, T.; Horn, S.; Strongin, D. R. Electronic Structure of Nanoscale Iron Oxide Particles Measured by Scanning Tunneling and Photoelectron Spectroscopies. *Phys. Rev. B* **2005**, *71* (16), 165409. https://doi.org/10.1103/PhysRevB.71.165409.

(73) Gonzalez, Y.; Lafont, M. C.; Pebere, N.; Chatainier, G.; Roy, J.; Bouissou, T. A Corrosion Inhibition Study of a Carbon Steel in Neutral Chloride Solutions by Zinc Salt/Phosphonic Acid Association. *Corros. Sci.* **1995**, *37* (11), 1823–1837. https://doi.org/https://doi.org/10.1016/0010-938X(95)00085-X.

(74) Minfray, C.; Martin, J. M.; Esnouf, C.; Mogne], T. [Le; Kersting, R.; Hagenhoff, B. A Multi-Technique Approach of Tribofilm Characterisation. *Thin Solid Films* **2004**, *447–448*, 272–277. https://doi.org/https://doi.org/10.1016/S0040-6090(03)01064-2.

(75) Varlot, K.; Martin, J. M.; Grossiord, C.; Vargiolu, R.; Vacher, B.; Inoue, K. A Dual-analysis Approach in Tribochemistry: Application to ZDDP/Calcium Borate Additive Interactions. *Tribol. Lett.* **1999**, *6* (3), 181–189. https://doi.org/10.1023/A:1019167808656.

(76) Eglin, M.; Rossi, A.; Spencer, N. D. X-Ray Photoelectron Spectroscopy Analysis of Tribostressed Samples in the Presence of ZnDTP: A Combinatorial Approach. *Tribol. Lett.* **2003**, *15* (3), 199–209. https://doi.org/10.1023/A:1024805001625.

(77) Rossi, A.; Piras, F. M.; Kim, D.; Gellman, A. J.; Spencer, N. D. Surface Reactivity of Tributyl Thiophosphate: Effects of Temperature and Mechanical Stress. *Tribol. Lett.* **2006**, *23* (3), 197–208. https://doi.org/10.1007/s11249-006-9051-6.

(78) Nedelcu, I.; Piras, E.; Rossi, A.; Pasaribu, H. R. XPS Analysis on the Influence of Water on the Evolution of Zinc Dialkyldithiophosphate–Derived Reaction Layer in Lubricated Rolling Contacts. *Surf. Interface Anal.* **2012**, *44* (8), 1219–1224.

https://doi.org/10.1002/sia.4853.

(79) Zhang, Z.; Yamaguchi, E. S.; Kasrai, M.; Bancroft, G. M. Interaction of ZDDP with Borated Dispersant Using XANES and XPS. *Tribol. Trans.* **2004**, *47* (4), 527–536. https://doi.org/10.1080/05698190490500725.

(80) Battez], A. [Hernández; Viesca, J. L.; González, R.; Blanco, D.; Asedegbega, E.; Osorio, A. Friction Reduction Properties of a CuO Nanolubricant Used as Lubricant for a NiCrBSi Coating. *Wear* **2010**, *268* (1), 325–328. https://doi.org/https://doi.org/10.1016/j.wear.2009.08.018.

(81) Peña-Parás, L.; Taha-Tijerina, J.; Garza, L.; Maldonado-Cortés, D.; Michalczewski, R.; Lapray, C. Effect of CuO and Al2O3 Nanoparticle Additives on the Tribological Behavior of Fully Formulated Oils. *Wear* **2015**, *332–333*, 1256–1261. https://doi.org/https://doi.org/10.1016/j.wear.2015.02.038.

(82) Kalyani; Jaiswal, V.; Rastogi, R. B.; Kumar, D. The Investigation of Different Particle Size Magnesium-Doped Zinc Oxide (Zn0.92Mg0.08O) Nanoparticles on the Lubrication Behavior of Paraffin Oil. *Appl. Nanosci.* **2017**, *7* (6), 275–281. https://doi.org/10.1007/s13204-015-0471-1.

(83) Song, X.; Zheng, S.; Zhang, J.; Li, W.; Chen, Q.; Cao, B. Synthesis of Monodispersed ZnAl2O4 Nanoparticles and Their Tribology Properties as Lubricant Additives. *Mater. Res. Bull.* **2012**, *47* (12), 4305–4310. https://doi.org/https://doi.org/10.1016/j.materresbull.2012.09.013.

(84) Chou, R.; Battez, A. H.; Cabello, J. J.; Viesca, J. L.; Osorio, A.; Sagastume, A. Tribological Behavior of Polyalphaolefin with the Addition of Nickel Nanoparticles. *Tribol. Int.* **2010**, *43* (12), 2327–2332. https://doi.org/https://doi.org/10.1016/j.triboint.2010.08.006.

(85) Viesca, J. L.; Hernández Battez, A.; González, R.; Chou, R.; Cabello, J. J. Antiwear Properties of Carbon-Coated Copper Nanoparticles Used as an Additive to a Polyalphaolefin. *Tribol. Int.* **2011**, *44* (7), 829–833. https://doi.org/https://doi.org/10.1016/j.triboint.2011.02.006.

Supporting Information

1) Chemical properties of plasma deposited borate-based polymer films and ZnO nanoparticles covered with borate-based films. Results of FTIR and XANES confirms deposition of borate based polymer films on ZnO nanoparticles.

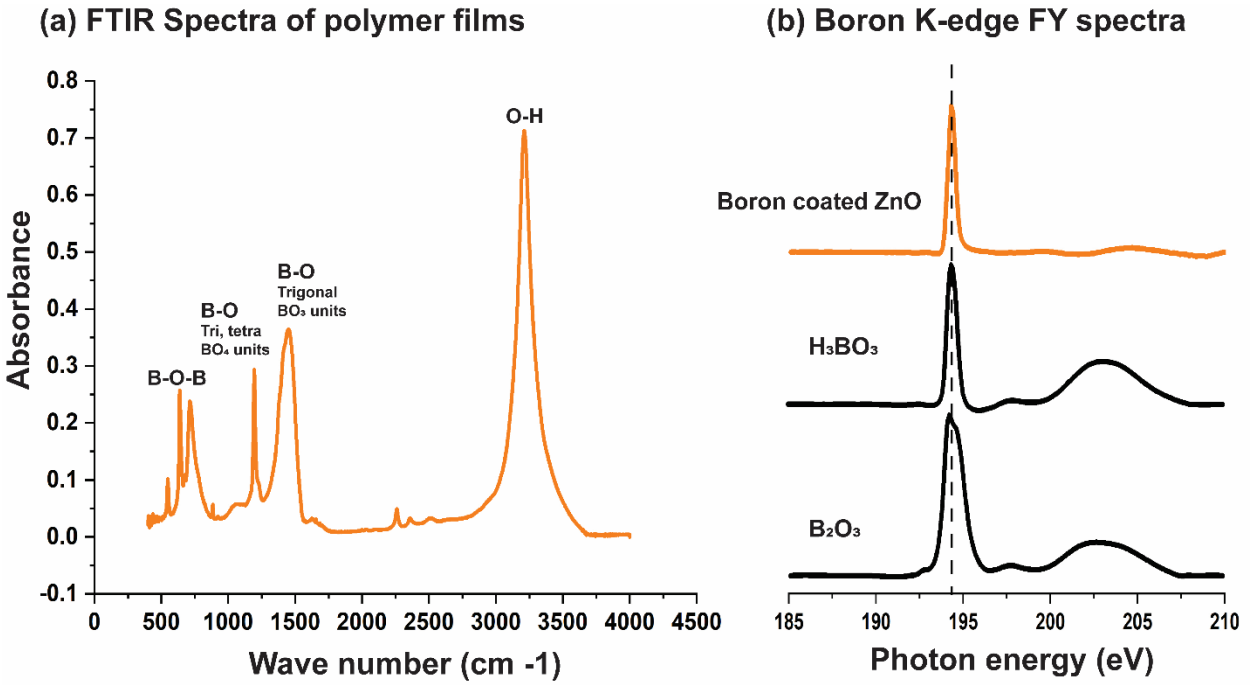

Figure S1. Surface characterization to confirm chemical nature of polymer films deposited on ZnO nanoparticles. (a) FTIR spectra of plasma films generated polymer films from trimethylboroxine monomer on KBr card (b) XANES Boron K-edge spectra of boron-coated ZnO nanopartciles developed using plasma polymerization.

2) Friction and wear results of tribological tests carried out to find optimum concentration of ZnO nanoparticles in mineral base oil.

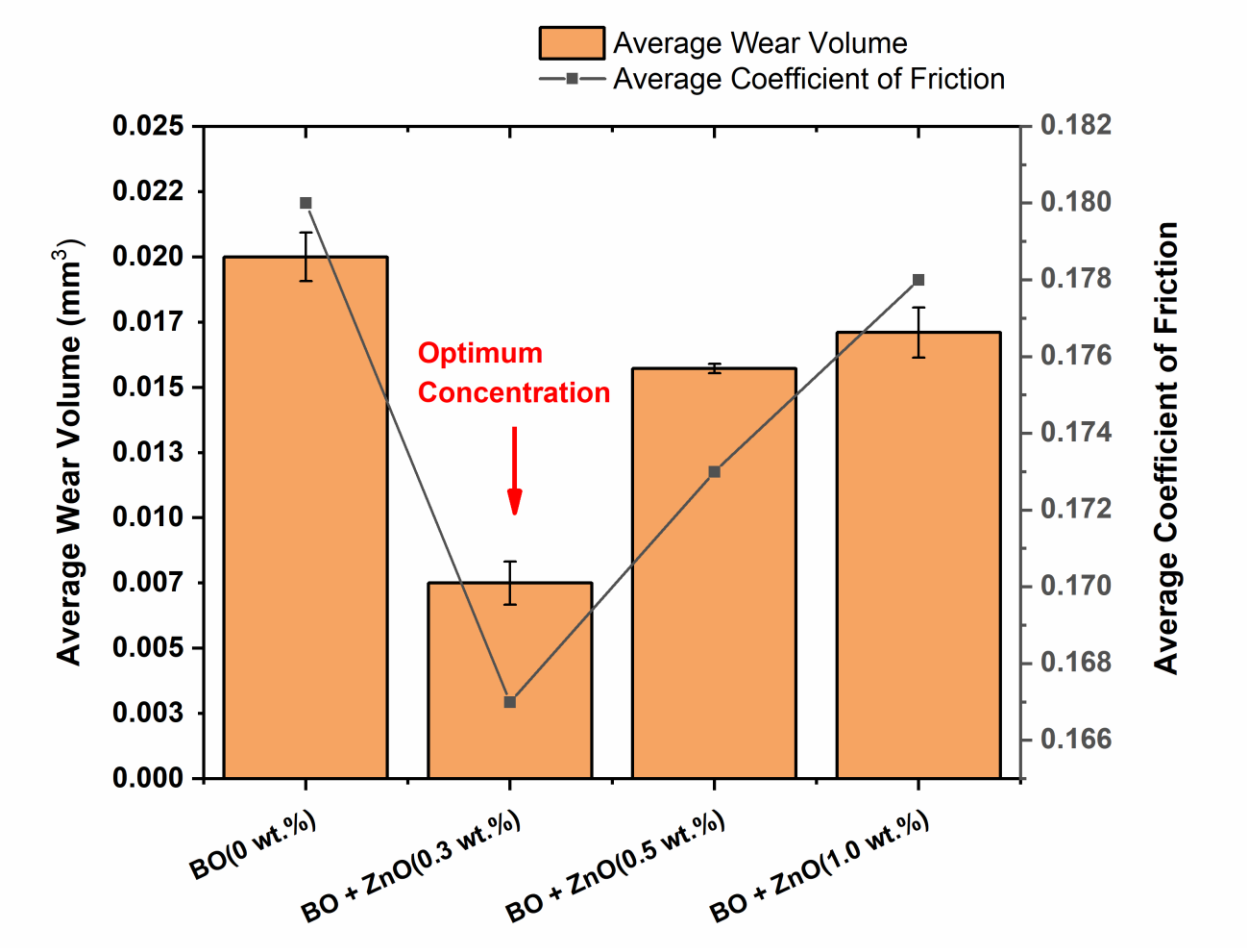

Figure S2. Average wear volume and average coefficient of friction test results of lubricants containing non-functionalized ZnO nanoparticles at different concentrations (0, 0.3, 0.5, 1 wt.%).

3) Optical images of the wear scar developed on flat steel specimen.

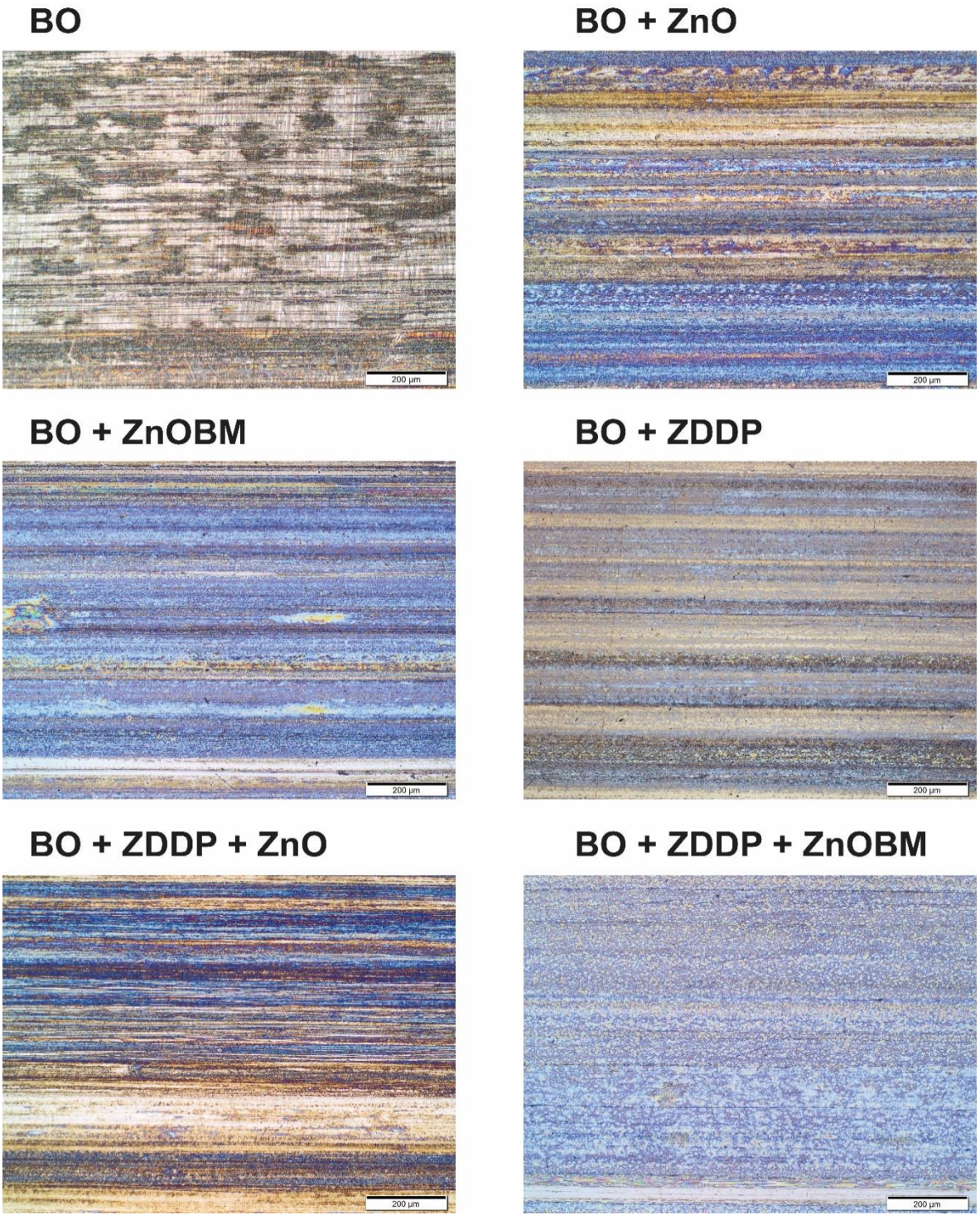

Figure S3. Optical images of the wear scar developed on flat steel specimen with test oils (A) BO; (B) BO + ZnO; (C) BO + ZnOBM; (D) BO + ZDDP; (E) BO + ZDDP + ZnO; (F) BO + ZDDP + ZnOBM.

4) Optical Profilometry Results

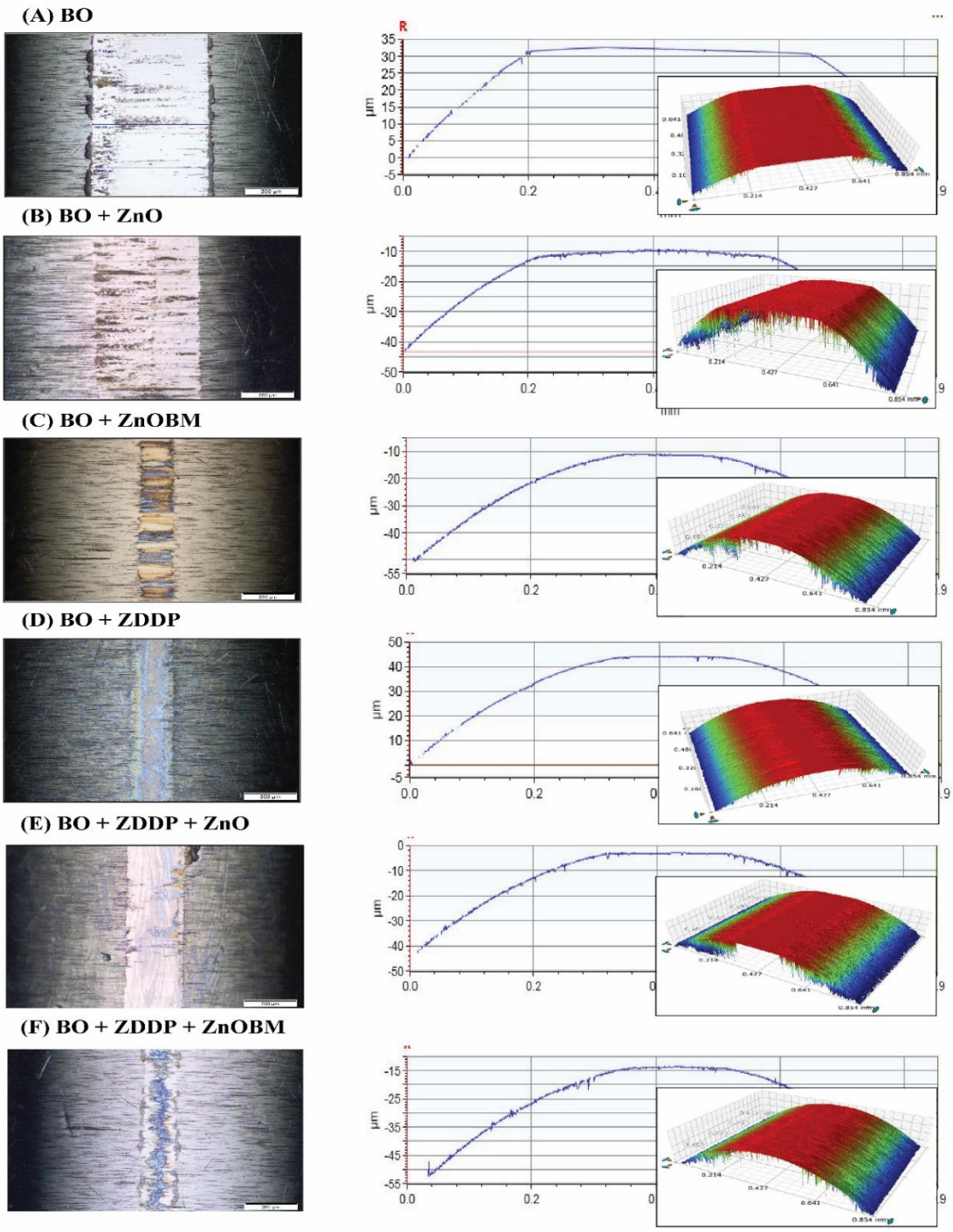

Figure S4. Optical micrographs (left) and profilometry 2D and 3D images (right) of the wear scar developed on cylindrical test specimen lubricated with formulations (A) BO; (B) BO + ZnO; (C) BO + ZnOBM; (D) BO + ZDDP; (E) BO + ZDDP + ZnO; (F) BO + ZDDP + ZnOBM.

CHAPTER 3

TRIBOFILM FORMATION, FRICTION, AND WEAR PROPERTIES OF A PLASMA FUNCTIONALIZED $CaCO_3$ NANOPARTICLES IN THE PRESENCE OF ASHLESS DITHIOPHOSPHATE AND ZDDP ANTI-WEAR ADDITIVES

Kimaya Vyavhare, Richard B. Timmons, Ali Erdemir, Brian Edwards, and Pranesh B. Aswath

Submission: In progress

Abstract

The surface-modified $CaCO_3$ nanoparticles were synthesized through plasma-enhanced chemical vapor deposition (PECVD) to develop eco-friendly lubricant additive technology for internal combustion engines with the focus on reducing and/ replacing harmful additives like zinc dialkyl dithiophosphate (ZDDP) in the engine oil. Various oil formulations were prepared with functionalized $CaCO_3$ nanoparticles in combination with ashless dialkyl dithiophosphate (DDP) and ZDDP at a very low concentration of phosphorus. Tribological test results indicate synergistic interaction of functionalized $CaCO_3$ nanoparticles with ZDDP and DDP providing enhanced friction and wear performance under boundary lubrication. A comparative study of the tribo-surfaces morphology and chemistry has been assessed by atomic force microscopy and X-ray absorption near-edge spectroscopy. Improved wear protection by functionalized $CaCO_3$BM nanoparticles under boundary lubrication was attributed to the formation of Calcium and Boron-rich 50-80 nm thick tribofilms on the worn surface. XANES results revealed that plasma functionalized $CaCO_3$ nanoparticles interact with ZDDP and DDP and participate in tribofilm formation through tribo-chemical reactions and metal cation supply to form stable and thicker tribofilms. These results strongly suggest the potential application of plasma functionalized $CaCO_3$ nano-additives to reduce the concentration of harmful P-based additives in automotive lubricants.

1. INTRODUCTION

The lubrication in mechanical devices like engines has always required continuous improvement to reduce emissions, improve fuel economy, increase durability, and reduce frictional losses – thus improving overall energy efficiency [1–6]. Lubrication at sliding/rolling contacts in the engine is an interfacial phenomenon with three regimes: boundary, mixed, and hydrodynamic lubrication, wherein hydrodynamic lubrication provides the lowest friction and wear. Maximum friction and wear losses occur at the boundary and mixed lubrication regimes in engine locations such as the top-ring-reversal region of the piston ring-cylinder liner interface, rolling-sliding contact at cam-follower surfaces, and sliding surfaces in the valve train [7]. Anti-wear additives play a crucial role in reducing wear and preventing the failure of boundary or mixed lubricated interfaces experiencing direct surface asperity collisions due to inadequate lubricant load support. Particularly, anti-wear additives are of prime importance in low viscosity oils which are currently being used in modern engines to substantially reduce viscous energy loss in the engine. Developing more effective automotive lubrication in combination with low viscosity base stock and high-performance additive package can be the most economical and effective route to improve engine efficiency and durability.

Anti-wear additives protect surfaces in relative motion from subsequent damage by undergoing mechanochemical dissociation and forming surface bond tribofilms. The capability of tribofilms to protect sliding contacts mainly depends on their intrinsic properties and their adhesion to the substrate. For example, zinc dialkyl dithiophosphate (ZDDP) is the additive used in current commercial automotive lubricants because of their ability to form effective tribofilms, which act as a sacrificial layer to protect the underlying metal surface [8]. ZDDP tribofilms are well known to form on steel-steel sheared contacts as a result of stress-assisted, thermally activated chemical

reactions [9–11]. To date, extensive research work has been conducted to study the properties and tribofilm forming mechanism of ZDDP. Several studies have shown that these tribofilms are formed at only high temperatures while at room temperature weakly bounded tribofilms are formed, while in some cases, no tribofilms are observed [12, 13]. ZDDP tribofilms exhibit patchy morphology and lower elastic modulus and hardness than that of materials of engine components (like steel), which allows them to sacrifice or distribute applied stresses under mild friction at the sliding interface to prevent wear [14]. However, despite being a cost-effective multipurpose additive, their application in engine oil is questioned in recent years due to their several disadvantages like poisoning of exhaust after-treatment systems by thiophosphate byproducts, inadequate wear protection in ultralow viscous lubricants, and micro-pitting in thin-film lubrication [14]. These disadvantages drive the need to eliminate or partially replace ZDDP in the oil. However, an alternative solution was found by introducing several engine oil specifications between 1994 to 2020 that subsequently reduced the permitted maximum concentration of phosphorus and sulfur in the engine oil [15]. Current engine oil specification allows phosphorus level up to 0.08 wt.%, however, there is a strong possibility that in the future permissible phosphorus content in an engine oil might be substantially reduced further [15, 16]. More crucially, any further reduction in ZDDP content than 0.08 wt.% of phosphorus will affect the tribological performance of currently used low viscosity lubricants (like GF6). Therefore, it is important to find novel additives capable of either replacing or reducing ZDDP content in the engine oil.

In recent years, various nanomaterials have been explored as additives in lubricant base oil from the perspective of developing energy-efficient lubrication which can impart superior tribological performance and lower emissions than conventional additives like ZDDP [17–24]. The integration of nanomaterials into tribological systems has several benefits over their micron-

sized counterparts mainly due to their extremely small size and high specific surface area [25]. Nanoscale materials are believed to have a different mechanism for friction and wear reduction as compared to P-based lubricant additives. For example, metal and metal oxide nanoparticles may get physically pressed or smeared on the rubbing surfaces at high contact pressure to form protective surface layers or tribo-sintered films, which helps to decrease resistance to shear stress and provides a cushion against direct asperities collision [19, 25, 26]. Hard carbon-based or ceramic particles are reported to act as mini-ball bearings at the sliding interface [27, 28]. On the other hand, soft carbon-based nanomaterials exfoliate to form a protective film upon rubbing [29, 30].

$CaCO_3$ nanoparticles are of our particular interest because of their excellent chemical stability, frictional and wear reduction properties, and potential to be used as a green lubricant additive in commercial oils [31–34]. Practical lubrication application of metal oxide nanoparticles faces major challenges like agglomeration and sedimentation in the base oil. Several studies have shown the efficacy of using a surface modification to improve the solubility of metal oxide nanoparticles in oils [18, 35–38].

In this study, we have encapsulated $CaCO_3$ nanoparticles with plasma polymerized acrylate ligands to molecularly surface tailored the $CaCO_3$ nanoparticles and improve their suspendability in the base oil. We are using the plasma-enhanced chemical vapor deposition (PECVD) technique to coat nanoparticles with two different polymer films not only to modify the surface of nanoparticles but also to use them as a carrier to deposit tribologically beneficial chemistries at the sliding interface to promote the formation of tribofilms. Initially, $CaCO_3$ nanoparticles were coated with boron-based polymer films, and then subsequently the second film of acrylate-based chemistry was deposited on top of boron-coated $CaCO_3$ nanoparticles. This plasma functionalized

calcium carbonate ($CaCO_3$BM) nanoparticles were characterized using Fourier transform infrared spectroscopy (FTIR) and X-ray absorption near-edge spectroscopy (XANES). The main objective of this study is to assess the anti-wear performance of plasma functionalized $CaCO_3$BM nanoparticles to partially replace P-containing anti-wear additives and develop environmentally friendly lubricants with 350 ppm of phosphorus (i.e. almost half of that is used in commercial lubricants). Secondly, we aim at elucidating the compatibility of novel $CaCO_3$BM nanoparticles with P-based additives like zinc dialkyl dithiophosphate (ZDDP) and ashless dialkyl dithiophosphate (DDP) and thoroughly examine their interaction, formation of tribofilms, and overall, anti-wear mechanism. For this purpose, oil formulations were prepared with $CaCO_3$BM nanoparticles in combination with/without ZDDP, and DDP and tribological properties were assessed through high frequency reciprocating tribometer under the boundary lubrication regime. In addition to friction and wear properties, electrical contact resistance data was acquired in-situ during tribological tests to evaluate the dynamics of tribofilm formation at the sliding interface. Furthermore, surface characterization techniques like atomic force microscopy (AFM) and XANES were employed to determine the morphology and chemical make-up of tribofilms. The results obtained provide fundamental insights into the anti-wear mechanism and nature of the tribofilms formed.

2. Experimental details

2.1 Materials

To synthesis functionalized nano-additives, $CaCO_3$ nanoparticles of size 30-40 nm were obtained from a commercial vendor, Sky Spring Nanomaterials. For plasma functionalization of $CaCO_3$ different precursors like trimethyl boroxine, and glycidyl methacrylate monomers were purchased from Sigma Aldrich and used in analytical grade reagents without further purification.

Test lubricants were formulated using ZDDP and DDP phosphorus-based anti-wear additives in Group III mineral base oil. Group III mineral base oil (Viscosity @100ºC - 4cst) was procured from GS Caltex, while ZDDP and DDP additives were obtained from Oronite. The chemical structure of all anti-wear additives used in this study is shown in Table 1.

Table 1. The coded names, structure, and chemical names of anti-wear additives.

Code	Chemical name	Structure	Wt.% P
DDP	Ashless dialkyl dithiophosphate	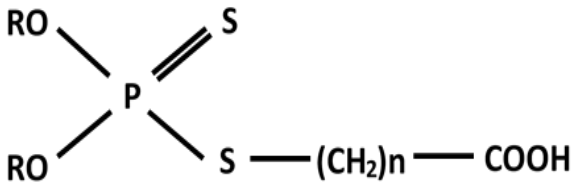	9.3
ZDDP	Zinc dialkyl dithiophosphate	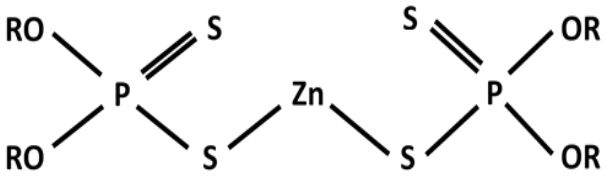	7.27
$CaCO_3$BM	Plasma functionalized $CaCO_3$ nanoparticles	 **Coating from Trimethyl boroxine** **Coating from Glycidyl Methacrylate**	N/A

2.2 Preparation of functionalized $CaCO_3$ nano-additives and test lubricants

A core-shell structure functionalized $CaCO_3$ nanoparticles were synthesized via a plasma processing technique, specifically plasma-enhanced chemical vapor deposition (PECVD). A home built 360º degree continuously rotatable plasma reactor was used in this study to ensure uniform and efficient coating of the $CaCO_3$ nanoparticles. It is believed that the effective mass transport

and agitation of the nanoparticles are achieved due to the rotating motion of the reactor, which in turn helps to continuously expose the fresh surface of $CaCO_3$ nanoparticles to the plasma generated reactive molecules and ions. Initially, 3g of $CaCO_3$ nanoparticles were loaded inside the borosilicate glass reactor and were exposed to a plasma generated with trimethyl boroxine monomer.

This deposition process was carried out using a continuous wave (CW) plasma for initial 20 mins, followed with pulsating wave plasma (PW) generated with sequentially reducing duty cycle from 20:30 (plasma on time: plasma off times in seconds) to 20:60, for 10 minute periods at each ratio. The technique of using both CW and PW plasma to achieve adhesive polymer film is reported in our previous work [39–41]. The monomer pressure was maintained at 120 mT and RF power was kept at 60 W throughout the process. To facilitate effective chemical characterization of plasma polymer films, Fourier transforms infrared (FTIR) analysis was carried out on trimethyl boroxine films deposited on a flat substrate like KBr card and Si wafer. Additionally, to confirm the uniform deposition of plasma polymer films on nanoparticles, $CaCO_3$ nanoparticles exposed to trimethyl boroxine monomer were characterized using the X-ray absorption near edge (XANES) technique. XANES boron K-edge spectra shown in figure 1(b) exhibit the presence of boron-based films on the surface of $CaCO_3$ nanoparticles. Subsequently, methacrylate-based polymer films were deposited on the top of boron-based coatings to assist the dispersion of the $CaCO_3$ nanoparticles in the base oil. For this purpose, glycidyl methacrylate monomer was used and the deposition process was carried out using power – 100 W, monomer pressure – 70 mT, continuous-wave plasma – 20 min, pulsating plasma with a duty cycle (20:50) – 40 min.

Table 2. Test lubricant details and additive composition.

Coded name	Lubricant	Additive Composition

BO	Group III mineral base oil	No additives were added
$CaCO_3$BM	Plasma functionalized $CaCO_3$ mixed with group III mineral base oil	$CaCO_3$BM – 0.5 wt.%
ZDDP350	Zinc dialkyl dithiophosphate mixed with group III mineral base oil	ZDDP – 0.035 wt.% of P
DDP350	Ashless dialkyl dithiophosphate mixed with group III mineral oil	DDP – 0.035 wt.% of P
ZDDP350_$CaCO_3$BM	Plasma functionalized $CaCO_3$ mixed with ZDDP in group III mineral base oil	$CaCO_3$BM – 0.5 wt.% ZDDP – 0.035 wt.% of P
DDP350_$CaCO_3$BM	Plasma functionalized $CaCO_3$ mixed with DDP in group III mineral base oil	$CaCO_3$BM – 0.5 wt.% DDP – 0.035 wt.% of P
ZDDP700	Zinc dialkyl dithiophosphate mixed with group III mineral base oil to mimic commercial oils	ZDDP – 0.07 wt.% of P

Different oil formulations were prepared by mixing functionalized $CaCO_3$BM nanoparticles to mineral group III base oil to assess their anti-wear and anti-friction performance. Initially, tribological tests were conducted to determine the optimum concentration of nano-additives by using oils containing non-functionalized $CaCO_3$ nanoparticles at different concentrations (0, 0.3, 0.5, 1), and results of which are shown as a bar graph in figure 1(c). Based on the friction and wear results of the concentration test, $CaCO_3$BM nanoparticles were added to the base oil at 0.5 wt.% percolation threshold. Table 2 details the coded name and concentration of additives used to prepare six oil formulations.

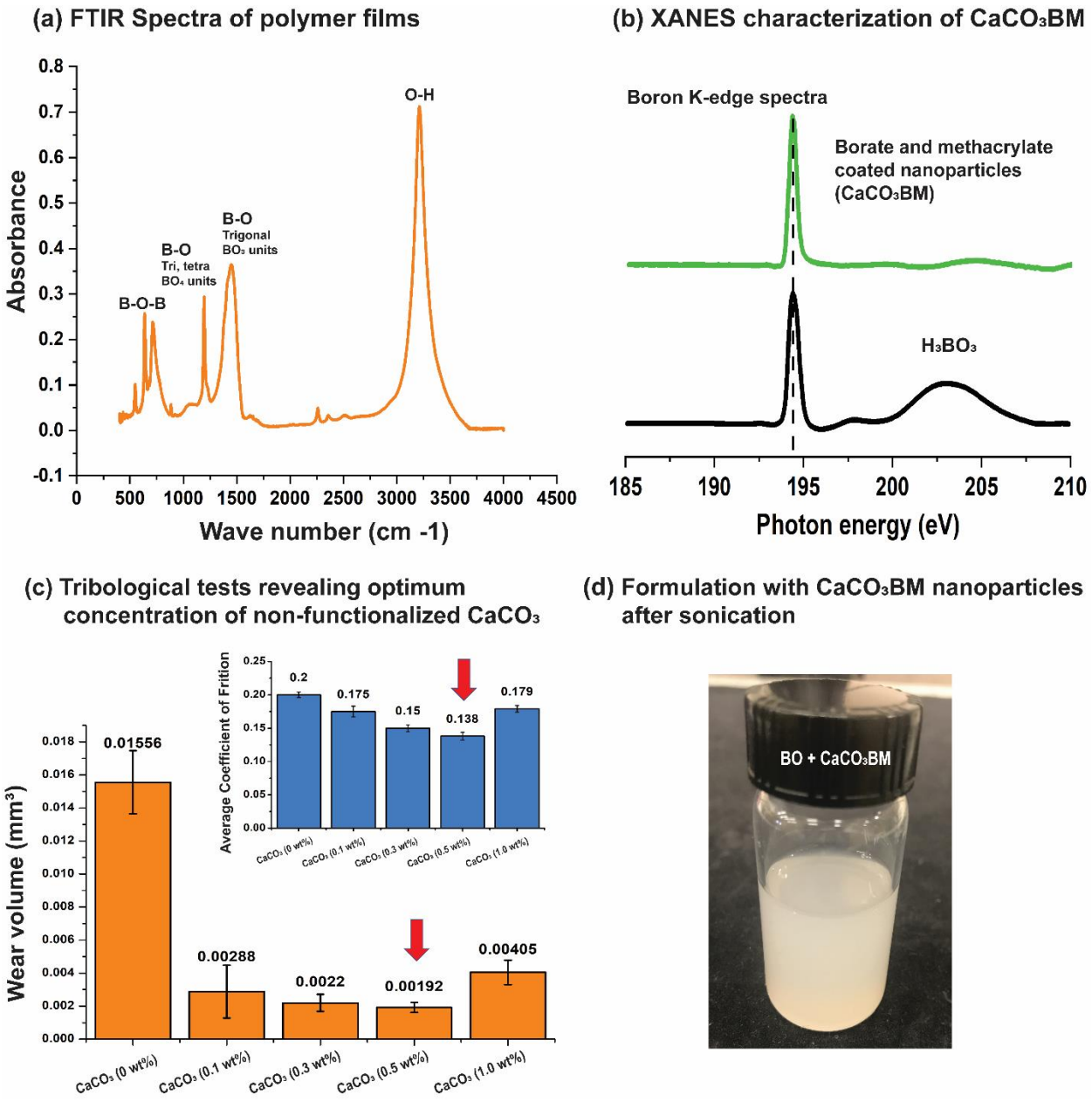

Figure 1 (a) FTIR characterization of plasma polymer films generated with trimethyl boroxine monomer; (b) XANES characterization of plasma functionalized nanoparticles; (c) Preliminary tribological test results with non-functionalized $CaCO_3$ nanoparticles indicating an optimum concentration of 0.5 wt.%; (d) Image of functionalized $CaCO_3$BM nanoparticles uniformly dispersed in the mineral base oil after probe sonication.

Here, P-containing additives were added to the base oil at 350 ppm of P concentration. It should be noted that 700 – 800 ppm of P is used in conventional engine lubricants, but as one of the aims of this study is to reduce the detrimental level of phosphorus in engine oil, test lubricants were formulated at 350 ppm. Probe sonication for 15 min was employed to ensure homogenous mixing of $CaCO_3$BM, ZDDP, and DDP additives in the base oil. Functionalized $CaCO_3$BM nanoparticles retained dispersion in the base oil for over a month of observation time.

2.3 Tribological Tests and Worn Surface Characterization

A linear reciprocating tribometer with the cylinder-on-flat configuration at Argonne National Laboratory was employed to evaluate the tribological performance of the oil dispersed with or without functionalized $CaCO_3$ additives and base oil. Tests were performed with an AISI 52100 steel cylinder (4mm × 6mm) reciprocating or sliding against AISI 52100 steel flat (12mm × 12mm × 4mm). The upper steel cylinder was a standard grade bearing steel of surface roughness ~15 nm (Sa) and the hardness was measured to be ~60 HRc. The steel flat surface was polished using 1200 grit SiC abrasive paper to reach a roughness of ~12 nm (Sa) and the hardness was measured to be in the range of 58-60 HRc. All contact surfaces were thoroughly cleaned with Stoddard solution, isopropanol, and acetone before the test. Tribological tests were conducted at 100 ºC temperature under a normal load of 82 N and speed of 300 rpm with a 6mm stroke for a sliding duration of 60 min. These test parameters were selected to closely simulate the contact pressure and sliding speed experienced at the cylinder liner-piston ring interface in the internal combustion engine. Lubricant film thickness was calculated using the Dowson-Higginson equation [42] to ensure all tests were run under the boundary lubrication regime. Three replicates were run for each lubricant. After completion of the tests, both cylinder and flat samples were cleaned using heptane to remove oil residue and were preserved for tribofilm characterization in

additive-free poly-alpha olefin oil. The coefficient of friction data was measured in-situ during tribological tests using DasyLab software. The non-contact 3D optical profilometer and optical microscope were used to measure the wear volume of cylinder test samples.

Worn surfaces generated on the steel flat samples were subjected to extensive surface characterization. The morphology and topography of interfacial tribofilms formed by additives were elucidated through analysis of worn surfaces generated on flat test specimens using atomic force microscopy (AFM). The high-resolution imaging capability of AFM allows us to acquire the 3D morphology of tribofilms at nanometer-scale resolution. AFM was used in the contact mode to obtain 3D scanning probe microscopic images of the rubbed surfaces detailing wear characteristics and mechanism in play at the tribological contact.

X-ray absorption near edge spectroscopic (XANES) was employed to determine the chemical make-up and properties of the tribofilms. XANES characterization was carried out at the Canadian Light Source synchrotron facility. For XANES analysis, flat steel samples were cleaned thoroughly using isopropyl alcohol and then loaded inside the vacuum chamber. Each sample was scanned at two different spots (left edge, or right edge, and center area of the wear scar) to ensure consistency in the results. The phosphorus L-edge and boron K-edge data were collected at a variable line spacing plane grating monochromator (VLS-PGM), operating at the energy range from 5.5 eV to 250 eV with a photon resolution of more than 10000 E/ΔE. The phosphorus, calcium, and sulfur K-edge data were acquired at a soft X-ray micro characterization beamline (SXRMB), which provides an energy range from 1.7 keV to 10 keV and a photon resolution of more than 3.3 x 10-4 InSb (111). The zinc L-edge, iron L-edge, and oxygen K-edge spectra were acquired at a spherical grating monochromator (SGM) beam station operating at the energy range of 250-2000 eV and a photon resolution of more than 5000 E/ΔE. Spectra at both VLS-PGM and

SGM beam stations were collected using 100 µm × 100 µm beam spot size, while the large spot size of 1 mm × 2 mm was used at the SXRMB beam station. Both high energy K-edge and low energy L-edge spectra were acquired in the total electron yield (TEY) and fluorescence yield (FY) two different detection modes. TEY mode provides chemical information of the surface layers/ near-surface region whereas the FY mode detects information from the bulk of the sample. For example, the sampling depth of P L-edge TEY mode is only ~ 5 nm, while in P L-edge FY mode ~60 nm of the bulk of the sample is probed.

3. Results and Discussion

3.1 Coefficient of Friction and Wear Volume

The coefficient of friction (COF) data recorded *in-situ* during the tribological test is plotted in figure 2 as the function of test time for all formulations. The average coefficient of friction is also provided in figure 3. Variance in the friction profile helps to speculate the presence or removal of smooth surface providing low shear strength at tribological contacts. The friction profile of the sample (A) BO exhibits unstable and high values of COF throughout the completion of tests. On the other hand, the friction response of sample (B) $CaCO_3$BM is relatively stable. For the first 25 min of sliding, rapid increase and drop in COF values are observed, but as the test continues COF value drops and becomes stable. Surprisingly, the ZDDP sample exhibits the most dramatic friction response, wherein for the initial 15 min some variance and high COF are observed, but after that COF values drop and increase and for the last 25 min becomes stable. Interestingly, sample (E) with the combination of ZDDP and $CaCO_3$BM exhibits lower COF values than the sample (C) with only ZDDP. Sample (F) with the mixture of ZDDP and $CaCO_3$BM nanoparticles exhibits the steadiest friction response of all, however, COF values near the end of the test are slightly higher than the COF values for sample (B) with only $CaCO_3$BM and sample (D) with only DDP. It is

important to note that after 40 min of the test, the friction profile for samples (B), (D), (E), and (F) appears to be stable and similar with low COF values. The stability in the friction profile indicates that the boundary tribofilms formed by these additives are very robust under applied normal load and high

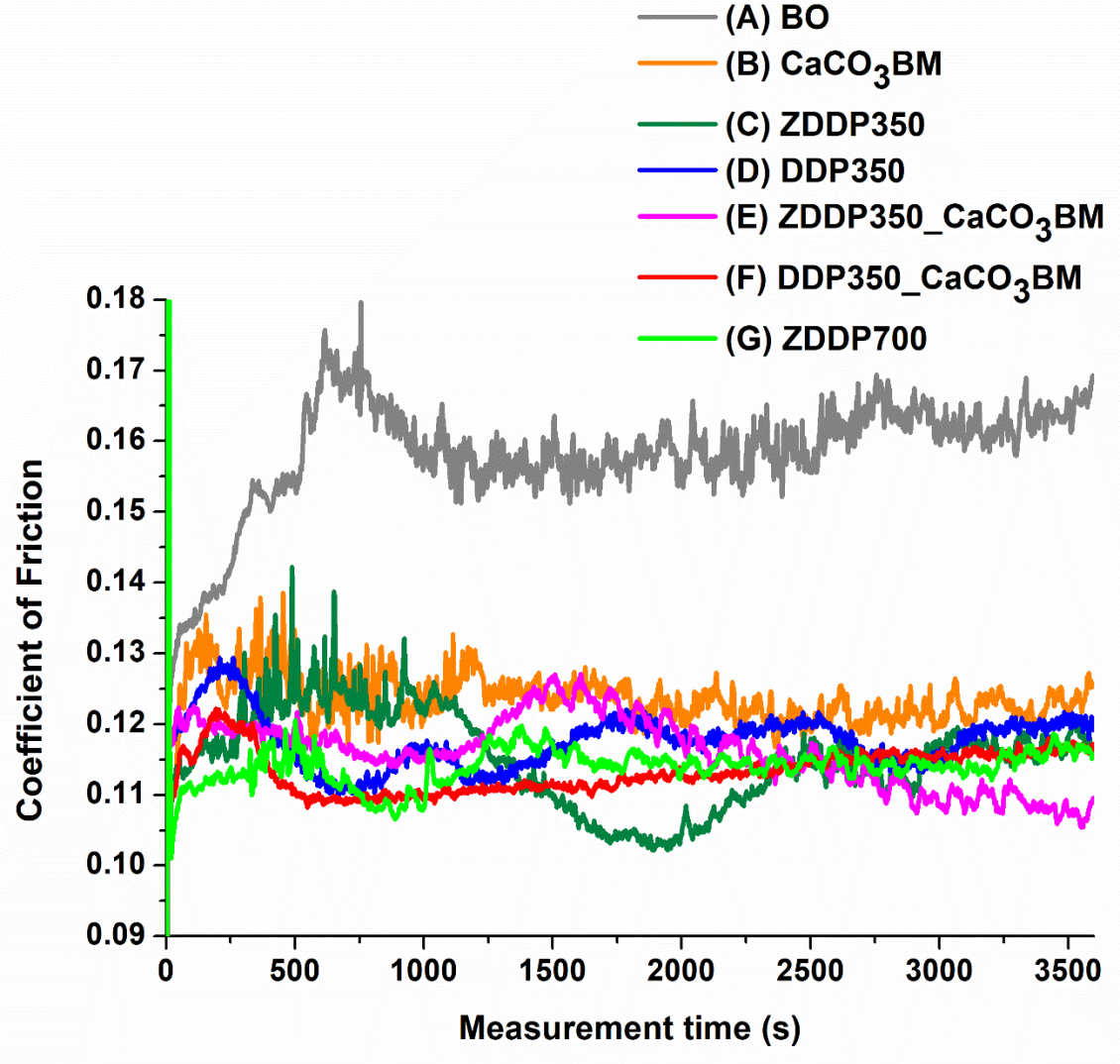

Figure 2. Friction results for samples BO, $CaCO_3$BM, ZDDP350, DDP350, ZDDP350_$CaCO_3$BM, DDP_$CaCO_3$BM, and ZDDP700.

contact pressure. As shown in figure 3, oil formulations containing only $CaCO_3$BM, only ZDDP, and only DDP exhibits the highest average COF value while binary additive formulations

containing $CaCO_3$BM with ZDDP and DDP displays the lowest average COF value. Notably, DDP_$CaCO_3$BM exhibits lower COF than ZDDP_$CaCO_3$BM. This indicates that the addition of $CaCO_3$BM to ZDDP and DDP results in an improvement of friction response.

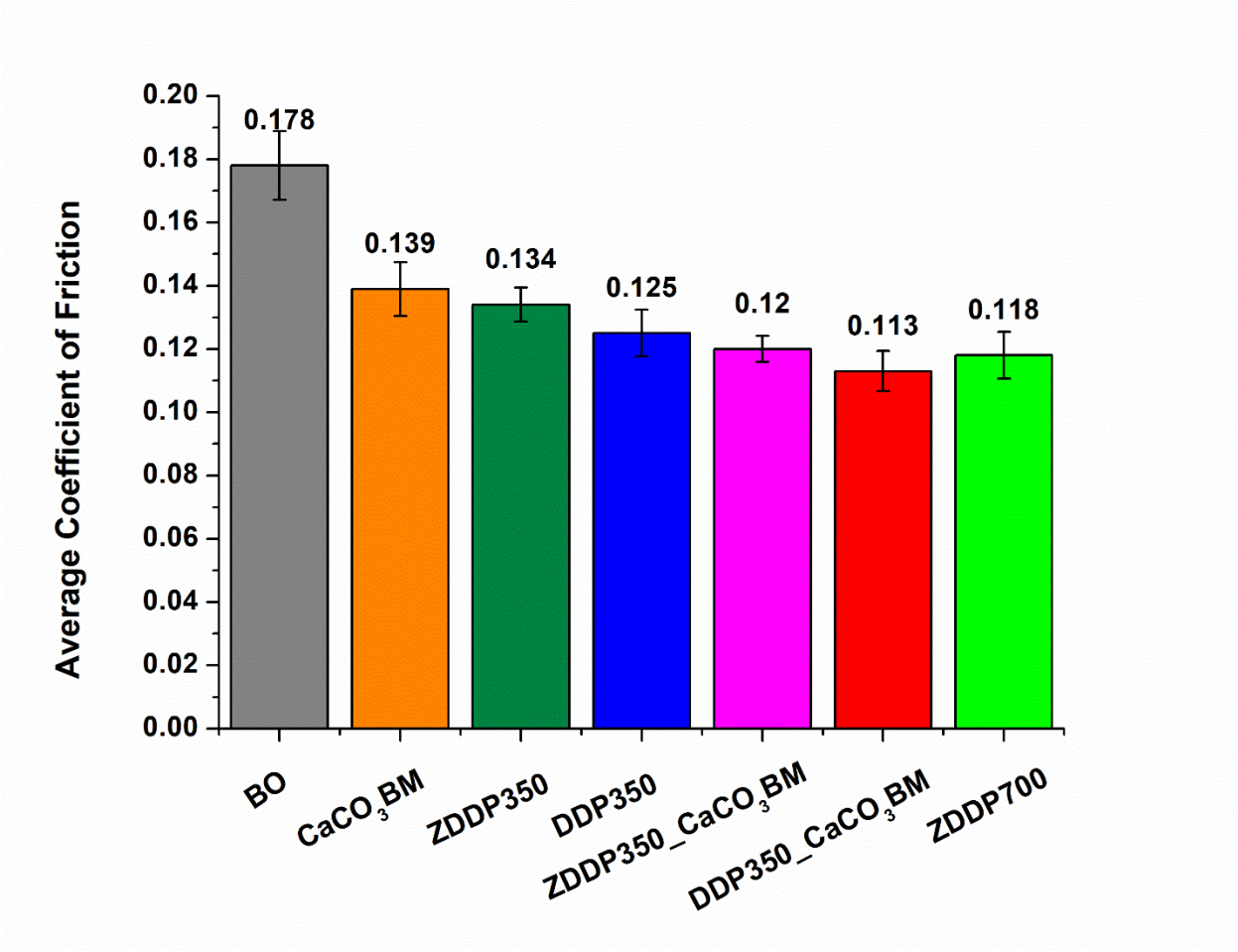

Figure 3. Average coefficient of friction calculated for 60 min duration tribological tests for all oil formulations.

The wear performance of $CaCO_3$BM nano-additives and binary additive mixtures of $CaCO_3$BM with ZDDP and DDP was benchmarked against the oil containing only ZDDP and only DDP additives. To assess wear appearance and surface deformation on worn surfaces, 3D and 2D surface profilometry images of the area of contact of cylinder sample were procured through

profilometer, which is added in the Supporting Information section for reference. Wear volume results of cylinder test specimens measured using optical profilometer are displayed in figure 4. The black color error bar on the bar chart represents the standard deviation of wear volume results of three repeat tests for each formulation. BO test oil exhibits the highest volume loss on the cylinder whereas the addition of both nano-additives and P-containing additives to the base oil led to a significant reduction in wear. Notably, the addition of plasma functionalized $CaCO_3$BM resulted in an 89.37% improvement in the wear performance of base oil. Interestingly, sample (C) with ZDDP at 350 ppm exhibited increased wear as compared to sample (D) with DDP at 350 ppm of P level.

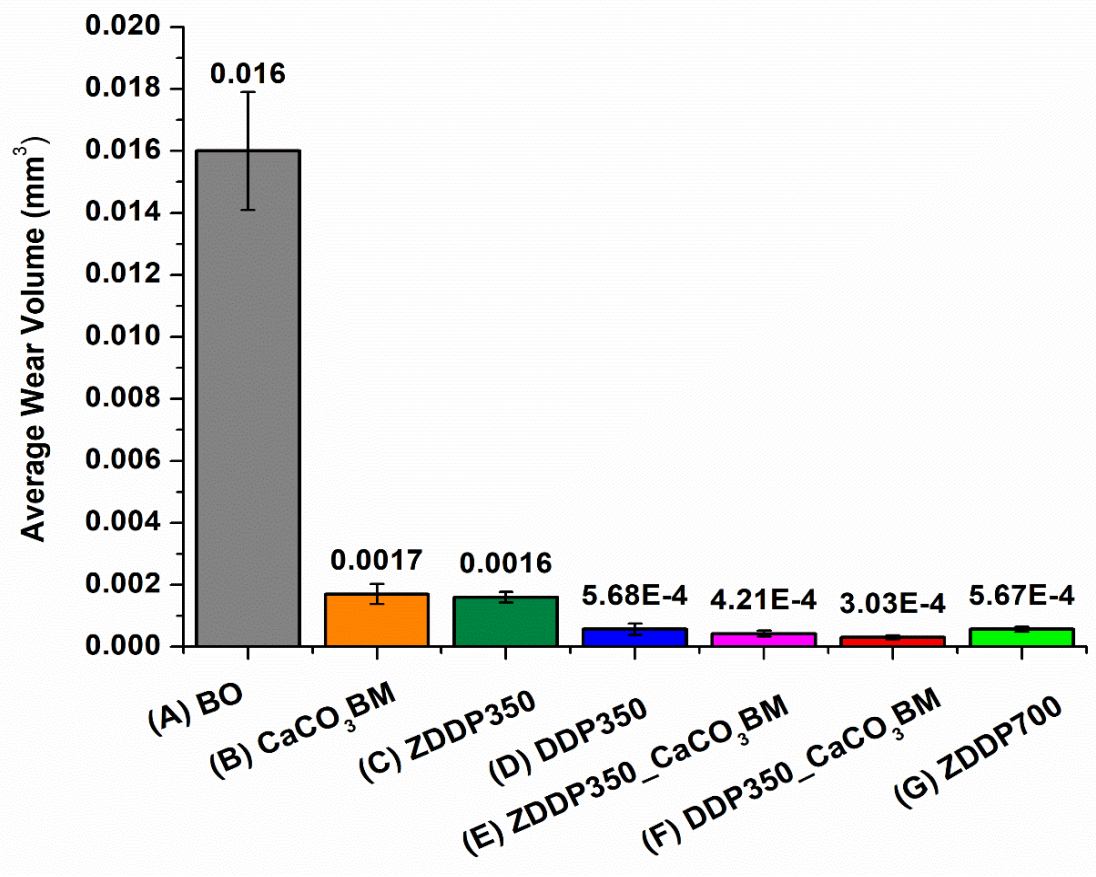

Figure 4. Wear volume results for samples (A) BO (B) $CaCO_3$BM (C) ZDDP350 (D) DDP350 (E) ZDDP350_$CaCO_3$BM (F) DDP350_$CaCO_3$BM and (G) ZDDP700.

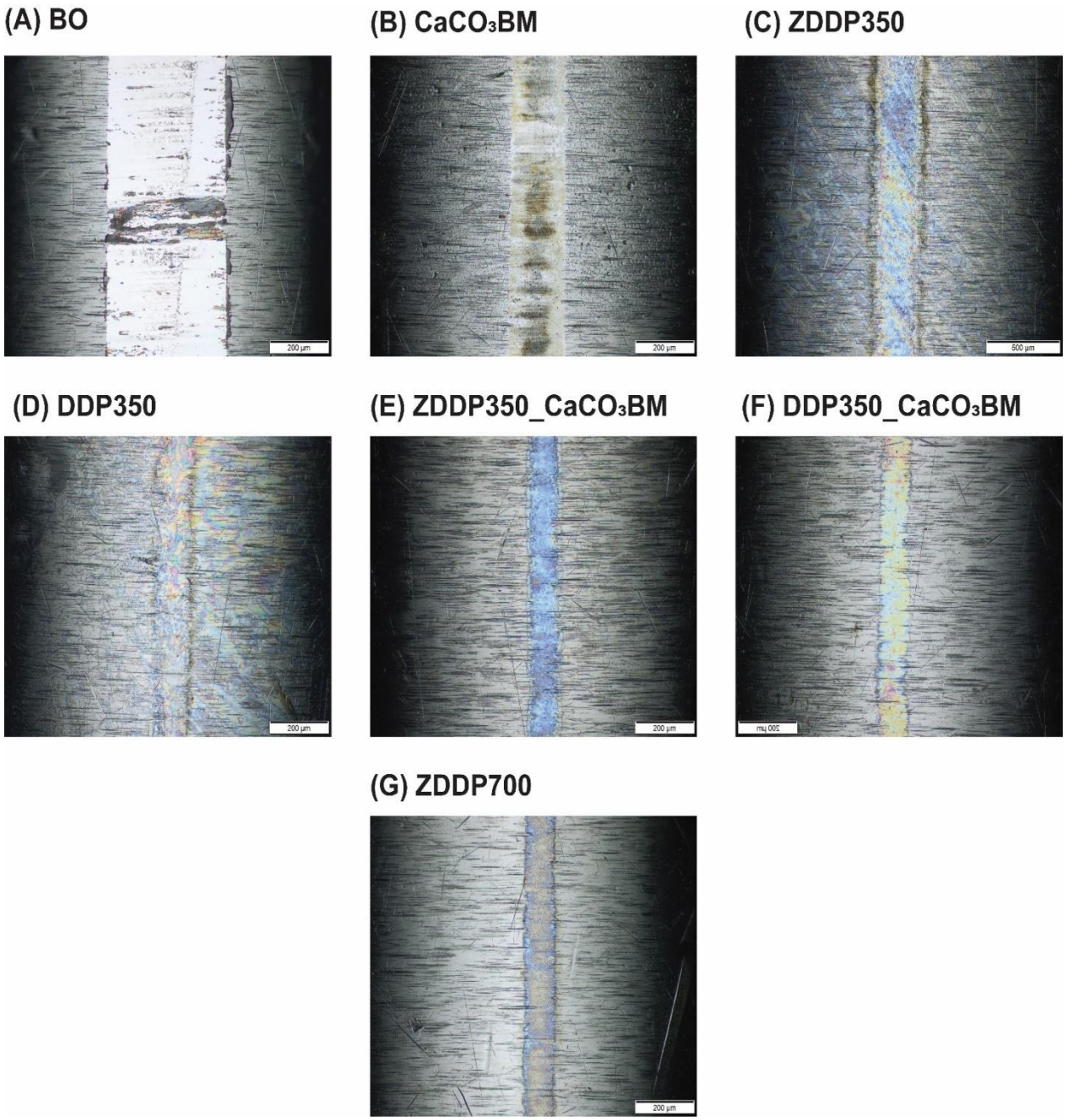

Figure 5. Optical microscopic images of the wear scar developed on cylinder test specimen with lubrications (A) BO; (B) $CaCO_3$BM; (C) ZDDP350; (D) DDP350; (E) ZDDP350_$CaCO_3$BM; (F) DDP350_$CaCO_3$BM; and (G) ZDDP700.

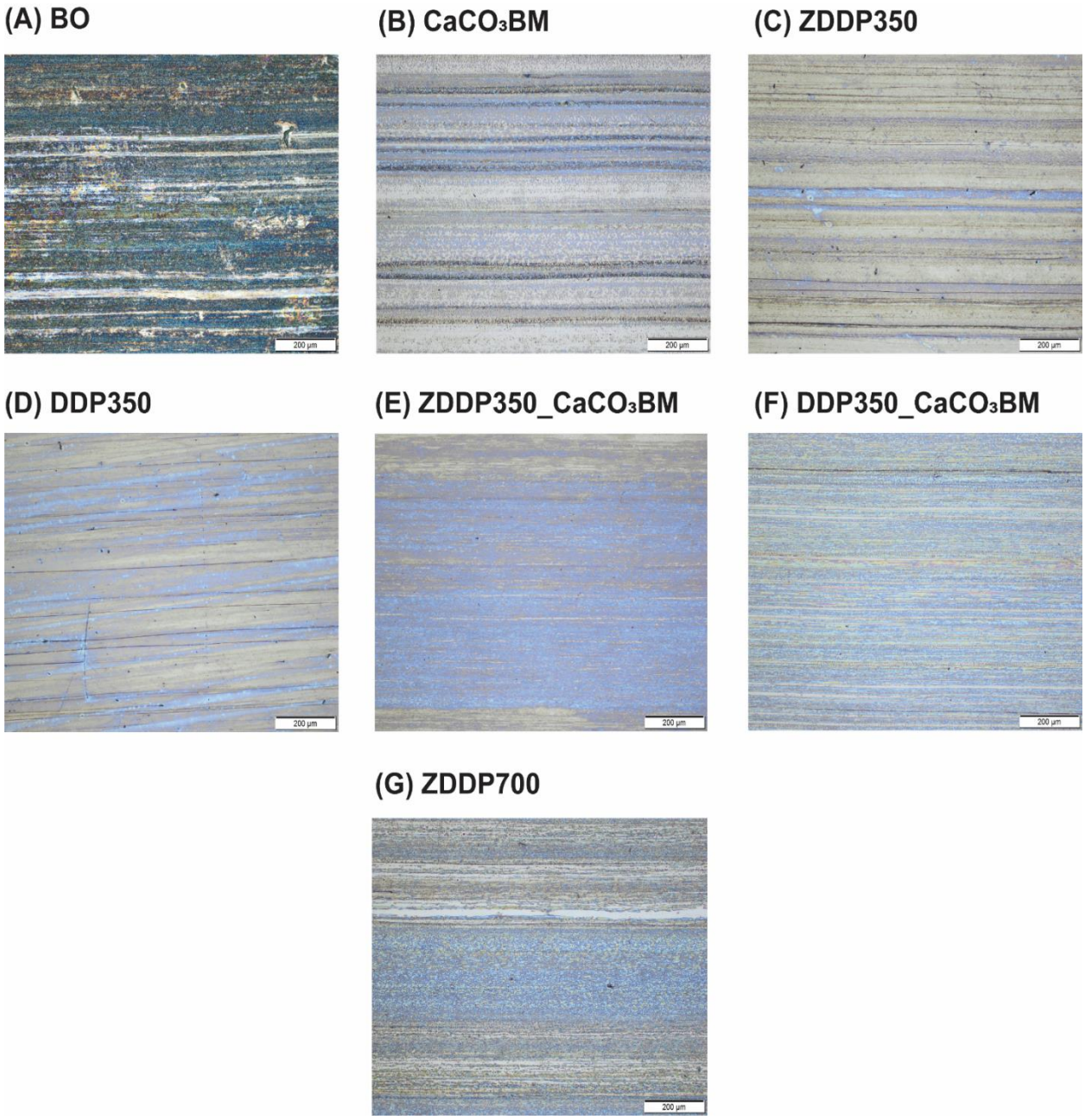

Figure 6. Optical micrographs of worn surfaces generated on flat steel specimen with formulations (A) BO; (B) $CaCO_3$BM; (C) ZDDP350; (D) DDP350; (E) ZDDP350_$CaCO_3$BM; (F) DDP350_$CaCO_3$BM; and (G) ZDDP700.

The mixture of $CaCO_3$BM with ZDDP and DDP (i.e. sample (E) and (F)) resulted in significant improvement in wear performance indicating synergistic interaction of developed $CaCO_3$BM

nanoparticles with ZDDP and DDP. It is important to note that formulation (F) of $CaCO_3$BM and DDP resulted in the lowest wear volume compared to all other formulations.

Figure 5 and 6 shows the optical microscopic images of wear scar generated on the cylinder and flat test specimen. Wear surfaces on both cylinder and flat have visually distinguishable features that reveal the formulation with an additive mixture of $CaCO_3$BM and DDP offered excellent wear protection compared to other lubricants. Additionally, wear volume results of the cylinder were calculated mathematically by measuring the width of the wear scar shown in figure 5, however, similar inferences were derived as of profilometry results and are therefore not included here. Overall friction and wear results highlight the advantage of extra chemistries deposited by $CaCO_3$BM in enhancing tribological properties without relying on reduced phosphorus concentration.

3.2 Tribofilm formation using electrical contact resistance

The high-frequency reciprocating rig tribometer used in this study was equipped with an electric setup design to record electrical contact resistance (ECR) across the counter bodies. Many researchers have shown that the highly resistive film is formed by P-based additives during the rubbing process and have successfully used the ECR technique to detect the presence or absence of lubricating films at the tribo-contact [43, 44]. Here, the potential of 100 mV was applied between the steel cylinder and flat, and the voltage drop recorded ranges from 0 to 100 mV. At the beginning of the stage, when the steel cylinder slides against flat and no tribofilm is formed, the resistance of the circuit is low, and the voltage drop value is close to 0 mV. As the rubbing continues, insulating tribofilms are formed which causes an increase in resistance of the circuit and then the voltage drop value shoots up close to 100 mV of ECR *in-situ* during tribological tests allows to effectively analyze overall dynamics of tribofilm formation.

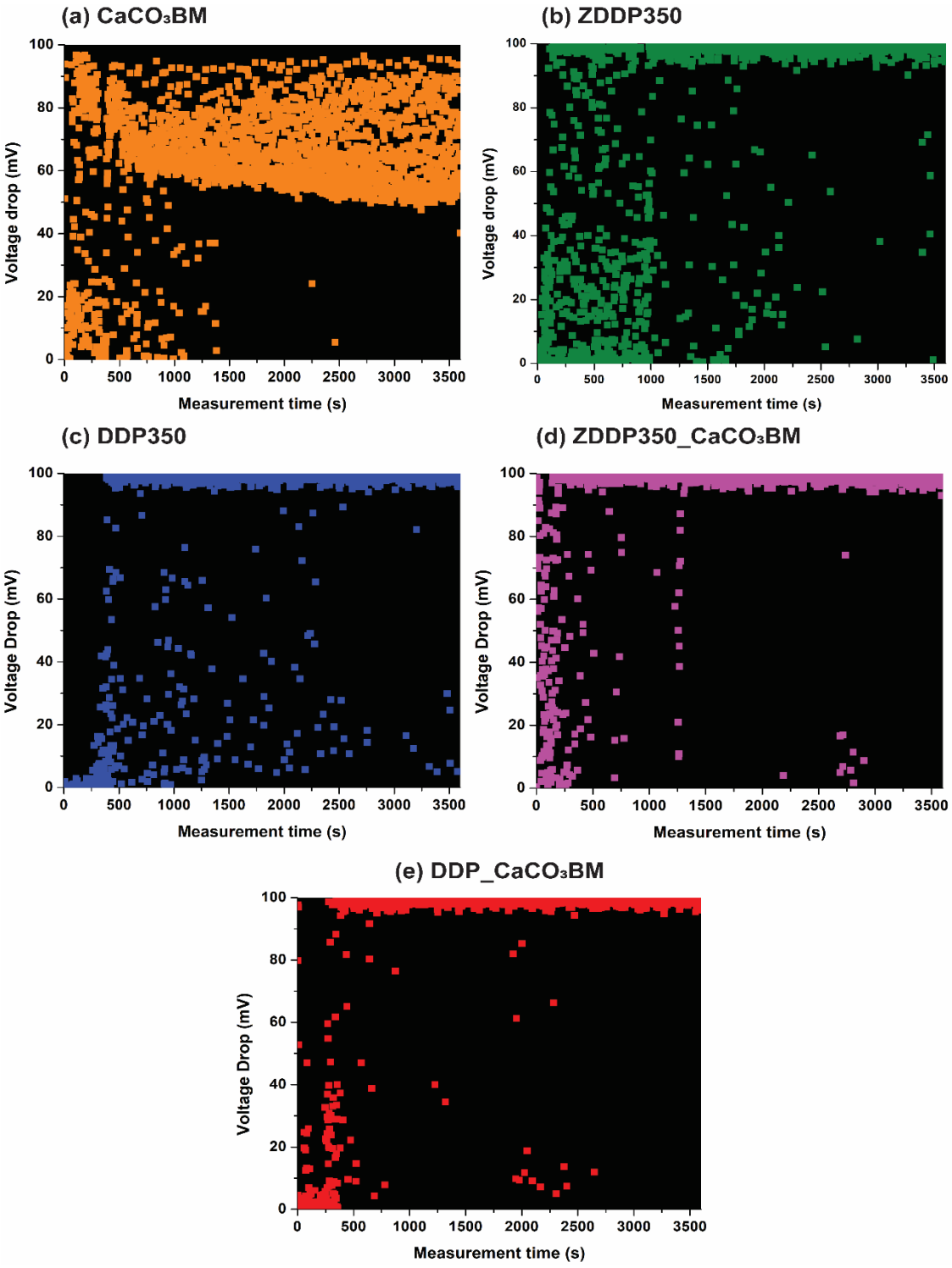

Figure 7. Electrical contact resistance data plotted as the function of test time for formulations (a) BO; (b) $CaCO_3$BM; (c) ZDDP350; (d) DDP350; (e) ZDDP350_$CaCO_3$BM; (f) DDP350_$CaCO_3$BM.

Importantly it helps to determine the incubation time required for anti-wear additives to form tribofilms at the interface.

Figure 7 shows ECR voltage drop signals plotted as the function of test time. Data points near 0 mV correspond to no tribofilm and near 100 mV to the presence of effective tribofilm. Sample (a) with functionalized $CaCO_3$BM nanoparticles exhibits the majority of data points in the upper half of the plot, apparently suggesting the formation of a thin protective film by nanoparticles at the interface after 15 min of sliding. In the case of ZDDP sample (b), data points appear to be dispersed for the first 15 min and after that are segregated near 100 mV. This indicates that tribofilms were forming and gradually breaking down during initial rubbing while later stability was achieved and maintained throughout the test. For sample (c) with DDP, tribofilm formation begins after 5 min of rubbing as opposed to sample (b) ZDDP. Additionally, tribofilms formed by DDP appears to be stable for the majority of test time with some minor breakdowns. Surprisingly, the voltage data points for the sample with a mixture of $CaCO_3$BM and ZDDP appear to be dispersed initially but after ~5 min numerous data points are close to 100 mV compared to sample (b) with only ZDDP, thus indicating that boron coated $CaCO_3$ nanoparticles available at the interface promote highly stable tribofilms of ZDDP even at a lower concentration of 350 ppm of P. Thus, ECR data for samples with an additive mixture of $CaCO_3$BM and ZDDP compliments wear volume results discussed in section 3.1. Additionally, the ECR plot of sample (e) is drastically different from the ECR plot of sample (c). Data points for sample DDP_$CaCO_3$BM reaches a maximum value in a slightly early stage and remains relatively stable than the sample with only DDP. These differences in incubation time and stability further supports that developed $CaCO_3$BM nano-additives interact synergistically with ZDDP and DDP additives and form robust tribofilms leading to enhanced anti-wear protection of boundary lubricated contacts.

3.3 Morphology and Topography of Tribofilms

AFM was used to observe and compare general topographical and morphological features of tribofilms formed due to the interaction of $CaCO_3$ nano-additives with ZDDP and DDP. Figure 8 shows AFM images of the 45 μm × 45 μm area probed around the wear scar along with the scale bar. Each sample was scanned at four spots close to the center region, while only one representative scan is shown in figure 8. It is apparent from all AFM images that in both nano-additives and P-containing additives a tribofilm is formed obscuring visibility of the ground steel surface. Looking first at $CaCO_3$BM, AFM image reveals several discrete small tribofilms or pad-like features along with evidence of directionality. It appears that pads are elongated in the direction of sliding. This nanoparticle reinforced tribofilm exhibits thinner and slightly rougher surface characteristics than ZDDP and DDP tribofilms. 3D topographical image of the ZDDP sample exhibits the presence of relatively homogenous tribofilms with thin and elongated pads oriented in sliding direction. These films have uniformly elevated features and appear to be smoother than $CaCO_3$BM. The observed morphology of ZDDP tribofilms resembles ZDDP films reported in the literature by various authors [45–49]. AFM image of the DDP sample as shown in figure 8(c) reveal that the surface of tribofilms is quite heterogenous with the combination of large and small size pads. However, it should be noted that the pads formed by DDP have a higher thickness and are covering a larger area than the pads formed by ZDDP. Najman et al. studied tribological properties of extreme pressure organo-sulfur additives and correlated poor anti-wear performance of additives to the formation of tribofilms containing smaller pads. Similarly, here the better wear volume results of DDP than ZDDP can be associated with the formation of wider and thicker pads. Interestingly, surface characteristics of tribofilms formed due to interaction of $CaCO_3$BM and ZDDP exhibits

better coverage of tribofilms with pad size larger than what is seen in the case of only ZDDP lubricated sample.

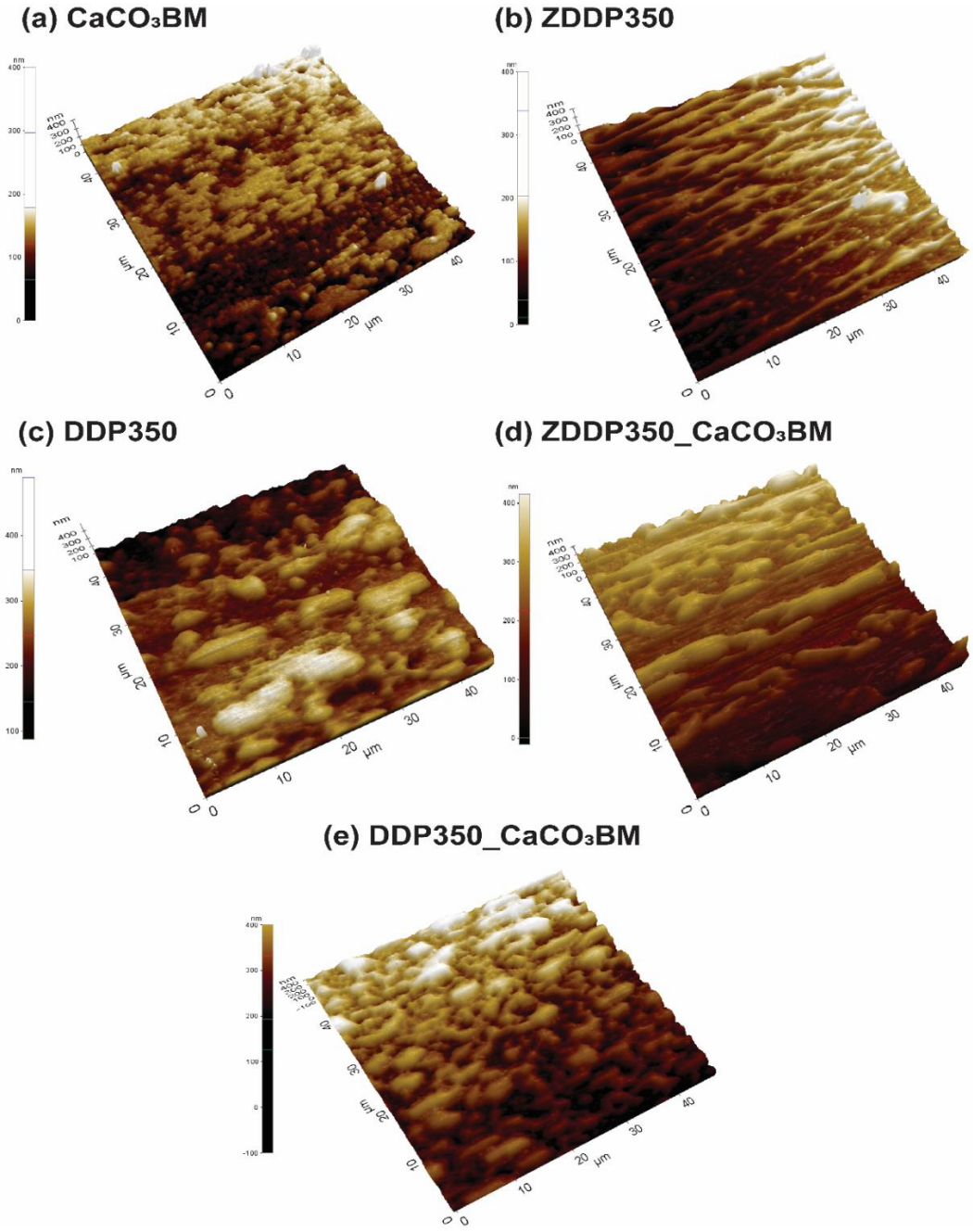

Figure 8. AFM topographical images of the wear scar generated on the flat steel specimen for formulations (a) $CaCO_3$BM; (b) ZDDP350; (c) DDP350; (d) ZDDP350_$CaCO_3$BM; (e) DDP350_$CaCO_3$BM.

Also, pads are continuous and elongated in the direction of sliding. Some areas of this sample appear to have deeper scratches in the sliding direction. On the contrary, surface lubricated with $CaCO_3$BM and DDP combined additive mixture reveal the best coverage of patchy tribofilms covering rough surface asperities. Although the pad appears to be smaller in diameter, the height (/thickness) of the pads is similar to that of the ZDDP_$CaCO_3$BM tribofilm sample. These topographical differences indicate the benefit of synergistic interaction of functionalized $CaCO_3$BM and DDP and/ ZDDP in strengthening properties of tribofilms and enhancing wear protection at the tribological interface.

3.4 Tribochemical analysis using XANES

3.4.1 XANES K-edge characterization

Calcium K-edge

To interpret the role of $CaCO_3$BM nanoparticles in promoting tribofilm formation and confirm interaction with P-based additives, calcium K-edge FY absorption spectra for all samples were recorded and compared with model compounds $Ca_2P_2O_7$, CaO, $CaCO_3$, $CaHPO_4$, $Ca_3(PO_4)_2$ as shown in figure 9(a). Ca K-edge FY has characteristic three discernable peaks labeled as **a**, **b**, and **c**. Details on the peak position and electronic transitions can be found elsewhere [50, 51]. The Ca K-edge spectra of $CaCO_3$BM nanoparticles-based lubrications reveal the presence of calcium chemistry on the tribo-surface. It is evident from these plots, that the sample with only $CaCO_3$BM has its pre-edge peak **a** aligned exactly with the $CaCO_3$ model compound, whereas its main peak the position is between the white line of $CaCO_3$ and CaO, which indicates a small contribution from CaO to the chemical makeup of tribofilms while the majority of calcium is associated with $CaCO_3$ in these tribofilms.

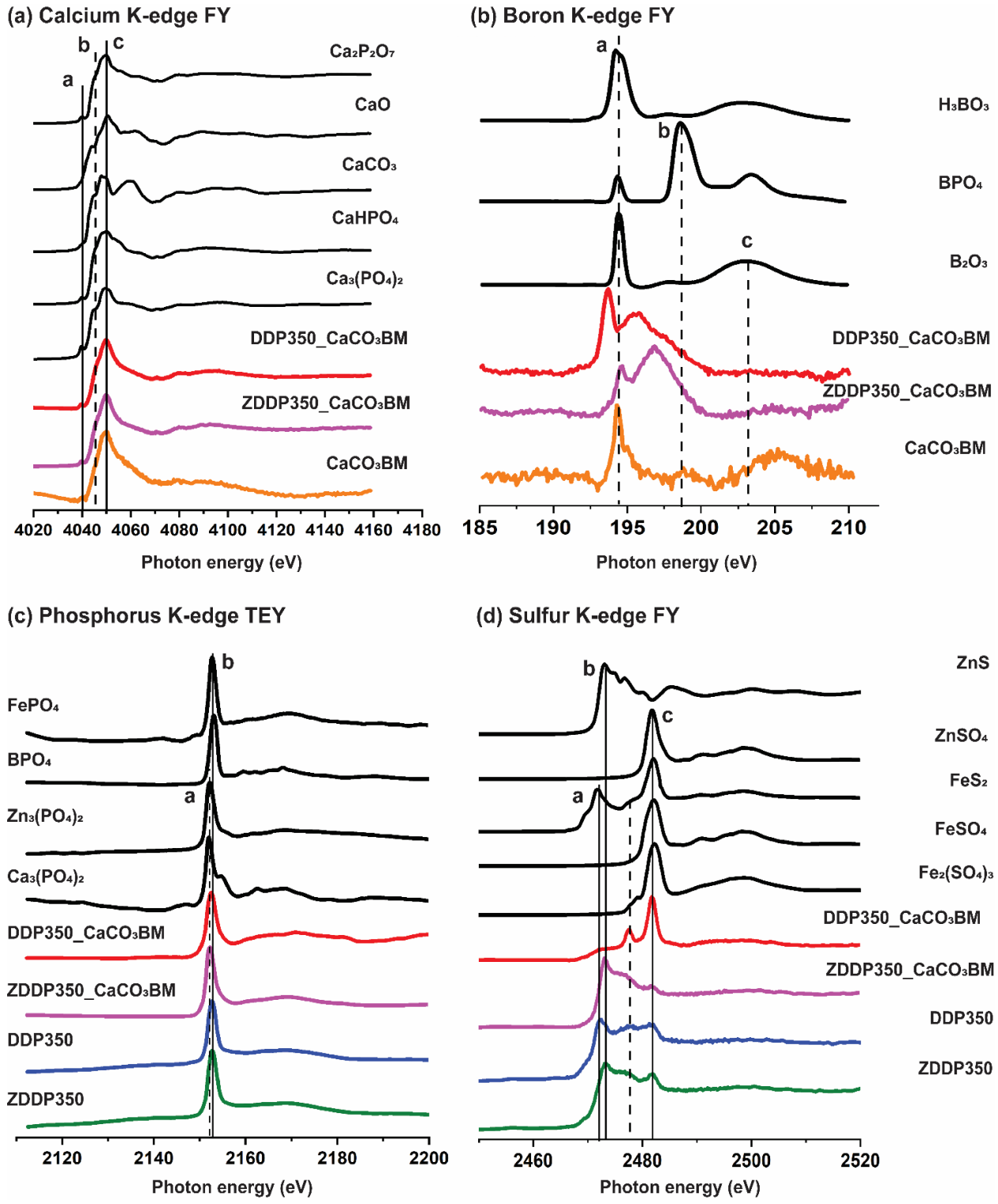

Figure 9. XANES K-edge characterization of tribofilms formed by all prepared oil formulations detailing information on (A) Calcium K-edge TEY; (b) Boron K-edge FY; (c) Phosphorus K-edge TEY; (d) Sulfur K-edge FY.

The peak positions and intensities in FY spectra from ZDDP_$CaCO_3$BM and DDP_$CaCO_3$BM reveal the presence of calcium phosphates in the tribofilms. It is difficult to distinguish among the calcium phosphate compounds, however, careful observation of peak **b** hints at the presence of $CaHPO_4$ in both tribofilms.

Boron K-edge

Boron K-edge was acquired for all formulations to confirm the capability of plasma functionalized $CaCO_3$BM nanoparticles to deliver coated boron chemistries at the tribological interface. Boron K-edge FY spectra of tribofilm samples compared with model compounds in figure 9(b) reveal important information on the co-ordination and intermediate-range structure of B in the tribofilms. Boron K-edge FY spectra exhibit characteristic three peaks **a**, **b**, and **c**. Peak **a** at 194.0 eV and **c** at 203 eV are attributed to boron in trigonal co-ordination, while peak **b** at 198.4 eV corresponds to boron in tetrahedral co-ordination [52, 53]. Spectra of B_2O_3 and H_3BO_3 are signatures of boron in trigonal co-ordination. On the other hand, the spectrum of BPO_4 represents boron in the tetrahedral form wherein small intensity peaks **a** and **c** possibly originates from surface modification. From figure 9(b) it is evident that, in the absence of ZDDP and DDP additives, $CaCO_3$BM forms tribofilms mainly composed of trigonal boron species. FY spectrum of sample $CaCO_3$BM exhibits a strong intensity peak **a** indicating that boron is present in the form of H_3BO_3/B_2O_3 in the tribofilm. Additionally, there is a low-intensity noisy peak **b** possibly suggesting that partial transformation might have occurred to produce tetrahedral boron species. Zhang et al. also reported that in tribofilms formed by borated additives, boron species transformed from trigonal co-ordination to tetrahedral co-ordination on rubbing. The spectrum of the sample with $CaCO_3$BM and ZDDP appears to be quite different than the spectra of model compounds. Spectra exhibits a strong intensity peak at 196.7 eV and a shoulder on the lower energy side at

194.6 eV which corresponds to trigonal boron in H_3BO_3 and B_2O_3. Here, the 196.7 eV peak is in between peak **a** and peak **b**. This unique peak position indicates the presence of a complex metal borate as calcium, zinc, and iron species are also present in this tribofilm [54, 55]. Interestingly, the blending of $CaCO_3$BM and DDP additives has resulted in different boron chemistries and distinct boron K-edge spectrum. The strong intensity peak at 193.3 eV matches with iron borates ($Fe_2Fe^{3+}BO_5$) in the literature [56] whereas the low-intensity shoulder around 195.5 eV corresponds to P 2s from the phosphate structure [57]. As the cross-section of B 1s is much larger than that of P 2s, B K-edge XANES peaks are at a higher intensity (i.e. peak at 193.3 eV) than the P 2s peak [57]. The P L-edge FY results (discussed later) suggests that these tribofilms contain $FePO_4$ and therefore, the shoulder around 195.5 eV seen in figure 8(b) can be assigned to $FePO_4$ present in the bulk of tribofilms.

Phosphorus K-edge

XANES phosphorus K-edge TEY spectra of tribofilm samples and model compounds, BPO_4, $Ca_3(PO_4)_2$, $FePO_4$, and $Zn_3(PO_4)_2$ are displayed in figure 9(c). The main absorption peak as seen in P K-edge spectra arises due to the transition of an electron from phosphorus 1s orbital to unoccupied 2p orbital. The main absorption peak **b** of $FePO_4$ is slightly at higher energy than peak **a** of $Zn_3(PO_4)_2$ and $Ca_3(PO_4)_2$ model compounds. Additionally, $FePO_4$ has distinctive pre-edge peak **a'** which is absent in $Zn_3(PO_4)_2$ and $Ca_3(PO_4)_2$. $Ca_3(PO_4)_2$ has a unique shoulder after the main absorption peak and BPO_4 has the main absorption edge at a higher energy level than $FePO_4$. Tribofilm samples, ZDDP and DDP contain iron phosphates as the main absorption peak exactly matches with peak **b** of $FePO_4$. The tribofilms formed due to the interaction of $CaCO_3$BM and ZDDP does not contain iron phosphates as the pre-edge peak **a'** is missing and the peak **b** of FePO4 does not match that of the tribofilm. The high-intensity peak aligns with peak **a** and thus, indicates

the dominance of $Zn_3(PO_4)_2$ in the chemical make up of these surface films. Phosphorus K-edge TEY spectra of DDP_$CaCO_3$BM sample exhibits peak position and features similar to TEY spectrum of $FePO_4$ model compounds and thus, indicates that these tribofilms are mainly comprised of iron phosphates in the bulk. Both ZDDP and DDP, when mixed with CaCO3BM nano-additives, give rise to zinc phosphate and iron phosphate-based tribofilms respectively and there is no formation of boron phosphate. Thus, the P K-edge results indicate that the boron chemistry from the shell of $CaCO_3$BM nanoparticles has no influence on the chemical environment of phosphorus in the tribofilms. However, Ca K-edge FY spectra for ZDDP_$CaCO_3$BM and DDP_$CaCO_3$BM did detect the presence of calcium phosphate in the bulk of tribofilms, suggesting that the core of $CaCO_3$BM nanoparticles does react with decomposition products of ZDDP and DDP. P K-edge FY spectra acquired for all samples were very similar to spectra obtained in TEY mode and hence, are not discussed here.

Sulfur K-edge

Sulfur K-edge is sensitive to oxidation states of sulfur and is useful in determining sulfur species in the sample containing complex composition. Sulfur K-edge FY spectra for model compounds, shown in figure 9(d) have characteristic peaks **a**, **b**, and **c**. The main absorption peak of sulfides is at lower photon energy i.e. FeS_2 (peak **a**) is at 2471.5 eV, and ZnS (peak **b**) is at 2473 eV. The peak positions for sulfate compounds ($ZnSO_4$, $FeSO_4$, and $Fe_2(SO_4)_3$ are at higher energy around 2482 eV. Tribofilms formed by all oil formulations have sulfur in several oxidation states as evident from peaks **a**, **b**, and **c**. The spectrum for the ZDDP sample has features similar to the ZnS model compound with the presence of additional peak **c** corresponding to the $ZnSO_4$ compound. This suggests zinc sulfide is the main chemical state of sulfur with a minimum concentration of zinc sulfates in these tribofilms. Likewise, the sulfur K-edge plot for

ZDDP_$CaCO_3$BM has its main feature aligned with ZnS. Looking at the XANES spectrum of DDP, we can see that peak **a** and **c** aligns perfectly with FeS_2, whereas the FY spectrum of DDP_$CaCO_3$BM has a high-intensity peak and mid-intensity peak (marked by dotted lines) at 2477.7 eV, which matches with a characteristic peak position of FeS in the literature [58]. Also, there is a low-intensity shoulder on the higher energy side of peak c' which can be probably attributed to a minor concentration of iron sulfates. These observations indicate that sulfur from the decomposing DDP additive reacts with iron or surface oxide to produce iron sulfide. This iron sulfide can then react partially with oxygen or iron oxide to form some sulfate (and sulfite) as in the case of DDP_$CaCO_3$BM.

3.4.2 XANES L-edge characterization

Phosphorus L-edge

The phosphorus L-edge TEY and FY spectra of tribofilms are plotted along with model compounds FePO4, $Zn_3(PO_4)_2$, $Ca_3(PO_4)_2$, and BPO_4 and are shown in figure 10(a) and 10(b), respectively. Compared to phosphorus K-edge, phosphorus L-edge provides detailed chemical information of near-surface region ~5 nm and of bulk ~60 nm depth of tribofilm. Additionally, phosphorus L-edge spectra help to determine the chain length of polyphosphate glasses present on the sample surface. The L-edge spectra are characterized by peaks **a**, **a'**, **b**, **c**, and **c'**. Details on these peak positions and electronic transitions can be found elsewhere. The TEY spectrum of ZDDP exhibits the strong presence of zinc phosphates at the near-surface region, while interestingly FY spectrum of this sample shows a very strong intensity peak at **c'** and thus, reveals the presence of iron phosphates in the bulk of these tribofilms. On the contrary, the phosphorus L-edge TEY and FY spectra of DDP reveal a strong presence of iron phosphates throughout the surface to the bulk of tribofilms.

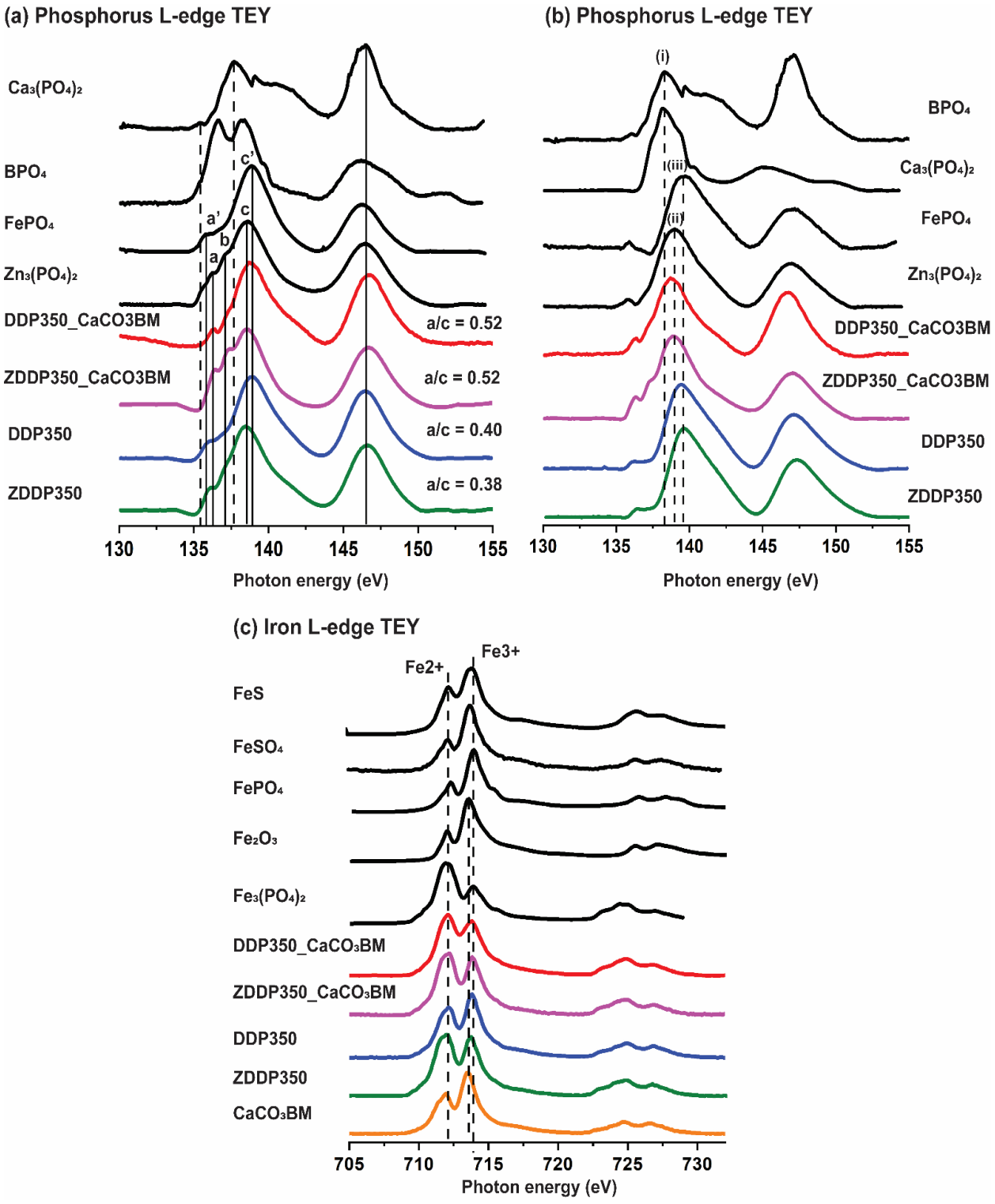

Figure 10. XANES L-edge characterization of tribofilms formed by all prepared oil formulations detailing information on (a) Phosphorus L-edge TEY; (b) Phosphorus L-edge FY; (c) Iron L-edge TEY.

TEY spectra for tribofilms generated with ZDDP_$CaCO_3$BM exhibit a strong main absorption peak aligned to that of the $Zn_3(PO_4)_2$ model compound. However, its corresponding FY spectra display a high-intensity characteristic peak in between **c** and **c'** peaks, thus indicating that the mixture of zinc phosphates and iron phosphates are present in the bulk of these tribofilms.

The chain length of detected zinc and iron phosphate glass can be determined from phosphorus L-edge spectra by calculating the ratio of intensity of **a**/**a'** peak to peak **c**/**c'** [59, 60]. The chain lengths are mentioned next to the respective spectrum in figure 10(a). An a/c ratio of less than 0.40 represents the presence of short-chain length polyphosphate glasses, while a chain length greater than 0.70 suggests long-chain polyphosphate glass [61]. A film with an a/c ratio between 0.40 and 0.60 is termed a medium-chain polyphosphate [62]. From a/c values in figure 10(a), it is evident that the interaction of $CaCO_3$BM nano-additives with ZDDP and DDP is resulting in the formation of tribofilms with increased chain length than the oils containing only ZDDP and DDP.

Iron L-edge

The Fe L-edge TEY spectra provide some vital information regarding the iron atoms present in the tribofilms for different test samples. From figure 10(c), we see that the L-edge spectra of model compounds display two main peaks at 707.1 eV and 708.5 eV irrespective of the oxidation state of Fe. The splitting and intensity ratios between the two main peaks are attributed to the interplay of crystal-field, spin-orbit, and electronic interactions (Coulomb and exchange) [63]. The most intense peak is used for fingerprint analysis i.e. to detect Fe^{2+} or Fe^{3+} compounds in the tribofilm sample. It is important to note that the intensity of the second peak increases noticeably when the oxidation states of iron are increased from Fe^{2+} to Fe^{3+}. The spectrum of the $CaCO_3$BM sample matches exhibits main absorption peaks in alignment with the Fe_2O_3 model

compound. The characteristic splitting as seen in the spectrum of both ZDDP and ZDDP_$CaCO_3$BM samples is almost the same, showing a slightly higher intensity of Fe^{2+} peak. This indicates that these tribofilms are comprised of a mixture of different iron phosphates with a slightly major concentration of $Fe_3(PO_4)_2$. Fe L-edge spectra of the DDP sample show the main intensity peak at 708.5 eV highlighting the strong presence of $FePO_4$ phosphates in the tribofilm. Interestingly, the interaction of DDP and $CaCO_3$BM has resulted in the formation of tribofilms containing $Fe_3(PO_4)_2$, as the main absorption peak and overall features of the sample, Fe L-edge spectra matches with $Fe_3(PO_4)_2$ compound. It is important to note that there might be a minor concentration of Fe_2O_3 present in the tribofilms formed with lubricants containing ZDDP and DDP additives, as the characteristic peak of Fe_2O_3 overlaps with the main absorption peak of these tribofilm samples. From the analysis of Fe L-edge spectra of all tribofilm samples, it can be concluded that iron is majorly associated with the phosphorus and not with the sulfur at ~50 nm beneath the top surface.

3.5 Discussion on Tribofilm formation and Wear Reduction Mechanism

This study has confirmed the ability of boron coated $CaCO_3$BM nanoparticles to interact synergistically with P-based additives to form thick tribofilms and improve anti-wear performance than ZDDP under comparable boundary lubrication conditions. Here, the aim is not just to seek alternative or supplement for ZDDPs but also to further understand the tribofilm formation and anti-wear mechanism of the developed binary additive system of $CaCO_3$BM and P-based anti-wear additives. Therefore, results from XANES and AFM were compiled to create phenomenological models of tribofilms and gain insight into the lubricating mechanism as shown in figure 11. In general, there are four feasible lubricating mechanisms for metal nano-additives: a) Ball bearing effect- where spherical nanoparticles act like tiny ball bearings at the contact zone

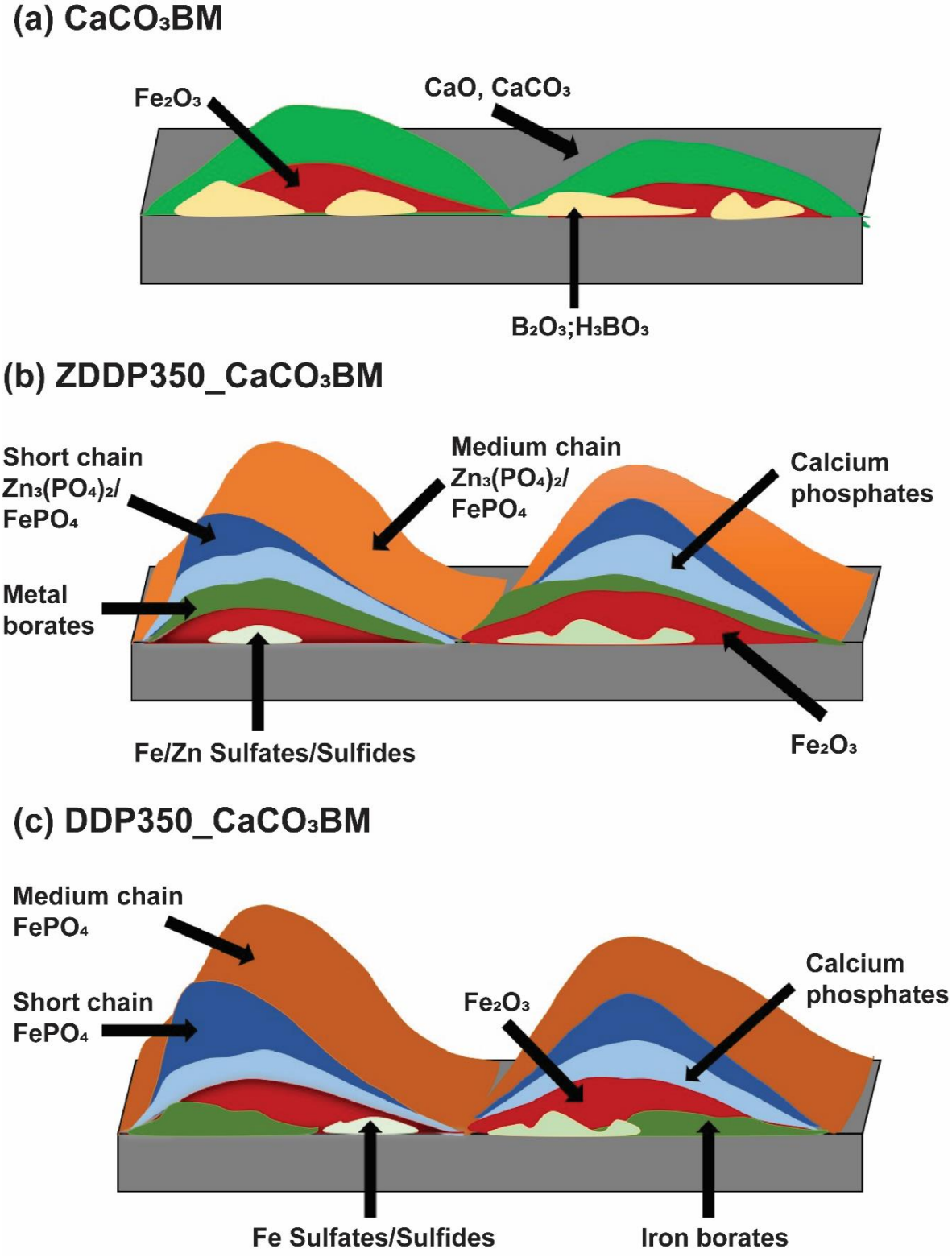

Figure 11. Tribofilm models created from the XANES and AFM results for samples (a) $CaCO_3$BM; (b) ZDDP350_ $CaCO_3$BM; and (c) DDP350_ $CaCO_3$BM.

and changes sliding motion to roll, thereby reducing the effective COF; (b) polishing effect- Hard nanoparticles smoothen off the surface asperities to reduce the roughness of the lubricating surface and improve tribological characteristics; (c) mending effect- nanoparticles deposit or fill the grooves and scars on the tribo-surface and compensate for the material loss; (d) Tribofilm formation- nanoparticles under high temperature and pressure get smeared or compacted to form adsorbed or tribo-sintered films or nanoparticles can participate in the tribo-chemical reactions with sliding metal surface to form tribofilms, which allows decrease resistance to shear for lower friction and prevent direct metal-metal contact to reduce wear. In this study, for plasma functionalized $CaCO_3$BM nanoparticles bearing effect and the smoothening effect was not observed since the worn surfaces produced with $CaCO_3$BM nanoparticles were slightly rougher. XANES analysis and comparison in figure 9 and 10 reveal that $CaCO_3$BM nanoparticles form tribofilms containing iron borates, B_2O_3, H_3BO_3, CaO, $CaCO_3$, and iron oxides. Zhang et al. reported the tribological behavior of the $CaCO_3$ nanoparticles in PAO base oil and XPS analysis revealed the deposition of similar tribofilms enriched with $CaCO_3$ on contact surfaces leading to friction and wear reductions. From figure 11(a), boron-based compounds are present near the sliding surface while the top surface of tribofilm patches is dominated by Ca-based compounds. This indicates that the boron chemistry was provided at the tribological surface through the removal of the outer polymer shell of $CaCO_3$BM nanoparticles under high tribo-stresses. Additionally, the presence of calcium oxide and iron borates hints that nanoparticles contributed to tribofilm formation through a chemical reaction and not simply by mechanical mixing. Tribo-chemistry plays a vital role in determining mechanisms of action of anti-wear additives. Here, figure 11(b) exhibits the chemical makeup of tribofilms formed due to interaction of $CaCO_3$BM and ZDDP, wherein the bottom layer close to steel substrate is comprised of iron oxides and iron

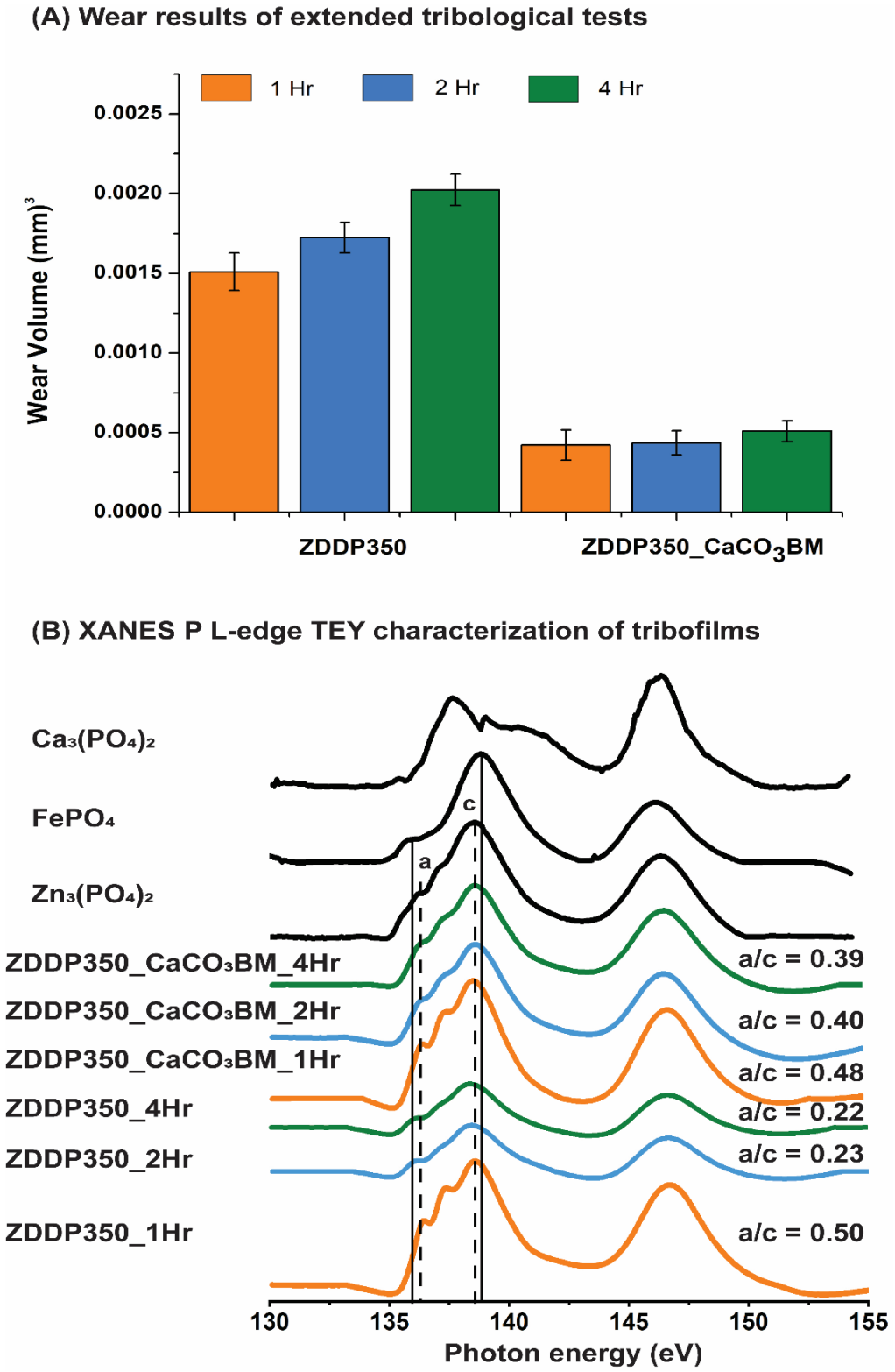

Figure 12. (A) Tribological test wear results for rubbing duration of 1 Hr, 2 Hr, and 4 Hr; (B) XANES P L-edge TEY spectra exhibiting a change in phosphate chain length with rubbing time.

and/ zinc sulfides/sulfates. The topmost region is dominated by medium-chain zinc phosphates with the presence of iron phosphates, calcium phosphates, and metal borates near the bulk region of the film. On the contrary, the tribofilm model formed due to the interaction of $CaCO_3$BM with DDP as shown in figure 11(c) is slightly different. These tribofilms are comprised of medium and short-chain length iron phosphates both in the near-surface and bulk of tribofilms along with the iron borates. These differences in the tribo-chemistry support the previous tribofilm forming mechanism proposed for both ZDDP and DDP [11, 15, 62, 64–67]. ZDDP is well-known to decompose and then self-react to deposit a tribofilm primarily composed of zinc and iron phosphates and oxides [9, 46, 68]. Such a mechanism does not apply to ashless DDP additive because they do not self-supply metal cations [62]. The two apparent sources of Fe cation supply for DDP are the contact surface and wear debris and therefore, the tribofilms formed due to ashless DDP in figure 10(c) majorly contain iron-based compounds. It is important to note that, in both cases, calcium phosphates are present deeper in the tribofilm which strongly indicates that the $CaCO_3$BM nanoparticles are participating in tribofilm formation by providing stabilizing Ca cations to assist Zn or Fe in forming phosphates in the tribofilm.

ECR results exhibited that the DDP by itself forms tribofilms at a slower rate than ZDDP, however, the addition of $CaCO_3$BM nanoparticles to DDP accelerated the formation of their tribofilms. It has been reported that ashless additives forms tribofilms much slower than ZDDP because they need Fe cations by initial wear or rubbing to develop a phosphate film [67]. However, here it can be proposed that the metal cation supply through $CaCO_3$BM nanoparticles promoted the stable formation of DDP tribofilms at a faster rate. Furthermore, additional Ca and B chemistries provided by $CaCO_3$BM nanoparticles boost the thickness of ZDDP and DDP tribofilms as illustrated in AFM figure 8.

To evaluate the durability of nanoparticle assisted tribofilms, tribological tests were carried out with ZDDP350 and ZDDP350_$CaCO_3$BM lubricants over 2 hours and 4 hours of extended sliding duration. The results of these tests (summarized in figure 12) indicate that the tribofilms formed through the interaction of $CaCO_3$BM and ZDDP are durable and effectively protect interacting surfaces over prolonged rubbing. XANES results exhibit that after extended rubbing the outermost longer-chain polyphosphates changes to shorter chain length phosphates i.e. orthophosphates. This depolymerization of both ZDDP350 and ZDDP350_$CaCO_3$BM tribofilms is attributed to the high tribo-stresses and temperature at the tribological contacts during extended rubbing. Many studies have proposed that the chain length of zinc polyphosphates decreases with the increase in rubbing time [69]. Here, the strength/durability of the tribofilms can be attributed to its phosphate chain length and thus change with rubbing time. Overall, it is evident from this study that the tribo-chemical reaction of $CaCO_3$BM nanoparticles with ZDDP and DDP promoted the formation of stable phosphate-rich tribofilms that lead to a corresponding improvement in tribological properties, especially wear.

4. CONCLUSION

In this study, high-performance surface-modified $CaCO_3$ nano-additives were synthesized using plasma polymerization technique to develop low phosphorus-based lubricants and seek a replacement for harmful P-based anti-wear additives. The addition of functionalized $CaCO_3$BM nanoparticles in the base oil reduced friction by up to 25% and wear by up to 89% in boundary lubrication. However, when used with P-based additives, the $CaCO_3$BM nano-additives displayed lower friction values, and especially with DDP additive, functionalized $CaCO_3$BM exhibited the lowest wear volume up to 97% improvement compared to all other formulations. Additionally, the additive mixtures of $CaCO_3$BM nano-additives with ZDDP and DDP at 350 ppm of P displayed

superior tribological performance than the lubricant containing industrially used ZDDP amount of 700 ppm of P. This significant improvement in tribological performance was attributed to the synergistic interaction of functionalized $CaCO_3$ nano-additives with ZDDP and DDP. ECR test results revealed that the interaction of $CaCO_3$BM nanoparticles with ZDDP and DDP promoted the stable formation of poly-phosphate based glassy tribofilms. Additionally, through AFM surface characterization, it was found out that for both ZDDP and DDP, the addition of $CaCO_3$BM nano-additives leads to the formation of thick patches of tribofilms, comparable to those formed by lubricants containing only ZDDP and only DDP. Further, tribo-surface chemical analysis by XANES indicated that the $CaCO_3$BM nanoparticles under high temperature and pressure conditions formed calcium oxide and iron borate enriched tribofilms on the sliding interface. Interestingly, in the presence of ZDDP and DDP, $CaCO_3$BM nano-additives participated in the tribofilm formation by tribo-chemical reactions and Ca metal cation supply. In conclusion, the additional Ca and B chemistries provided by plasma functionalized $CaCO_3$BM nanoparticles at the tribological interface compensated for reduced phosphorus concentration in the lubricants without affecting the tribological performance.

Acknowledgments

Tribological tests were conducted at Argonne National Laboratory. The support provided by Dr. Ali Erdemir is gratefully acknowledged. XANES experiments were conducted at the Canadian Light Source, Saskatoon, Saskatchewan, Canada that is supported by NSERC, NRC, CIHR and the University of Saskatchewan.

References

1. Boyde, S.: Green lubricants. Environmental benefits and impacts of lubrication. Green Chem. 4, 293–307 (2002). doi:10.1039/B202272A

2. Holmberg, K., Erdemir, A.: Influence of tribology on global energy consumption, costs and emissions. Friction. 5, 263–284 (2017). doi:10.1007/s40544-017-0183-5

3. Holmberg, K., Erdemir, A.: Global impact of friction on energy consumption, economy and environment. FME Trans. 43, 181–185 (2015). doi:10.5937/fmet1503181H

4. Hsu, S.M., Zhang, J., Yin, Z.: The Nature and Origin of Tribochemistry. Tribol. Lett. 13, 131–139 (2002). doi:10.1023/A:1020112901674

5. Jaiswal, V., Kalyani, Umrao, S., Rastogi, R.B., Kumar, R., Srivastava, A.: Synthesis, Characterization, and Tribological Evaluation of TiO2-Reinforced Boron and Nitrogen co-Doped Reduced Graphene Oxide Based Hybrid Nanomaterials as Efficient Antiwear Lubricant Additives. ACS Appl. Mater. Interfaces. 8, 11698–11710 (2016). doi:10.1021/acsami.6b01876

6. Gusain, R., Khatri, O.P.: Ultrasound assisted shape regulation of CuO nanorods in ionic liquids and their use as energy efficient lubricant additives. J. Mater. Chem. A. 1, 5612–5619 (2013). doi:10.1039/C3TA10248C

7. Bovington, C., Anghel, V., Spikes, H.A.: Predicting Sequence VI and VIA Fuel Economy from Laboratory Bench Tests. In: SAE Technical Paper. SAE International (1996)

8. Spikes, H.: The History and Mechanisms of ZDDP. Tribol. Lett. 17, 469–489 (2004). doi:10.1023/B:TRIL.0000044495.26882.b5

9. Gosvami, N.N., Bares, J.A., Mangolini, F., Konicek, A.R., Yablon, D.G., Carpick, R.W.: Mechanisms of antiwear tribofilm growth revealed in situ by single-asperity sliding contacts. Science (80-.). 348, 102–106 (2015). doi:10.1126/science.1258788

10. Mosey, N.J., Woo, T.K., Kasrai, M., Norton, P.R., Bancroft, G.M., Müser, M.H.: Interpretation of experiments on ZDDP anti-wear films through pressure-induced cross-linking. Tribol. Lett. 24, 105–114 (2006). doi:10.1007/s11249-006-9040-9

11. Zhang, J., Spikes, H.: On the Mechanism of ZDDP Antiwear Film Formation. Tribol. Lett. 63, 24 (2016). doi:10.1007/s11249-016-0706-7

12. Tse, J.S., Song, Y., Liu, Z.: Effects of Temperature and Pressure on ZDDP. Tribol. Lett. 28, 45–49 (2007). doi:10.1007/s11249-007-9246-5

13. Fujita, H., Spikes, H.A.: The formation of zinc dithiophosphate antiwear films. Proc. Inst. Mech. Eng. Part J J. Eng. Tribol. 218, 265–278 (2004). doi:10.1243/1350650041762677

14. Erdemir, A.: Review of engineered tribological interfaces for improved boundary lubrication. Tribol. Int. 38, 249–256 (2005). doi:https://doi.org/10.1016/j.triboint.2004.08.008

15. Luiz, J.F., Spikes, H.: Tribofilm Formation, Friction and Wear-Reducing Properties of Some Phosphorus-Containing Antiwear Additives. Tribol. Lett. 68, 75 (2020). doi:10.1007/s11249-020-01315-8

16. ILSAC GF-5 Standard for Passenger Car Engine Oil. (2009).

17. Uflyand, I.E., Zhinzhilo, V.A., Burlakova, V.E.: Metal-containing nanomaterials as lubricant additives: State-of-the-art and future development. Friction. 7, 93–116 (2019). doi:10.1007/s40544-019-0261-y

18. Wu, L., Zhang, Y., Yang, G., Zhang, S., Yu, L., Zhang, P.: Tribological properties of oleic acid-modified zinc oxide nanoparticles as the lubricant additive in poly-alpha olefin and diisooctyl sebacate base oils. RSC Adv. 6, 69836–69844 (2016). doi:10.1039/C6RA10042B

19. Battez], A. [Hernández, González, R., Viesca, J.L., Fernández, J.E., Fernández], J.M. [Díaz, Machado, A., Chou, R., Riba, J.: CuO, ZrO2 and ZnO nanoparticles as antiwear additive in oil lubricants. Wear. 265, 422–428 (2008). doi:https://doi.org/10.1016/j.wear.2007.11.013

20. Xue, Q., Liu, W., Zhang, Z.: Friction and wear properties of a surface-modified TiO2 nanoparticle as an additive in liquid paraffin. Wear. 213, 29–32 (1997). doi:https://doi.org/10.1016/S0043-1648(97)00200-7

21. Zhou, J., Wu, Z., Zhang, Z., Liu, W., Xue, Q.: Tribological behavior and lubricating mechanism of Cu nanoparticles in oil. Tribol. Lett. 8, 213–218 (2000). doi:10.1023/A:1019151721801

22. Seymour, B.T., Wright, R.A.E., Parrott, A.C., Gao, H., Martini, A., Qu, J., Dai, S., Zhao, B.: Poly(alkyl methacrylate) Brush-Grafted Silica Nanoparticles as Oil Lubricant Additives: Effects of Alkyl Pendant Groups on Oil Dispersibility, Stability, and Lubrication Property. ACS Appl. Mater. Interfaces. 9, 25038–25048 (2017). doi:10.1021/acsami.7b06714

23. Tunckol, M., Durand, J., Serp, P.: Carbon nanomaterial-ionic liquid hybrids. Carbon N. Y. 50, 4303–4334 (2012). doi:10.1016/j.carbon.2012.05.017

24. Guo, Y.-B., Zhang, S.-W.: The Tribological Properties of Multi-Layered Graphene as Additives of PAO2 Oil in Steel–Steel Contacts. Lubricants. 4, 30 (2016). doi:10.3390/lubricants4030030

25. Khare, H.S., Lahouij, I., Jackson, A., Feng, G., Chen, Z., Cooper, G.D., Carpick, R.W.: Nanoscale Generation of Robust Solid Films from Liquid-Dispersed Nanoparticles via in Situ Atomic Force Microscopy: Growth Kinetics and Nanomechanical Properties. ACS Appl. Mater. Interfaces. 10, 40335–40347 (2018). doi:10.1021/acsami.8b16680

26. Battez], A. [Hernández, Viesca, J.L., González, R., Blanco, D., Asedegbega, E., Osorio, A.: Friction reduction properties of a CuO nanolubricant used as lubricant for a NiCrBSi coating. Wear. 268, 325–328 (2010). doi:https://doi.org/10.1016/j.wear.2009.08.018

27. Tao, X., Jiazheng, Z., Kang, X.: The ball-bearing effect of diamond nanoparticles as an oil additive. J. Phys. D. Appl. Phys. 29, 2932–2937 (1996). doi:10.1088/0022-3727/29/11/029

28. Chou, C.-C., Lee, S.-H.: Tribological behavior of nanodiamond-dispersed lubricants on carbon steels and aluminum alloy. Wear. 269, 757–762 (2010). doi:https://doi.org/10.1016/j.wear.2010.08.001

29. Dou, X., Koltonow, A.R., He, X., Jang, H.D., Wang, Q., Chung, Y.-W., Huang, J.: Self-dispersed crumpled graphene balls in oil for friction and wear reduction. Proc. Natl. Acad.

Sci. (2016). doi:10.1073/pnas.1520994113

30. Lee, J., Cho, S., Hwang, Y., Lee, C., Kim, S.H.: Enhancement of Lubrication Properties of Nano-oil by Controlling the Amount of Fullerene Nanoparticle Additives. Tribol. Lett. 28, 203–208 (2007). doi:10.1007/s11249-007-9265-2

31. Machado, A.H.E., Lundberg, D., Ribeiro, A.J., Veiga, F.J., Lindman, B., Miguel, M.G., Olsson, U.: Preparation of Calcium Alginate Nanoparticles Using Water-in-Oil (W/O) Nanoemulsions. Langmuir. 28, 4131–4141 (2012). doi:10.1021/la204944j

32. Zhang, M., Wang, X., Fu, X., Xia, Y.: Performance and anti-wear mechanism of CaCO3 nanoparticles as a green additive in poly-alpha-olefin. Tribol. Int. 42, 1029–1039 (2009). doi:https://doi.org/10.1016/j.triboint.2009.02.012

33. Jiusheng, L., Lifeng, H., Xiaohong, X., Tianhui, R.: Tribological synergism of surface-modified calcium borate nanoparticles and sulfurized olefin. Ind. Lubr. Tribol. 64, 217–223 (2012). doi:10.1108/00368791211232762

34. Gupta, R.N., Harsha, A.P.: Synthesis, Characterization, and Tribological Studies of Calcium–Copper–Titanate Nanoparticles as a Biolubricant Additive. J. Tribol. 139, (2016). doi:10.1115/1.4033714

35. Sánchez-López, J.C., Abad, M.D., Kolodziejczyk, L., Guerrero, E., Fernández, A.: Surface-modified Pd and Au nanoparticles for anti-wear applications. Tribol. Int. 44, 720–726 (2011). doi:https://doi.org/10.1016/j.triboint.2009.12.013

36. Kolodziejczyk, L., Mart\'\inez-Mart\'\inez, D., Rojas, T. ~C., Fernández, A., Sánchez-López, J. ~C.: Surface-modified Pd nanoparticles as a superior additive for lubrication. J. Nanoparticle Res. 9, 639–645 (2007). doi:10.1007/s11051-006-9124-3

37. Viesca, J.L., Hernández Battez, A., González, R., Chou, R., Cabello, J.J.: Antiwear properties of carbon-coated copper nanoparticles used as an additive to a polyalphaolefin. Tribol. Int. 44, 829–833 (2011). doi:https://doi.org/10.1016/j.triboint.2011.02.006

38. Sunqing, Q., Zhou, Z., Junxiu, D., Chen, G.: Preparation of Ni Nanoparticles and Evaluation of Their Tribological Performance as Potential Additives in Oils . J. Tribol. 123, 441–443 (1999). doi:10.1115/1.1286152

39. Cho, J., Denes, F.S., Timmons, R.B.: Plasma Processing Approach to Molecular Surface Tailoring of Nanoparticles: Improved Photocatalytic Activity of TiO2. Chem. Mater. 18, 2989–2996 (2006). doi:10.1021/cm060212g

40. Sumitsawan, S., Cho, J., Sattler, M.L., Timmons, R.B.: Plasma Surface Modified TiO2 Nanoparticles: Improved Photocatalytic Oxidation of Gaseous m-Xylene. Environ. Sci. Technol. 45, 6970–6977 (2011). doi:10.1021/es2012963

41. Savage, C.R., Timmons, R.B., Lin, J.W.: Molecular Control of Surface Film Compositions via Pulsed Radio-Frequency Plasma Deposition of Perfluoropropylene Oxide. 575–577 (1991). doi:10.1021/cm00016a005

42. Hamrock, B.J., Dowson, D.: Isothermal Elastohydrodynamic Lubrication of Point Contacts: Part III—Fully Flooded Results. J. Lubr. Technol. 99, 264–275 (1977). doi:10.1115/1.3453074

43. Yamaguchi, E.S., Ryason, P.R., Hansen, T.P.: Electrical contact resistance studies on zinc dithiophosphates. Tribol. Lett. 3, 27–33 (1997). doi:10.1023/A:1019175509680

44. So, H., Lin, Y.C., Huang, G.G.S., Chang, T.S.T.: Antiwear mechanism of zinc dialkyl dithiophosphates added to a paraffinic oil in the boundary lubrication condition. Wear. 166, 17–26 (1993). doi:https://doi.org/10.1016/0043-1648(93)90274-P

45. Topolovec-Miklozic, K., Forbus, T.R., Spikes, H.A.: Film thickness and roughness of ZDDP antiwear films. Tribol. Lett. 26, 161–171 (2007). doi:10.1007/s11249-006-9189-2

46. Spikes, H.A.: The History and Mechanisms of ZDDP. Tribol. Lett. 17, 469–489 (2004). doi:10.1023/B:TRIL.0000044495.26882.b5

47. Dawczyk, J., Morgan, N., Russo, J., Spikes, H.: Film Thickness and Friction of ZDDP Tribofilms. Tribol. Lett. 67, 34 (2019). doi:10.1007/s11249-019-1148-9

48. Li, Y.-R., Pereira, G., Lachenwitzer, A., Kasrai, M., Norton, P.R.: X-Ray Absorption Spectroscopy and Morphology Study on Antiwear Films Derived from ZDDP Under Different Sliding Frequencies. Tribol. Lett. 27, 245–253 (2007). doi:10.1007/s11249-007-9213-1

49. Morina, A., Green, J.H., Neville, A., Priest, M.: Surface and Tribological Characteristics of Tribofilms Formed in the Boundary Lubrication Regime with Application to Internal Combustion Engines. Tribol. Lett. 15, 443–452 (2003). doi:10.1023/B:TRIL.0000003065.37526.84

50. Hesse, B., Salome, M., Castillo-Michel, H., Cotte, M., Fayard, B., Sahle, C.J., De Nolf, W., Hradilova, J., Masic, A., Kanngießer, B., Bohner, M., Varga, P., Raum, K., Schrof, S.: Full-Field Calcium K-Edge X-ray Absorption Near-Edge Structure Spectroscopy on Cortical Bone at the Micron-Scale: Polarization Effects Reveal Mineral Orientation. Anal. Chem. 88, 3826–3835 (2016). doi:10.1021/acs.analchem.5b04898

51. Cebe, T., Ahuja, N., Monte, F., Awad, K., Vyavhare, K., Aswath, P., Huang, J., Brotto, M., Varanasi, V.: Novel 3D-printed methacrylated chitosan-laponite nanosilicate composite scaffolds enhance cell growth and biomineral formation in MC3T3 pre-osteoblasts. J. Mater. Res. 35, 58–75 (2020). doi:DOI: 10.1557/jmr.2018.260

52. Varlot, K., Kasrai, M., Bancroft, G.M., Yamaguchi, E.S., Ryason, P.R., Igarashi, J.: X-ray absorption study of antiwear films generated from ZDDP and borate micelles. Wear. 249, 1029–1035 (2001). doi:10.1016/S0043-1648(01)00586-5

53. Zhang, Y., Zeng, X., Wu, H., Li, Z., Ren, T., Zhao, Y.: The Tribological Chemistry of a Novel Borate Ester Additive and Its Interaction with ZDDP Using XANES and XPS. Tribol. Lett. 53, 533–542 (2014). doi:10.1007/s11249-013-0292-x

54. Fofanov, D.: Synthesis, characterization and physical properties of metal borides, http://ediss.sub.uni-hamburg.de/volltexte/2009/2995, (2006)

55. Fleet, M.E., Muthupari, S.: Coordination of boron in alkali borosilicate glasses using XANES. J. Non. Cryst. Solids. 255, 233–241 (1999). doi:10.1016/S0022-3093(99)00386-5

56. Fleet, M.E., Muthupari, S.: Boron K-edge XANES of borate and borosilicate minerals. Am. Mineral. 85, 1009–1021 (2000). doi:10.2138/am-2000-0716

57. Zhang, Z., Yamaguchi, E.S., Kasrai, M., Bancroft, G.M.: Interaction of ZDDP with borated dispersant using XANES and XPS. Tribol. Trans. 47, 527–536 (2004).

doi:10.1080/05698190490500725

58. Sharma, V., Timmons, R., Erdemir, A., Aswath, P.B.: Plasma-Functionalized Polytetrafluoroethylene Nanoparticles for Improved Wear in Lubricated Contact. ACS Appl. Mater. Interfaces. 9, 25631–25641 (2017). doi:10.1021/acsami.7b06453

59. Yin, Z., Kasrai, M., Fuller, M., Bancroft, G.M., Fyfe, K., Tan, K.H.: Application of soft X-ray absorption spectroscopy in chemical characterization of antiwear films generated by ZDDP Part I: the effects of physical parameters. Wear. 202, 172–191 (1997). doi:https://doi.org/10.1016/S0043-1648(96)07272-9

60. Fuller, M., Yin, Z., Kasrai, M., Bancroft, G.M., Yamaguchi, E.S., Ryason, P.R., Willermet, P.A., Tan, K.H.: Chemical characterization of tribochemical and thermal films generated from neutral and basic ZDDPs using X-ray absorption spectroscopy. Tribol. Int. 30, 305–315 (1997). doi:10.1016/S0301-679X(96)00059-X

61. Nicholls, M., Najman, M., Zhang, Z., Kasrai, M., Norton, P., Gilbert, P.: The contribution of XANES spectroscopy to tribology. Can. J. Chem. 85, 816–830 (2007). doi:10.1139/V07-093

62. Najman, M.N., Kasrai, M., Bancroft, G.M., Frazer, B.H., Stasio, G. De: The Correlation of Microchemical Properties to Antiwear (AW) Performance in Ashless Thiophosphate Oil Additives. Tribol. Lett. 17, 811–822 (2004). doi:10.1007/s11249-004-8089-6

63. Yang, S., Wang, D., Liang, G., Yiu, Y.M., Wang, J., Liu, L., Sun, X., Sham, T.-K.: Soft X-ray XANES studies of various phases related to LiFePO4 based cathode materials. Energy Environ. Sci. 5, 7007–7016 (2012). doi:10.1039/C2EE03445J

64. Spikes, H.: The history and mechanisms of ZDDP. Tribol. Lett. 17, 469–489 (2004). doi:10.1023/B:TRIL.0000044495.26882.b5

65. Najman, M.N., Kasrai, M., Bancroft, G.M.: Chemistry of Antiwear Films from Ashless Thiophosphate Oil Additives. Tribol. Lett. 17, 217–229 (2004). doi:10.1023/B:TRIL.0000032448.77085.f4

66. Kim, B., Mourhatch, R., Aswath, P.B.: Properties of tribofilms formed with ashless dithiophosphate and zinc dialkyl dithiophosphate under extreme pressure conditions.

Wear. 268, 579–591 (2010). doi:10.1016/j.wear.2009.10.004

67. Najman, M., Kasrai, M., Michael Bancroft, G., Davidson, R.: Combination of ashless antiwear additives with metallic detergents: interactions with neutral and overbased calcium sulfonates. Tribol. Int. 39, 342–355 (2006). doi:10.1016/j.triboint.2005.02.014

68. Mosey, N.J., Müser, M.H., Woo, T.K.: Molecular Mechanisms for the Functionality of Lubricant Additives. Science (80-.). 307, 1612–1615 (2005). doi:10.1126/science.1107895

69. Ueda, M., Kadiric, A., Spikes, H.: On the Crystallinity and Durability of ZDDP Tribofilm. Tribol. Lett. 67, 123 (2019). doi:10.1007/s11249-019-1236-x

CHAPTER 5

GENERAL CONCLUSIONS

In pursuit of tribological solutions to improve the fuel economy and the energy efficiency of passenger car vehicles, in this research work, we have developed an innovative technology to prepare high-performance environmentally friendly nano-additives for the automotive engine oils. Currently, the automotive lubricant market is dominated by P-containing additives like ZDDP. ZDDP in engine oil provides exceptional wear protection of engine components experiencing direct contact during sliding, however, at the same time ZDDP affects service-life and performance of exhaust catalytic converters leading to increased automotive emissions in the atmosphere. Considering the contribution of the automotive sector to greenhouse gases, ZDDP must be eliminated or at least reduced in modern lubrication technology. In addition to problems of increased emissions, existing additive technology is not sufficient to minimize frictional losses and fuel usage in modern automobile engines. Therefore, it is important to develop novel high-performance additives for engine oils to benefit both industry and society.

In this study, the plasma polymerization technique especially plasma-enhanced chemical vapor deposition (PECVD) was applied to develop novel nano-additives and solve problems of engine lubrication. PECVD coating method was employed to functionalize nano-particles and achieve their adequate dispersion in a polar base oil. Additionally, the aim was to use PECVD coated nanoparticles as the carrier to deposit polymer film chemistries at the tribological contacts to ultimately improve the anti-wear and anti-friction performance of lubricants. To achieve this, surface tailored nanoparticles were subjected to the tribological tests, and their performance was compared with conventional additives like ZDDP. Furthermore, to resolve problems of ZDDP, test

lubricants were formulated with a low concentration of ZDDP (approximately 50% reduced than commercial oils). The study includes a comprehensive and fundamental scientific approach to elucidate the tribological mechanism of novel core-shell structure nano-additives.

Initially, the experimental methodology was designed with a 360º rotating plasma reactor to synthesize core-shell structure ZnO nanoparticles. Here, the ZnO core was encapsulated with a bi-layer shell coating of fluorocarbon and methacrylate-based polymer films. These fluorinated ZnOFM nanoparticles were later mixed with a mineral base oil and formulations were prepared with and/without ZDDP. Methacrylate coating encapsulating fluorocarbon coating successfully provided an effective dispersion of nanoparticles for several weeks. Tribological test results indicated that ZnOFM nanoparticles by themselves or in combination with ZDDP provide superior anti-wear and anti-friction protection. Chemical surface analysis exhibited stable formation of tribofilms under nanoparticles based lubrication, these tribofilms were comparatively thick and continuous as to ZDDP formed tribofilms. Results proved that extra chemistries delivered through plasma coated ZnO nanoparticles can contribute to enhance properties of tribofilms formed at sliding contacts and enhance overall tribological performance.

Considering the positive results of fluorinated ZnO nanoparticles, the developed PECVD technique was extended to coat ZnO nanoparticles with another tribological beneficial chemistry. A similar experimental methodology was applied to synthesize core-shell nano-additives with ZnO nanoparticles and boron-based polymer films. The boron coated ZnO nano-additives were subjected to boundary lubrication tribological tests. The results of this study exhibited synergistic interaction between functionalized ZnO nanoparticles and ZDDP additive. Tribochemical analysis of worn surfaces collected after tribological tests revealed that interaction of ZDDP and non-functionalized ZnO nanoparticles did not lead to the formation of tribofilms, on the other hand,

synergistic interaction between functionalized ZnO and ZDDP promoted the formation of beneficial zinc phosphate-based tribofilms.

To explore the versatility of plasma polymerization technology for the preparation of lubricant additives, further experiments were conducted with $CaCO_3$ nanoparticles and boron-based monomer. Similar to the previous chapter, functionalized $CaCO_3$BM nanoparticles were prepared by initially coating them with boron-based films followed with methacrylate coating. However, in this study, the compatibility of plasma functionalized ZnO nanoparticles was assessed with other environmentally friendly P-containing additives, DDP. A linear reciprocating tribometer was employed to evaluate tribological performance and interaction of $CaCO_3$BM nanoparticles with both DDP and ZDDP additives. Again, it was observed that functionalized $CaCO_3$BM nanoparticles interacted synergistically with the ashless DDP additives and exhibited enhanced anti-wear and anti-friction behavior.

In conclusion, core-shell structure polymer-coated metal oxide nanoparticles delivered tribological beneficial chemistries at tribological contacts and promoted the robust formation of tribofilms leading to enhanced anti-wear and anti-friction performance. This dissertation work established a new class of lubricant nano-additives via plasma polymerization technique. This research work effectively exhibited the applicability of the developed plasma surface modification technique to different nanoparticles and coating chemistries. Additionally, the knowledge gained here on the tribological performance of plasma functionalized metal-oxide nanoparticles and their tribofilm properties will help promote the future development of nano-lubricants containing a mixture of surface-modified nanoparticles for the tribological applications that will extend the durability and energy efficiency of a multitude of different mechanical systems in addition to automotive engines.